Rutin and barley starch modification using subcritical water, ultrasonication and electrolysis technologies

by

Idaresit Uyai Ekaette

A thesis submitted in partial fulfillment of the requirements for the degree of

Doctor of Philosophy

in
Bioresource and Food Engineering

Department of Agricultural, Food, and Nutritional Science

University of Alberta

© Idaresit Uyai Ekaette, 2020

Abstract

The barley grain is a rich source of starch and dietary fibre but over the years, barley grain uses in Canada has been more popular in animal feeding and brewing, than for food uses. With the large barley production and increasing demand for starch by the food and biobased industries, barley starch has become an item of economic value. Therefore, the objective of this research was to isolate barley starch and modify the barley starch properties for suitability in functional food applications. Towards the development of a functional ingredient, rutin, a flavonoid compound was selected to be added to the isolated barley starch. The incorporation of rutin into the barley starch matrix was enhanced by thermal treatments using subcritical water, ultrasonication and electrolysis technologies. In the first study, barley starch (0%, 22%, 37% amylose) with rutin treated at 80 $^{\circ}$C and subcritical water temperatures of 100-160 $^{\circ}$C/7 MPa/30 min resulted in the addition of 0.19-0.87 mg rutin/g starch dry matter. Comparison of barley starches with and without rutin showed a loss of amylose, for the 37% amylose starch at 100 $^{\circ}$C, and 22% amylose starch at 120 $^{\circ}$C, indicating that rutin was involved in V-amylose inclusion complexation. The 37% amylose starch with 0.34 mg rutin/g starch dry matter had the highest observed expansion (specific volume) of 6.10 $\pm$ 0.12 mL/g at 160 $^{\circ}$C; a 392% increase from 1.24$\pm$0.01 mL/g of native 37% amylose starch at room temperature (23 $^{\circ}$C). In the second study, ultrasonication treatment at energy density (3.6-36 kJ/mL, 47 $^{\circ}$C) and change in energy density (0.1-7.0 kJ/mL, 86 $^{\circ}$C) was carried out on rutin hydrate in water, 0.01 g/mL citric acid, and 0.01 g/mL sodium chloride. The highest increase in total flavonoid content of 74% was observed in the water media (27 kJ/mL). Quercetin, an aglycone of rutin was produced (with treatment in the citric acid media) as change in energy density increased

from 0.1 kJ/mL (0.34±0.09%) to 7.0 kJ/mL (2.23±0.04%). In the third study, further characterization on the recrystallized rutin after ultrasonication (insoluble fraction) showed long, and slender strands of rutin nanocrystals (100-820 nm) bound as agglomerates (SEM images). According to DSC endotherms, new rutin polymorphs were formed with all solvent treatments at 3.9 kJ/mL, and 7.0 kJ/mL, and with water, 36 kJ/mL. The new rutin polymorphs used in pyrodextrinization (2.2 M HCl, 90 ºC, 1 h) of barley starch did not significantly change the quantity of malto-oligosaccharides (DP 1-7) produced from the control barley starch (without rutin). In the final study, waxy barley flour (0% amylose content) slurry (1:6 w/w in water) was treated by electrolysis at voltages of 5-30 V, and electrode length of 4-8 cm. Starches isolated from the electrolysed barley flour slurry had higher metal content (magnesium 2.9% and phosphorus 13.0%) compared to magnesium 0.8% and phosphorus 3.5% of the alkali-treated starch (starch isolated by conventional method). The electrolysed freeze-dried starch gel had a high absorption capacity in water as 1659±24%, observed for treatment at 15 V, and 8 cm. However, the effect of rutin addition in the freeze-dried starch gels inhibited rehydration. All electrolysed starch gels with and without rutin were opaque and exhibited no change of firmness at 40 days of storage at room temperature. The structural behavior of the electrolysed starches was related to enhanced crystallinity by electrolysis (FT-IR results). Based on the technologies and thermal treatments utilized, modified barley starches loaded with rutin have been produced with the unique characteristics of expanded starch (lighter mass per volume), dextrin (as a soluble starch), and opaque superabsorbent hydrogels (to enhance light protection of rutin). These starches can find applications in functional foods, cosmetics, and the pharmaceutical industry.

Preface

This thesis is made up of four research studies each representing the application of cutting-edge processing technologies, for generating scientific data relevant to the contemporary bioresource and food engineering field. Each study is presented per chapter and focuses on a different type of processing technology, and a different type of modified starch, except for Chapter 4, which is part (1) of the following chapter - Chapter 5 part (2). This thesis explored options for the incorporation of rutin into modified starch products from barley grain.

This thesis is an original work of Idaresit Ekaette, and data from this thesis have been presented at scientific conferences relevant to the subject areas. Also excerpts, of this thesis have either been published or submitted to peer-reviewed scientific journals. The research studies in this thesis were sponsored by the financial support of the Natural Sciences and Engineering Research Council of Canada (Dr. Saldaña's NSERC-Discovery Grant).

Chapter 2 is the literature review on the subject areas related to the objectives of this thesis. I, and my supervisor developed the titles and sections. I drafted the manuscript. Dr. Saldaña helped with discussion and revision of the manuscript.

Chapter 3 was published as "Ekaette, I., and Saldaña, M.D.A. (2020). Barley starch behavior in the presence of rutin under subcritical water conditions. *Food Hydrocolloids* 100, 105421." I was responsible for the experimental design, performed the experiments, carried out the data collection and analysis, interpreted the results and discussion, and prepared the manuscript. Dr. Saldaña provided the topic research area and helped with discussion and revisions of the manuscript.

Excerpts of Chapter 4, and Chapter 5 will be submitted for publication to the journal, Food Research International as "Ekaette, I., and Saldaña, M.D.A. Ultrasonication processing of rutin: Derivative compounds, antioxidant activities and optical rotation." And as "Ekaette, I., and Saldaña, M.D.A. Ultrasonication treatment for production of rutin nanocrystals." I was responsible for the experimental design, carried out the experiments, data collection and analysis, interpreted the results and discussions, and drafted the manuscript. Carla Valdivieso helped me with some HPLC analysis for malto-oligosaccharides. Dr. Saldaña provided the topic research area and helped with the discussion and revision of the manuscript.

Chapter 6 will be submitted for publication to Journal of Food Engineering as "Ekaette, I., and Saldaña, M.D.A. Structural characterization of starch isolates from the electrolysis treatment of barley flour, and the influence of rutin." I developed the experimental design, performed the experiments, carried out the data collection and analysis, interpreted the results and discussion, and drafted the manuscript. Dr. Saldaña helped with discussion and revision of the final manuscript.

Dedication

To Comfort and Uyai

Acknowledgements

I wish to express my gratitude to my supervisor, Dr. Marleny Aranda Saldaña for her support and tutelage throughout my studies, and the encouragements towards my career goals. I am also thankful to the Natural Sciences and Engineering Research Council of Canada (Dr. Saldana's NSERC Discovery Grant) for supporting my research. I also wish to express my gratitude to Dr. Feral Temelli and Dr. Jianping Wu, for being on my supervisory committee. Thank you for your availability, contributions, and support to the end of this thesis.

Special thanks to my kind-hearted neighbors of the Grain Processing Technology Laboratory (Dr. Thava Vasanthan's lab), you made many things easy: Jun Gao, Natalie Lopez, and Brasathe Jeganathan. Jun Gao, thank you for sharing your expertise, your availability, the trainings, and the accessibility to resources. I also like to thank Dr. Nakano for his valuable help. My lab mates were of great assistance to me. Thank you for contributing to a conducive learning environment: Carla Valdivieso, Raquel Huerta, Yujia Zhao, Angelica Chavez, Azadeh Aghashashi, and Jasreen Sekhon. I am also grateful to my other colleagues and friends for the encouragement through the years.

The last, but not the least, I am thankful to my parents, Comfort and Uyai Ekaette, my amazing heros of education, and my siblings, Edidiong, John, Emem, Unwana, Aniekan, and Nkechi who were there during the difficult times. Thank you to my family for believing in me, for the financial support towards some student costs, and for your prayers.

To the One who makes all things possible, my Provider, the Author and Perfecter of my faith, the Alpha and Omega, the One True God: I give you all the Praise!!!

Table of contents

List of tables

List of figures

List of abbreviations and symbols

5-HMF   5-(Hydroxymethyl) furfural

5-MF   5- Methyl furfural

ΔED Change in energy density

ΔE Total color difference

ANOVA   Analysis of variance

ABTS   2,2'-Azino-bis(3-ethylbenzothiazoline-6-sulphonic)

ASTM   American Society for Testing Materials

BHA   Butylated hydroxy-anisole

C   Carbon

CO_2 Carbon dioxide

dm   Dry matter

DMSO   Dimethyl sulfoxide

DPPH   1,1-Diphenyl-2-picrylhydrazine

DSC   Differential Scanning Calorimetry

ED   Energy density

EDTA   Ethylenediamine tetra-acetic acid

EGCG   Epigallocatechin gallate

$FeCl_2$	Ferric chloride
FRAP	Ferric Reducing Antioxidant Power
FT-IR	Fourier Transform-Infrared
G''	Loss modulus
G'	Storage modulus
H^+	Hydrogen ion
H_2O	Water
H_3O^+	Hydronium ion
H_3PO_4	Phosphoric acid
H_2SO_4	Sulfuric acid
HCl	Hydrochloric acid
H-NMR	Proton Nuclear Magnetic Resonance
HPLC	High Performance Liquid Chromatography
I	Iodine
KI	Potassium iodide
KOH	Potassium hydroxide
LC-MS/MS	Liquid chromatography Tandem mass spectrometry
MW	Molecular weight

NaCl	Sodium chloride
NaOH	Sodium hydroxide
Na_2CO_3	Sodium carbonate
OH^-	Hydroxide ion
$OH^\bullet$	Hydroxyl radical
rpm	Revolutions per minute
RVA	Rapid Visco Analyzer
SEM	Scanning Electron Microscopy
SCW	Subcritical water
TFC	Total flavonoid content
TPC	Total phenolic content
TPTZ	2,4,6-Tripyridyl-s-triazine
UTR	Ultrasound treated rutin
UVB	Ultraviolet B
WI	Whiteness index
YI	Yellowness index

Chapter 1. Introduction and thesis objectives

1.1. Introduction

Functional foods for the delivery of phytochemicals are widely accepted for their health-promoting benefits. Some of the functional foods are whole foods such as fruits, vegetables, and grains, while some are processed foods enhanced or fortified with the target functional ingredient (Hasler, 2002). Common grains like buckwheat has been harnessed for its rich content of rutin (Ahmed et al., 2013). The presence of this flavonoid compound has promoted the traditional use of buckwheat in breakfast cereals, soups, stews and salads. Buckwheat flour, with its rutin content of 18-1148 mg/100 g per dry matter (Andrea et al., 2009) has often been utilized as an antioxidant ingredient in the formulation of other flour breads (Watanabe et al., 1997), e.g. wheat breads, biscuits, crackers, and noodles (Szawara-Nowak et al., 2014; Yoo et al., 2012; Filipčev et al., 2011; Sedej et al., 2011; Lin et al., 2009). However, the use of rutin for food purposes has been limited to buckwheat-based products, and therefore, there is a need to extend the application of rutin to other food types.

Rutin (3,3′,4′,5,7-pentahydroxyflavone-3-rutinoside) is a known phytochemical (Khalifa et al., 1983), with proven antioxidant, antimicrobial, anti-inflammatory, anticancer, antidiabetic, and antiallergic capacities (Gullón et al., 2017). Rutin usually co-exists with other phytochemicals such as isoquercetin (Valentová et al., 2014) and quercetin (Ożarowski et al., 2018) found in buckwheat, and amaranth plants (Kraujalis et al., 2013; Kalinova and Dadakova, 2009; Watanabe et al., 1997). However, isoquercetin (quercetin-3-O-β-D-glucopyranoside) and the quercetin (3,3′,4′,5,7-pentahydroxyflavone) aglycone are also obtained from the hydrolysis of rutin (Ravber et al., 2016). These rutin derivatives

(isoquercetin and quercetin) were identified as rutin hydrolysates from the subcritical water treatment of rutin (Kim and Lim, 2017; Vetrova et al., 2017; Ravber et al., 2016); and also in the extracts of the ultrasonic extraction of flavonoid compounds from red grape skins (Novak et al., 2008). The limitations of rutin are in its low water solubility (13 mg/100 mL, Khalifa et al., 1983; Krewson and Naghski, 1952) and low bioavailability. Therefore, it is often complexed with cyclodextrins, which are water-soluble drug carriers (Miyake et al., 2000). In addition, advances have been made to incorporate rutin in other food matrices like soy protein isolates (Chen et al., 2016), and cheese spreads (Přikryl et al., 2018) but its application in non-buckwheat starch processing is limited.

Starch is the energy storage of plants and is structurally a large polymer composed of two major α-D-glucan macromolecules, namely amylose and amylopectin. In amylose, the glucose molecules are connected by α-1,4-linkages within a linear chain, while the amylopectin polymer is a highly branched molecule characterized by α-1,4 and α-1,6-linkages (Bergthaller and Hollman, 2007). In a starch granule growth ring, amylose and the α-1,6-linkages of amylopectin are contained in the amorphous lamellae, while the left-handed helical side chains of amylopectin are found in the crystalline lamellae (Bergthaller and Hollman, 2007). These characteristics make amylose and amylopectin the amorphous and the crystalline components of starch, respectively. Furthermore, native starch because of its composition of large molecular weight polymers (0.15-700×10^6 Da, Bergthaller and Hollman, 2007) is insoluble in water, and in this native state may not exhibit certain functional characteristics suitable for food purposes. Therefore, starch modification methods including chemical, physical and thermal treatments are often employed to disrupt

the starch's structural components. A commonly used starch modification process is gelatinization.

Gelatinization is the disintegration of starch granule structure by heat and water treatment (Bergthaller and Hollman, 2007). During gelatinization in excess water, starch granules swell, absorb water, lose structural integrity such as crystallinity, and leach amylose (He et al., 2018; Bergthaller and Hollman, 2007). This starch structural disintegration enables the accessibility of other compounds into the starch granules, e.g. flavonoids to form starch-flavonoid complexes (Zhu, 2015a; Kasemwong and Itthisoponkul, 2013). Apart from starch-flavonoid complexes being a delivery vehicle for flavonoids in starch-based foods, the presence of flavonoids also affects starch properties. For example, when a mixture of 5 mg of rice starch (amylose content of 1.6-32%) and 5 mg rutin were treated at 130 $^{\circ}$C, the presence of rutin hindered starch retrogradation at 4 $^{\circ}$C for 7 days and reduced the retrograded starch yield by 65% in the 32% amylose rice starch (Zhu and Wang, 2012). Similarly, in the thermal treatment of tartary buckwheat starch (3 mg) with rutin (0.5%) at solid-to-water ratio (1:3, w/v) at 100 $^{\circ}$C, the enthalpy of retrograded starches after storage at 4 $^{\circ}$C for 7 days was reduced by 7.5% (He et al., 2018). This reduction was related to the decreased starch crystallinity during retrogradation. Other physicochemical changes in the tartary buckwheat starch (3 g) treated with rutin (0.5%) in 25 mL water were the reduced peak viscosity (364 rapid visco unit, RVU), and breakdown viscosity (171 RVU) compared to 369 RVU and 205 RVU, respectively, of the tartary buckwheat starch without rutin (He et al., 2018).

Thermal treatment of starch has been achieved with different technologies, including autoclaving, extrusion, heat-moisture treatment, and subcritical water, but among

the emerging technologies with environmentally friendly potential, subcritical water technology is unique for its high chemical reactivity due to the modified properties of water at high temperatures (100-374 ^{o}C) kept under pressure up to 22 MPa (Saldaña and Valdivieso, 2015; Brunner, 2014). Subcritical water acts as an acid, base or organic solvent due to its tunable properties of dissociation constant, dielectric constant, surface tension, and viscosity (Brunner, 2014; Saldaña and Valdivieso, 2015). In subcritical water applications, cassava starch was modified at conditions of 100-150 ^{o}C, 8.5 MPa, and 10 min, showing reduced relative X-ray crystallinity of 7.0-11.3% compared to 24.4% of the native starch. Also observed was the production of low molecular weight starch hydrolysates (100 kDa) at 150 ^{o}C and 15.5 MPa (Zhao and Saldaña, 2019a). Subcritical water has also been reported to hydrolyze ginger bagasse starch (176-200 ^{o}C, 15 MPa, 15 min) to oligosaccharides and sugars (Moreschi et al., 2004), and sweet potato starch (180-240 ^{o}C, 10-30 min) to glucose (Nagamori et al., 2004). Decomposition products from the subcritical water treatment of sweet potato starch, including 5-hydroxymethyl furfural (5-HMF), and furfural were also produced at 200-240 ^{o}C for 10 min, and 220-240 ^{o}C for 10 min, respectively (Nagamori et al., 2004). However, there are other methods to produce oligosaccharides and dextrins from starch with no water requirement. Pyrodextrinization of dry starch carried out at temperature >90 ^{o}C and 2.2M hydrochloric acid produced indigestible starch (pyrodextrins) from lima bean starch (Orozco-Martínez and Betancur-Ancona, 2004), and banana starch (Olvera-Hernández et al., 2018). Further investigation on the subcritical water and pyrodextrinization treatments of starch of A-type crystallinity like barley can enhance understanding towards the production of different modified starch products.

Another emerging technology is ultrasonication, which utilizes sound waves >20 kHz to cause mechanical disintegration of plant tissues, commonly applied for the extraction of phytochemicals, e.g. rutin from flower bud of *Sophora japonica* (Liao et al., 2015; Wang and Zuo, 2011; Paniwnyk et al., 2001). The efficiency of ultrasonication on the increased yield of extractable compounds has often been related to its capacity to accelerate heat and mass transfer, thereby enhancing the release of phytochemicals from disrupted plant tissues (Chemat et al., 2011). However, it is unclear if the increased yield of extractable compounds was only from the disruption of plant tissues or influenced by the acoustic cavitation impact on the individual compounds. Therefore, it is important to investigate the effect of direct ultrasonication on individual phytochemicals, in this case rutin.

Recently, modified starches have also been produced using electrolysis in sodium chloride media, e.g. retrograded sweet potato starch at 45-180 V for 30-120 min (Xijun et al., 2012), and oxidized rice starch at 7.5 mA/cm^2 for 60 min (Shaarwy et al., 2009). Electrolysis is a chemical process driven by the passage of electrical voltage through metal electrodes into an electrically conductive solution (electrolyte) to create ionic species and new chemical compounds (Petrucci et al., 2007). Electrolysis can affect the energy and electrical charge of starch granules, influencing its swelling, water absorption, and retrogradation characteristics (Xijun et al., 2012). However, the functional properties of electrolysis-modified starches have not been fully explored.

Each of the technologies mentioned above are similar in their chemical effects on water molecules (H_2O) by the breaking of hydrogen bonds, dissociation of water molecules, and reactions that form ions or radicals. In subcritical water, hydronium, and hydroxide

ions (H_3O^+, OH^-) are formed (Brunner, 2014). Ultrasonication in water produces hydrogen and hydroxyl radicals ($H^\bullet$, $OH^\bullet$), OH^-, hydrogen peroxide (H_2O_2), oxygen (O_2) and electrons (e^-) (Bermudez-Aguirre, 2017). Electrolysis of water decomposes water to hydrogen, hydronium and hydroxide ions (H^+, H_3O^+, OH^-) to form hydrogen and oxygen gas (Shultz, 2007). Based on research findings, any substance placed in any of these systems can experience enhanced solubility, electron transfer, hydrogen atom abstraction, formation of new bonds and new compounds, and a structural modification.

To the best of my knowledge, there is a dearth of information on the application of subcritical water, ultrasonication, and electrolysis for modification of barley starch structure, in the presence of the flavonoid, rutin. Barley *Hordeum vulgare*, is an important cereal crop in Canada, known for its health benefits of lowering cholesterol because of its beta-glucan content (AAFC, 2019) but the utilization of barley for food purposes in Canada is currently below 2% (Statistics Canada, 2018). Therefore, there is need to promote barley in food and industrial applications. This thesis is focused on maximizing the utilization of barley grain's high starch content (52-68%) for starch-based products, and thereby will provide the food and biobased industries with an alternative starch to meet their demands.

1.2. Rationale

Thermal and acid treatment of rutin produced isoquercetin and quercetin, which have better physiological activities than rutin, including the inhibition of α-Glucosidase, protective activity in HepG2 cells, and anti-adipogenic activity (Yang et al., 2019; Li et al., 2009). Barley starch has lower gelatinization enthalpy compared to maize starch (Li et al., 2001). The gelatinization enthalpy is the energy required to unwind and melt double helices of starch (Li et al., 2001) for incorporation of rutin. Barley starch compared to β-

cyclodextrin showed higher retention capability for encapsulation of benzaldehyde and benzothiazole flavors (Jeon et al., 2003).

1.3.   Hypothesis

It is hypothesized that rutin and barley starch can interact during thermal treatments, and this interaction can modify starch behavior. Barley starch structure can be altered by hydrothermal, acidic, and electrical treatments.

1.4.   Thesis objectives

The main objective of this thesis was to modify barley starch and rutin in a matrix suitable as a functional food ingredient using green technologies such as subcritical water, ultrasonication, and electrolysis to enhance the desirable functional properties.

Specific objectives were to:

1. Understand the effects of barley starch amylose content and subcritical water temperature on starch properties in the presence of rutin (Chapter 3).

2. Understand the effect of ultrasonication energy, pH of common food solvents (modified with citric acid, and sodium chloride), and temperature, on rutin, its derivatives, and antioxidant activities (Chapter 4).

3. Characterize the structural modification of the ultrasound-treated rutin in objective 2, and to understand its effect on the production of barley starch pyrodextrins (Chapter 5).

4. Determine the effects of electrical voltage, and electrode length on structural properties of barley starch isolates, and to study the effect of rutin on the structural properties of electrolysed-barley starch gels (Chapter 6).

1.5.   Justification of study

Barley grain is a low-cost source of starch. The modified barley starches from this research will find applications as bakery ingredient, and thickener (Chapter 3), coating material in nutraceutical products (Chapter 5), and hydrogel in personal care products (Chapter 6).

Chapter 2. Literature review

2.1.   Flavonoids

Flavonoids are a group of secondary metabolites of plants, which have the chemical structure-activity relationships for pharmacological benefits, including antioxidant, antiviral, anti-inflammatory, and antitumor activities (Menezes et al., 2016). Natural flavonoids are part of polyphenols and are present in flowers, fruits, seeds, vegetables, leaves, barks, and roots (Middleton, 1998; Montanari et al., 1998). The basic chemical structure of flavonoids consists of two benzene rings designated as A and B as shown in Figure 2.1, linked via a heterocyclic pyrane ring designated as C.
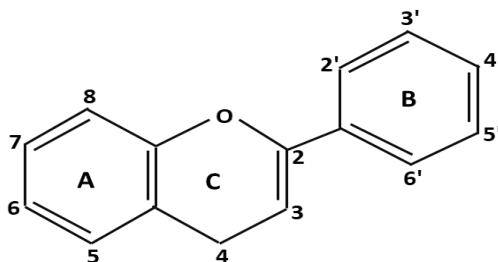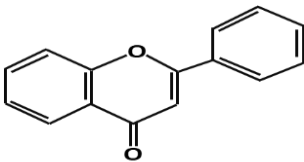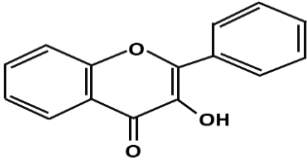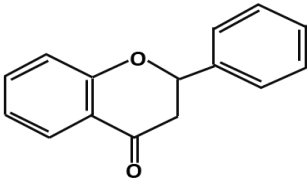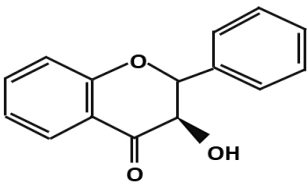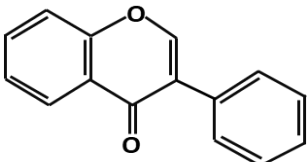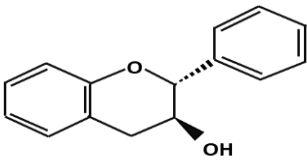
Figure 2.1. Basic flavonoid structure

The subclasses of flavonoids (flavones, flavonols, flavanones, flavanonol, isoflavones, and flavan-3-ols) differ in their saturation level of the bond between the C2-C3 position shown in Table 2.1 (Kumar and Pandey, 2013). These subclasses are further divided into individual compounds varying in the degree of hydroxylation, glycosylation or methoxylation (or other substituent moieties) in the A, B, and C rings and the presence or absence of a carbonyl group at position 4 (Middleton, 1998). Examples of glycosylated flavonols are rutin, and isoquercetin. An example of a glycosylated flavonone is naringin.

Table 2.1. Structure of flavonoids

Group of flavonoid	Structure skeleton	Examples
Flavone		Luteolin, Apigenin, Chrysin
Flavonol		Kaempferol, Quercetin, Rutin
Flavanone		Hesperidin, Naringenin
Flavanonol		Taxifolin
Isoflavone		Genistin, Daidzein
Flavan-3-ol		Catechin, Epicatechin

Kumar and Pandey (2013); Medvidović-Kosanović et al. (2010).

2.1.1. Chemistry of flavonoids and functionality

The antioxidant activity of flavonoids is determined by the nature of substitutions on rings B and C of the basic flavonoid structure (Medvidović-Kosanović et al., 2010), which provides them with the ability to scavenge free radicals (Elia et al., 2012), donate hydrogen atoms or electrons (Huang et al., 2005), or chelate metal ions (Afanas'ev et al., 1989). For example, in the electrochemical processing of catechin, quercetin, and rutin, the investigation indicated the oxidation of catechol 3′,4′-dihydroxy group on the B-ring, and the transfers of $2e^-$ and $2H^+$ ions (Medvidović-Kosanović et al., 2010). Some of the identified structural features on rings B and C that enhanced antioxidant activities of flavonoids are: 1) The degree of hydroxylation and positions of the hydroxyl groups in the B-ring, 2) Substitution of hydroxyl groups in ring B by methoxyl groups, 3) A double bond between C-2 and C-3, conjugated with the 4-oxo group in ring C, and 4) A double bond between C-2 and C-3 combined with a 3-OH group in ring C (Balasundram et al., 2006). The antioxidant activities of flavonoids (e.g. rutin, quercetin, myricetin, kaempferol, morin) have been attributed to the prevention of many diseases, including the free-radical oxidative hemolysis of red blood cells (Dai et al., 2006), and human low-density lipoprotein oxidation (Hou et al., 2004). The flavonol rutin has also proven biological activities of anti-diabetic-induced erectile dysfunction (Al-Roujeaie et al., 2017), anti-chronic cerebral hypoperfusion (Qu et al., 2014) and anti-acute gastric mucosal lesions (Liu et al., 2013).

2.1.2. Rutin

Rutin, also known as quercetin-3-O-rutinoside, vitamin P, or Eldrin, is a common dietary flavonoid (Khalifa et al., 1983). The rutin structure consists of a flavonol, known as quercetin, and a disaccharide, named rutinose [6-O-(α-L-rhamnopyranosyl)-D-glucose]

(Figure 2.2). Rutin is abundant in buckwheat plant parts (*Fagopyrum esculentum Moench.*) such as leaves, grains, and flowers, containing 126 to 40,011 mg/g of dry matter (Ahmed et al., 2013), and green and black teas, containing 18 to 37 µg/ mL tea infusion (Jeszka-Skowron et al., 2015). Other sources of rutin are apple skin (Hossain et al., 2009), *Sophora japonica* (Paniwnyk et al., 2001), and onion (Chua, 2013). The physicochemical properties of rutin are summarized in Table 2.2.

Quercetin ($C_{15}H_{10}O_7$, MW: 302.24 g/mol)   Rutinose ($C_{12}H_{22}O_{10}$, MW: 326.30 g/mol)

Rutin ($C_{27}H_{30}O_{16}$, MW: 610.52 g/mol)
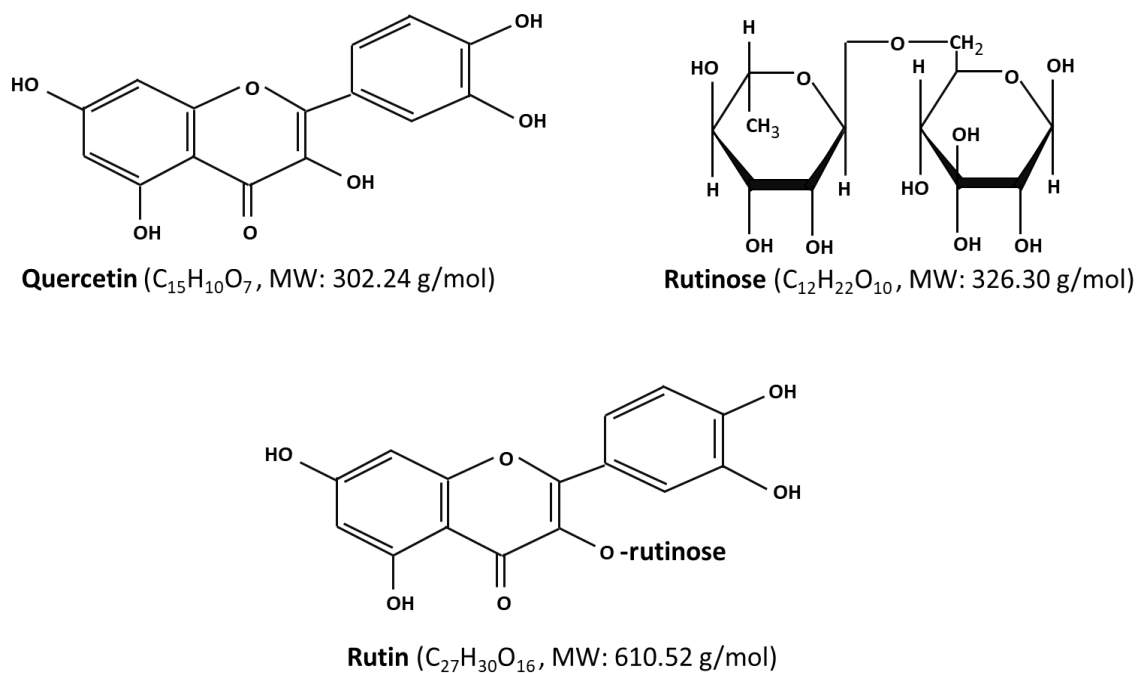
Figure 2.2. Chemical structure of rutin

(Redrawn from 'The Merck Index, 2006').

2.1.2.1. Thermal treatment of rutin

Flavonoids can be modified during thermal processing. The thermal effects on flavonoid glycosides often lead to the hydrolysis of parent compounds to lower molecular weight compounds, free aglycones, and the formation of new compounds (Kim and Lim, 2017; Zhang et al., 2014). Degradation of flavonoid compounds by pyrolysis have also been reported by Kim and Lim (2017) and Sharma et al. (2015).

Table 2.2. Physico-chemical properties of rutin

Empirical formula	$C_{27}H_{30}O_{16}$	
Molecular weight	610.52 g/mol	
Elemental composition	C: 53.12%, H: 4.95%, O: 41.93%	
Appearance and color	Pale yellow needles which darken with exposure to light.[a] Dilute solutions give green color with ferric chloride.[b] Forms deep yellow color in alkaline solution, and with polyvalent metal ions.[c]	
Water of crystallization	Water crystals contain 3 molecules of H_2O, and becomes anhydrous at 110 °C, and 1.3×10^{-3} MPa.[a]	
Melting point	Becomes brown at 125 °C. [a,b] Melts at 188.7 °C. [a] Plastic at 195-197 °C. [a,b] Decomposes with effervescence at 214-215 °C.[b]	
Solubility	Water	0.13 mg/mL[d]
	Boiling water	5 mg/mL [a]
	80% methanol	70% solubility [e]
	Boiling methanol	140 mg/mL [a]
	Alkaline solution, [a] pyridine, [a] DMSO [f]	Soluble
	Chloroform, benzene, ether	Insoluble[b]
Stability	More stable to oxidation than quercetin in the presence of low concentrations of alkali (0.01 M NaOH). [g] In acid solutions (0.1-1 M HCl), it is hydrolyzed to quercetin. Rate of hydrolysis is higher in acidic ethanolic solution than in aqueous solution.[h] Requires light protection. Ultraviolet-B radiation reduced rutin content by 13.6%.[i]	
Complexation with metals	Throrium (Obeys Beer-lambert law at 435 mµ)[j] Iron (III), Copper (II), Cobalt (II), Nickel (II)[k]	

[a]Khalifa et al. (1983), [b]The Merck Index (2006), [c]Chen et al. (2010), [d]Krewson and Naghski (1952), [e]Chua et al. (2017), [f]Sigma Aldrich, [g]Lin et al. (2010), [h]Yang et al. (2019), [i]Savic et al. (2016), [j]Dev and Jain (1962), [k]Escandar and Sala (1991). DMSO - dimethyl sulfoxide, H_2O - water, NaOH - sodium hydroxide, HCl - hydrochloric acid.

The degree of hydrolysis of rutin depends on the processing factors such as temperature and pH. Rutin treated with subcritical water at 171 °C under CO_2 pressure of 11 MPa for 10 min produced maximum yields of rutin hydrolysates as isoquercetin (13.7%) and quercetin (53.3%) along with thermal degradation products such as 2,5-dihydroxyacetophenone and protocatechuic acid (Kim and Lim, 2017). However, in the hydrothermal treatment of rutin at 140 °C for 50 min, quercetin, 3,4-dihydroxybenzoic acid,

catechol, 5-(hydroxymethyl) furfural (degradation from glucose), and 5-methylfurfural (dehydration from rhamnose) were identified as degradation products (Ravber et al., 2016). Thermal treatment can also be applied to rutin while in a complex matrix.

Polyphenols, like rutin, are often incorporated into the starch matrix via gelatinization to enhance the nutritional and physicochemical properties of starch (Zhu et al., 2015). The polyphenol-starch interactions are driven by hydrophobic effects forming amylose-polyphenol inclusion complexes or by glycosidic bonding of amylopectin-polyphenol interactions (Zhu et al., 2015). These interactions have been utilized to produce functional starch-based foods. For example, Takahama and Hirota (2010) reported the formation of amylase-digestion resistant starch (lower glycemic index) caused by interactions between rutin and buckwheat starch. Another rutin-starch interaction, which involved the addition of rutin to rice starch, altered the melting of starch, hindered retrogradation, and modified the flow behavior (increased yield stress, consistency coefficient, and decreased the flow behaviour index modeled by Herschel–Bulkley equation; Zhu and Wang, 2012). Table 2.3 shows interactions between tea polyphenols and different types of starch. The findings from these studies explain the effect of polyphenols on the starch molecular structure, by disruption of the starch crystallites. The polyphenol-starch interactions also apply to rutin-starch interactions, as rutin coexists with tea polyphenols and have the same flavonoid structure. Furthermore, Table 2.4 shows some examples of thermal processing, involving rutin and starch interactions, and their influence on the nutritional and physicochemical properties of starch.

Table 2.3. Interactions between tea polyphenols and starch

Source of polyphenols	Type of starch	Experiment	Analysis	Findings and suggested hypothesis for interaction	Reference
Green and black teas	Wheat (amylose 34%) Corn (amylose 22%) Potato (amylose 22%) Rice (amylose 9%)	Pasting starch with tea extracts (RVA profile: 37 $^{\circ}$C to 95 $^{\circ}$C, and from 95 $^{\circ}$C to 37 $^{\circ}$C)	Enzymatic hydrolysis and Free polyphenols	Green and black teas reduced the hydrolysis kinetics of starch: -By reducing number of binding sites for the enzymes or -By being an enzyme inhibitor or -Was influenced by structural differences in starches. -Interactions between starch and black tea polyphenols occurred during the heating phase -Interactions between starch and green tea polyphenols occurred in the cooling phase	Guzar et al. (2012)
Green tea[a]	Rice amylose content (28.3%,13.7%,1.15%) Maize (amylose 27.6%) Potato (amylose 20.3%)	Thermal analysis (DSC)	Gelatinization Retrogradation	Gelatinization temperature and degree of retrogradation of starch decreased with increasing concentration of green tea polyphenols -Green tea polyphenols disrupted the starch crystallites.	Xiao et al. (2011; 2013)

[a]Green tea total polyphenols of 99.97% : 46.8% (−) epigallocatechin-3-gallate (EGCG), 24% (−) epicatechin- 3-gallate (ECG), 12.8% (−) epigallocatechin (EGC), 8% (−) epicatechin (EC). Tea polyphenols of 97%: 50% EGCG, 20% ECG, 18% EGC, 7% EC. RVA: rapid visco analysis. DSC: Differential Scanning Calorimeter.

Table 2.3. Continued.

Source of polyphenols	Type of starch	Experiment	Assay	Findings and suggested hypothesis for interaction	Reference
Tea[b]	Rice (amylose 21%)	Thermal analysis (DSC)	X-ray diffraction	Typical B-type crystallinity pattern characterized by well defined peak of 16.9°(2θ) disappeared on addition of tea polyphenols. -Tea polyphenols retarded recrystallization behavior of starch	Wu et al. (2009)
Tea[b]	Rice (amylose 21%)	Pasting starch with tea extracts (RVA profile: 50 ºC to 95 ºC, and from 95 ºC to 50 ºC)	H-NMR	NMR-Coupling constant (a measure of interactions between protons) was different for A (blend of rice and tea polyphenol gelatinized together), and B (blend of tea polyphenols and gelatinized rice starch). A had two coupling constants, and B had one coupling constant. -Samples A and B differed in H-H interaction -Size of coupling was inversely proportional to hydrogen bond strength -Sample A interaction strength was suggested as stronger than B.	Wu et al. (2011)
			Quantitative FT-IR	Bandwidth of OH- stretching was broader than in sample B. The C-O-H bending frequency was lower in sample A, than in sample B -Sample A had stronger capability to form hydrogen bonding interactions than sample B.	

Tea total polyphenols of 97%: 50% EGCG, 20% ECG, 18% EGC, 7% EC. RVA: rapid visco analysis. H-NMR: Proton Nuclear Magnetic Resonance. FT-IR: Fourier Transform-Infrared.

Table 2.4. Thermal processing of rutin in starch-based foods

Starch/flour or food type	Composition	Process (Temperature, rate, time)	Result	Reference
Rice starch High amylose 32% Normal rice 22% Waxy rice 1.6%	9 mg starch:1 mg rutin	Gelatinization test 25 -130 ºC/5 min/5 ºC/min	Peak melting temperature T_p *Without rutin:* High amylose 32%, T_p = 76.0 ºC Normal rice 22%, T_p = 67.0 ºC Waxy rice 1.6%, T_p = 67.9 ºC *With rutin:* High amylose 32%, T_p = 75.7 ºC Normal rice 22%, T_p = 66.6 ºC Waxy rice 1.6%, T_p = 66.6 ºC	Zhu and Wang (2012)
High amylose 32% Normal rice 22%		Retrogradation test: Gelatinized samples at 4 ºC for 7 days Rescanned from 25 to 130 ºC	*Without rutin:* High amylose 32%, T_p = 52.6 ºC Normal rice 22%, T_p = 51.5 ºC *With rutin:* High amylose 32%, T_p = 51.9 ºC Normal rice 22%, Not observed	
Bread	90% white wheat flour:10% unhusked buckwheat flour	Baking 250 ºC/30 min	Rutin: 12.12±0.21 µg/g dm Quercetin: 8.75±0.15 µg/g dm	Szawara-Nowak et al. (2014)
	50% wheat flour:50% unhusked buckwheat flour		Rutin: 25.59±0.12 µg/g dm Quercetin: 57.20±0.39 µg/g dm	
	90% white wheat flour:10% white buckwheat groats		Rutin: 12.29±1.00 µg/g dm Quercetin: 2.70±0.05 µg/g dm	
	50% white wheat flour:50% roasted buckwheat groats		Rutin: 71.98±0.64 µg/g dm Quercetin: 9.40±0.18 µg/g dm	

Table 2.4. Continued.

Starch/flour or food type	Composition	Process (Temperature, rate, time)	Result	Reference
Bread	85% white wheat flour:15% unhusked buckwheat flour	Baking 200 ºC/40 min	Rutin: 0.90±0.40 mg/100 g dm Quercetin: 0.04±0.01 mg/100 g dm	Lin et al. (2009)
	85% white wheat flour:15% husked buckwheat flour		Rutin: 1.75±0.21 mg/100 g dm Quercetin: 0.03±0.01 mg/100 g dm	
Noodles	35 g wheat flour + 15 g native buckwheat grains	Dough mixing 3 min, sheeting and cutting	Rutin: 0.27 g/100 g noodle Quercetin: 0.43 g/100 g noodle Dough water absorption: 52.70% Dough stability time: 10.89 min Dough development time: 5.63 min	Yoo et al. (2012)
	35 g wheat flour + 15 g buckwheat grains (steamed with boiling water for 10 min), dried at 25 ºC and ground to flour		Rutin: 0.83 g/100 g Quercetin: very low amounts Dough water absorption: 56.37% Dough stability time: 8.63 min Dough development time: 7.21 min	
	35 g wheat flour + 15 g buckwheat grains (autoclaved at 120 ºC for 10 min) dried at 25 ºC and ground to flour		Rutin: 0.83 g/100 g Quercetin: very low amounts Dough water absorption: 55.90% Dough stability time: 7.25 min Dough development time: 8.64 min	

Table 2.4. Continued.

Starch/flour or food type	Composition	Process (Temperature, rate, time)	Result	Reference
Tartary buckwheat flour	100% buckwheat whole meal flour	-	Raw tartary buckwheat flour: Hydroxyl radical scavenging activity: 93.13±2.58% Superoxide radical scavenging activity: 92.74±2.22% Lipid peroxidation inhibitory activity: 34.28±0.45%	Zhang et al. (2010)
		Roasting 80 ºC/40 min	Hydroxyl radical scavenging activity: 87.90±3.75% Superoxide radical scavenging activity: 77.70±3.22% Lipid peroxidation inhibitory activity: 29.07±0.81%	
		Pressurized steam-heated 0.1 MPa/40 min	Hydroxyl radical scavenging activity: 20.17±5.75% Superoxide radical scavenging activity: 63.33±2.91% Lipid peroxidation inhibitory activity: 23.50±1.08%	
		Microwave processing, 700 W/10 min	Hydroxyl radical scavenging activity: 30.63±0.91% Superoxide radical scavenging activity: 71.47±0.65% Lipid peroxidation inhibitory activity: 23.23±0.42%	

- Not available

Table 2.4. Continued.

Starch/flour or food type	Composition	Process (Temperature, rate, time)	Result	Reference
Pasta	30% tartary buckwheat sprout powder 70% durum wheat semolina	Extrusion 9.1-12.1 MPa, vacuum 9x10^{-3} MPa	Raw material tartary buckwheat powder: Rutin: 24.6±1.2 mg/g Quercetin: 0.8±0.2 mg/g	Merendini et al. (2014)
		Drying 50-58 ^{o}C/4 h	Uncooked pasta: Rutin: 0.8±0.0 mg/g Quercetin: 3.0±1.2 mg/g	
		Cooking and boiling	Cooked pasta: Rutin: 0.6±0.4 mg/g Quercetin: 2.7±0.2 mg/g	

2.1.2.2. Prospects of rutin in functional foods

Rutin-starch interactions via buckwheat products, including breads, flour, groats, and leaves, have often served as rutin-based functional foods (Zhang et al., 2012; Kreft et al., 2006) as shown in Table 2.4. Also, rutin has been incorporated in protein-based products (Table 2.5) for functional modification of soy protein isolate (Chen et al., 2016), and textural modification of cheese spread (Přikryl et al., 2018).

2.2. Barley grain

Barley *Hordeum vulgare* is a cereal grain with high nutritive value. Hulless barley grains have high starch 52-68%, protein 9-15%, and beta-glucan 2.5-7% contents (Gao et al., 2009; Anderson et al., 2001). The differences in composition of barley grain may be related to growth conditions and genotypes (Martínez et al., 2018; You and Izydorcyk, 2002; Bhatty and Rossnagel, 1998), which yield varieties with different amylose contents (Gao et al., 2009; Anderson et al., 2001; Bhatty, 1999). Barley varieties are based on amylose contents and are classified as 'zero' (0% amylose), waxy (0-6% amylose), regular (15-25% amylose), and high amylose (37-42% amylose) barley (Gao et al., 2009). Common food hulless barley varieties in Canada are waxy (CDC Alamo, CDC Ascent, Enduro, CDC Fibar, CDC Rattan, and CDC Marlina), high amylose (CDC Hilose) (Canadian Grain Commission, 2019), and regular amylose (Peregrine) barley (Field Crop Development Centre, Lacombe, Alberta, Canada).

Table 2.5. Rutin used in non-starch foods

Source	Compound	Food product	Functionality	Reference
Buckwheat hull extract	3,4-Dihydroxybenzoic acid, 4-hydroxybenzoic acid, gallic acid, isovanillic acid and *p*-coumaric acid, and flavonoids: isoorientin, quercetin, quercetin 3-D-glucoside, rutin (0.37 mg/g extract), and vitexin	Frozen-stored fried meatballs made from ground pork	Increased lipid stability (antioxidant)	Hęś et al. (2017)
Mulberry polyphenol extract	Cyanidin 3-O-glucoside (C-3-O-G), Cyanidin 3-O-rutinoside (C- 3-O-R), caffeic acid, quercetin, and rutin (2mg extract/g protein)	Lean pork sausage	Rutin compared to other phenolic compounds increased surface hydrophobicity, solubility, emulsifying activity and stability of myofibrillar protein	Cheng et al. (2020)
Rutin commercial powder (≥94% purity)	Rutin (2 mg/mL isolate)	Soy protein isolate	Rutin reduced protein surface hydrophobicity, but increased antioxidant activity	Chen et al. (2016)
Rutin commercial powder (≥94% purity) Quercetin commercial powder (≥94% purity)	Rutin (0.5% rutin to cheese) Quercetin (0.5% rutin to cheese)	Cheese spread	Increased complex modulus (rigidity and gel strength) of cheese	Přikryl et al. (2018)

2.2.1. Barley production

World production of barley decreased over the past decade from 155.3 million metric tonnes in 2008/2009 to 142.37 million metric tonnes in 2017/2018 with Canada being the seventh largest producer, contributing 7.9 million metric tonnes to the world barley production in 2017/2018 (Statista, 2019). In Western Canada (Alberta, Saskatchewan, and Manitoba), in 2019, the barley seeded area for general purpose was 37.3%, for malting 55.1%, and for food uses 2.2% (McMillan et al., 2019).

2.2.2. Barley food uses

In Canada, the proportion of scientific publications on the utilization of barley for food and biofuel uses in the past decade (2009-2019) has increased to 68% compared to 32% between 2001-2008. This data was based on 84 papers (2001-2019) sourced from a collection of 1595 related publications on barley studies, including plant and animal breeding, brewing, and related topic areas. The protein component was the most researched (Figure 2.3), followed by whole kernels and flour (22.8%), beta-glucan (19.3%), starch (14.0%) and barley hull and straw (12.3%). Most of the research interests of the barley components have been on the extra health benefits (functionality) other than the basic purpose of nutrition, for example, the enzymatic hydrolysis of barley glutelin to obtain antioxidant peptides (Xia et al., 2012), the effect of processing on phenolic acids and radical scavenging activities of barley pasta (Paula et al., 2017), the protective effects of beta-glucan on ethanol-induced gastric damage in rats (Chen et al., 2019), and the use of beta-glucan aerogels as a carrier for flax oil (Comin et al., 2012). Barley hull (Sarkar et al., 2014), barley straw (Huerta and Saldaña, 2018), and barley grass (Cao et al., 2017) have also been processed for their phenolic contents. However, the research on barley starch has

less target towards functional ingredients, but more on understanding starch structure. The research interests in barley starch reported for potential food and industrial purposes are summarized in Table 2.6.
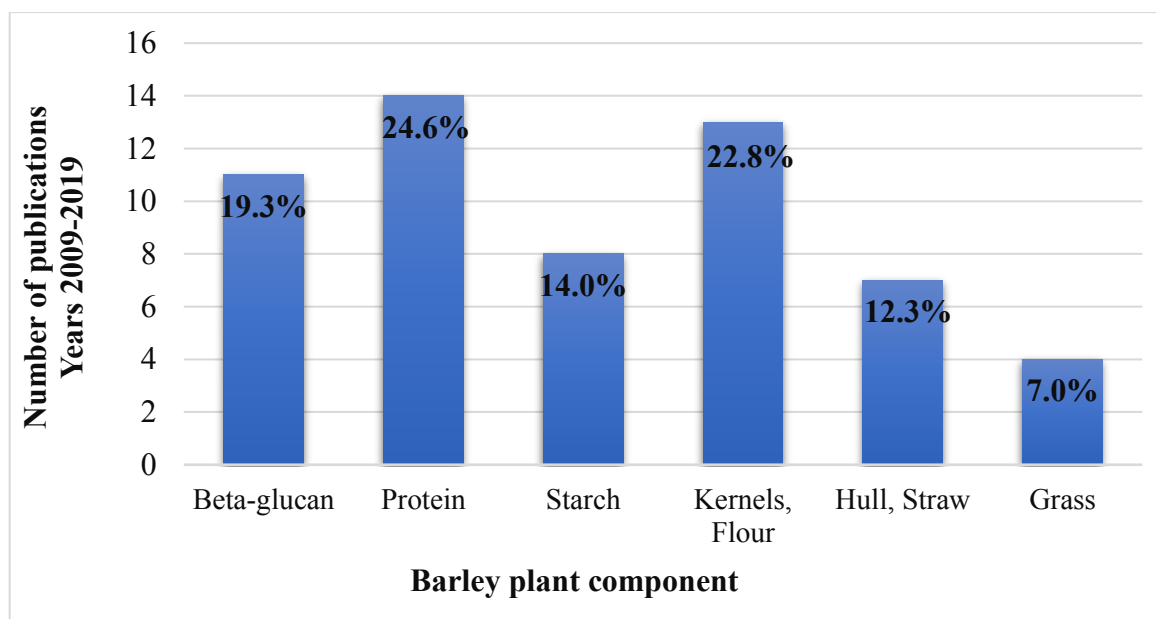
Figure 2.3. Distribution of scientific publications on barley components for food uses in Canada between 2009 and 2019.

(Source: University of Alberta Library/Web of Science Database).

2.2.3. Barley grain fractionation for starch isolation

Barley grain fractionation for the purpose of isolating high purity starch can be carried out through dry or wet processes. The dry fractionation processes may involve a combination of dry milling and sieving, or dry milling and air-classification while the wet fractionation processes utilize aqueous medium for extraction in combination with alkaline, acid, and enzymatic treatments (Vasanthan and Temelli, 2008; You and Izydorczyk, 2002). Enzymes such as lichenase and β-xylanase can enhance the disruption of cell walls and release of starch granules (You and Izydorczyk, 2002).

Table 2.6. Research studies in Canada between 2009 and 2019 on barley starch for food and industrial applications

Modification treatment	Result	Suggested application	Reference
Acetylation Oxidation	Increased hydrophobicity Promotes low retrogradation and viscosity	Biodegradable films	El Halal et al. (2015)
Annealing	Susceptibility towards amylolysis	-	Samarakoon et al. (2020)
Isolation of amylopectin units by α-amylolysis	Interconnection of clusters and random distribution of building blocks	-	Källman et al. (2013)
Amylolysis (α- and glucoamylase)	High degree of hydrolysis of native granules caused by high proportion of short-chains in amylopectin	Production of sugar derivatives and bioethanol	Naguleswaran et al. (2014a)
Dissolution in 90% DMSO/2 M KOH	Molecular characterization with less amylopectin degradation	-	Naguleswaran et al. (2014b)
Annealing	Low gelatinization temperature and increase in melting temperatures after annealing	-	Vamadevan et al. (2013)
Fractionation into large and small granules	Proportion of small granules in high amylose barley was higher than in waxy and normal types	-	Naguleswaran et al. (2013)
Thermal treatment	Retrogradation was promoted by short chains in the amylopectin	-	Källman et al. (2015)

- Not reported. DMSO: Dimethylsulfoxide

The aqueous alkaline extraction method favors the removal of beta-glucan (Maheshwari et al., 2017; Wood et al., 1989) and proteins, based on the selective solubility of individual proteins.

Barley cytoplasmic proteins (albumins and globulins) are soluble in salt solution and alkaline solution, hordeins are soluble in ethanol, while barley glutelins are soluble in alkaline solution (Wang et al., 2010). Other solvents used in the isolation of starch from protein matrix are mercury chloride (to soften the endosperm, Adkins and Greenwood, 1966), and toluene (to remove small starch granules and protein impurities from the interface, McDonald and Stark, 1988; Bathgate and Palmer, 1972). Table 2.7 shows further details on the methods and solvents used in the isolation of barley starch from flour. Isolation processes with multiple steps of sieving and filtration, with the use of solvents produced starch isolates with >88% purity.

2.2.4. Barley starch

2.2.4.1. Morphology, particle size, and X-ray crystallinity

Barley starch, like other cereal starches, is made up of a linear α-D-glucan polymer known as amylose, and a highly branched α-D-glucan polymer known as amylopectin (Figure 2.4). Barley starch granules observed for 2 Tibetan hulless barley starches are semi-crystalline in nature and have typical bimodal size distributions of 10-30 μm of lenticular shaped (large A granules) and 1-5 μm of spherical shaped (small B granules) granules (Yangcheng et al., 2016).

Table 2.7. Barley grain fractionation methods

Barley variety	Starch content (%)	Amylose content (%)	Method	Solvent and enzyme	Starch isolate yield (%)	Starch purity (%)	Reference
CDC Candle	63.46	6.02	Dry milling, filtration, sonication	50 and 95% Ethanol, 0.25% (w/w) SDS	35.69	99.39	Gao et al. (2009)
CDC Freedom	67.91	26.35			33.44	99.25	
SH99250	58.08	41.28			25.60	98.58	
SW 906129	56.60	8.00	Crushed grains, soaking, wet-milling, filtration	3% NaOH (pH 11.5)	30.00	96.00	Anderson et al. (2001)
Golf	63.80	28.00			34.00	96.00	
High-Amylose Glacier	52.10	42.00			25.00	96.00	
CDC Alamo	52.70	0	Soaking coarsely-ground grains, alkaline, acid, and enzymatic treatments	0.02 N HCl, 0.2 N NaOH, 0.5% $NaHSO_3$ (pH 7.0) in 0.1M Tris-HCl, proteinase 15 U/g, lichenase 2 U/g, β-xylanase 8 U/g	55.50	>99.00	You and Izydorczyk (2002)
M-16 (*Hordeum sativum jess*)	-	-	Soaking, draining, blending, sieving	0.02 mol/L (pH 6.5) sodium acetate containing 0.01 mol/L mercury chloride, 0.1 mol/L aqueous NaCl: toluene (7:1)	-	-	Bello-Pérez et al. (2010)
Merlin	54.70	-	Dry milling, alkaline treatment, precipitation, filtration	NaOH solution, 2 N HCl, 50 v/v ethanol	51.40	87.80	Liu and Barrows (2017)

- Not available. SDS - sodium dodecyl sulfate, NaOH – Sodium hydroxide, HCl – Hydrochloric acid, $NaHSO_3$ – sodium bisulfite, NaCl – sodium chloride.

This morphology reported by Yangcheng et al. (2016) was also consistent with various barley starches of different botanical origins, such as CDC Fibar from Canada (Figure 2.5), and cultivars from China.
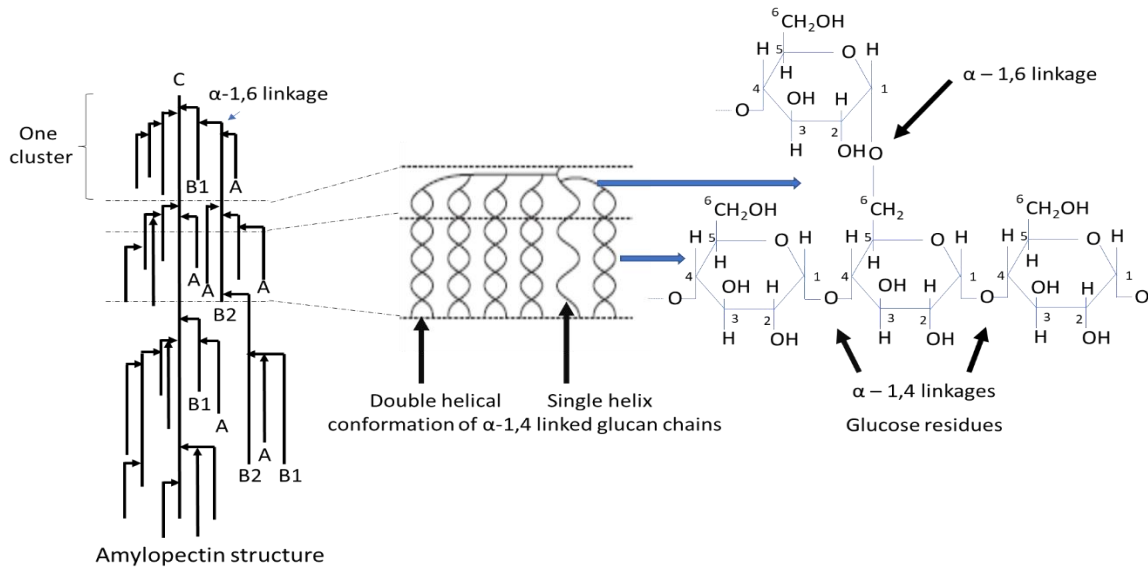
Figure 2.4. Starch structure

(Amylopectin structure redrawn, and double and single helical conformations of glucan chains, adapted from Bergthaller and Hollman, 2007).

Scanning electron micrographs (SEM) of starch granules from 4 hulless barley cultivars grown in different parts of China also showed lenticular, oval or disc-like shaped granules (Kong et al., 2016), with a bimodal size distribution of large granules of 10-25 μm in diameter and small granules of 2-5 μm in diameter (Kong et al., 2016).
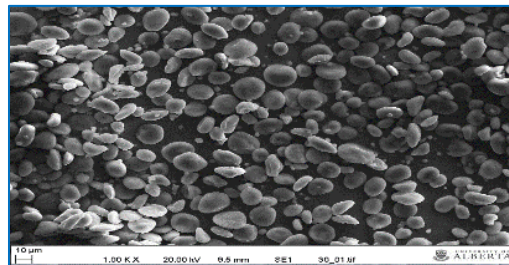
Figure 2.5. Morphology of native barley starch granules

(Scanning electron micrographs SEM image of CDC Fibar barley starch, this thesis, University of Alberta).

In addition to the size, Yangcheng et al. (2016) observed that amylose contents of the 2 Tibetan hulless barley starches were positively correlated (R^2=0.99, p<0.01; and R^2=0.90, p<0.05) to the size of A granules (10-30 μm). This was confirmed by Tang et al. (2002) on barley starch varieties in Japan where the amylose content (29.9%) in large granules of normal starch was higher than amylose content (3.3%) of waxy barley starches. Furthermore, for hulless barley cultivars in Canada, small granule starches were not observed in the waxy starches (amylose 1-6%) but were present in the normal (amylose 24-28%) and high amylose (34-41%) starches (Gao et al., 2009). The starches from hulless barley cultivars grown in Canada, including normal (CDC McGwire), waxy (CDC Candle), and high amylose (SH 99250) had relative crystallinity of 31.5%, 39.1%, and 29.1 %, respectively. All exhibiting A-type X-ray pattern crystallinity (Gao et al., 2009), which are similar to the 2 Tibetan hulless barley starches with strong peaks at 2θ of 15.1°, 16.8°, 17.8°, and 23.0° (Yangcheng et al., 2016), and also for the 7 barley cultivars grown in China with strong peaks at 2θ of 15°, 17°, 18°, 20°, and 23.0° (Li et al., 2014). Some of the barley starch characteristics compared with other starch characteristics for food and industrial applications are outlined in Table 2.8.

2.2.4.2. Gelatinization, Thermal properties, and Retrogradation

Starch gelatinization is a pre-requisite step to starch utilization. Gelatinization is the application of heat to starch in excess water. During gelatinization, starch granules undergo hydration, forming ghost remnants from the external layers, and swell in radial and tangential dimensions (Li et al., 2004). Also involved is the leaching of amylose and amylopectin chains, loss of birefringence and crystallinity, and changes in viscosity (Li et al., 2004).

Table 2.8. Comparison of barley starch characteristics with other starches

Starch type	Treatment	Application/investigation	Advantages of barley starch	Disadvantages of barley starch	Reference
Barley Corn	Succinylation, Octenyl succinylation	Wall material for encapsulation of volatile synthethic flavors: benzaldehyde, dimethyl trisulfide, 2-mercaptopropionic acid and benzothiazole	Succinylated barley and corn starches showed better retention capabilities than octenyl succinylated, native starches, and β-cyclodextrin	-	Jeon et al. (2003)
Barley Corn Potato Rice	Annealing	Mechanism of annealing without amylose	-	-Increased susceptibility towards amylolysis in waxy corn and waxy barley starches -Relative crystallinity of barley, potato, and rice starches did not change, but increased for waxy corn starch from 42.4 to 46.1 %	Samarakoon et al. (2020)
Barley, waxy barley, oat, rye. Waxy maize, rice, waxy rice, sago	Annealing	Effect of internal structure of amylopectin on annealing	Amylopectin from barley, oat, and rye starches have higher number of unpacked double helices.	-	Vamadevan et al. (2013)

   -    Not available

Table 2.8. Continued.

Starch type	Treatment	Application/investigation	Advantages of barley starch	Disadvantages of barley starch	Reference
Barley Corn Wheat Triticale	Isolation of starch molecular polymers: amylose and amylopectin	Molecular characteristics and amylolysis of amylose and amylopectin	The highest average chain length was observed for amylopectin isolated from waxy barley starch	Amylopectin from normal barley, corn, and triticale starches	Naguleswaran et al. (2014a)
			The highest degree of branching, and dispersed-molecular density was observed for amylopectin, and amylose, isolated high-amylose barley starch	Amylose from normal barley and triticale starches showed the highest degree of hydrolysis at 30 °C, after 72 h	
			Amylopectin, and amylose isolates of normal barley and normal AC reed wheat starch had the highest z-average radius of gyration (nm)		
Barley Corn	Dissolution in different solvents (DMSO, and 2M KOH)	Role of molecular characteristic in starch dissolution	-	Higher degradation of amylopectin molecular weight and size of waxy barley starch compared to waxy corn starch	Naguleswaran et al. (2014b)
Barley Corn	Characterization of molecular structure	-	Waxy, normal, and high-amylose barley starches, and waxy and normal corn have A-type X-ray pattern	-	Naguleswaran et al. (2013)

\- Not available

Figure 2.6 illustrates starch granules disintegration during gelatinization. Starch gelatinization usually occurs at 50-80 °C, as observed in thermal studies on barley starches using differential scanning calorimetry (Yangcheng et al., 2016; Ao and Jane, 2007; Tang et al., 2002). Gelatinized starches during cooling and storage undergo a process of retrogradation where starch molecules re-associate into more ordered structures, enhancing crystallinity (Wang et al., 2015). Gelatinized starches after storage at 4 °C for 7 days were re-scanned at a heating rate of 10 °C per min over a temperature range of 25-120 °C. It was observed that these starches had retrograded starch contents of 37-45% (Ao and Jane, 2007). Table 2.9 shows thermal properties of retrograded starches produced from barley starches.
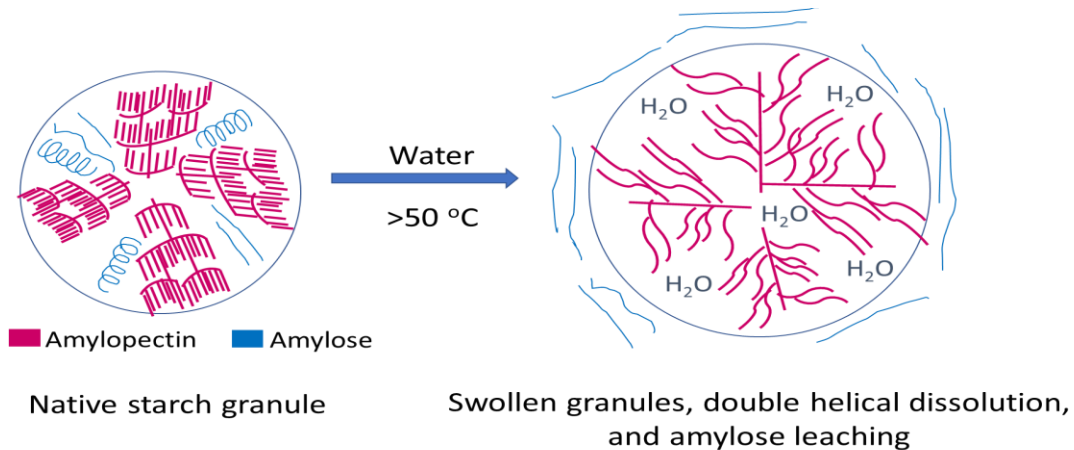
Figure 2.6. Illustration of starch gelatinization showing the effect of heat and water on starch granule swelling and disruption.

Table 2.9. Thermal properties of hulless barley starches

Barley starch amylose content (%)	Gelatinization[a]				Dissociation of retrograded starch					Reference
	T_o (°C)	T_p (°C)	T_c (°C)	ΔH (J/g)	T_o (°C)	T_p (°C)	T_c (°C)	ΔH (J/g)	R%[b]	
24	54.9	nr	64.3	10.6	39.9	nr	59.5	2.6	25.0[c]	Yangcheng et al. (2016)
27.1	57.9	62.6	nr	12.6	43.1	52.8	59.3	5.5	43.7[c]	Ao and Jane (2007)
A-granule 28.1	57.0	61.5	nr	12.2	42.8	52.6	59.7	5.5	45.1[c]	
B-granule 23.0	58.2	66.3	nr	12.7	44.1	53.4	59.3	4.7	37.1[c]	
30.0	53.5	57.3	60.7	9.3	nr	nr	nr	0.6	6.5[c]	Kong et al. (2016)
0.6	52.6	57.8	63.6	9.9	nd	nd	nd	nd	nr[d]	Källman et al. (2015)
					nd	nd	nd	nd	nr[e]	
					46.9	57.8	68.1	0.8	nr[f]	
30.3	50.9	55.0	61.7	10.4	43.5	54.9	64.9	0.8	nr[d]	
					45.2	56.6	68.4	1.9	nr[e]	
					45.5	55.6	65.5	2.4	nr[f]	
47.8	52.7	60.2	71.9	15.4	44.5	56.1	68.6	6.0	nr[d]	
					46.5	56.5	69.3	9.4	nr[e]	
					47.1	56.0	70.4	11.0	nr[f]	

[a]T_o, T_p, and T_c = onset, peak and conclusion temperatures of endotherm, ΔH = enthalpy change. [b]Retrogradation (%) = (ΔH of dissociation of retrograded starch/ ΔH of native starch gelatinization) x 100. [c]Retrogradation after storage at 4 °C for 7 days, [d]Retrogradation after storage at 4 °C for 3 days, [e]Retrogradation after storage at 4 °C for 6 days, [f]Retrogradation after storage at 4 °C for 10 days, nr = not reported, nd = not detectable.

2.2.4.3. Thermal treatment of starch above 80 °C

Waxy barley starch granules heated at 80 °C in the presence of water had lost the granule shape due to full fragmentation of the granules, and further heating to 90 °C enhanced homogeneity of the gelatinized/solubilized starch (Li et al., 2004). At 100 °C, the solubilized starch remnants formed a looser filamentous network compared to prior heating at 80 °C (Li et al., 2004). However, at 100 °C, the normal barley starch gel, which also had fragmented and melted starch remnants formed a coarse honeycomb-like network structure. Similarly, at 100 °C, the high-amylose starch formed a honeycomb-like network structure (Li et al., 2004). These ultrastructural changes in barley starch granules indicated depolymerization of starch chains. In the pressurized hot-water treatment of cassava starch (16.9% amylose), 13 g/270 mL at different temperatures (75, 100, and 150 °C), and fixed static pressure (15.5 MPa), and treatment time (10 min), it was observed that the reducing end yield increased from <12.5 mg glucose equivalent/g starch at 75 °C to 38.6 mg glucose equivalent/g starch at 150 °C, which indicated depolymerization and hydrolysis of starch polymers to lower molecular weight starch molecules (Zhao and Saldaña, 2019a).

Heat-induced hydrolysis of starch with little or no moisture has also been utilized with or without acid to produce dextrins (Bai and Shi, 2016; Orozco-Martínez and Betancur-Ancona, 2004). Pyrodextrinization or roasting of starch leads to depolymerization, transglycosidation, and internal elimination reactions in starches (Bai and Shi, 2016). Waxy maize starch (100 g/150 mL water) with pH 3.0 adjusted using 0.5 M HCl was dried to a moisture content of 10-15% (Bai and Shi, 2016), and treated at 170 °C for 4 h to a final moisture content of 7%. The dextrinized products were soluble in water (100%), and as studied by one dimensional ^{1}H and ^{13}C NMR; the pyrodextrins showed

chemical structures indicative of reducing end-groups, and degree of branching (17.8%, 3 times higher than 5.8% in maltodextrin) (Bai and Shi, 2016). Table 2.10 shows studies on advances in starch modification by pyrodextrinization of different types of starches.

2.3.   Green processing technologies

Innovative techniques have been developed to meet the food processing demands of the 21st century. Some of these techniques are pressurized fluid processing, ultrasonication, pulsed electric field, ohmic heating, cold plasma, supercritical CO_2, high hydrostatic pressure, high-intensity pulsed light, infrared food processing, and membrane separations (Proctor, 2018; Chemat et al., 2017). The choice of a technique for food processing depends on the food matrix, the aim of processing, and the desired product e.g. agricultural biomass treatment with pressurized fluids for the extraction of value-added compounds. In terms of thermal treatment of starch, pressurized fluids (like subcritical water), high hydrostatic pressure, ohmic heating, and superheated steam, have been utilized for starch modification (Zhao and Saldaña, 2019a; Zhu, 2018; Hu et al., 2018; Pei-Ling et al., 2010). Of these four techniques, subcritical water has received less attention for wet starch processing (11 scientific publications versus literature review publications on high hydrostatic pressure of starch (Pei-Ling et al., 2010), and ohmic heating of starch (Zhu, 2018). However, subcritical water is unique in its application for chemical reactions.

2.3.1. Subcritical water technology

Subcritical water (SCW) technology utilizes hot liquid water, at temperature and pressure conditions between 100-374 ^{o}C and 0.3-21 MPa, respectively, for the treatment of biomass to separate cross-linked polymers and to cause subsequent hydrolysis (Brunner, 2014).

Table 2.10. Pyrodextrinization

Source/Type of starch	Material	Treatment parameter	Modification	Reference
Borlotti bean (BB) White kidney bean (WKB) Chickpea (C)	Starch/acid (2.2 M HCl) ratio (80:1 w/v) Reaction for 16 h, at room temperature	Drying 110 ºC, 3 h Grinding and sieving (100 μm)	Increased solubility (%): Native BB: 11.8±1.3 PD BB: 77.7±5.1 Native WKB: 9.9±0.9 PD WKB: 77.2±6.1 Native C: 9.3±0.6 PD C: 81.2±4.6	Güzel and Sayar (2010)
Lima bean (LB) Cowpea bean (CB)	Starch/acid (2.2 M HCl) ratio (80:1 w/v) Reaction for 16 h, at room temperature	Drying 100 ºC, 3 h Grinding and sieving (175 μm)	Available starch (%, dm): Native LB: 97.7±0.9 PD LB: 40.8±0.1 Native CB: 94.8±1.9 PD CB: 59.2±2.6	Campechano-Carrera et al. (2007)
	Starch/acid (2.2 M HCl) ratio (40:1 w/v) Reaction for 16 h, at room temperature	Drying 140 ºC, 1 h Grinding and sieving (175 μm)	Available starch (%, dm): PD LB: 71.7±0.4 PD CB: 80.2±0.3	
Corn starch	Starch (10 g dm, MC 2%) Concentration of glacial acetic acid in starch (2.5%)	Incubation at 140 ºC–180 ºC, 3 h, 100 rpm	Digestible starch content (%, dm) Native: 99.0±0.6 At 140 ºC: 73.4±0.4 At 150 ºC: 72.7±1.2 At 160 ºC: 69.2±0.8 At 170 ºC: 52.6±1.5 At 180 ºC: 47.8±0.9	Lin et al. (2018)
Lima bean	Starch/acid (2.2 M HCl) ratio (160:1 w/v) Reaction for 16 h, at room temperature	Convection oven 90 ºC, 1-3 h	Indigestible starch content (%, dm) Native: 5.5 At 1 h: 49.5 At 3 h: 47.6	Orozco-Martínez and Betancur-Ancona (2004)

PD – pyrodextrin. Solubility (%) = M_2/M_0 x 100, where M_0 is initial dry weight of starch. M_2 is constant weight of recovered solids from drying supernatant at 130 ºC. Supernatant was from gelatinization of M_0 at M_0 (0.6 g in 30 mL water) heated at 85 ºC for 30 min.

This type of treatment utilizes the properties of water in the subcritical region (Figure 2.7), which makes it act as an acid and a base, improving its effectiveness as a catalyst and a bond-breaking agent (Brunner, 2014; Jin et al., 2006). This is possible because water at high temperatures and pressures (maintained in the liquid state) has more hydronium and hydroxide ions thereby increasing its ionizing tendency and lowering the dielectric constant and polarity of the subcritical water compared to water at ambient conditions (Liang and Fan, 2013).
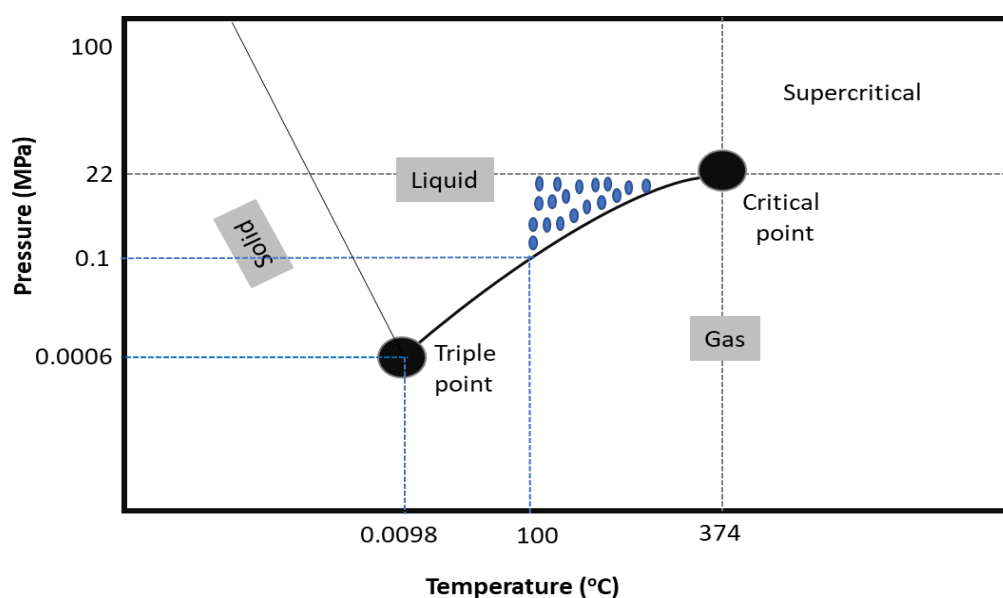
Figure 2.7. Phase diagram of water: Dotted area is the subcritical water region.

Table 2.11 shows a comparison of the properties between normal water and subcritical water. Jin et al. (2006) reported that SCW can act as a 0.02 mol/L of H_2SO_4 or NaOH at condition of 300 °C at a saturation temperature where its ionizing strength is at maximum. SCW is also referred to as liquid hot water, pressurized hot water, near-critical water, superheated water or pressurized water (Saldaña et al., 2012).

Table 2.11. Comparison of properties of solvents

Property	Water[a]	Subcritical water[b]	Methanol[a]
Temperature, °C	25	350	25
Dielectric constant	78.30	30.00 at 250°C[c] 14.87 at 350 °C[b]	32.70
Acid dissociation constant, pKa	13.99[b]	11.55[b], 11.42[d]	-
Density, kg/m^3	997.10	625.45	790.00
Surface tension, mN/m	71.98	3.70 at 17 MPa[e]	22.43 at 23.82 °C[f]
Viscosity, cP	0.89	0.073	0.54
Dipole moment, Debye	1.85	1.85[e]	1.70

Values are at 25 °C for water and methanol unless otherwise stated. [a]Covington and Dickinson (1973), [b]Brunner (2014), [c]Doctor and Yang (2018), [d]Fisher and Barnes (1972), [e]Plaza and Turner (2015), [f]Součková et al. (2008). – not available.

The advantages of using SCW either as a solvent or reaction medium compared to the use of other ionic liquids or organic solvents in treatments, extractions or chromatography processes have been repetitively proven by many researchers (Doctor and Yang, 2018; Sarkar et al., 2014; Liang and Fan, 2013; Cheng et al., 2009). Generally, water is environmentally friendly and cheap, and the recovery of valuable bioproducts using a SCW treatment is an attractive and economical way to disintegrate and fractionate lignocellulosic materials (Pińkowska et al., 2013). Since there is no need for a washing/neutralization step in the SCW process, SCW reduces process time but the large volumes of water necessary for a large-scale application can be energy demanding (Agbor et al., 2011). However, the excess of water used in SCW process can prevent condensation reactions (Alvarez et al., 2014).

In addition, Sarkar et al. (2014) reported higher recovery of total carbohydrates (192.7 mg of glucose equivalent/g) from barley hull with SCW (150 °C, 15 MPa, 15 min) compared to 16.1 mg of glucose equivalent/g of solid-liquid extraction using aqueous

ethanol (70 °C). Also, Singh and Saldaña (2011) extracted higher yields of phenolics (81.83 mg/100g) using SCW (180 °C, 6 MPa and 2 mL/min) compared to methanol extraction (46.36 mg/100 g) or ethanol extraction (29.52 mg/100 g) at 65 °C and at atmospheric pressure. But a concern with this process is the formation of degradation products, which can be minimized by maintaining the SCW pH between 4 and 7, for example, in the catalytic degradation of sugars (Hendriks and Zeeman, 2009), or by carefully determining the extreme conditions and hydrolysis rates at which the degradation products are produced (examples of degradation products from hemicellulose hydrolysis are acetic acid, 5-hydroxymethylfurfural, and furfural). Degradation products can vary for different lignocellulosic materials due to their differences in chemical composition, cell wall composition and structure, and existing linkages (Prado et al., 2014).

2.3.2. Ultrasonication

Ultrasonication is a process of transmitting sound energy in the range of 20 kHz to 2 MHz via a liquid phase for the purpose of creating the physical phenomenon called cavitation (Chatel and Colmenares, 2017). During cavitation, vapor-filled cavities or bubbles are formed due to pressure differences in the liquid system (Soria and Villamiel, 2010). Based on the rectified diffusion phenomenon of expansion and compression cycles (Figure 2.8), the bubbles grow and implosively collapse, causing local mechanical, physical or chemical effects on the molecules and particles of the liquid medium (Chatel and Colmenares, 2017; Soria and Villamiel, 2010). The degree of these acoustic cavitation effects is influenced by factors such as the power intensity (W/cm^2), frequency, medium viscosity, surface tension, vapour pressure, temperature and time of treatment, and type and concentration of dissolved gas (Bermudez-Aguirre, 2017; Soria and Villamiel, 2010).
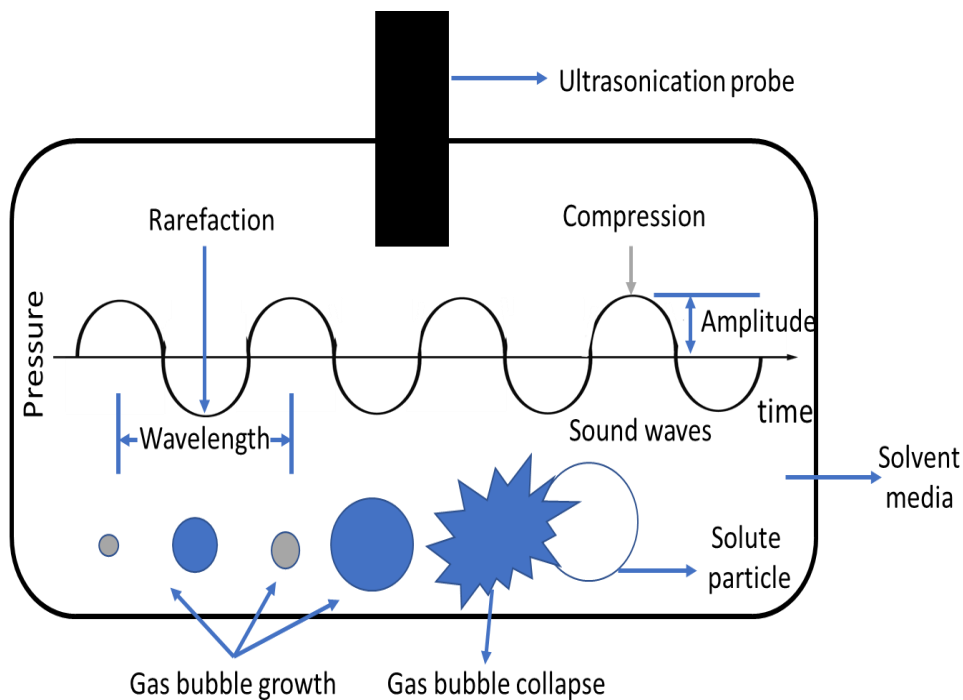
Figure 2.8. Cavitation phenomenon during ultrasonication showing the formation, and growth of gas bubbles in successive cycles of rarefaction and compression, and the gas bubble collapse on solute particle.

Low ultrasonic frequency (20-90 kHz) was applied in the extraction of rutin from the dried flower buds of *Sophora japonica* (Liao et al., 2015). Other parameters utilized were solvent (aqueous ethanol 50-80%), solvent-to-solid ratio (5-50 mL/g), ultrasound power (100-300 W), particle size (0.841-0.420, 0.420-0.250, 0.250-0.177, 0.177-0.149 mm), temperature (15-40 °C) and an extraction time of 15 min. The maximum extraction yield of rutin was 182.25±13.38 mg/g obtained in the range of 60-62 kHz using ethanol (70%) to solid ratio of 25 mL/g with 150 W, particle size of 0.420-0.250 mm and at 20 °C (Liao et al., 2015). These results proved that the extent of cavitation shear forces on the flower cells and tissue matrix were influenced by the ultrasonic parameters. Also, the advantage of ultrasonication over conventional Soxhlet extraction method was observed in

the lower extraction yield of rutin (153.93 ± 9.41 mg/g) obtained after 60 h Soxhlet extraction at 90 °C (Liao et al., 2015).

Paniwnyk et al. (2001) reported ultrasonic extraction yields of rutin from dried flower buds of *Sophora japonica* in methanol (20 kHz, 27 W, and room temperature) and compared with the yields from the conventional (reflux) method in methanol (room temperature). They observed that ultrasonic extraction method resulted in higher rutin yield (1.18 and 1.20 g) compared to the reflux method (0.80 and 1.12 g) at 20 and 30 min, respectively. However, at 60 min of extraction, the yield (1.1 g) was the same for both extraction methods, possibly due to the degradation of rutin after 30 min (Paniwnyk et al., 2001).

2.3.3. Electrolysis and electrical conductivity of starch

In electrolysis (Figure 2.9), electrical energy supplies electrons through a metal or other material (electrode) into a liquid (electrolyte), where the liquid cationic molecules are reduced at the negative electrode (cathode), and the liquid anionic molecules lose electrons and are oxidized at the positive electrode (anode). Thus, electrolysis is a process that creates non-spontaneous chemical reactions for the formation of new products (Petrucci et al., 2007). Electrolysis of water is the simplest form of electrolysis. At the cathode, the transfer of electrons breaks the bond between oxygen and hydrogen, causing water molecules to decompose to hydrogen and hydroxide ions. Two of such hydrogen ions gain electrons and link to form hydrogen gas (Shultz, 2007). With the shortage of electrons, and an attraction of anions to the positive electrode, the hydroxide ions lose electrons, and two oxygen atoms join to form oxygen gas, which is liberated at the anode (Shultz, 2007). Equations shown in Figure 2.9 describe the redox reactions for water electrolysis.
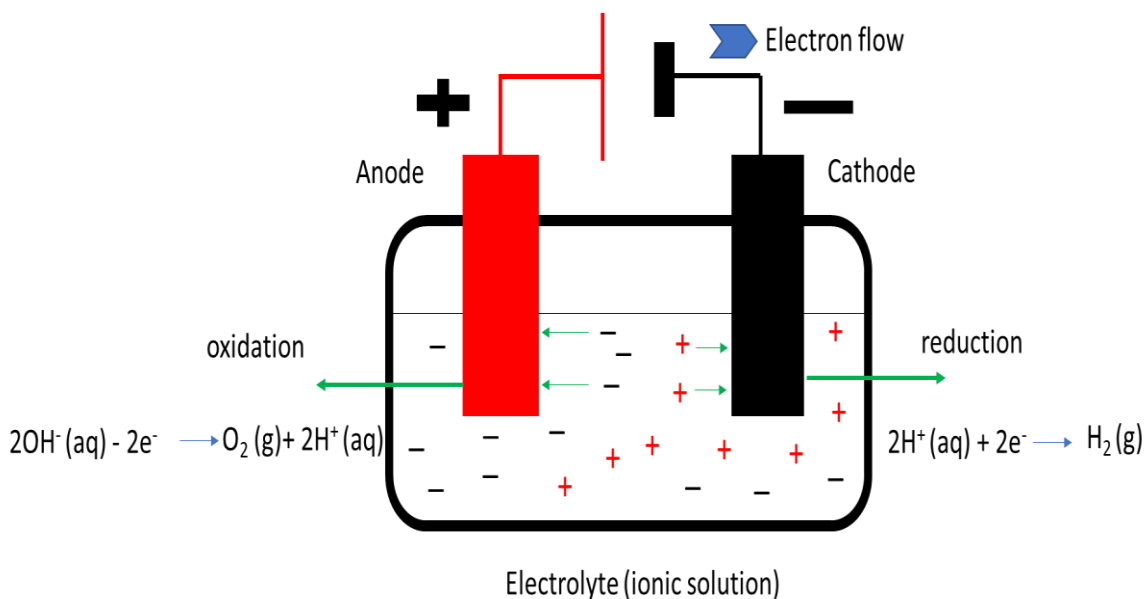
Figure 2.9. An electrolysis cell: Cations are reduced at the negative electrode while anions are oxidized at the positive electrode

In a mixed ionic aqueous solution, where other metal ions are present, the competition for preferential discharge of ions for reduction or oxidation reactions at the cathode or anode, respectively, is governed by three factors: 1) the relative position of ions in the electrochemical series, 2) the concentration of ions in the electrolyte, and 3) the nature of electrode (Ababio, 1990). For example, in an aqueous solution of sodium chloride (NaCl) with higher concentrations of sodium ions (Na^+) and chlorine ions (Cl^-), H^+ and OH^- are preferentially discharged because of lower electropositivity, and lower electronegativity, respectively (Ababio, 1990). However, if a mercury cathode is used, which has affinity for Na^+, the preferential ion at the cathode would be Na^+ because the discharge of Na^+ requires less energy, but H^+ would be discharged at a platinum (inert) electrode (Ababio, 1990). The minimum electrode potential required to drive the electrolysis of aqueous sodium chloride with inert electrodes is -2.06 V (Petrucci et al., 2007).

Sodium chloride aqueous solution was utilized in the electrolysis of sweet potato starch (10 g starch: 1 g NaCl: 100 mL water, using platinum anode at 90 V for 30 min, and at room temperature) (Xijun et al., 2012). This treatment was followed by heating of the starch solution (pH 6) at 95 $^{\circ}$C for 20 min, and further autoclaving at 120 $^{\circ}$C for 30 min. Results showed that the presence of sodium chloride produced 33.1% retrograded (resistant) starch compared to 13.9% yield of retrograded starch from the control electrolysis of starch without NaCl addition (Xijun et al., 2012). The effect of the whole process was attributed to leaching of starch granules during electrolysis, uniform distribution of lamellae during gelatinization, and contribution of NaCl to crystal nucleation (Xijun et al., 2012). Application of electrolysis in sodium chloride media was also reported for rice starch oxidation (Shaarwy et al., 2009).

The electrical conductivity of starch (sweet potato, wheat, maize, potato) and flour (Japanese rice, waxy rice) suspensions (50 g/kg) was studied during the gelatinization process at 20-95 $^{\circ}$C, measured with a conductivity probe at a frequency of 200 kHz (Chaiwanichsiri et al., 2001). Electrical conductivity of potato starch increased gradually and linearly from 3.0 x 10^{-5} S/cm at 20 $^{\circ}$C to 5.5 x 10^{-5} S/cm at 62 $^{\circ}$C, but a rapid linear increase was observed from 5.5 x 10^{-5} S/cm at 62 $^{\circ}$C to 14.0 x 10^{-5} S/cm at 72 $^{\circ}$C (Chaiwanichsiri et al., 2001). The increase in electrical conductivity upon gelatinization was related to the increase in ions from starch granules, and this behavior was similar for all the other starches and flours studied (Chaiwanichsiri et al., 2001).

Electrical conductivity of heated corn starch-water mixtures (10:90-70:30 w/w) was also investigated as a function of temperature at a heating rate of 5 $^{\circ}$C /min, using an external resistive heating system coupled with monitoring device for electrical conductivity

in real time (Morales-Sanchez et al., 2007). The monitored stage temperatures were 25-41 ºC, 41-64 ºC, 64-78 ºC, 78-92 ºC, and the observations are summarized in Table 2.12 (Morales-Sanchez et al., 2009).

Table 2.12. Electrical conductivity of gelatinized starches

Temperature range (ºC)	Electrical conductivity (EC)	Possible reason
25-41	Increasing rate of EC	Starch hydration
41-64	Lower rate than stage 25-41 ºC	Related to starch granule swelling
64-78	EC dependent on water content. Water content >50 % increased EC but decreased when water content was <50%	Related to starch gelatinization
78-92	Steady increase in EC	Total solubilization in water

Adapted from Morales-Sanchez et al. (2009).

2.4.   Final Remarks

Functional food ingredients are the leading specialty food ingredients in the market, but the application of rutin in functional foods has been limited to buckwheat products. To make rutin more available to consumers within the wide spectrum of food preferences, the incorporation of rutin in starch ingredients is a feasible option. Starch-based ingredient is an economically viable option, because most processed foods already contain modified starch ingredients. In addition, starch is abundant, cheap, and renewable.

The technologies outlined in previous sections (subcritical water, ultrasonication, and electrolysis), and the method of starch pyrodextrinization have advantages and disadvantages in processing. These technologies can be applied creatively, to incorporate rutin into barley starch for functional food ingredients.

Even though buckwheat starch has similar characteristics to cereal starches, currently its production is low (<50 kilo tonnes) in Canada, but the increasing production of barley grain (>7 Million Tonnes) makes barley starch available for industrial production. Barley starch characteristics compete favorably with A-type crystallinity starches from cereals such as wheat, and corn. The objective of blending rutin and barley starch in a product, can promote the accessibility of rutin, and the development of the barley industrial sector. Also, the application of green emerging technologies for rutin-barley starch processing keeps the promise of a green environment.

Chapter 3. Barley starch behavior in the presence of rutin under subcritical water conditions[1]

3.1.   Introduction

Starch is composed of two α-D-glucan polymer molecules, amylose and amylopectin. Amylose is majorly a linear chain of α-1,4-linkage units, with about 0.1% branches of α-1,6-linkage units. Amylose structure is characterized by a left-handed helix made up of six anhydroglucose units per turn of the helix (Jane, 2009). Amylopectin, the predominant glucan molecule of most starches has a highly branched structure. Like amylose, amylopectin also contains α-1,4-linked glucose units but with more branches, about 4-6% of α-1,6-linkage units (Bergthaller and Hollman, 2007). Amylopectin is larger than amylose, with its molecular weight in the range of $200\text{-}700\text{x}10^6$ Da while the molecular weight of amylose is around $0.15\text{–}0.4\text{x}10^6$ Da (Bergthaller and Hollman, 2007). Based on their differences in molecular structures, they can form different types of complexes with certain compounds. For example, the helix coil of amylose has a hydrophobic cavity due to the presence of hydrogen atoms, and therefore forms a clathrate type of complex with phenolic compounds as the guest molecules (Zhu, 2015a). Also, complexation through hydrophobic interactions may occur with linear fragments of amylopectin (Barros et al., 2012).

Studies on starches from various origins with varying amylose contents and their interactions with phenolics have been reported by Chai et al. (2013), Barros et al. (2012), and Zhu et al. (2008). These starch-phenolic interactions were initiated at starch gelatinization temperatures above 50 °C. Starch gelatinization is important as an initial step

---

[1] A version of this chapter has been published as Ekaette, I., and Saldaña, M.D.A. (2020). Barley starch behavior in the presence of rutin under subcritical water conditions. Food Hydrocolloids, 100, 105421.

for starch interaction with other compounds because during heat treatment in excess water, starch granules swell, lose structural integrity and compounds can penetrate the starch granules (Kasemwong and Itthisoponkul, 2013). Particularly, temperatures above 100 ºC were required to unwind the double helices of amylose to single helices thereby creating a central channel for inclusion complexation to occur (Conde-Petit et al., 2006).

Subcritical water is water at elevated temperatures in the range of 100-374 ºC, which is maintained in liquid state under pressure up to 22 MPa. Water at these conditions has unique physical and chemical properties due to the reduction of hydrogen bonds, which leads to a decrease in polarity, viscosity and surface tension. Subcritical water also has increased ionic products H^+ and OH^- compared to ambient water, and thereby acts as an acid or base catalyst (Saldaña and Valdivieso, 2015). Subcritical water has been used for the hydrolysis of rutin into its respective aglycones, including isoquercetin, quercetin, and degradation compounds 3,4, dihydrobenzoic acid, and catechol (Kim and Lim, 2017; Ravber et al., 2016).

Rutin (quercetin-3-O-rutinoside) is a flavonoid glycoside found in plants such as tartary buckwheat (Kim et al., 2016), and apple skin (Hossain et al., 2009). The chemical composition of rutin consists of the flavonol quercetin and a disaccharide rutinose (α-L-rhamnopyranosyl-(1−6)-β-D-glucopyranose), conferring rutin with pharmacological activities such as antioxidant, anticancer, and anti-inflammatory (Gullón et al., 2017). Rutin also known by other names as rutoside, birutan, eldrin or vitamin P, is a tasteless yellow crystalline powder with a melting point of 196 ºC (Gullón et al., 2017).

Most rutin delivery systems for rutin require rutin complexation with biopolymers to enhance its solubility and oral bioavailability for example, by complexation with β-

cyclodextrin (Miyake et al., 2000). With respect to subcritical water, Chen et al. (2016) reported that subcritical water (120 ºC, 30 min) induced structural changes in soybean protein isolate and further enhanced rutin binding capacity due to the exposed hydrophobic sites of the soybean protein isolate from the treatment. Flour-rutin interactions, during the extraction of buckwheat flour at 100 ºC, yielded amylase-resistant flour after heat treatment, producing bread of lower glycemic indices (Takahama and Hirota, 2010). Rice starch (1.6 to 32% amylose) and rutin mixtures were studied for their rheological and thermal properties *in situ* at 25 ºC–95 ºC, and 25 ºC–130 ºC, respectively (Zhu and Wang, 2012). However, these studies did not elucidate behaviors of starches of varying amylose contents with rutin above 130 ºC. To the best of my knowledge, starch-rutin interactions have not been studied under subcritical water conditions. It was hypothesized that rutin will interact with the molecular components of barley starch, amylose and amylopectin.

Barley *Hordeum vulgare* is the seventh important grain in the world, and Canada produces approximately 7.7 Million Tonnes (Mcallister and Meale, 2015) but less than 2% of barley in Canada is used for food purposes (Statistics Canada, 2018). Therefore, barley grain was selected as the starch source in this study to promote the utilization of barley in food applications. The objectives of this study were to: 1) determine if barley starch-rutin complexation occurs under subcritical water conditions, and 2) compare barley starch behavior with and without rutin under the same subcritical water conditions.

3.2 Materials and Methods

3.2.1. Materials

Three cultivars of hulless barley grains CDC Hilose (37% amylose), Peregrine (22% amylose) and CDC Rattan (0% amylose) were obtained from the Field Crop Development

Centre at Alberta Agriculture and Forestry (Lacombe, AB, Canada) and Crop Development Centre at University of Saskatchewan (Saskatoon, SK, Canada). Rutin hydrate (purity ≥94%) was purchased from Sigma Aldrich (Oakville, ON, Canada). All other chemicals such as dimethyl sulfoxide (Fisher Scientific, Ottawa, ON, Canada), iodine ACS solid reagent ≥99.8% (Sigma Aldrich, Oakville, ON, Canada), and potassium iodide (BioUltra, ≥99.5% (AT) Sigma Aldrich, Oakville, ON, Canada), were of analytical grade and solvents were of high-performance liquid chromatography (HPLC) grade.

3.2.2. Methods

3.2.2.1. Starch isolation

Hulless barley grains were milled into flour, shorts, and bran fractions using a roller mill (Buhler Automatic Laboratory mill MLU-202, Uzwil, Switzerland). The flour fractions (17-29% of whole grains) were collected, mixed and stored at room temperature (23 °C) until needed for starch isolation. Each flour cultivar (300 g) was mixed briefly with deionized water (1.5 L) in the ratio 1:5 w/w, and centrifuged at 1593 g for 10 min. The supernatant was discarded and the brown bran at the bottom of the residue removed. This centrifugal washing stage was repeated with 20% less amount (1.2 L) of initial deionized water. The final residue was mixed with 50% less amount (0.6 L) of initial deionized water, and sodium carbonate was used to adjust the pH of the mixture to 10.4 for enhanced removal of beta-glucan (Maheshwari et al., 2017; Wood et al., 1989). The alkali-treated residue mixture was stirred for 5 min at room temperature (23 °C) until the aggregation and a color change of protein was observed. The mixture was further centrifuged at 1593 g, for 10 min, and the top dark brown protein layer was removed carefully to isolate the white starch residue fraction. The centrifugation and protein removal steps were carried out twice.

The total extraction time was >2 h. The white starch isolate was dispersed with ~20 mL volume of 95% ethanol and dried at 40 °C for 12 h. The dried starch isolates were milled using a Rsetch ZM 200 laboratory mill (Retsch Inc. Newton, PA, USA) equipped with a 0.5 mm sieve, and stored in air-tight containers at room temperature (23 °C).

3.2.2.2. Chemical composition of starch isolates

Dried starch isolates were analyzed for total amylose content according to the method of Hoover and Ratnayake (2002). Briefly, barley starch (2 g) was defatted by boiling the native starch in 75% (v/v) propan-2-ol/H_2O for 7 h. The resulting defatted barley starch (20 mg) was dissolved in 8 mL of 90% dimethylsulfoxide and shaken vigorously, then left on a shaker at 150 rpm for 12 h to fully solubilize the starch. The mixture was diluted to 25 mL in a volumetric flask. An aliquot of diluted solution (1 mL) was mixed with 40 mL deionized water and 5 mL iodine/potassium iodide solution (0.0025M I_2 and 0.0065M KI), and the final volume adjusted to 50 mL. After 15 min at room temperature (23 °C), sample absorbance was read at 600 nm. These absorbances were translated to percent amylose content from the calibration curve in the concentration range of 0-100% amylose contents using pure potato amylose and pure amylopectin mixtures. The final amylose contents were calculated based on dry matter (dm) of defatted starch.

Moisture contents of starch isolates were determined at 130 °C for 1 h according to the AACC Method 44-15A (AACC, 1995). Starch purity was determined according to the total starch procedure (Megazyme International Ireland Limited, Wicklow, Ireland). Protein analysis of starch isolates was carried out using Flash 2000, Organic Elemental (CHN-O) analyzer (Thermo Fisher Scientific, Mississauga, ON, Canada). Total ash was determined

by first carbonizing starch samples on a hot plate and thereafter incinerating at 525 °C for 2 h according to the AACC Method 08-17 (AACC, 1995).

3.2.2.3. Preparation of rutin solution

The suspension of rutin hydrate powder (66.7 mg) in deionized water (400 g) was stirred briefly for 1 min and filtered using Whatman filter paper (No. 1) into a glass amber bottle. The supernatant was used as the rutin solution. To determine the concentration of rutin in the solution, two methods were used: UV spectrophotometric method, and HPLC method. This solution was prepared fresh for every experimental condition. In the UV spectrophotometric method, a calibration curve was prepared for rutin hydrate in 90% dimethyl sulfoxide (DMSO) using serial dilutions of $0.92–18.40 \times 10^{-3}$ mg rutin/mL. From a freshly prepared rutin supernatant, 5 mL was diluted to 10 mL using 90% DMSO, absorbances of serial dilutions and rutin supernatant in DMSO were measured using quartz cuvettes at 358 nm (Savic et al., 2016). Determination of rutin concentration was carried out in triplicates. The calculated concentration of rutin in the supernatant was 1.96 ± 0.00 mg/100 mL.

In the HPLC method, the rutin supernatant was further filtered through a Basix 0.2 μm nylon syringe filter into amber glass vials and injected into the HPLC system. A Shimadzu LC 20 Prominence 20 (Agilent Technologies, Santa Clara, CA, USA) system consisting of an autosampler, a column oven and a diode array detector was utilized. Separation of rutin from quercetin was carried out on a Zorbax SB-C18 column (Agilent Technologies, Santa Clara, CA, USA) of 250 mm x 3.0 mm i.d., 5 μm particle size, set at a temperature of 30 °C in a column oven. The mobile phases used were 0.5% formic acid in water (elution A) and 0.5% formic acid in methanol (elution B) at a flow rate of 1 mL/min

using gradients: 0 min, 8% B; 5 min, 10% B; 20 min, 75% B; 21 min, 100% B; 23 min, 100% B; 24 min, 8% B; and 26 min, 8% B. The quantifications of rutin and quercetin in the rutin supernatant and standard solutions were performed at a detection wavelength of 268 nm. Calibration curves of standard solutions were obtained for rutin (0.013-0.645 mg/mL), and quercetin (0.001-0.510 mg/mL). Determination of rutin and quercetin concentrations was carried out in duplicates. The calculated concentration of rutin in the supernatant was 1.50±0.00 mg/100 mL, while quercetin was 0.74±0.00 mg/100 mL.

3.2.2.4. Subcritical water experiments

The subcritical water experimental unit earlier utilized and described by Zhao and Saldaña (2019) is shown in Figure 3.1. Barley starch (9 g) was mixed with 270 mL rutin solution (4.9 mg) and poured into a stainless-steel reactor (270 mL). The helical stirrer was inserted into the reactor, while closing the reactor. This caused an overflow loss of 0.3 g starch /20 mL starch-rutin suspension. The starch-rutin suspension in the reactor was stirred for 2 min. The stirring continued for 1 min during which purging was carried out by pumping fresh rutin solution using the HPLC pump, into the reactor to eliminate air bubbles. Stirring was stopped, and only purging was continued for another 2 min. After purging, the safety valve was closed, and the suspension was heated to the desired temperature. The final starch-suspension concentration was 8.70 g barley starch in 250 mL rutin solution (3.36% w/w). Temperature levels studied were 80, 100, 120, 140, and 160 °C. At each set temperature, a constant pressure of 7 MPa was applied to the starch-rutin sample (pressure was achieved using the HPLC pump). Static time to reach the set temperature varied for 80, 100, 120, 140, and 160 °C as 10, 15, 17, 20, and 23 min, respectively. The experimental run time after reaching the set temperature and pressure was

constant at 30 min. At the end of each run, the reactor was cooled down with ambient water to 45 °C. Mixing was stopped, and the system depressurized. The final starch-rutin solution was poured into 1.2 L of ethanol to precipitate the starch and remove the free flavonoid compounds. Starch precipitate was recovered by vacuum filtration using a Büchner funnel. Starch precipitate was washed off the filter paper with deionized water and then freeze-dried. The weights of final subcritical water (SCW) treated starch samples were recorded. This procedure was the same for SCW treatment of starch without rutin at the same experimental conditions. All experiments were carried out at least in duplicates.
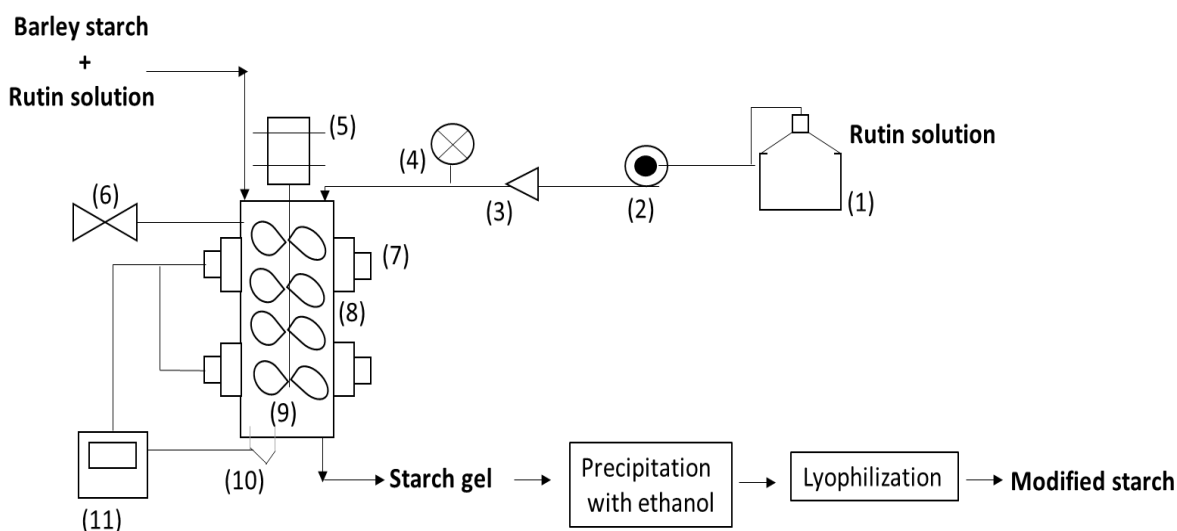
Figure 3.1. Subcritical water system

(1) Solvent reservoir, (2) HPLC pump, (3) One-way valve, (4) Pressure gauge, (5) Motor stirrer controlled by the control panel, (6) Safety valve, (7) Band heaters, (8) Reactor, (9) Stirrer, (10) Thermocouple, and (11) Temperature controller.

3.2.2.5. Preparation of starch powders

Freeze-dried starches with and without rutin were milled using a Retsch ZM 200 laboratory mill (Retsch Inc. Newton, PA, USA) equipped with a 0.5 mm sieve. The powders were stored at room temperature in air-tight containers covered with aluminium foil.

3.2.2.6. Characterization of barley starch powders

3.2.2.6.1. Total rutin content

Starch-rutin powder (20 mg) was vortexed for 5 min with 3 mL of 90% DMSO in 10 mL test tubes covered with aluminium foil and left on a shaker at 150 rpm for 12 h. Rutin hydrate (2 mg) was weighed into 10 mL of 90% DMSO and ten serial dilutions were performed at concentrations of 0.4-20.0 µg/mL. A calibration curve was prepared by reading absorbances of the dilutions in quartz cuvettes against 90% DMSO as blank, at a wavelength of 358 nm using a UV spectrophotometer (Savic et al., 2016). The calibration curve was used to determine the total rutin content in the starch-rutin powders. The results were calculated based on mg rutin/g starch-rutin powder.

3.2.2.6.2. Apparent amylose content

The apparent amylose contents of 37% amylose and 22% amylose starch powders were carried out according to the modified method of Hoover and Ratnayake (2002) described in Section 3.2.2.2, without the defatting step.

3.2.2.6.3. Fourier Transform Infrared (FT-IR) spectroscopy

A Nicolet iS50 FT-IR spectrometer (Thermofisher Scientific, Madison, WI, USA) fitted with an ATR cell and Omnic software was used to obtain FT-IR spectra of starch powders. Each starch powder sample was subjected to 32 scans at 4 cm^{-1} resolution in the wavenumber range of 4000–400 cm^{-1}.

3.2.2.6.4. Expansion

Expansion or specific volume of starch powders was determined according to the method of bulk density determination described by Nyombaire et al. (2011), with slight modifications. Starch powder was weighed into 2.0 mL MCT graduated centrifuge tube

(Fisher Scientific, Ottawa, ON, Canada) and gently tapped on a flat surface until a constant volume at 0.5 mL was obtained. The mass of the sample in 0.5 mL was recorded. Expansion of starch powder was calculated at a constant volume of 0.5 mL divided by the corresponding mass (g). The pictorial diagram for the starch powders was carried out by weighing 0.5 g starch into culture tubes (16x125 mm), without the tapping step.

3.2.2.6.5. Viscoelasticity

Dynamic oscillatory test was performed on starch powders using a rheometer (Discovery HR-1, TA Instruments, Mississauga, ON, Canada). Rehydrated starch gels (25% w/w solids) were prepared by mixing starch powders with deionized water in appropriate amounts, then allowed to stand for 10 min to enhance equilibration. The solid percent (25% w/w) was chosen to accommodate the highly viscous starch gel of the 0% amylose starch. The equilibrated starch gels were then placed between 25 mm parallel plate Sandblasted, Peltier plate steel with a gap of 2000 μm. Linear viscoelastic region (LVR) was identified by running amplitude sweeps at constant frequency (1 Hz) from strain 0.1 to 15% at 25 °C, at 5 points per decade. Frequency sweeps were then run at a constant strain (2%) at frequency of 0.1 to 25 Hz, constant temperature of 25 °C, at 5 points per decade. Storage (elastic) modulus (G'), loss (viscous) modulus (G''), and loss tangent (tan δ = G''/G') were obtained for each test.

3.2.2.6.6. Color analysis

Hunter Lab colorimeter (CR-400/CR-410, Konica Minolta, Ramsey, NJ, USA) was used for color determination of starch powders using D65 illuminant, opening of 14 mm, and 10° standard observer, according to the ASTM D2244 method. A white reference plate was used to calibrate the colorimeter (L* = 93.49, a* = −0.25, b* = −0.09). Lightness,

chroma and hue were measured for the samples and the total color difference (ΔE), yellowness index (YI) and whiteness index (WI) were calculated according to Boun and Huxsoll (1991):

$$\Delta E = \sqrt{(L^* - L)^2 + (a^* - a)^2 + (b^* - b)^2} \qquad (3.1)$$

$$YI = 142.86 \; b/L \qquad (3.2)$$

$$WI = 100 - [(100 - L)^2 + a^2 + b^2]^{0.5} \qquad (3.3)$$

where, L*, a* and b* are the color values of the standard white plate, and L, a and b are the color values of the starch powders, where L scale represents light versus dark, a scale represents red versus green, b scale represents yellow versus blue.

3.2.3. Statistical analysis

Statistical analyses were performed using R Studio software (Version 0.99.903, R studio, Inc., Boston, MA, USA). Characterizations of the SCW starch powders were carried out in triplicates for colorimetric analyses and duplicates for other methods. One-way Analysis of Variance (ANOVA) was carried out for temperature and amylose content as independent factors for the SCW treated starches with and without rutin. The means were compared for significant differences at $p < 0.05$ by Tukey's test.

3.3.   Results and Discussion

3.3.1. Chemical composition of barley starch isolates

The barley starch isolates used for the subcritical water experiments had 96% starch (Table 3.1). The other components (protein and ash) were below 1%. The high amylose (37%) starch has higher protein and ash compared to the normal (22%), and waxy (zero) amylose starch.

Table 3.1. Chemical composition of native barley starch isolates

Cultivar	Total starch (% dm)	Protein (% dm)	Ash (% dm)	Amylose (% dm)
CDC Hilose	95.53±1.18[a]	0.377±0.004[a]	0.452±0.051[a]	37.220±0.026[a]
Peregrine	95.94±0.99[a]	0.222±0.002[b]	0.275±0.003[b]	22.260±0.017[b]
CDC Rattan	96.57±0.49[a]	0.244±0.036[b]	0.227±0.008[b]	nd

Data shown as mean±standard deviation ($n = 3$). [a-b]Data with same letters within each column are not significantly different.   nd: not detectable.

3.3.2. Total rutin content

Total rutin content (Figure 3.2) decreased with an increase in temperature from 140 °C to 160 °C for all starches of varying amylose contents. The starch cultivars used were CDC Hilose (37 % amylose), Peregrine (22% amylose), and CDC Rattan (0% amylose). This trend was expected as rutin is degraded at temperatures >120 °C to its respective aglycones isoquercetin, and quercetin, and other degradation products, including 3,4 dihydrobenzoic acid and catechol (Kim and Lim, 2017, Ravber et al., 2016) thereby making rutin less available for complexation reactions at these temperatures.
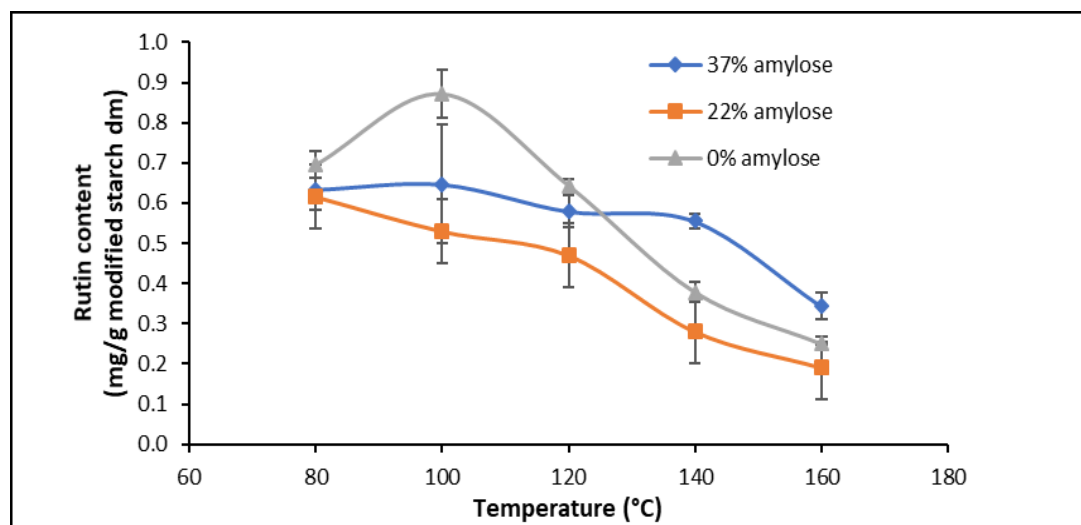
Figure 3.2. Effect of subcritical water temperature on total rutin content of barley starches with different amylose contents at 7 MPa and 30 min.

The degradation of rutin is further supported by a study on heat treatment of buckwheat groats at 160 °C, 30 min, and 0.588 MPa, in which rutin content decreased from

198.1±3.3 μg/g raw groats (dm) to 34.1±0.9 μg/g roasted groats (dm) (Zieliński et al., 2009). Ravber et al. (2016) also reported that rutin in SCW was converted to quercetin at temperatures of 120 °C-220 °C, treated for 2 h.

The highest rutin content in Figure 3.2 was 0.87±0.06 mg/g modified starch (dm) in the 0% amylose content starch at 100 °C. Based on the starting rutin content of 4.90 mg (1.96 mg/100 mL x 250 mL) before SCW treatment, the highest amount of rutin complexed was ~6.13 mg based on the total recovered mass, and purity (total starch content) of the freeze-dried modified starch. The freeze-dried 0% amylose starch at 100 °C weighed 7.38±0.18 g (dry matter), and its total starch content was 95.47±3.29% (Table A.2., Appendix A). Since 6.13 mg is higher than the starting rutin content, the increased yellow colour intensity may be due to presence of quercetin hydrolysed from rutin or the deprotonation of rutin in SCW media (Berlim et al., 2018). The total starch contents of all freeze-dried modified starches ranged from 87% to 98% as reported in Appendix A, Table A.2.

The behavior of rutin content in Figure 3.2 suggests that amylose content of starch, besides temperature, plays an important role in starch-rutin complexation. Generally, heated starch dispersions are characterized by swollen starch granules and leached amylose molecules (Bergthaller and Hollmann, 2007; Doublier and Nantes, 1981). However, if leaching is incomplete, remaining amylose is found between amylopectin molecules inside the collapsed starch granules (Bergthaller and Hollmann, 2007; Doublier and Nantes, 1981). Although leached amylose from the granules recrystallizes upon cooling (retrogradation), it is possible that rutin complexation occurred within the starch granule with unleached amylose molecules. At 140 °C and 160 °C, 37% amylose had higher rutin

contents of 0.55±0.02 and 0.34±0.03 mg/g modified starch, respectively, compared to rutin content of 0% amylose and 22% amylose at the same temperatures. The starch behaviors at these temperatures may be related to its amorphous versus crystalline regions to be discussed further under the FT-IR analysis results.

The highest rutin content at 100 °C was obtained as a sharp rise from rutin content at 80 °C (0.69±0.03 mg/g modified starch), and thereafter decreased to 0.64±0.02 mg/g modified starch at 120 °C. This result may be related to the unwinding of starch double helices, which occurs at temperatures above 100 °C necessary to keep the helix central cavity free for ligand binding as reported for amylose-flavour complexation (Conde-Petit et al., 2006). Studies on amylose helix central cavity for complexation were confirmed by Raman spectroscopy (Carlson et al., 1979) and X-ray diffraction (Takeo et al., 1973; Hinkel and Zobel, 1968). The amylopectin molecular structure is generally accepted as a cluster model of straight short chains interconnected by longer B-chains (Bertoft et al., 1993) and within the crystalline lamellae of the molecule, each straight chain carries a double helical conformation of α, 1-4 linked glucans, similar to the amylose double helical structure (Ball et al., 1998). It is therefore hypothesized in this study that at 100 °C, the highest rutin content is due to enough unwinding of double helices in amylopectin molecules of 0% amylose starch granules coupled with relatively higher availability of rutin at 100 °C compared to temperatures above 100 °C. Furthermore, amylose helix polymorphs may have contributed to rutin content complexation. Studies have shown that amylose helices can take different polymorphs, such as the native double-helical A-form and the single-stranded V_h, depending on the temperature of complex formation (Immel and Lichtenthaler, 2000; Kowblansky, 1985). Based on these findings, starch may have interacted with rutin via

different binding or complexation mechanisms (Barros et al., 2012). Other components present in the starch isolates may also have competed with starch for complexation with rutin, such as protein (Chen et al., 2016), beta-glucan, ash (e.g. iron metal) (Chirug et al., 2018), and lipids. However, in this study, complexation of these compounds was not determined due to minor amounts of protein and ash (Table 3.1).

3.3.3. Apparent amylose content

The apparent amylose contents of 37% and 22% SCW modified starches were determined to estimate how much amylose was non-complexed, and to evaluate the possible types of complexation between starch and rutin based on non-complexed amylose. The loss of amylose (difference in amylose content) between the starches treated with rutin and without rutin (Figure 3.3) was observed at 100 °C for 37% amylose starch with rutin as 7.16% loss. Other losses at 80 °C and 120 °C were 1.16% and 1.82%, respectively. These losses could be attributed to amylose involved in inclusion complexation with rutin.
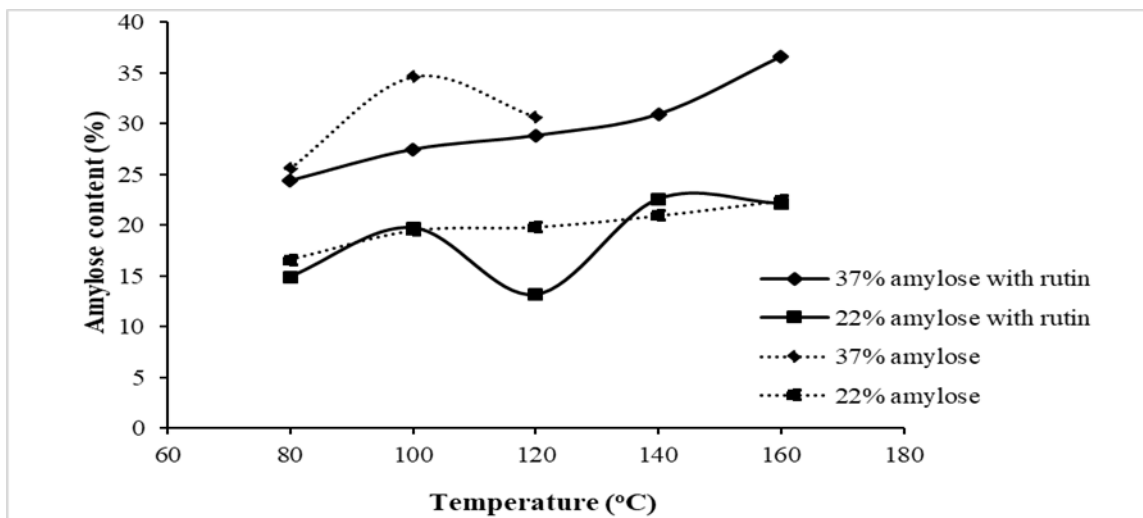
Figure 3.3. Effect of subcritical water temperature and presence of rutin on apparent amylose contents of barley starches with varying amylose contents at 7 MPa and 30 min.

Amylose-phenolic compounds complexation is possible via hydrophobic interactions, which is the driving force for the formation of clathrate compounds, where phenolics are guest molecules inside the cavity of the left-handed amylose single helix coil (Zhu, 2015a). This type of interaction forms V-amylose inclusion complexes that was reported for the formation of starch-phenolic inclusion complexes prepared via co-precipitation method, involving the acidification (H_3PO_4) of alkali starch solution (potato and maize amylose in KOH) to produce amylose-genistein complexes (Cohen et al., 2008). The co-precipitation method did not work for the formation of maize starch V-amylose-ferulic acid complexation as reported by Karunaratne and Zhu (2016). They mentioned the possibility of limited capacity of helix cavity size (Obiro et al., 2012) to accommodate the ferulic acid molecule; poor hydrophobicity of ferulic acid, and/or poor solubility of ferulic acid in water (Karunaratne and Zhu, 2016). Furthermore, for enhanced V-amylose inclusion complexes with ferulic acid, its hydrophobicity needed to be improved. Steam jet cooking at 140 ºC and a flow rate of 1 L/min was utilized to complex a lipophilic ferulic acid ester, octadecyl ferulate with high amylose corn starch (Kenar et al., 2016). Another example was reported when aliphatic chain was grafted onto chlorogenic acid to produce 4-*O*-palmitoyl chlorogenic acid-amylose complexes at 90 ºC (Lorentz et al., 2012). However, in this study, rutin was complexed with amylose directly in SCW.

Interestingly, Figure 3.3 shows that amylose content was decreasing in the 37% amylose starches (rutin) with decreasing temperatures from 140 ºC to 80 ºC. There was no amylose loss at 160 ºC (36.59±0.02%). The decreasing amount of amylose from higher to lower temperatures may be related to the modified structure of amylose at increasing temperatures. The effect of SCW on amylose retention requires further investigation. The

61

same trend was observed for 37% amylose without rutin at 80 $^{\circ}$C and 120 $^{\circ}$C with amylose contents of 25.59±0.00%, and 30.68±0.00%, respectively. Freeze-dried modified starches weighed from 7.06±0.05 g to 7.97±0.03 g (dm), which also proved the loss of starch after SCW treatment (recovered freeze-dried weights for individual samples are not shown). It is possible that amylose-rutin complexation may have taken several helical conformations: hexagonal or orthorhombic, or both (Takeo et al., 1973), either in the crystalline (V-hydrate) or amorphous state (Whittam et al., 1989; Hinkle and Zobel, 1968). The crystalline state also known as the V-hydrate form, is similarly formed by the driving forces behind amylose-iodine inclusion complex, which are van der Waals forces, hydrogen bonding and hydrophobic effect (Whittam et al., 1989). Further studies may be required to understand if the molecular dimensions of rutin influence the helix conformation/packing diameter or state of the amylose complexes (Takeo et al., 1973).

Amylose contents for 22% amylose were low at 80-120 $^{\circ}$C but there was retention (no losses) of amylose at 140 $^{\circ}$C and 160 $^{\circ}$C (22.560±0.003% and 22.120±0.002%, respectively) for 22% amylose with rutin, and 22.420±0.001% at 160 $^{\circ}$C for 22% amylose without rutin. This behavior was similar to 37% amylose. Therefore, it is possible that at these temperatures (where there was no amylose loss), amylopectin was the major complexing molecule with rutin. Other studies also suggest amylopectin-phenolic interactions like starch with a cyanidine catechin pigment - vignacyanidin (Takahama et al., 2013); and amylopectin interactions with C6 aroma compounds (hexanal; hexanol; t-2-hexenal; 2-hexanone) by Jouquand et al. (2006). In this study, rutin interaction with amylopectin could also be the reason for the amylose retention at 100 $^{\circ}$C, for 22% amylose with rutin 19.750±0.008%, and without rutin 19.460±0.004%. Amylose losses between

22% amylose with rutin and without rutin at 80 ºC and 120 ºC were 1.69% and 6.67%, respectively, due to possible formation of amylose-rutin inclusion complexes. Experiments were not completed for 37% amylose without rutin at 140 ºC and 160 ºC due to overpressure in the reactor possibly caused by excessive expansion of starch gels. This was not the case with 37% amylose with rutin at the same temperatures of 140 ºC and 160 ºC.

3.3.4. Fourier Transform Infrared (FT-IR) spectroscopy

The FT-IR spectra are provided in Figure 3.4. Band at 994 cm^{-1} is sensitive to water and represents intramolecular hydrogen bonding of the hydroxyl group at C6. The ratios of intensities of bands at 1047 cm^{-1} to 1022 cm^{-1} indicate the amount of crystalline (ordered starch) to amorphous starch (van Soest et al., 1995). Lower ratios were correlated with the loss of crystalline order (Dupuis et al., 2017; El Halal et al., 2015).

In this study, the bands were observed at 994-997 cm^{-1}, 1015-1017 cm^{-1}, and a distinct shoulder at 1077 cm^{-1}. Calculated intensity ratios 1077/1017 cm^{-1} for the SCW starch powders ranged between 0.489-0.548. It was also observed that certain starches had both bands at 994-997 cm^{-1} and 1017 cm^{-1}, while other modified starches had bands either at 994-997 cm^{-1} or 1017 cm^{-1}. All the modified starches had bands at 1077 cm^{-1}. In Figure 3.4A,B, comparing the intensities of bands at 994-997 cm^{-1} between starches with rutin and without rutin: for 37% amylose starch, at 80 ºC and 100 ºC, the higher intensities of starches with rutin showed increased hydrogen bonding due to possible starch-rutin complexation. Increased hydrogen bonding and/or CH-OH functional group stretching, was also observed for 22% amylose at 120 ºC, and 140 ºC (Figure 3.4C,D), and for 0% amylose at 80-160 ºC (Figure 3.4A-E).
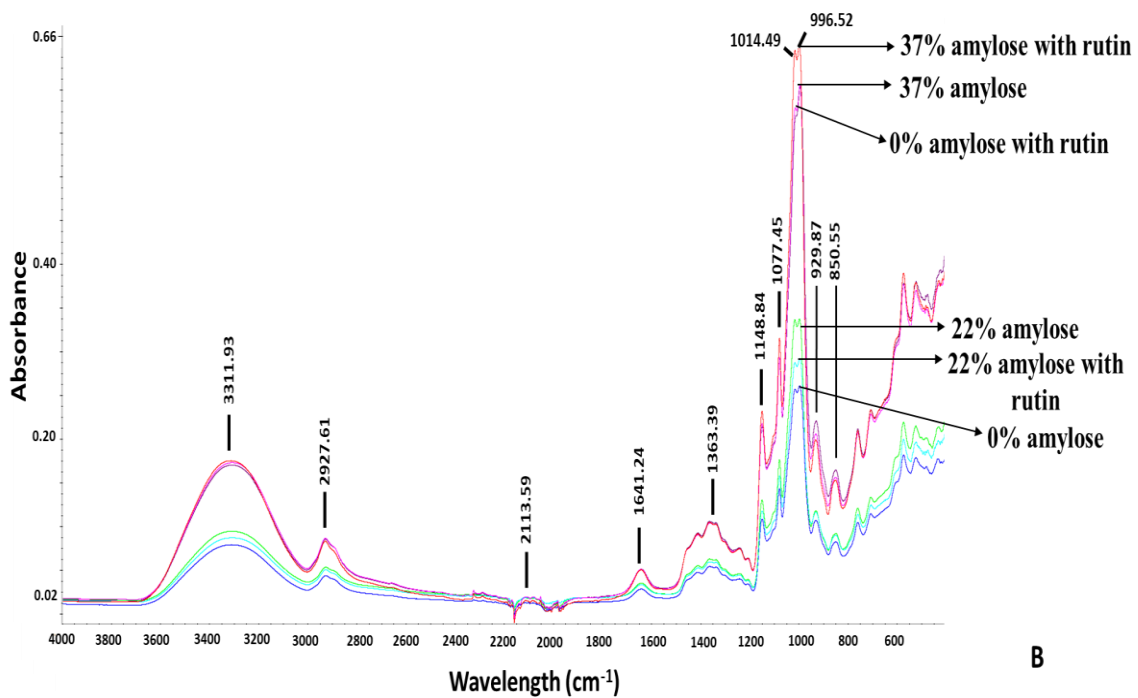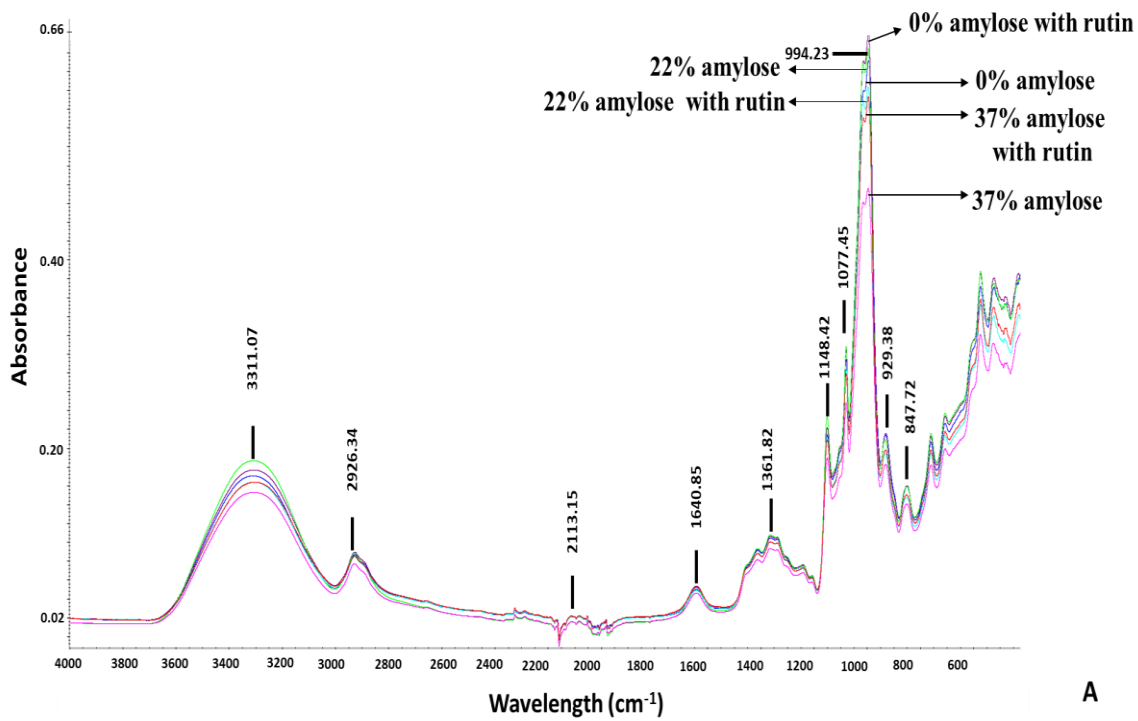
Figure 3.4. FT-IR spectra of subcritical water treated barley starches with and without rutin at 80 °C (A), 100 °C (B), at 7 MPa and 30 min, showing hydrogen bonding interactions at 994-997 cm^{-1}.
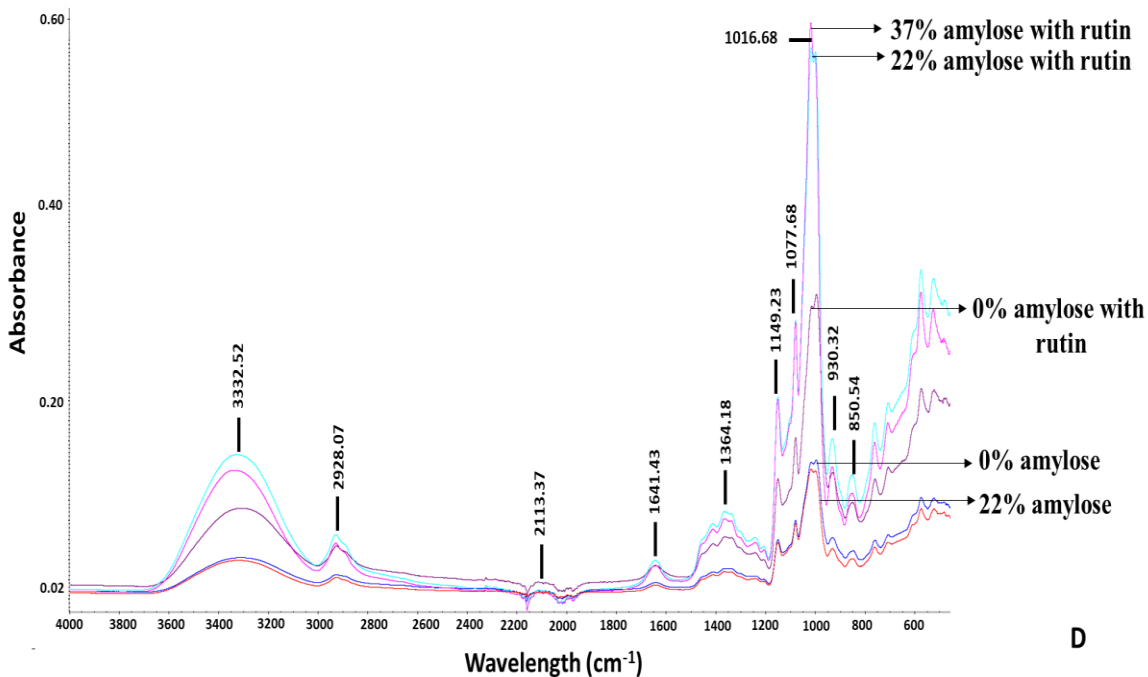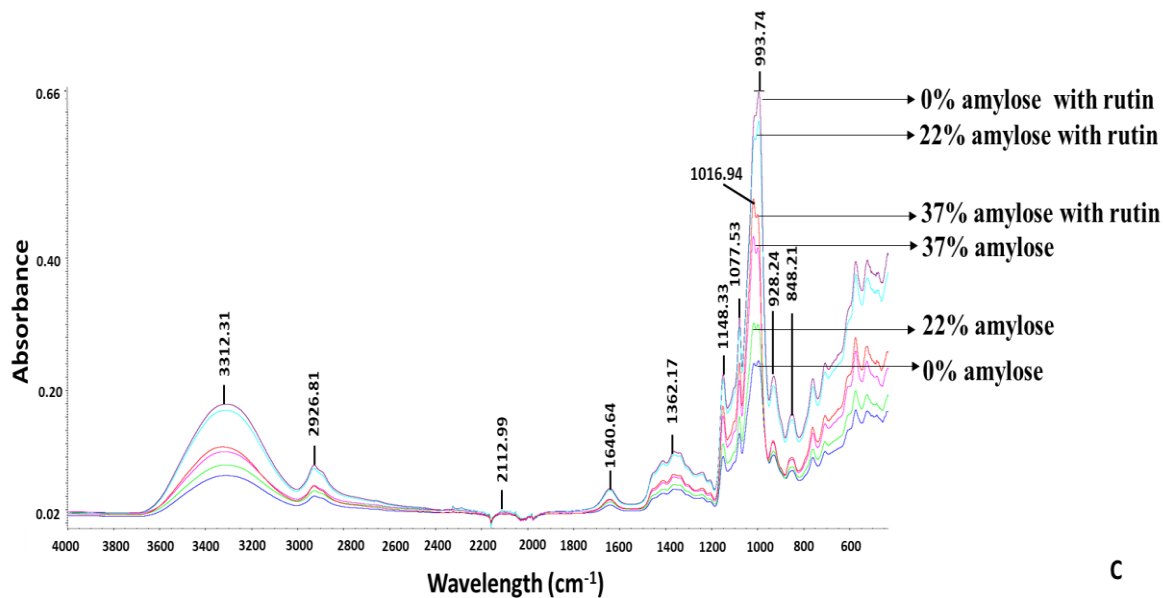
Figure 3.4. FT-IR spectra of subcritical water treated barley starches with and without rutin at 120 ºC (C), 140 ºC (D), at 7 MPa and 30 min, showing hydrogen bonding interactions at 994-997 cm⁻¹.
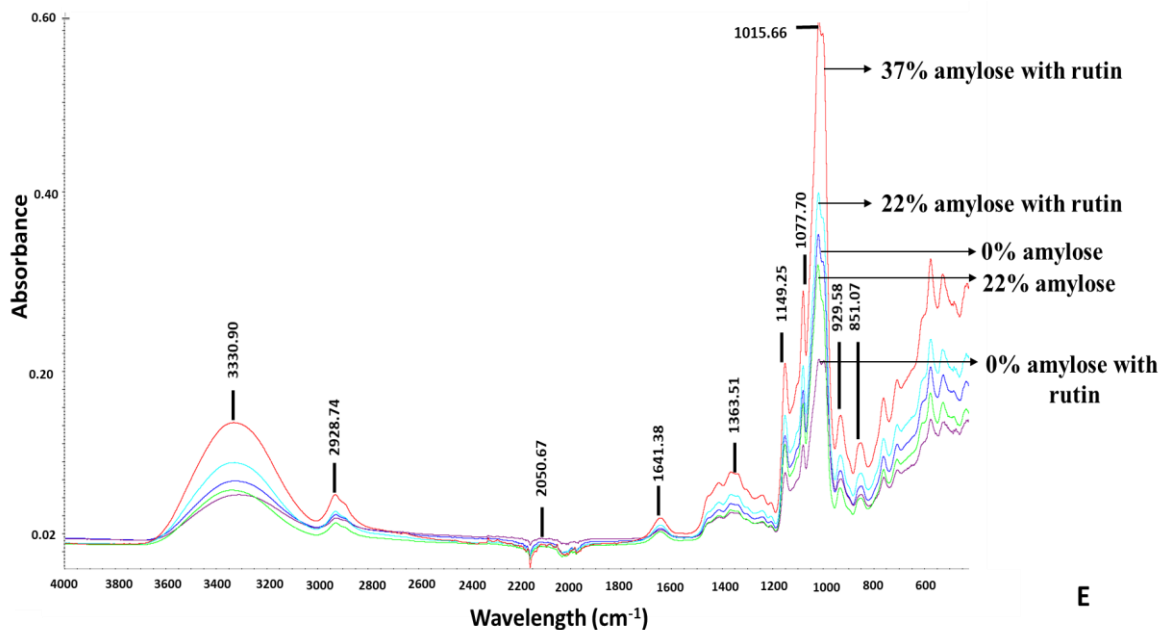
Figure 3.4. FT-IR spectra of subcritical water treated barley starches with and without rutin at 160 °C (E), at 7 MPa and 30 min showing hydrogen bonding interactions at 994-997cm^{-1}.

The inclusion complexation speculated for 37% amylose at 100 °C, and 22% amylose at 120 °C (Figure 3.3) may be supported by the presence of a band at 994-997 cm^{-1}, indicating complexation reaction. There were no bands at 994-997 cm^{-1} for 37% amylose with rutin at 120-160 °C, therefore the possibility of starch-rutin complexation at these temperatures may have been controlled by amylose-amylose or amylose-amylopectin interactions. There are other FT-IR studies that supported amylose-polyphenol complexation. Chai et al. (2013) hypothesized that tea polyphenols disrupted self-assembly of amylose molecules, which led to less double helices and loss of crystalline order of maize starch. Also, Komulainen et al. (2013) suggested decreased hydrogen bonding between hydroxyl groups of oxidized starch and Fe (III) with increasing pH values.

There were no bands at 994/997 cm^{-1} for 22% amylose and 0% amylose starches without rutin at 140 °C and 160 °C; and 160 °C, respectively, but at 140 °C this band was

66

present for 22% amylose starch with rutin, and at 160 °C for 0% amylose starch with rutin, attributed to hydrogen bonding (starch-rutin complexation).

The lack of a band at 1017 cm⁻¹ might mean that 37% amylose starches at 80 °C, and at 100 °C (without rutin) had higher crystallinities compared to 37% amylose starches at 100 °C (with rutin), and 120 to 160 °C. Other starches with no band at 1017 cm⁻¹ were 22% amylose with rutin (120 °C), and 0% amylose (80 °C, and 100-140 °C) without rutin. This lack of band might indicate high crystalline order of these starches. With respect to the effect of rutin on crystallinity, the 1077/1017 cm⁻¹ ratio for rutin complexed starches at 80 °C (0.497) and 140 °C (0.504) were lower compared to ratios of 22% amylose starch without rutin at 80 °C (0.506) and 140 °C (0.582). Dupuis et al. (2017) attributed a decrease in the ratio 1045/1015 cm⁻¹ from the spectra of amylose-vanillic acid inclusion complexation to degraded short range order (loss of crystalline order) caused by increased alkaline conditions. However, for the same 22% amylose starch, 1077/1017 cm⁻¹ ratio increased with rutin at 100, 120, and 160 °C.

Rutin content related behavior discussed in Figure 3.2 may be similar to the trend of intensities at band 1077 cm⁻¹. Particularly for 0% amylose, intensity at 100 °C (0.292) indicates a decrease in the amorphous region (higher crystalline order) of the starch compared to 80 °C (0.303), and 120 °C (0.308), which corresponds with the peak rise in rutin content between 80 °C and 120 °C (Figure 3.2). However, the 1077 cm⁻¹ intensities reduced as 0.162 (140 °C) and 0.117 (160 °C). Therefore, rutin content might not have influenced the crystalline order at 140 °C and 160 °C. With respect to amylose-rutin inclusion complexation at 100 °C for 37% amylose, and 120 °C for 22% amylose, intensities at band 1077 cm⁻¹ showed that inclusion complexation increases crystallinity at

0.314, and 0.295, respectively, as observed for 37% amylose (0.293 at 100 $^{\circ}$C) and 22% amylose (0.160 at 120 $^{\circ}$C).

3.3.5. Expansion of subcritical water modified starches

Many studies on starch expansion have previously been reported for processes involving heat and shear, like extrusion (Ye et al., 2018). Subcritical water is also a medium for producing expanded starches as shown in Figure 3.5. All starches with varying amylose contents, in native state had similar specific volumes (37% amylose 1.24±0.00 mL/g, 22% amylose 1.19±0.02 mL/g, and 0% amylose 1.32±0.03 mL/g) but with SCW treatments (80-160 $^{\circ}$C, 7 MPa, and 30 min), with and without rutin, the starches increased in specific volume.

The amylose/amylopectin ratio plays an important role in swelling of starches as supported by Schirmer et al. (2013), who observed restricted granule swelling (average diameter size) in confocal laser micrographs of regular maize and barley starches (22.7% and 24.7% amylose content, respectively) compared to waxy maize and barley starches (2.5% and 3.4% amylose content, respectively). These starches were treated as starch-water suspensions of 10 g/kg heated in boiling water bath for 0.5-4 min. In this study, there was similar behavior of lower expansion as a result of higher amylose content observed in 37% amylose starches compared to 22% amylose as seen in Figure 3.5A (without rutin) at temperatures of 80-120 $^{\circ}$C. The 22% amylose starch had the highest expansion of 3.37±0.03 mL/g at 80 $^{\circ}$C compared to 37% amylose (2.10±0.08 mL/g) and 0% amylose (1.91±0.14 mL/g).
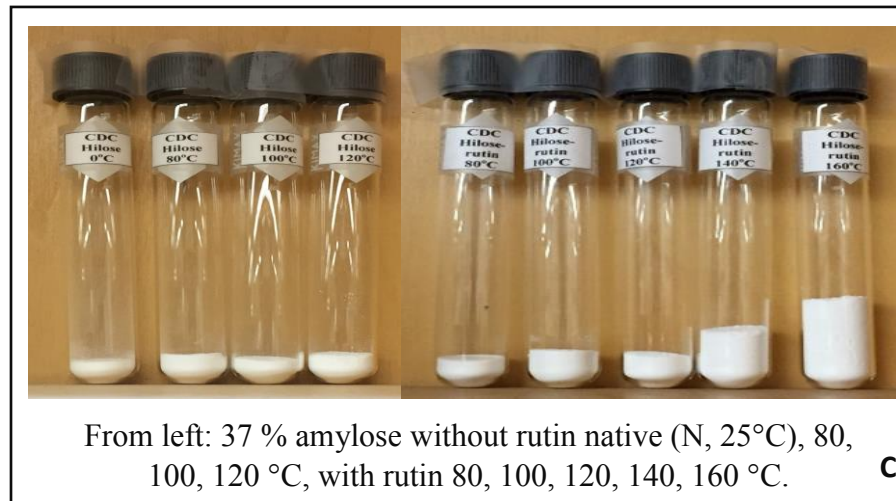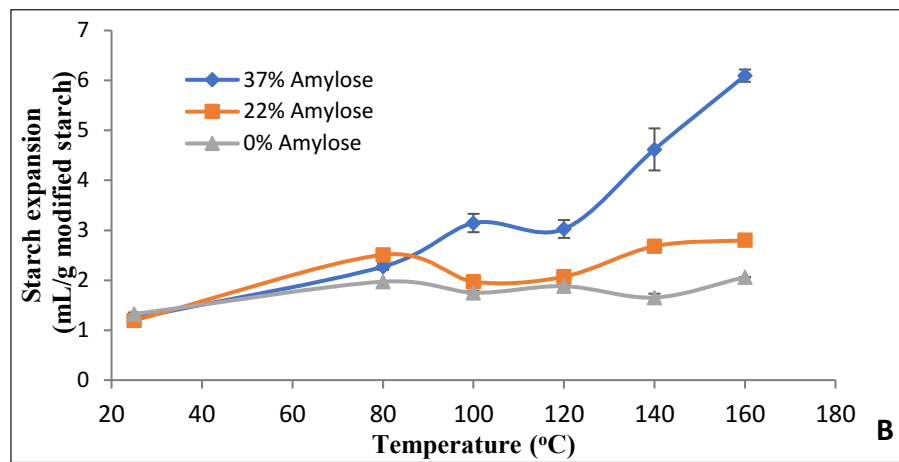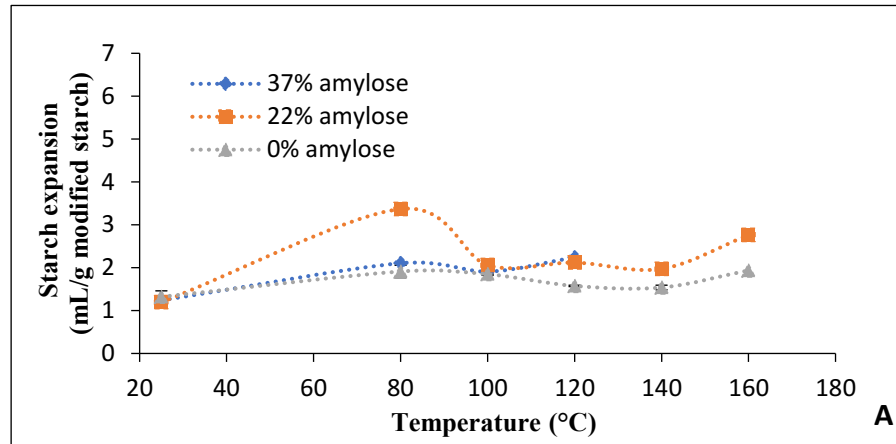
Figure 3.5. Effect of subcritical water temperature on expansion of barley starches with varying amylose contents: A) without rutin, and B) with rutin, at 7 MPa for 30 min, and C) expansion of 37% amylose starch without rutin, and with rutin.

These differences may also be related to the degree of starch gelatinization, as starch expansion increases with increasing degree of gelatinization (Tongdang et al., 2008; Cheow and Yu, 1997). Degree of gelatinization of starches describes the gelatinization behavior of starches with respect to its crystalline part, i.e. starches may have the same onset gelatinization temperature (first crystallite melting) but different conclusion gelatinization temperature at which gelatinization of most perfect crystallites is completed (Baks et al., 2007). However, in this study, measuring the degree of gelatinization of the modified gelatinized starches was not practical, but from the FT-IR results, there is possible correlation between crystallinity and expansion of starches. For example, crystallinity decreases for 22% amylose starch at 80 $^{\circ}$C, and 140 $^{\circ}$C (ratio 1077/1017 cm^{-1}), and expansion is observed only at these conditions as an effect of rutin complexation. Also, the lack of expansion difference between 37% amylose starches at 80 $^{\circ}$C (with and without rutin) may be attributed to their close ratio of 1077/1017 cm^{-1}, that is 0.248, and 0.278. Furthermore, in Figure 3.5A, as temperature increased from 80 $^{\circ}$C to 100 $^{\circ}$C, the expansion of 22% amylose decreased to 2.06±0.02 mL/g and there was no significant difference in expansion at 100 $^{\circ}$C among all the starches. The two starches with amylose contents of 22% and 37% had higher expansion 2.12±0.05 mL/g and 2.24±0.07 mL/g, respectively, at 120 $^{\circ}$C, while at the same temperature 0% amylose had a lower expansion of 1.58±0.03 mL/g (Figure 3.5A). This behavior was expected as the 0% amylose has >99% amylopectin where amylopectin represents the crystallinity of starch and contributes largely to the structural integrity of starch granule. However, there was an increased expansion from 140 $^{\circ}$C to 160 $^{\circ}$C for the 22% and 0% amylose starches (without rutin). The increase in

temperature may have caused further breakdown of starch structure, and molecular degradation influencing starch expansion (Chinnaswamy, 1993).

The starches with rutin treated in SCW also increased in specific volume (mL/g) compared to their native state. This is the first study that reported starch expansion in SCW media. At 80 $^\circ$C, 22% amylose starch had still the highest expansion of 2.51±0.00 mL/g compared to 37% amylose (2.27±0.07 mL/g), and 0% amylose (1.97±0.00 mL/g).

As temperature increased in the SCW region to 100-160 $^\circ$C, 37% amylose became the leading starch in expansion. Therefore, amylose content plays an important role in expansion as the specific volume (mL/g) increases with increasing amylose content, especially at 140 $^\circ$C and 160 $^\circ$C. This behavior may be related to rutin content in Figure 3.2. The consistent no band at 1017 cm^{-1} for 0% amylose starch with rutin may also be related to its almost steady expansion values from 80 $^\circ$C to 140 $^\circ$C.

There was no remarkable difference in the expansion behavior of the starches (Figure 3.5B) between 100 $^\circ$C and 120 $^\circ$C, especially for 22% and 0% amylose starches. However, there was a significant difference at 140 $^\circ$C and 160 $^\circ$C for all starches. This further confirms that amylose content and temperature contributed towards expansion of starches in SCW media. Among the starches, the highest expansion was observed for 37% amylose with rutin at 160 $^\circ$C as 6.10±0.12 mL/g, and the lowest expansion was 1.54±0.02 mL/g for 0% amylose without rutin at 140 $^\circ$C. Effects of rutin on starch expansion were observed for 37% amylose (100 to 160 $^\circ$C), 22% amylose (80 $^\circ$C and 140 $^\circ$C), and 0% amylose (120 $^\circ$C). The images in Figure 3.5C illustrate the extent of expansion and were not used to measure specific volume.

3.3.6. Viscoelastic properties of starch powders

For all SCW starch gels with and without rutin, storage modulus (G′) and loss modulus (G″) magnitudes increased with increasing frequencies (Figure 3.6A-F), even though the increase in G″ magnitudes was smaller and less responsive to the range of 0.1-25 Hz compared to G′ values (Figure 3.6A-F). The increase in G′ and G″ with increasing frequency is similar to results obtained between 0.1-10 Hz, strain 3%, and 25 °C for 10% w/w xanthan-rice starch gels with different amylose contents: high amylose 37.85%, medium amylose 27.55%, and low amylose 9.98% dm which were previously produced by dry-heating at 130 °C for 4 h (Su et al., 2018). The range of frequency applied in oscillatory sweep tests assesses the structural response of a material to oscillatory deformations based on longer and shorter timescales. As G″ magnitudes are less dependent on frequency, and magnitudes of G′ and G″ are in the order G′> G″, it shows that all the heat-treated starches were weak gels.

For the 37% amylose starch without rutin, G′ magnitude decreased with increase in temperature from 20193 ± 3284 Pa at 80 °C/25Hz to 11994 ± 1242 Pa at 120 °C/25Hz (Figure 3.6A). However, in the case of 37% amylose starch with rutin, G′ magnitude was the highest (24268 ± 288 Pa) at 160 °C/25Hz compared to 21879 ± 1185 Pa at 80 °C/25Hz (Figure 3.6D).

Interestingly, some G′ magnitudes do not correspond to increasing or decreasing order for temperatures studied, e.g. 160°C>80°C>140°C,100°C,120°C (Figure 3.6B), 160°C>80°C>140°C>100°C,120°C (Figure 3.6D), and 160°C>140°C,80°C>100°C,120°C (Figure 3.6E); which may be due to varying starch-rutin complexation mechanisms occurring at different temperatures, and extent of retrogradation of starch.
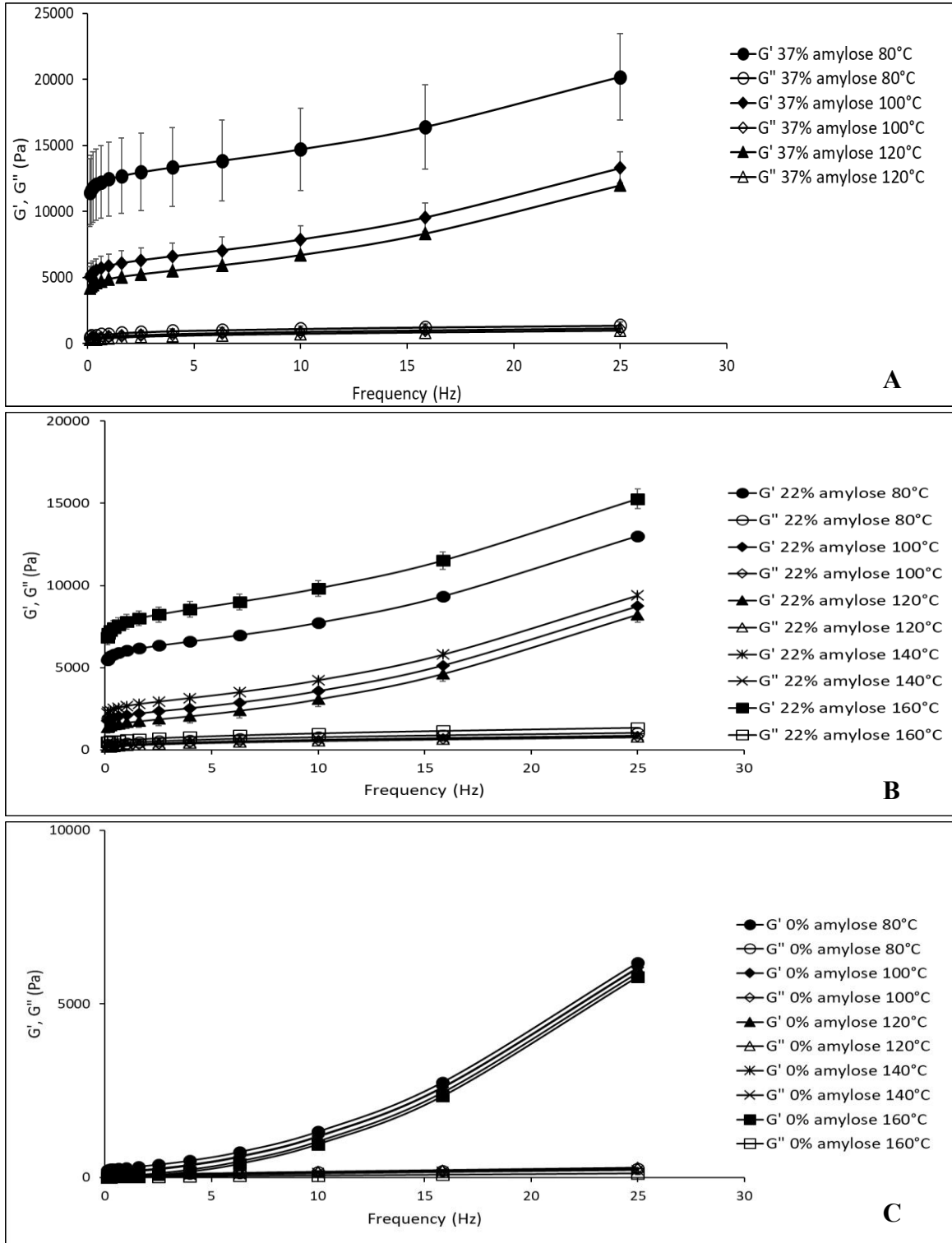
Figure 3.6. Influence of subcritical water treatment at 80-160 °C, 7 MPa, and 30 min on the storage modulus G', and loss modulus G" of barley starches with different amylose contents: without rutin (A-C).
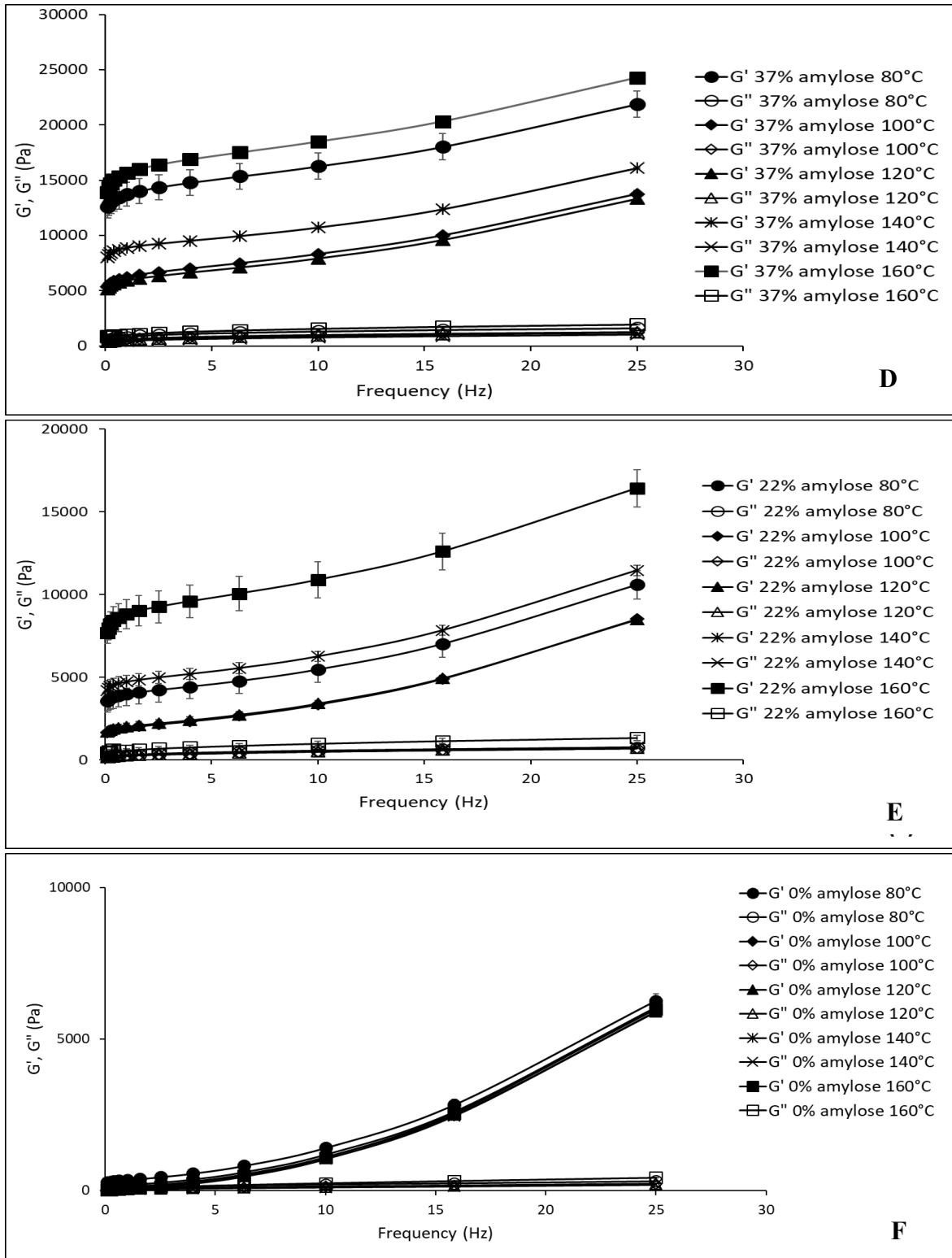
Figure 3.6. Influence of subcritical water treatment at 80-160 °C, 7 MPa, and 30 min on the storage modulus G′, and loss modulus G″of barley starches with different amylose contents: with rutin (D-F).

Retrogradation is the re-association of leached amylose and amylopectin fragment chains of a starch gel into a more ordered structure upon cooling (Wang et al., 2015). Therefore, retrogradation modified the crystallinity of the starch gels. Starch-rutin complexation mechanisms hypothesized in this study as discussed earlier include V-amylose inclusion complexes, rutin molecules trapped between self-associated non-complexed amylose molecules and swollen/collapsed granules, and rutin-amylopectin complexation occurring inside the swollen/collapsed granules.   Such complexation mechanisms are sustained by hydrophobic interactions (V-amylose), and hydrogen bondings.

The inconsistent order in G′ magnitudes among temperatures studied was also observed with 22% amylose starches (with and without rutin) with maximum G′ magnitudes at 160°C/25 Hz as 16424 ± 1137 Pa (with rutin) in Figure 3.6B, and 15270 ± 597 Pa (without rutin) in Figure 3.6E. Also, the 0% amylose starch (with and without rutin) unlike the 37% amylose starch and 22% amylose starches had no significant difference in G′ magnitudes among 80 °C to 160 °C (Figure 3.6D,F). The reason for maximum G′ magnitudes at 160 °C for 37% and 22% amylose starch gels could be attributed to stiffer networks developed during retrogradation from recrystallization of smaller molecular weight amylopectin (Modig et al., 2006) and reinforcement of amylose matrix (Miles et al., 1985). Possibly, the lack of reinforcement of amylose in 0% amylose starch made its gel less stiff.

Figure 3.7 compares the tan δ values for the different starches at 10 Hz. The 0% amylose starch had the highest tan δ value as 0.220±0.002 at 160 °C, which means it was the most viscous starch. Starches with high elastic components were 37% amylose at 80 °C

(0.081±0.001), 160 °C (0.083±0.000), and 22% amylose at 140 °C (0.089±0.008) and 160 °C (0.091±0.003). Byars et al. (2013) suggested that the presence of V-amylose-lipid complexes lowers the availability of amylose for retrogradation. This may be the reason 37% amylose with rutin at 100 °C, and 22% amylose with rutin at 120 °C had lower elastic components of 0.117±0.000, and 0.148±0.014, respectively, compared to 80 °C, 140 °C and 160 °C (Figure 3.6A) because of possible V-amylose-rutin complexation (Figure 3.3). At 160 °C, for both starches (37% amylose and 22% amylose), rutin was assumed to be complexed in amylopectin molecules or trapped between retrograded non-complexed amylose molecules (Figure 3) as there was no loss of amylose. The viscous behavior of 0% amylose at 160 °C was probably due to structural disintegration of starch granules and poor retrogradation characteristics of amylopectin molecules. Morita et al. (2002) earlier reported that breads made from waxy (0-2.3% amylose) wheat flours were softer than breads from non-waxy (24-37.5% amylose) wheat flours. At 80 °C, tan δ decreased with increase in the amylose content (Figure 3.7), which agrees with Noosuk et al. (2005) on the tan δ measurements of rice starch gels of varying amylose contents (2.08% - 22.43%) treated at 80-95 °C.

Furthermore, the addition of rutin made a significant difference in viscoelastic behavior (tan δ) between 22% amylose with rutin (0.089 ± 0.008) and without rutin (0.147±0.003) at 140 °C (Figure 3.7). Also, there was significant difference in tan δ between 0% amylose with rutin (0.22±0.002) and 0% amylose without rutin (0.057±0.016) at 160°C. This behavior agrees with the study of Li et al. (2018), where the peak viscosity, hot paste and cold paste viscosities of maize amylopectin-phenolic acids complexes were significantly lower than the similar viscosities of processed maize amylopectin without

phenolic acids. The presence of rutin may have formed interactions with amylopectin in the amorphous regions (Li et al., 2018). With the 22% amylose, rutin content increased elasticity at 140 °C. This may be related with the effect of starch-rutin complexation on expansion as observed in Figure 3.5. Expanded starch probably resulted from more leached amylose, which also enhanced retrogradation, causing stronger network structures.
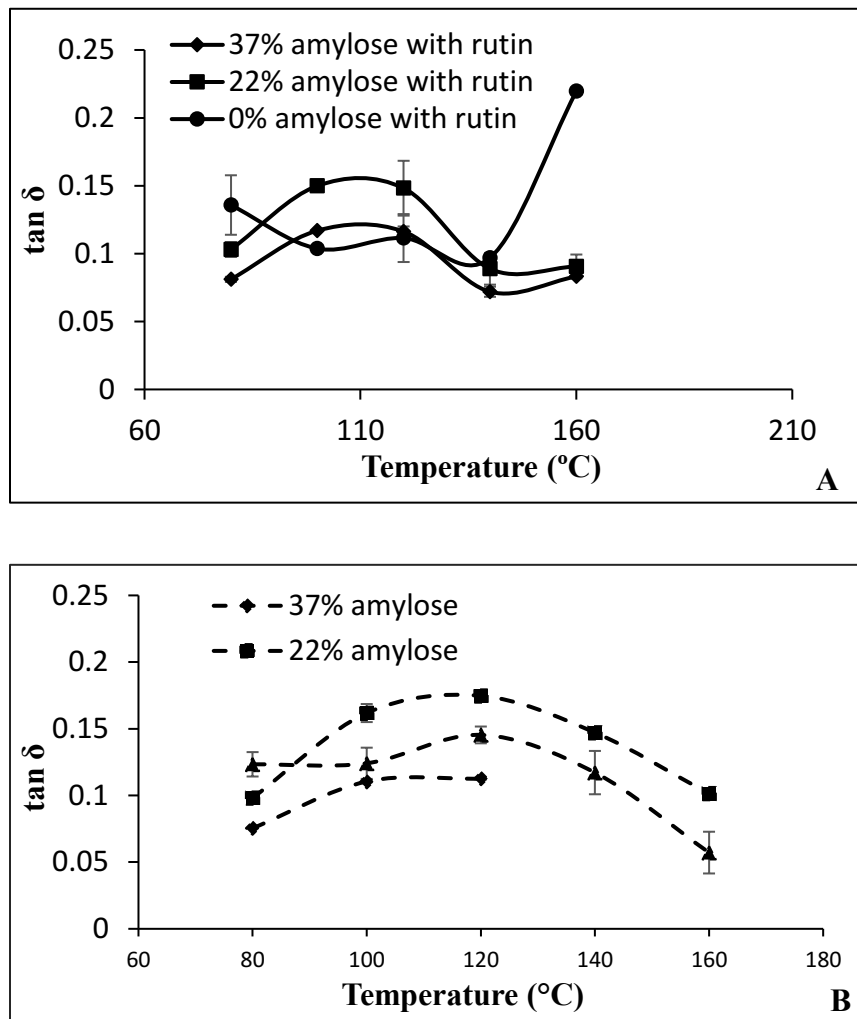
Figure 3.7. Influence of subcritical water treatment at 80-160 °C, 7 MPa, and 30 min on the shear response of barley starches with different amylose contents, determined at 10 Hz, with rutin (A), and without rutin (B).

Other authors have shown that swelling power influences viscoelastic properties of gelatinized starch dispersions (Singh et al., 2004; Okechukwu and Rao, 1996), particularly

increased volume fraction of starch granules increased elasticity (Morikawa and Nishinari, 2000). However, this behavior between tan δ and expansion did not reflect when comparing 22% amylose with and without rutin at 80 °C. This may have been related to thermal properties of water, or heat transfer between starch and water at these temperatures of 80 °C, and >100 °C. Analysis of retrogradation capacity of the 22% amylose starches may provide insight to why starches with similar elastic component (tan δ = 0.1) have different specific volumes (with rutin 2.510±0.003 mL/g, and without rutin 3.370±0.032 mL/g). Nevertheless, when comparing 0% amylose starches with and without rutin at 160 °C, the presence of rutin resulted in 16% higher viscous component.

3.3.7. Color

Subcritical water treated starches with rutin were evaluated for total color difference, yellowness index, and whiteness index (Figure 3.8). The total color difference (ΔE) accounts for the overall difference in lightness, redness/greenness, or blueness/yellowness of the starches from the white standard. Figure 3.8A shows significant difference in total color difference among the starches within each temperature and amylose contents. At 80 °C, 22% amylose starch was significantly different from 0% amylose, and 37% amylose starches. At 140 °C, and 160 °C, 37% amylose starch was significantly different in total color difference compared to 0% amylose, and 22% amylose starches. These differences may be related to rutin content of the SCW treated starches.

The yellowness index in Figure 3.8B is relevant to the complexed rutin in the starches. It was not surprising that 0% amylose at 100 °C had high yellowness index as 6.94 ±0.00 because this starch had the highest rutin content of all the starches (Figure 3.2).
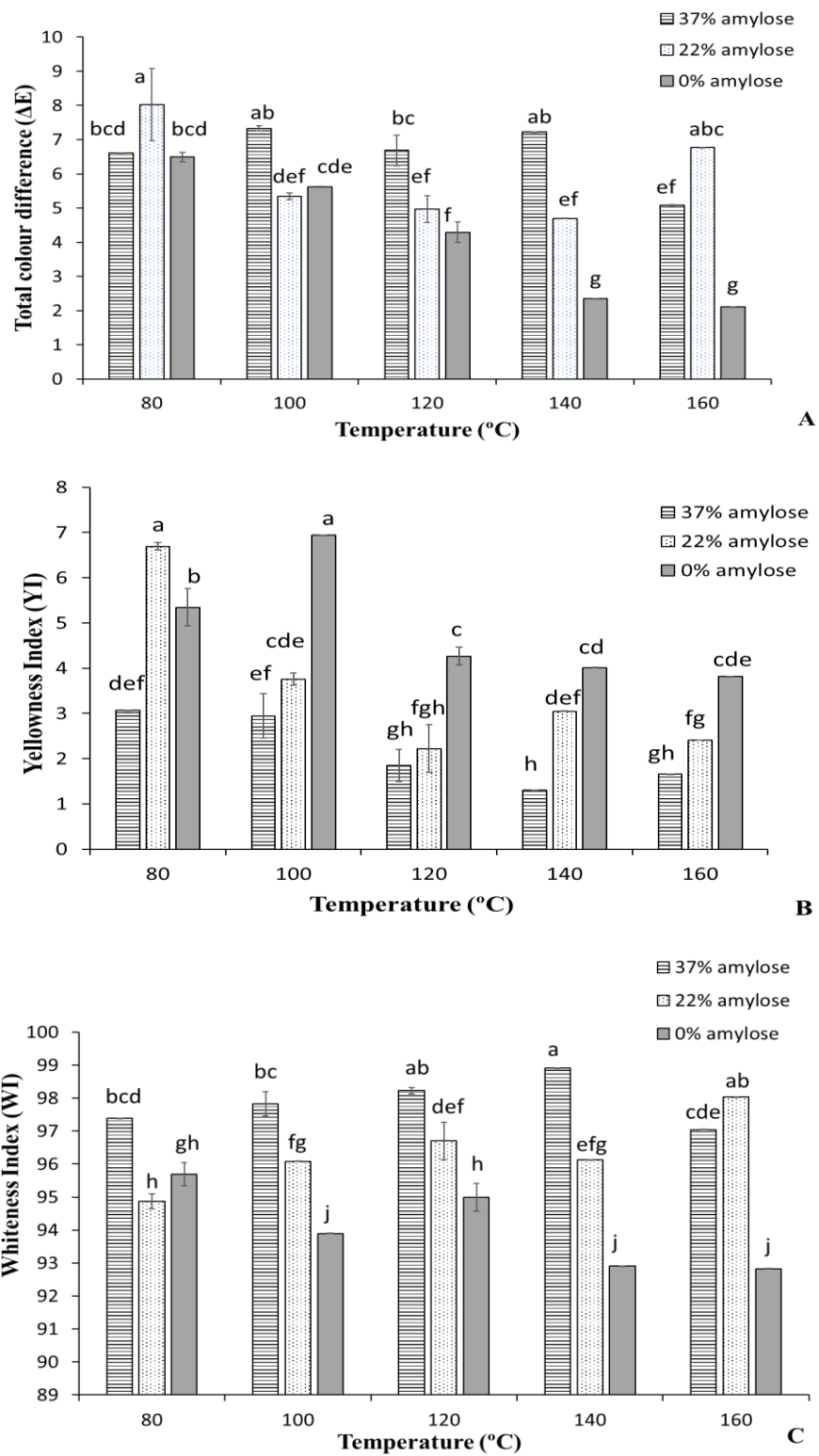
Figure 3.8. Color parameters of subcritical water treated barley starches at 80-160 °C, 7 MPa, and 30 min in the presence of rutin. Total color difference (A), Yellowness index (YI) (B), and Whiteness index (WI) (C).

However, the yellowness index of 6.69 ± 0.06 of 22% amylose starch at 80 $^\circ$C was not significantly different from that of 0% amylose at 100 $^\circ$C even though their rutin contents were significantly different as 0.62 ± 0.05 mg/g modified starch (dm) and 0.87 ± 0.06 mg/g modified starch (dm), respectively.

Therefore, the yellowness index may not be based on rutin content only. This is also more evident with SCW temperatures of 140 $^\circ$C to 160 $^\circ$C, where the yellowness indices of 0% amylose starch were significantly different and higher than the other starches even though the rutin content of 0% amylose at 140 $^\circ$C and 160 $^\circ$C was lower than that of 37% amylose. A possible reason for the deeper yellow color intensity could be due to reactions involving deprotonation of hydroxyl groups of rutin caused by pH change in the SCW media (Berlim et al., 2018; Klein et al., 2016; Lemańska et al., 2001), as earlier stated SCW can act as an acid or a base.

Generally, deprotonation of hydroxyl groups of flavonoids is pH dependent (Berlim et al., 2018). For rutin, the number of deprotonated sites increase with increasing pH (Chen et al., 2010). The acid dissociation constant (pK$_a$ value) for deprotonation of 3'-OH group in rutin radical to occur was reported as 4.3 (Jovanovic et al., 1994). Berlim et al. (2018) also reported that as concentration of flavonoids increased in solution, acidity increased, which led to deprotonation of 7-OH, 3'-OH and 4'-OH groups of eight flavonoids extracted from *Syngonanthus nitens*. They also reported color changes using different pH buffers (pH range of 4-9) at bands around 325 nm and 425 nm. Therefore, it is possible that under SCW conditions, many deprotonated sites of rutin occurred and formed glycosidic bonds with amylopectin molecules. Further research is required to evaluate pH during SCW experiments.

The whiteness index in Figure 3.8C was significantly different for all starches compared within each isotherm. The 0% amylose starch was the darkest starch at SCW temperatures, while 37% amylose starch was the whitest except at 160 °C. Amani et al. (2005) also observed that starch gels with higher amylose content had less clarity than starch gels from waxy or no amylose. However, at 160 °C, the whiteness index of 22% amylose was significantly higher than the whiteness index of 37% amylose. This could be related to the new alignment of amylose molecules that influences opacity (Amani et al., 2005).

3.4.   Conclusions

The structure of barley starches was modified in excess water (3.36% w/w) at temperatures of 80, 100, 120, 140, and 160 °C, 7 MPa and 30 min. The extent of modification was influenced by amylose and amylopectin contents in the starch granule, and the presence of rutin. These factors together had influenced and enhanced varying behavior characteristics of SCW-treated barley starches. Rutin content in starch decreased at elevated temperatures of 140 °C and 160 °C. Starch-rutin interaction modes included V-amylose inclusion complexation, and amylopectin-rutin complexation strengthened by hydrogen bonding. The highest content of amylose (37%) also resulted in maximum expansion value of 392%. All SCW-treated starches were weak gels, with 37% amylose starch, showing stiffer networks. Starches modified with rutin had high yellowness indices, useful for aesthetic applications. SCW treatment had the advantage of producing high value starches with rutin content, and high expansion characteristics. Overall, the variety of modified starch characteristics produced in this study offers a range of choices for target functional food applications.

Chapter 4. Effect of ultrasonication on rutin: Identification of derivative compounds and antioxidant activities[2]

4.1. Introduction

The utilization of ultrasonication for the processing of polyphenols from plant parts and various biomass has gained interest due to its non-thermal, short-time, and high intensity power characteristics. Ultrasonication process is the transfer of ultrasonic waves >16kHz (McClements, 1995) in a liquid medium via cavitation phenomena, which involves the creation, growth and collapse of gas bubbles due to pressure differences, expansion, and compression cycles, respectively, in the liquid medium (Zhu, 2015b). When utilizing low frequencies below 100 kHz and high power (10–1000 W/cm^2), the collapse of bubbles generates localized high temperatures (<4727 °C) and pressures (<101 MPa), which causes high shear rates on solid surfaces and chemical reactions like oxidation (Cárcel et al., 2012; McClements, 1995). Ultrasonic extraction at 25 kHz, 27 W, and room temperature was employed for the extraction of rutin in aqueous medium from 10 g of dried *Sophora japonica* flower buds, and a loss was reported after 30 min of processing as 0.18 g rutin compared to 0.28 g rutin from a conventional aqueous (reflux) extraction method (Paniwnyk et al., 2001). This reduced yield was possibly due to rutin degradation reactions with the hydroxyl radicals generated from the aqueous medium during sonication (Paniwnyk et al., 2001). However, the degradation compounds from ultrasonication of rutin were not reported.

---

[2] A version of this chapter will be submitted as Ekaette, I., and Saldaña, M.D.A. Ultrasound processing of rutin: Derivative compounds, antioxidant activities and optical rotation. Food Research International.

Rutin, also known as quercetin-3-O-rutinoside or 3′,4′,5,7-tetrahydroxy- flavone-3-rutinoside is an important phenolic flavonoid of the class of flavanols known for the prevention of microbial, inflammatory, cancer, and diabetic ailments (Gullón et al., 2017; Chua, 2013). The hydrothermal hydrolysis of rutin at 120-220 °C yielded derivatives and degradation compounds, including isoquercetin, quercetin, 3,4-dihydrobenzoic acid, catechol, 5-hydroxymethyl furfural, 5-methyl furfural, protocatechuic acid, 2,5-dihydroxyacetophenone, isorhamnetin, myricetin, and kaempferol (Kim and Lim, 2017; Ravber et al., 2016; Ravber et al., 2015). Isoquercetin reportedly has more antiproliferative effect than rutin or quercetin (de Araujo et al., 2013), and quercetin has higher antioxidant activity (2.3-fold) than rutin (Scherer and Godoy, 2014; Zhang et al., 2014). Therefore, the hydrolysis of rutin into its respective aglycones can enhance the functionality of rutin for other pharmacological benefits.

Furthermore, on the degradation of rutin, onion which is a source of rutin (Simin et al., 2013) was fresh cut and washed with a combination of nisin (50 μg/mL) and citric acid (1% w/v), which led to increased total phenolic contents after 15 days storage. Particularly, quercetin, a rutin derivative had increased from 2.03 mg/g dm of untreated fresh-cut onions to 3.13 mg/g dm with nisin treatment, and from 1.80 mg/g dm of untreated fresh-cut onions to 3.94 mg/g dm with citric acid treatment (Chen et al., 2016). This might have been caused by hydrolysis of rutin to quercetin by nisin and citric acid.

In another report, there was increased degradation rate of the phenolic compounds, 4-chlorophenol, phenol, catechol and resorcinol by ultrasonication (200 kHz, 16 W, 60 min, 20 °C) in the presence of an aqueous salt (0.45 M sodium chloride) medium (Uddin et al., 2016). Sodium chloride acts as a catalyst for sonochemical reactions by creating a partition

coefficient and salting out effect of phenolic compounds from the bulk solution to the cavitation interface, thereby enhancing the rate of degradation of the compounds (Uddin et al., 2016; Sutkar and Gogate, 2010). The utilization of sodium chloride in an ultrasonication process can enhance cavitationally induced transformation of chemical compounds for the selective production of its degradation products.

To the best of my knowledge, rutin hydrolysis using ultrasonication assisted with citric acid and sodium chloride has not been reported. It was hypothesized that the influence of ultrasound-generated heat on rutin would increase rutin solubility in aqueous solvent and might catalyze the process of rutin hydrolysis. Krewson and Naghski (1952) reported the highest solubility of rutin in water near the boiling point (100 °C). Therefore, the objective of this study was to understand the effects of ultrasound energy, pH of aqueous media, and temperature control on the hydrolysis, and properties of rutin.

4.2. Materials and Methods

4.2.1. Materials

Rutin hydrate (purity ≥94%), citric acid, sodium chloride, sodium carbonate, Folin-Ciocalteau's phenol, gallic acid, sodium nitrite, sodium hydroxide, isoquercetin, quercetin, epigallocatechin gallate, catechin, naringin, 1,2-dihydrobenzene, 2,4-dihydrobenzoic acid, 3,4- dihydrobenzoic acid, 4-dihydrobenzoic acid, 5-(hydroxymethyl) furfural, 2,2'-azino-bis(3-ethylbenzothiazoline-6-sulphonic acid (ABTS), potassium persulfate, butylated hydroxy-anisole (BHA), L-ascorbic acid, 2,4,6-tripyridyl-s-triazine (TPTZ), iron III chloride hexahydrate, glacial acetic acid, sodium acetate trihydrate, 1,1-diphenyl-2-picrylhydrazine (DPPH), ferric chloride, 3-(2-pyridyl)-5,6-diphenyl-1,2,4-triazine-4′,4″-disulfonic acid sodium salt (ferrozine), copper sulfate, pyridine, pyrocatechol, and

trisodium trimetaphosphate were purchased from Sigma Aldrich (Oakville, ON, Canada). Dimethyl sulfoxide, methanol, hydrochloric acid, and ethylenediamine tetra-acetic acid (EDTA) were purchased from Fisher Scientific (Ottawa, ON, Canada). Aluminium chloride, and trolox were purchased from Acros Organics (Thermo Fisher Scientific, Morris Plains, NJ, USA). Morin and hesperidin were purchased from Indofine Chemical Company Inc. (Hillsborough, NJ, USA) and Fisher Scientific (Ottawa, ON, Canada), respectively. All other chemicals were of analytical grade and solvents were of high-performance liquid chromatography (HPLC) grade.

4.2.2. Methods

4.2.2.1. Ultrasonication

High intensity ultrasonic processor (Model FS-1200N, Shanghai Sonxi Ultrasonic Instrument Co., Shanghai, ZJ, China) was utilized for the experiments with a 20 mm diameter probe at 20 kHz. The power was fixed at 600 W, while varying time of 2, 5, 10, 15, and 20 min. Deionized water (pH 5.0), and two aqueous solvents of low concentration: 0.01 mg/mL citric acid (pH 2.2), and 0.01 mg/mL sodium chloride (pH 6.3) were prepared as the media for the ultrasonication process. For each experiment, rutin hydrate (20.0±0.9 mg) was mixed with 20 mL of the desired solvent. The media was stirred briefly and transferred to an ice-water bath. Stirring of the media continued with a magnetic stirrer while the ultrasound probe was immersed at 1.3 cm length into the media. The stirring speed (0.5 level of magnetic plate) was kept constant for all experiments. Temperature of the ultrasound-treated rutin suspension or solution was recorded immediately after the experimental run time. Samples treated with an ice-water bath at a constant volume of 20 mL and a final temperature of 47 °C (Table 4.1) were tagged as 'with temperature control',

and the energy densities were calculated according to Equation 4.1 (3.6, 9.0, 18.0, 27.0, and 36.0 kJ/mL). Specific final temperatures are reported in Table 4.1. Experiments were repeated for samples without an ice-water bath and tagged as 'without temperature control'. The samples 'without temperature control' had loss in volume and final temperature of 86 °C (Table 4.1). Final volumes after the ultrasonication experiment times were 19.5 mL (2 min), 19.0 mL (5 min), 18.5 mL (10 min), 17.5 mL (15 min), and 16.75 mL (20 min). The change or gain in energy density (ΔED) was calculated according to Equation 4.2 (0.1, 0.5, 1.5, 3.9, and 7.0 kJ/mL). After the ultrasonication treatments, sample suspensions/solutions were transferred quantitatively and made up to 50 mL with methanol in a volumetric flask. The >60% v/v methanol solutions of ultrasound treated rutin samples were left at 6 °C overnight, before being transferred to 50 mL Kimax culture tubes. Samples were tightly sealed, reinforced with parafilm, and stored at -26 °C until further characterizations. All experiments were repeated in at least duplicates. Controls of rutin hydrate in the various media without ultrasonication treatment were also prepared with the same procedure.

$$\text{Ultrasound Energy Density (ED)} = \frac{\text{Power (W) x Time (s)}}{\text{Volume (mL)}} \tag{4.1}$$

$$\text{Change in Ultrasound ED (}\Delta\text{ED)} = \frac{\text{Power (W) x Time (s)}}{\text{Final Volume (mL)}} - \frac{\text{Power (W) x Time (s)}}{\text{Initial Volume (mL)}} \tag{4.2}$$

Table 4.1. Final temperature of rutin in media after ultrasound treatment

Time (min)	Temperature (°C) With temperature control*		Temperature (°C) Without temperature control
	Water media	Citric acid and NaCl media	All media
2	42	42	68
5	47	47	86
10	47	47	86
15	47	50	86
20	47	55	86

* using an ice-water bath

4.2.2.2. Total phenolic content

Total phenolic content (TPC) was determined according to the methodology of Sarkar et al. (2014) with minor modifications. An aliquot of ultrasound treated rutin (0.10 mL) was mixed with 3.46 mL of deionized water in a test tube and vortexed for 10 s. Folin-Ciocalteau's phenol reagent (0.2 mL) was added and vortexed for 10 s, then left for 6 min of reaction. Thereafter, 0.6 mL of 0.25 g/mL sodium carbonate was added to the mixture and vortexed for 10 s. Solvent (60% v/v methanol) was used as a blank. The final mixture was incubated in the dark at room temperature (23 °C) for 2 h. The absorbance was measured at 765 nm using a Jenway Genova spectrophotometer (Stone, Staffordshire, UK). The measurements were compared with the standard curve of gallic acid serial solutions (0.03-0.39 mg/mL). TPC was expressed as mg of gallic acid equivalent per mg rutin hydrate.

4.2.2.3. Total flavonoid content

Total flavonoid content (TFC) was measured using the method described by Huang et al. (2009) with slight modifications. An aliquot of ultrasound treated rutin (0.125 mL), 0.037 mL $NaNO_2$ solution (5% w/v), 0.075 mL $AlCl_3$ (10% w/v), 0.25 mL NaOH (1 mol/L) and 0.765 mL deionized water were added and mixed in a test tube. A blank sample of 60% v/v methanol was prepared with the aliquots. The mixture was left to stand for 5 min, and absorption was measured at 507 nm using a Jenway Genova spectrophotometer (Stone, Staffordshire, UK). The measurements were compared with the standard curve of catechin serial solutions (0.02-0.39 mg/mL). TFC was expressed as mg of catechin equivalent per mg rutin hydrate.

4.2.2.4. Identification and quantification of compounds by High Performance Liquid Chromatography (HPLC)

Aliquots of ultrasound treated rutin were filtered using a Basix 0.2 μm nylon syringe filter into amber HPLC vials and injected into a Shimadzu LC 20 Prominence 20 (Agilent Technologies, Santa Clara, CA, USA) system consisting of an autosampler, a column oven set at 30 °C, and a diode array detector. Separation of rutin, isoquercetin, quercetin, naringin, morin, catechin, hesperidin, epigallocatechin gallate, 1,2 dihydrobenzene, 2,4-dihydrobenzoic acid, 3,4-dihydrobenzoic acid, 4-dihydrobenzoic acid, and 5-(hydroxymethyl) furfural was carried out on a Zorbax SB-C18 column (Agilent Technologies, Santa Clara, CA, USA) of 250 mm x 3.0 mm i.d., 5 μm particle size. The mobile phases used were 0.5% formic acid in water (elution A) and 0.5% formic acid in methanol (elution B) at a flow rate of 1 mL/min using gradients: 0 min, 8% B; 5 min, 10% B; 20 min, 75% B; 21 min, 100% B; 23 min, 100% B; 24 min, 8% B; and 26 min, 8% B. The quantifications of individual compounds in standard solutions and ultrasound treated rutin aliquots were performed at a detection wavelength of 268 nm. Calibration curves were fitted for standard solutions of rutin (≥94%), isoquercetin (≥98%), quercetin dihydrate (≥98%), naringin (95%), morin (pure), (+)-catechin hydrate (≥98%), hesperidin (95%), (-)-epigallocatechin gallate (≥80%), 1,2-dihydrobenzene (≥99), 2,4-dihydrobenzoic acid (≥97%), 3,4- dihydrobenzoic acid (≥97%), and 5-(hydroxymethyl) furfural (≥99%). Determination of individual compound concentrations was carried out in triplicates and presented as yield (%) based on the starting mass of rutin hydrate (20.0±0.9 mg).

4.2.2.5. Antioxidant activity of ultrasound treated rutin

4.2.2.5.1. Ferric Reducing Antioxidant Power (FRAP)

Ferric Reducing Antioxidant Power (FRAP) of ultrasound treated rutin aliquots was determined following previous methodologies reported by Benzie and Strain (1996) and Szeto et al. (2002). The FRAP reagent was prepared by mixing 0.3 M sodium acetate buffer, 10 mmol/L TPTZ-HCl, and 20 mmol/L $FeCl_3.6H_2O$ at the volumetric ratio of 10:1:1, respectively. An aliquot of the ultrasound treated rutin (0.025 mL) was mixed with the FRAP reagent (37 ºC) and deionized water (0.375 mL) and placed in a water bath at 37 ºC for 30 min. The absorbance of the mixture was measured at 593 nm using a Jenway Genova spectrophotometer (Stone, Staffordshire, UK). This procedure was repeated for Trolox standard, but the absorbance was measured after 4 min from incubation in a water bath at 37 ºC. The measurements of ultrasound treated rutin were compared with the standard curve of Trolox serial solutions (0.06-0.88 µmol/mL). The FRAP of ultrasound treated rutin was presented as µmol Trolox per mg rutin hydrate.

4.2.2.5.2. DPPH free radical scavenging assay

Scavenging activity of ultrasound treated rutin on DPPH free radical was assessed following the method of Bamdad et al. (2011) with slight modifications. An aliquot of ultrasound treated rutin (0.1 mL) was diluted with 60% v/v methanol (0.4 mL) and then mixed with 0.1 mM DPPH in methanol (0.5 mL). The mixture was vortexed vigorously and left to stand in the dark for 30 min. The blank used was 60% v/v methanol. The absorbance of the reduction of DPPH radicals was measured at 517 nm with Jenway Genova spectrophotometer (Stone, Staffordshire, UK). L-Ascorbic acid at concentrations of 0.2

mg/mL, and 2.0 mg/mL were used as positive controls. The scavenging activity of the ultrasound treated rutin samples was calculated according to Equation 4.3.

DPPH free radical scavenging (%) = 1- (A_S/A_B) x 100   (4.3)

where, As and A_B are the absorbances of ultrasound treated rutin and the blank solution, respectively.

4.2.2.5.3. ABTS cation inhibition assay

The ABTS inhibition assay was adapted from Dudonné et al. (2009) with slight modifications. The ABTS cation (ABTS$^{\bullet+}$) solution was prepared by mixing 7 mM ABTS stock solution with 2.45 mM potassium persulfate in equal quantities. The mixture in an amber bottle was covered with aluminium foil and placed in the dark for 12 h to stabilize the ABTS cation solution. After 12 h, the ABTS$^{\bullet+}$ solution was diluted with deionized water to an absorbance of 0.70 (±0.02) at 734 nm. Diluted ABTS$^{\bullet+}$ solution (3.0 mL) was added to the ultrasound treated rutin (0.1 mL) and mixed for 5 s. The mixture was incubated at 30 ºC for 10 min. The blank used was 60% v/v methanol. Positive controls used were L-ascorbic acid (4.7 mg/mL in 60% v/v methanol), BHA (1.2 mg/mL in 60% v/v methanol), and trolox (6.3 mg/mL in 100% methanol). Decolorization of ABTS cation was measured as absorbance at 734 nm using a Jenway Genova spectrophotometer (Stone, Staffordshire, UK). The inhibition percentage was calculated using Equation 4.4:

Inhibition (%) = 1- (A_S/A_B) x 100   (4.4)

where, As is the absorbance of ultrasound treated rutin sample, and A_B is the absorbance of the blank solution.

4.2.2.5.4. Metal ion chelating activity

The ability of ultrasound treated rutin to chelate the prooxidative transitional metal ions Fe^{2+} and Cu^{2+} was investigated following the method of Bamdad et al. (2011), and Kong and Xiong (2006), respectively, with slight modifications. In the Fe^{2+} chelating assay, ultrasound treated rutin (0.25 mL) was mixed with 0.5 mL of 20 μM $FeCl_2$, then 0.5 mL of 0.5 mM ferrozine was added to initiate the reaction, which produces a pink chromophore (ferrozine-Fe^{2+}) that absorbs strongly at 562 nm. The mixture was left to stand for 10 min and the color change caused by ultrasound treated rutin due to dissociation of Fe^{2+} was measured at 562 nm. The blank used was 60% v/v methanol. A strong metal chelator EDTA (0.1 mg/mL) was used as a positive control. In the Cu^{2+} chelating assay, 1 mL of 2 mM $CuSO_4$, 1 mL of 10% pyridine, and 20 μL of 0.1% pyrocatechol violet were mixed, followed by addition of ultrasound treated rutin to cause dissociation of Cu^{2+} monitored as the disappearance of blue color, and measured as absorbance at 632 nm. The blank used was 60% v/v methanol. L-Ascorbic acid in 60% v/v methanol (5 mg/mL) was used as a positive control. Both metal chelating activities were calculated using Equation 4.5:

Chelating activity (%) = 1- (A_S/A_B) x 100   (4.5)

where, A_s is absorbance of the ultrasound treated rutin sample, and A_B is the absorbance of the blank solution.

4.2.2.6. Optical rotation

Ultrasonication of rutin hydrate was carried out at 27 kJ/mL (with temperature control), and at 3.9 kJ/mL (ΔED, without temperature control). The suspension was freeze-dried, and the dried mass was dissolved in dimethyl sulfoxide (DMSO), methanol, and ethanol, at concentrations of 0.5% w/v, 0.3% w/v, and 0.1% w/v. The optical rotation of the

rutin solutions in DMSO, methanol, and ethanol was measured at 20±0.02 °C, using a cylindrical quartz cell of length 100 mm at wavelength λ=589 nm ± 0.001° accuracy (Anton Paar OptoTec GmbH, Seelze-Letter, Germany). The quartz cell was fitted in a Modular Circular Polarimeter (MCP, 5500 model) (Anton Paar OptoTec GmbH, Seelze-Letter, Germany), and operating on the instrument software version: 5.10. Controls used for measurements were D-(+)-glucose (+52.7°, c=10% in H_2O), D-(+)-galacturonic acid monohydrate (+53±2°, 5 h, c=10% in H_2O), and D-(−)-fructose (-92±2°, 1 h, c=10% in H_2O). Samples solutions were left to equilibrate for 18 h at room temperature (23 °C) before measurement. The specific rotation was calculated using Equation 4.6:

$$[\alpha]_D^{20°C} = 100\alpha/ \ c. \ l \tag{4.6}$$

where $[\alpha]_D^{20°C}$ is specific rotation of the ultrasound treated rutin, α is the observed optical rotation by ultrasound treated rutin at 20 °C, c is concentration of optically active component (ultrasound treated rutin) expressed as g sample/ml solution, and l is cell length in decimetre.

4.2.3. Statistical analysis

Experiments were carried out in at least duplicates, and in triplicates for colorimetric methods. All values were reported as mean ± standard deviation. One-way Analysis of Variance (ANOVA) were performed using Minitab 18 statistical software (Minitab Inc., State College, PA, USA) comparing the means for significant differences at $p < 0.05$ by Tukey's test.

4.3. Results and Discussion

4.3.1. Total phenolic and flavonoid content

Phenolic compounds consist of flavonoids, phenolic acids, anthocyanins, and tannins, all of which contain one or more hydroxyl groups bonded to an aromatic hydrocarbon (phenyl) group. The TPC determination is based on the transfer of electrons from the hydroxyl group of phenolic compounds to phosphomolybdic/phosphotungstic acid complexes (Ainsworth and Gillespie, 2007).

In Figure 4.1A, the controls (untreated rutin hydrate) in water, citric acid, and NaCl media showed TPC as 0.28 ± 0.02, 0.29 ± 0.00, and 0.27 ± 0.02 mg gallic acid equivalent/mg rutin hydrate, respectively. At 36 kJ/mL, ultrasound treatment increased TPC by 56% from the control in water and citric acid media, and by 69% in NaCl media. This may be related to the catalytic degradation effect of NaCl on phenolic compounds (Uddin et al., 2016), thereby producing more degradation compounds compared to in the other media.
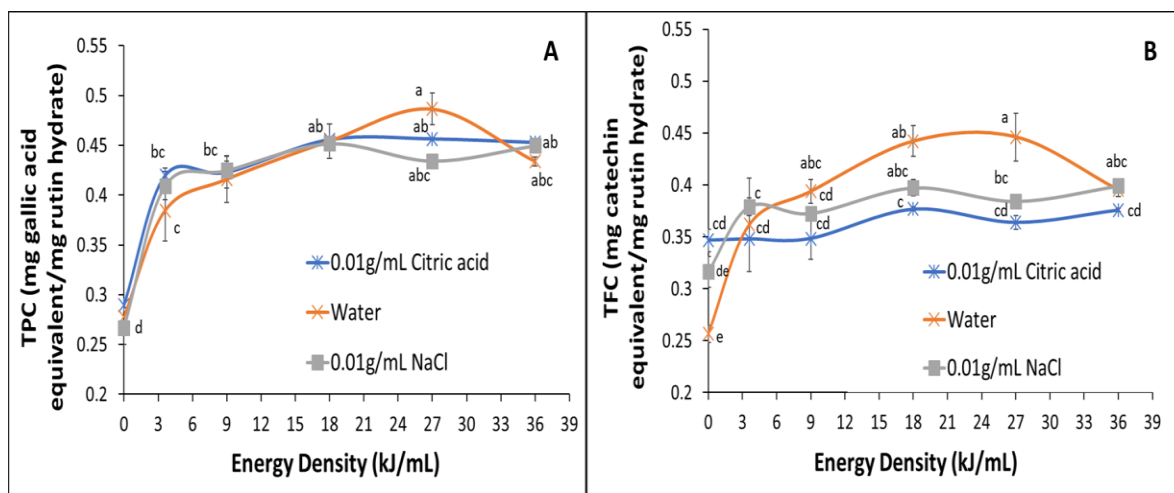
Figure 4.1. Total phenolic content TPC (A), and total flavonoid content TFC (B) after ultrasonication of rutin with temperature control.

(Values with the same lowercase letters (a-c) are not significantly different at p>0.5, across all values).

From the TFC results (Figure 4.1B) at 27 kJ/mL, TFC in water media (0.44±0.02 mg catechin equivalent/mg rutin hydrate) is significantly higher than TFC in citric acid (0.36±0.01 mg catechin equivalent/mg rutin hydrate) and NaCl (0.38±0.00 mg catechin equivalent/mg rutin hydrate) media. At 27 kJ/mL, the TFC increased from the control by 73% and 21% in water and NaCl media, respectively, possibly influenced by the pH of the media. This was related to the hydrolysis of rutin involving the breaking of glycosidic bonds to release aglycones and sugars. In an earlier study, rutin was hydrolysed in pressurized hot water to isoquercetin and quercetin, and sugar moieties such as rhamnose, glucose (Ravber et al., 2016) or rutinose. Therefore, in this study, it is possible that interfering substances such as sugars influenced TPC additively (Lee et al., 2014). The increases in TPC and TFC may also be from the production of rutin nanosuspensions which increased the number of rutin and derivative particles, surface areas, and consequently the hydroxyl groups required for the chemical reactions in TPC and TFC assays. Mauludin et al. (2009) reported the production of rutin nanosuspensions (547 nm) using high-pressure homogenization (150 MPa, at room temperature) in the treatment of rutin/polyvinyl alcohol/water (10:2:88 w/w/v %) mixture.

The TPC or TFC in citric acid and NaCl media did not increase above TPC or TFC in water media as expected. A reason may be increased solute/ion concentration in 0.01 g/mL citric acid and 0.01 g/mL NaCl media, in competition for cavitation impact available for target rutin molecules compared to water. Akulichev (1966) reported that in NaCl-water solutions, ions were distributed at the surface of gas bubbles, reducing cavitation threshold with respect to distilled water. Another factor with respect to solute concentration could have been from the kinetics in the production of hydrolysates, as solutes concentration at 2

min remained in the system, and consequently influenced cavitation as the experiment progressed to the fifth, tenth, fifteenth, and twentieth minute. This may explain the lack of significant difference observed in TPC and TFC between 3.6 to 36 kJ/mL, except TFC at 27 kJ/mL, in all the media studied. Contrary to the possible negative effect of increased ion concentration on cavitation, Atchley et al. (1984) reported that cavitation threshold of water increases with an increase in ion concentration. Therefore, in this study, the ionic concentrations in 0.01 g/mL citric acid and 0.01 g/mL NaCl may have been too low for pronounced TPC or TFC increment effects over water.

Some chemical reactions in the systems may include the increase in hydrogen ions in the citric acid media available for formation of hydrogen bonding with functional groups of the derivative compounds of rutin, and the chlorination or oxidation of hydroxide ions of the derivative compounds in the NaCl media. All these reactions may have limited availability of hydroxyl functional groups for nitration in the TFC assay (Pękal and Pyrzynska, 2014). The TFC assay is based on the nitrite-scavenging effect of catechol group in flavonoids, which is related to the positions of the hydroxyl groups (Lu et al., 2016). Since the method described in this study refers to nitration (NO_2), and not nitrosation (NO) reactions, it is possible that the presence of other flavonoids (e.g. EGCG) could be involved in nitrosation (NO) reactions (Lu et al., 2016) and influenced the TFC behavior. Determination of TFC by nitration (NO_2) is more specific to flavonoids, such as rutin, luteolin and catechins (Pękal and Pyrzynska, 2014).

There was similar behaviour between TPC with and without temperature control as TPC for ultrasound treated rutin without temperature control increased from control at 0.28±0.02 mg gallic acid equivalent/mg rutin hydrate (water), 0.29±0.00 mg gallic acid

equivalent/mg rutin hydrate (citric acid), and 0.27±0.02 mg gallic acid equivalent/mg rutin hydrate (NaCl) by 63% within all change in energy density (ΔED) studied.

Also, TFC increased from control to ΔED of 7.0 kJ/mL by 47%, 15%, and 19% in water, citric acid and NaCl media, respectively. Citric acid media did not favor hydrolysis and production of flavonoids similarly observed in Figure 4.1. This may be related to the electron donating capacity of citric acid in ionized state, which may have led to the formation of citric acid-catechol esters, thereby limiting catechol hydroxy groups for TFC determination. At ΔEDs of 1.5 kJ/mL, and 3.9 kJ/mL, all TPC (0.45 mg gallic acid equivalent/mg rutin hydrate) were significantly higher than all TFC (0.38 mg catechin/mg rutin hydrate) within each media. This could be related to the increased production of sugars, interfering additively with TPC determination.

4.3.2. Identification and quantification of derivative compounds

The flavonoid compounds identified in water and NaCl media included rutin, isoquercetin, quercetin, and EGCG (also present in the starting rutin). The same compounds and other flavonoid compounds including naringin, morin, and catechin were also detected in citric acid media (Table 4.2), possibly due to enhanced stability of flavonoids in low pH (acidic) during the ultrasonication process. It was reported by Friedman and Jürgens (2000) that rutin, epigallocatechin, and catechin resisted pH (7-11) induced degradation, as a result of relative resonance stabilization of phenoxide ions and quinone oxidation intermediates, and Jurasekova et al. (2014) also reported that quercetin is highly unstable in alkaline solution (pH of 8.6-13.4) due to oxidation. Therefore, in this study, it is possible that ultrasonication combined with the various pH (2.2-6.3) levels either stabilized or enhanced oxidation of the flavonoids. Furthermore, rutin content increased in water media from the

control to 27 kJ/mL by 42%, which is lower than the percentage of TPC increase of 56% (Figure 4.1A). The difference between rutin levels may be related to other unidentified derivative compounds from the HPLC analysis. The unexpected increase in rutin yield above 100% was observed in all ultrasound treated rutin, and in rutin dissolved in 100% methanol. The yield in Tables 4.2, and 4.3 was calculated as (quantified mass in mg of identified compound/starting mass of rutin hydrate in mg)*100. The yield between 130-152% for rutin is not supported by the increase in the TPC and TFC results (Figure 4.1), for example TPC in water at 27 kJ/mL has a yield of 48%. However, TPC or TFC results do not provide individual compound contents. Therefore, it is possible that new compounds of same molecular weight as rutin were formed in the methanolic solutions. Krewson & Naghski (1952) reported the formation of rutin solvates in methanol (rutin methanolates), and in ethanol (rutin ethanolates). They observed an increase in rutin content with the rutin ethanolate cake and mentioned inferior quality of the additional rutin compared to the main rutin crop. However, more details were not provided. The starting rutin in this study was rutin hydrate, and its dissolution in anhydrous methanol may have provided opportunity for methanol molecules to fill cavities in rutin hydrate, and/or the rutin hydrate crystals may have seeded the formation of new crystals.

The increase in rutin content caused by ultrasonication (3.6-36 kJ/mL) in Table 4.2 might be as a result of chiral amplification of rutin crystals. This is a possibility since rutin is an optically active compound. Medina et al. (2011) observed the enantioselective crystallization of DL-threonine (2.7 g in 10 mL of water) during ultrasonication (3 min, 1 cm^2 titanium horn, 20 kHz, 40 W, ice-water bath).

Table 4.2. Yield of derivative compounds from ultrasonication with temperature control

Treatment		Yield of Derivative Compounds (%)						
Media	ED (kJ/mL)	Rutin	Isoquercetin	Quercetin	EGCG	Naringin	Morin	Catechin
Water	0.0	107.71±4.06 ^{d}	0.65±0.06^{fgh}	nd	0.012±0.000^{d}	nd	nd	nd
	3.6	131.59±3.07 ^{c}	0.71±0.05^{defg}	nd	0.028±0.007^{cd}	nd	nd	nd
	9.0	130.02±2.28 ^{c}	0.71±0.01^{defg}	nd	0.013±0.000^{d}	nd	nd	nd
	18.0	148.43±6.37^{ab}	0.82±0.03^{abcde}	nd	0.045±0.013^{c}	nd	nd	nd
	27.0	152.63±5.52^{a}	0.90±0.07^{ab}	0.43±0.08^{b}	0.048±0.007^{c}	nd	nd	nd
	36.0	138.82±7.92^{abc}	0.91±0.01^{a}	nd	0.041±0.000^{cd}	nd	nd	nd
Citric acid	0.0	102.47±6.14 ^{d}	0.52±0.01^{h}	0.34±0.09^{bc}	0.823±0.014^{ab}	2.27±0.02^{b}	0.096±0.002^{a}	0.141±0.002^{a}
	3.6	132.83±0.47^{c}	0.64±0.00^{fgh}	0.84±0.04^{a}	0.848±0.002^{a}	2.79±0.13^{a}	0.102±0.005^{a}	0.100±0.003^{b}
	9.0	134.55±2.46 ^{bc}	0.65±0.02^{fgh}	0.77±0.01^{a}	0.812±0.001^{b}	2.80±0.04^{a}	0.099±0.004^{a}	0.091±0.012^{b}
	18.0	140.17±0.51^{abc}	0.69±0.01^{efg}	0.74±0.01^{a}	0.811±0.013^{b}	2.94±0.03^{a}	0.097±0.001^{a}	0.086±0.008^{b}
	27.0	139.03±1.11 ^{abc}	0.69±0.01^{efg}	0.73±0.02^{a}	0.817±0.003^{b}	2.85±0.27^{a}	0.131±0.048^{a}	0.087±0.006^{b}
	36.0	138.11±0.06 ^{abc}	0.69±0.01^{efg}	0.36±0.00^{b}	0.810±0.005^{b}	2.60±0.08^{ab}	0.164±0.009^{a}	0.092±0.000^{b}
NaCl	0.0	99.99±6.40 ^{d}	0.63±0.07^{gh}	nd	nd	nd	nd	nd
	3.6	134.00±1.05 ^{bc}	0.72±0.01^{cdefg}	0.18±0.01^{c}	0.036±0.003^{cd}	nd	nd	nd
	9.0	135.90±1.40 ^{bc}	0.77±0.04^{bcdef}	nd	0.040±0.004^{cd}	nd	nd	nd
	18.0	139.01±0.63 ^{abc}	0.80±0.01^{abcde}	nd	0.030±0.008^{cd}	nd	nd	nd
	27.0	136.65±0.51 ^{bc}	0.86±0.06^{abc}	nd	0.028±0.008^{cd}	nd	nd	nd
	36.0	136.72±1.35 ^{bc}	0.84±0.02^{abcd}	nd	0.026±0.003^{cd}	nd	nd	nd
100% MeOH	0.0*	143.74±0.58	0.67±0.01	0.66±0.01	0.86±0.01	3.02±0.12	0.10±0.00	0.20±0.00

Energy Density (ED). nd - not detectable. Epigallocatechin gallate (EGCG). Temperatures of 42-55 ºC. $^{a-g}$Means in the same column considering all three media, sharing same letters are not significantly different at p>0.05. *Not included in ANOVA. MeOH: methanol.

Table 4.3. Yield of derivative compounds from ultrasonication without temperature control

Treatment		Yield of Derivative Compounds (%)					
Media	ΔED (kJ/mL)	Rutin	Isoquercetin	Quercetin	EGCG	Naringin	Catechin
Water	0.0	107.71±4.06[b]	0.65±0.06[bc]	nd	0.012±0.000[d]	nd	nd
	0.1	132.91±10.09[a]	0.10±0.02[d]	nd	0.036±0.000[cd]	nd	nd
	0.5	132.01±3.98 [a]	0.70±0.04[abc]	nd	0.020±0.004[cd]	nd	nd
	1.5	138.04±2.85 [a]	0.72±0.01 [abc]	nd	0.035±0.007[cd]	nd	nd
	3.9	140.26±1.34 [a]	0.74±0.00 [abc]	0.25±0.04[e]	0.043±0.000[cd]	nd	nd
	7.0	136.91±3.36 [a]	0.75±0.02 [abc]	nd	0.057±0.006[c]	nd	nd
Citric acid	0.0	102.47±6.14[b]	0.52±0.01[c]	0.34±0.09[e]	0.823±0.014[a]	2.27±0.02[a]	0.141±0.002[a]
	0.1	133.86±1.89 [a]	0.57±0.01[bc]	0.72±0.03[d]	0.439±0.006[b]	2.36±0.28[a]	0.016±0.000[b]
	0.5	137.77±1.42 [a]	0.60±0.01[bc]	0.89±0.05[d]	0.428±0.017[b]	2.47±0.19[a]	0.010±0.000[b]
	1.5	138.26±1.49 [a]	0.71±0.00[abc]	1.35±0.01[c]	0.417±0.022[b]	2.14±0.01[a]	0.020±0.004[b]
	3.9	138.32±7.13 [a]	0.81±0.04[ab]	1.69±0.08[b]	0.416±0.027[b]	2.61±0.12[a]	0.007±0.002[b]
	7.0	142.33±9.70 [a]	0.97±0.06[a]	2.23±0.04[a]	0.415±0.012[b]	2.62±0.27[a]	0.009±0.006[b]
NaCl	0.0	99.99±6.40[b]	0.63±0.07[bc]	nd	nd	nd	nd
	0.1	131.65±5.01 [a]	0.73±0.01[abc]	*traces*	*traces*	nd	nd
	0.5	131.32±1.66 [a]	0.75±0.04[abc]	nd	*traces*	nd	nd
	1.5	140.80±0.59 [a]	0.78±0.01[abc]	*traces*	*traces*	nd	nd
	3.9	138.28±2.51 [a]	0.63±0.27[bc]	nd	*traces*	nd	nd
	7.0	136.78±1.06 [a]	0.82±0.00[ab]	nd	0.002±0.000[d]	nd	nd

Energy Density (ED). nd - not detectable. Epigallocatechin gallate (EGCG). Temperatures of 68-86 °C. 3,4 DHB was detectable in water, at 7.0 kJ/mL as 0.374±0.034%. *traces* means ≤0.002. [a-g]Means in the same column considering all three media, sharing same letters are not significantly different at $p > 0.05$.

The DL-threonine solutions during ultrasonication had crystal nucleation and were enriched with the D-enantiomer (dextrorotatory) of threonine (Medina et al., 2011). Furthermore, the rutin yield also increased for the ultrasound treatment samples, without temperature control (Table 4.3). The increase in temperature from 47 to 86 °C (Table 4.1) might have influenced cavitation effect during the ultrasonication process and also enhanced chiral amplification of rutin. The different pH of media used had no influence on the rutin content.

With respect to yield of isoquercetin, and EGCG, there were no significant differences from the controls within each energy density, and media studied. This was similar for naringin and morin in the citric acid media. However, in the same citric acid media, quercetin yield increased from control as 0.34±0.09% to 0.73±0.02% and 0.84±0.04% at 3.6 kJ/mL and 27 kJ/mL, respectively. At 27 kJ/mL, the quercetin yield reduced to 0.36±0.00% but was not significantly different from quercetin yield produced in water media at 27 kJ/ml, as 0.43±0.08%, and in NaCl media at 3.6 kJ/mL, as 0.18±0.01%. There was loss in catechin yield with ultrasonication on citric acid media, which may be due to degradation of catechin or formation of catechin epimers such as epicatechin (Chen et al., 2001).

A similar trend was observed in rutin yield (Table 4.3) with >30% increase, and no increase in isoquercetin from the control in all media studied. An increase in ΔED increased the production of quercetin in citric acid media from 0.72±0.03% at 0.1 kJ/mL to 2.23±0.04% at 7.0 kJ/mL, which supports the hypothesis of the effect of ultrasonication-citric acid assisted hydrolysis of flavonoids. Similar to Table 4.2, the production of quercetin was observed in water and NaCl media, as 0.25±0.04% and 0.002±0.000%, respectively (Table 4.3), but these lower values indicate that the effect of ultrasonication

with heat was detrimental to quercetin in water and NaCl media. This detrimental effect by heat (86 °C) was also observed for catechin in citric acid media. Therefore, ultrasonication was selective in either the hydrolysis or degradation of compounds, depending on the media. Morin was not detected in any of the media, without temperature control. Also, degradation compounds such as 2,4-dihydrobenzoic acid, 1,2-dihydrobenzene, or 5-(hydroxymethyl) furfural were not detected in any of the media, either with or without temperature control, but 3,4- dihydrobenzoic acid was detected in the water media (Table 4.3).

4.3.3. Antioxidant activities of ultrasound treated rutin

Figure 4.2 shows the FRAP, and DPPH results in each media. There were increases in FRAP from the control to 36 kJ/mL for water and citric acid media (57%), and for NaCl media (55%). These increases correspond to increases observed for TPC in Figure 4.1A. However, at 3.6 kJ/mL, and at 27 kJ/mL, FRAP is favoured in citric acid media above NaCl media. This may be related to more derivative compounds produced in the citric acid media (Table 4.2). The FRAP assay reaction, which is carried out at low pH (3.6), is non-specific to reductants (antioxidants) (Benzie and Strain, 1996). Interferences into the total FRAP include half-reactions with less-positive redox potential that could also drive the reduction of ferric-tripyridyltriazine (Fe^{III} – TPTZ) complex to the ferrous (Fe^{II}) form (Benzie and Strain, 1996). The plummeting effect between 27 and 36 kJ/mL in water media reflects the similar behaviour in TPC and TFC. This may be related to the degradation of compounds (rutin, isoquercetin, quercetin, and EGCG) in water media as ED increased from 27 to 36 kJ/mL (Table 4.2).

The DPPH inhibition effect was the highest at 95%, and not significantly different after 9 kJ/mL among the different energy densities. Positive controls of 0.2 mg/mL and 2.0

101

mg/mL L-ascorbic acid also had 96% and 95% DPPH inhibition effect, respectively. This corresponds to the total identified compounds concentration (~27 mg in 50 mL) from the HPLC results, as 0.54 mg/mL.
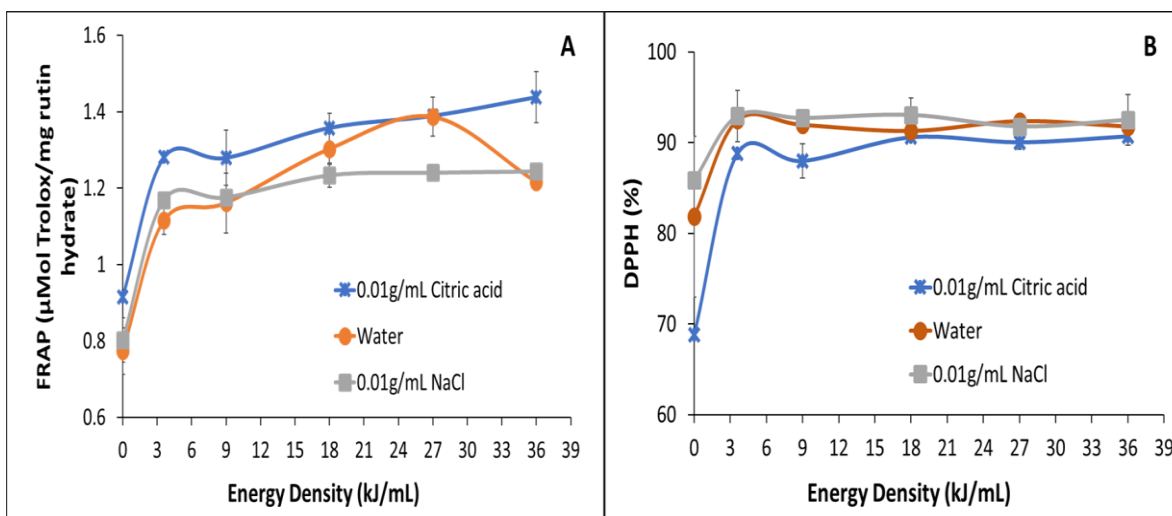
Figure 4.2. Influence of ultrasonication on rutin carried out with temperature control on the FRAP (A) and DPPH (B) antioxidant activities of rutin derivatives.

The ABTS (%) was constant at >99% for control and ultrasound treated rutin samples in water and NaCl media, but ABTS (%) for all ultrasound treated rutin samples in citric acid increased from 45.64±1.55% (control) to 54.29±0.32%. The results indicate that ABTS (%) was not favoured in low pH. The limitations of the different antioxidant capacity assays were discussed earlier by Dudonné et al. (2009) and Magalhães et al. (2008). Ferrous-ion chelating ability for ultrasound treated rutin without temperature control was only observed in citric acid media at 18 kJ/mL (12.34±1.23%), 27 kJ/mL (16.73±0.24%), and 36 kJ/mL (16.46±1.48%). Copper ion chelating ability was also only evident in citric acid samples from the control sample as 42.67±1.22% to 67.97±4.03% at all energy densities. The metal-ion chelating ability observed only in citric acid samples maybe related to the media.

The effect of media on FRAP is more distinct with change in energy density without temperature control (Figure 4.3) compared to the energy densities in Figure 4.2 with temperature control.
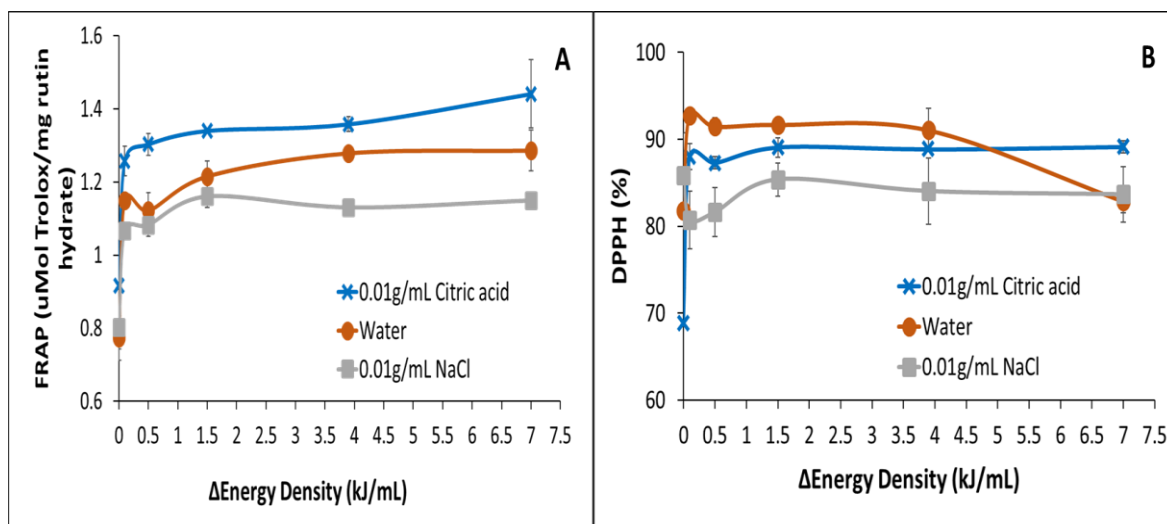
Figure 4.3. Influence of ultrasonication on rutin carried out without temperature control on the FRAP (A) and DPPH (B) antioxidant activities of rutin derivatives.

The FRAP values in the citric acid media may be related to the higher quantity of identified flavonoid compounds compared to the quantified flavonoids in water and NaCl media (Table 4.3). At 15 min (3.9 kJ/mL), and 20 min (7.0 kJ/mL), the NaCl media had the lowest FRAP compared to the other media. FRAP values at 3.9 kJ/mL were 1.36±0.02 µmol Trolox/mg rutin hydrate (citric acid), 1.28±0.00 µmol Trolox/mg rutin hydrate (water), and 1.13±0.02 µmol Trolox/mg rutin hydrate (NaCl). The DPPH (93%) was the highest in water media (0.1-1.5 kJ/mL), but the lowest in NaCl media (85%) from 0.1-3.9 kJ/mL. According to Foti et al. (2004), there are different pathways in which the nitrogen-centered DPPH radical reacts with phenols, either by abstraction of phenol H-atom by the radical, or by an electron-transfer from the phenol to the radical, and either route can be predominant depending on the presence of oxidizing radicals. Therefore, either mechanism may have been a preferential route in these media and contributed to the DPPH results. The

plummeting effect in water media is also evident in DPPH between 3.9 kJ/mL and 7.0 kJ/mL, which is related to lesser flavonoids at 7.0 kJ/mL. The ABTS inhibiting capacity in the control and all ultrasound treated rutin in water and NaCl media were >98%. The ABTS (%) in citric acid samples were not significantly different between 0.1-7.0 kJ/mL as 53.39±1.17% to 57.96±2.08%, from the control 45.64±1.55%. Ferric ion chelating ability without temperature control was only observed in water media at 7.0 kJ/mL, as 47.67±0.90%. This indicates that the presence of phenolic or flavonoid compounds (Table 4.3) at this condition, maybe acting as chelating agents. Chelating agents are chemical compounds with structures capable of linking two or more donor atoms (or sites) to the same metal ion simultaneously to form ring-like structures called chelates or metal complexes (Flora et al., 2015). With respect to copper ion chelating ability observed only in citric acid media, copper ion chelating ability increased from 42.67±1.22% in control to 75.81±2.15%, which was not significantly different between 0.1-7.0 kJ/mL. However, this was higher than the copper chelating ability in ultrasound treated rutin with temperature control as 64.73±2.28-67.95±4.02% between 3.6-36 kJ/mL. These results indicate the influence of temperature on the structure of ultrasound treated rutin derivatives in different media. Iron and copper ions are known to catalyze oxygen radicals that trigger oxidative chain reactions in food systems (Bamdad et al., 2011; Stohs and Bagchi, 1995). Therefore, a system with metal-binding and radical scavenging capacities has dual functionalities. In summary, Table 4.4 shows the media with the highest antioxidant activities based on the different methods.

4.3.4. Specific optical rotation

Rutin hydrate (0.1% w/v) in DMSO, had a specific optical rotation $[\alpha]_D^{20°C}$ of -32.04±3.23° (levorotatory). This was close to -38.38° (levorotatory) in 100% pyridine based on a 0.5% w/v solution reported by Krewson & Naghski (1952).

Table 4.4. Solvent media with antioxidant capacity

Antioxidant assay	Mechanism	Media with the highest antioxidant capacity of ultrasound treated rutin	
		With temperature control	Without temperature control
Ferric reducing antioxidant power	Reduction of Fe^{3+}-TPTZ to Fe^{2+}	Citric acid	Citric acid
DPPH radical scavenging	Reduction of radical	NaCl and water	Water
ABTS$^{•+}$ radical scavenging	Reduction of radical	NaCl and water	NaCl and water
Ferric ion chelating	Fe^{2+}-binding	Citric acid	Water
Copper ion chelating	Cu^{2+}-binding	Citric acid	Citric acid

FRAP, DPPH, and ABTS$^{•+}$ assays are based on electron transfer (Huang et al., 2005).

Rutin hydrate (0.1% w/v) in methanol showed both levorotatory $[\alpha]_D^{20°C}$ of -26.31±11.62°, and dextrorotatory $[\alpha]_D^{20°C}$ of +7.59±0.36° compounds. The presence of both levorotatory and dextrorotatory compounds was also observed at higher concentration of rutin hydrate in anhydrous methanol solution (0.3% w/v, -4.06±2.08°, and +0.80±0.38°). However, rutin showed only dextrorotatory compound $[\alpha]_D^{24°C}$ of +4.63°, in 99.8% methanol, based on 0.5% w/v solution (Krewson & Naghski, 1952). In this study, rutin hydrate (0.1% w/v) in ethanol showed only dextrorotatory $[\alpha]_D^{20°C}$ of +33.83°±7.25, and +13.29°±0.90, but at different magnitudes. These results in methanol, and ethanol indicate that the control (rutin hydrate) contain both levorotatory and dextrorotatory enantiomers. The specific rotation of rutin hydrate in ethanol (0.1% w/v), is similar to $[\alpha]_D^{23°C}$ of +13.82°

of rutin in ethanol according to the report by Khalifa et al. (1983). They also reported a Deca-methyl derivative of rutin in ethanol with $[\alpha]_D^{19°C}$ of -33°.

Further analysis of optical rotation on the ultrasound treated rutin (UTR) was carried out in 0.5% w/v solution in DMSO. The DMSO solvent was chosen to avoid the variations observed in methanol, or ethanol. Also, the manufacturer's description was that rutin hydrate was soluble in DMSO. Figure 4.4. shows that rutin is optically active, its chiral molecules (two forms of the same material) may have influenced the HPLC results (Tables 4.2 and 4.3). It should be noted too, that other optically active compounds present in the solutions like glucose may have contributed to the optical rotation of the rutin solutions. Ultrasound treated rutin at 27 kJ/mL in water, citric acid, and at ΔE=3.9 kJ/mL in citric acid were not significantly different from the control (Figure 4.4A). This might indicate that these samples have same amount of rutin enantiomers.
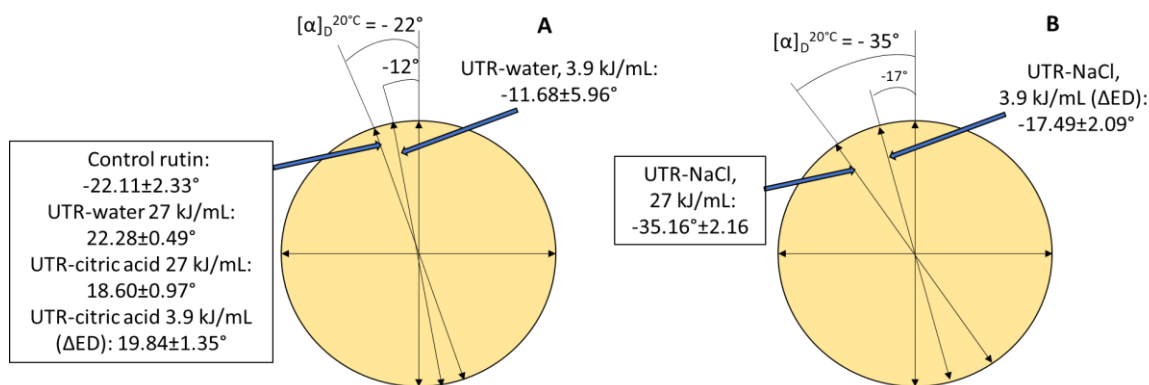
Figure 4.4. Specific optical rotation of plane polarised light by rutin hydrate and ultrasound treated rutin in different media. 0.5% w/v solution in DMSO (A), 0.23% w/v solution in DMSO (B).

*Angles not drawn to scale.

The UTR at ΔE=3.9 kJ/mL in water contained a higher number of levorotatory rutin ($[\alpha]_D^{20°C}$ of +11.68±5.96°. It is possible that dextrorotatory rutin was also present at this condition which cancelled out some of the levorotatory rutin. However, for the UTR in 0.01

g NaCl, the optical rotation measurement was not possible with 0.5% w/v solution in DMSO because of the insoluble NaCl crystals in DMSO and possible increased concentration of the filtrate. Therefore, UTR in NaCl at 27 kJ/mL, and at ΔE=3.9 kJ/mL, was diluted with DMSO to 0.23% w/v solution before optical rotation measurements. Figure 4.4B shows that the quantity of levorotatory enantiomers in UTR NaCl was higher at ΔE=3.9 kJ/mL (86 °C) than at 27 kJ/mL (47 °C). Similar to UTR in water, the UTR in NaCl at ΔE=3.9 kJ/mL might contain dextrorotatory molecules.

4.4.   Conclusions

The application of ultrasonication treatment on rutin hydrate at 3.6-36 kJ/mL (with temperature control, 47 °C), and without temperature control (86 °C) resulted in increased total phenolic and total flavonoid contents. There was also an increase in rutin derivatives including rutin (131-152%), and quercetin (0.18-2.23%). The effect of citric acid as a media was observed in the identification of flavonoids such as naringin, morin and catechin. The water media was selective to produce quercetin, at 600 W, and 15 min (27 kJ/mL or 3.9 kJ/mL, ΔED) irrespective of temperature control (47 and 86 °C). However, the behavior of derivative compounds in different media varied with the antioxidant activity assays because of the specific principles involved in the assay measurements, and/or the structure of the modified rutin. The specific optical rotation of the rutin solutions indicated the presence of levorotatory and dextrorotatory enantiomers.

Chapter 5. Effect of ultrasonication on rutin: Characterization of insoluble fractions and effects in barley starch pyrodextrin[3]

5.1. Introduction

Ultrasonication is a processing technique characterized by the mechanical disintegration of crystals, particles, and substrates, via sound energy in a liquid medium. During ultrasonication, sound waves in the liquid result in regions of pressure differences, within which gas bubbles are formed. The gas bubbles grow and implode on the particles in the liquid, a phenomenon known as cavitation (Zhu, 2015b). Due to the cavitation principle, ultrasonication has gained attention as a top-up method for particle size reduction in the production of pharmaceutical nanosuspensions for enhanced dissolution rate and oral bioavailability of hydrophobic drugs (Phaechamud and Tuntarawongsa, 2016; Antunes et al., 2013; Liu et al., 2012).

The top-up technique, which utilizes mechanical and heat energy to impact or shear surface properties was reported in the ultrasonication of febantel (Antunes et al., 2013). Antunes et al. (2013) employed an indirect contact of titanium tip operating at 20 kHz and 20 W/cm^2 with the aqueous drug via a glass wall. The aqueous drug inside in a glass tube was surrounded by an ambient water-cooling system via which ultrasonic waves was transmitted from the tip to the aqueous drug suspension. Febantel (232 μm) was reduced to 0.1-10 μm at an operating time of 60 min. Other studies on direct ultrasonication of drug suspensions include the production of irbesartan nanocrystals using 20-23 kHz, and 50% amplitude for 5 min to produce 146-320 nm of freeze-dried powder (Sridhar et al., 2016), and nanocrystals formulation containing ezetimibe using 20% power, for 1 min to reduce

---

[3] A version of this chapter will be submitted Ekaette, I., and Saldaña, M.D.A. Ultrasound treatment for production of rutin nanocrystals. Food Research International.

ezetimibe from 6432±1024 nm to 1736±88 nm (Gulsun et al., 2011). However, these latter reports did not indicate the use of either a cooling system, or a temperature control system such as ice bath for the ultrasonication process employed. In the bottom-up techniques, which involve controlled molecular self-assembly of dissolved drug components in organic solvents, Liu et al. (2012) utilized anti-solvent precipitation with ultrasonication at 400 W, 15 min, and 10 °C (temperature control with ice bath), to produce flake-shaped, amorphous, mean size 212 nm carvedilol nanosuspensions. Also, Phaechamud and Tuntarawongsa (2016) produced ibuprofen nanosuspension (331 nm) utilizing a combined method of eutectic emulsion solvent evaporating with ultrasonication (amplitude 50%, 30-second on, and 2-second off pulse, and 30 min) using an ice bath for temperature control. These ultrasonication methods for nanosuspensions have been employed on synthetic drug compounds, but not on naturally occurring polyphenols like flavonoids.

Rutin, also known as quercetin-3-O-rutinoside, is a dietary flavonoid that contains the flavonol quercetin and a disaccharide rutinose. Rutin is abundant in buckwheat grains and leaves (Ahmed et al., 2013), and green teas (Jeszka-Skowron et al., 2015) and exhibits pharmacological activities including antioxidant, antiviral, anti-inflammatory, and anticancer properties (Chua, 2013). Rutin, being poorly soluble in water at 13 mg/100 mL (Khalifa et al., 1983; Krewson and Naghski, 1952), is often complexed with cyclodextrins to enhance its oral delivery (Paczkowska et al., 2015).

Pyrodextrinization is the dry heating of starch at 90-180 °C, either with or without acid to produce lower molecular weight, cold-water soluble and lower viscosity products compared to the parent material (Lin et al., 2018; Bai and Shi, 2016). Chemical reactions during pyrodextrinization are hydrolysis, transglycosidation, and repolymerization producing highly branched pyrodextrins with new glycosidic linkages such as α-1,6, β-1,6,

α-1,2, and β-1,2 (Han et al., 2018; Bai and Shi, 2016). In the application of pyrodextrins for drug release, pyrodextrinized rice starch produced at 130 ºC, 0.5% HCl, 0.5% citric acid, and for 1-3 h, was further heat-moisture treated (HMT) at 115 ºC, for 1 h, and the final product was used as a wall material in the encapsulation of tocopheryl acetate via spray drying (Subpuch et al., 2016). However, to the best of my knowledge, interactions between pyrodextrins and rutin have not been studied. It was hypothesized that the presence of nanosized rutin in the reactions to form pyrodextrins (hydrolysis, transglycosidation, and repolymerization) might influence the new linkages and structures of pyrodextrin. Therefore, the objectives of this study were to: 1) characterize rutin treated at constant ultrasonication power of 600 W, for 15 min in water, citric acid and NaCl media, and for 20 min in water, and 2) understand rutin interactions with barley starch pyrodextrin. The conditions of 15, and 20 min were the extreme conditions evaluated in Chapter 4.

5.2.   Materials and Methods

5.2.1. Materials

Rutin hydrate (purity ≥94%), citric acid, sodium chloride, isoquercetin, quercetin, epigallocatechin gallate, catechin, naringin, 1,2-dihydrobenzene, 2,4-dihydrobenzoic acid, 3,4-dihydrobenzoic acid, 4-dihydrobenzoic acid, 5-(hydroxymethyl) furfural, trisodium trimetaphosphate, 2,2'-azino-bis(3-ethylbenzothiazoline-6-sulphonic acid (ABTS), and potassium persulfate were purchased from Sigma Aldrich (Oakville, ON, Canada). Methanol was purchased from Fisher Scientific (Ottawa, ON, Canada), hesperidin was purchased from Fisher Scientific (Ottawa, ON, Canada), other chemicals were of analytical grade and solvents were of high-performance liquid chromatography (HPLC) grade.

Waxy barley white flour was provided by GrainFrac Inc. (Edmonton, AB, Canada). Megazyme total starch kit was purchased from Megazyme International Ireland Limited (Wicklow, Ireland).

5.2.2. Methods

5.2.2.1. Preparation of insoluble fraction

The ultrasonication process was carried out according to the method described in Chapter 4, Section 4.2.2.1. Briefly, a high intensity ultrasonics processor (Model FS-1200N, Shanghai Sonxi Ultrasonic Instrument Co., Shanghai, ZJ, China) with a 20 mm diameter probe at 20 kHz was utilized for the experiments. Rutin hydrate (20±0.9 mg) was mixed with 20 mL of the desired solvent: deionized water, 0.01 mg/mL citric acid, and 0.01 mg/mL sodium chloride, NaCl. The suspension was transferred to either an ice-water bath (with temperature control) or without the ice-water bath (without temperature control). The suspensions were subjected to ultrasound-treatment at 600 W for 15 min (deionized water, citric acid and NaCl), and 600 W for 20 min (deionized water). These conditions were the extreme conditions (27 and 36 kJ/mL) in the experimental design of Chapter 4, Section 4.2.2.1. The ultrasound-treated rutin (UTR) samples were left to crystallize for 24 h at 4 °C. The UTR samples were centrifuged at 2325 g for 5 min. The recovered residue was freeze-dried, and the dried samples stored with light protection at room temperature (23 °C). The preparation of insoluble fraction was carried out in triplicates. The Energy Density (ED) was calculated according to Equation 5.1 for the samples 'with temperature control' and Equation 5.2 for the samples 'without temperature control'.

$$\text{Ultrasound Energy Density (ED)} = \frac{\text{Power (W) x Time (s)}}{\text{Volume (mL)}} \qquad (5.1)$$

$$\text{Change in Ultrasound ED } (\Delta ED) = \frac{\text{Power (W) x Time (s)}}{\text{Final Volume (mL)}} - \frac{\text{Power (W) x Time (sec)}}{\text{Initial Volume (mL)}} \qquad (5.2)$$

5.2.2.2. Zeta potential

Ultrasonication of rutin in water media was carried out at 27 kJ/mL, and 36 kJ/mL. The colloidal suspensions of rutin were measured for zeta potential using disposable folded capillary cells (Zetasizer nano series, Malvern Instruments, Malvern, UK). The Zeta potential and size was measured at 25 °C in a Zetasizer (Malvern Instruments, Malvern, UK).

5.2.2.3. Transmission Electron Microscopy (TEM)

Diluted solution of ultrasound treated rutin in water media, was placed on regular grids without support film, and transmission electron microscopy was carried out using a Philips – FEI Transmission Electron Microscope (Model, Morgagni 268, FEI Company, Hillsboro, Oregon, USA) operating at 80 kV. The images were captured using a Gatan Orius CCD camera, and collected using a Gatan DigitalMicrograph™ Ver. 1.81.78 software.

5.2.2.4. Identification and quantification of rutin and derivatives by High Performance Liquid Chromatography (HPLC)

The freeze-dried UTR was dissolved in ethanol (1 mg/mL) as the stock solution. The stock solution (2.5 mL) was diluted to 10 mL with 60% methanol. The HPLC analysis was carried with the same method described in Chapter 4 (Section 4.2.2.4). Aliquots of UTR methanolic solutions were filtered using a Basix 0.2 μm nylon syringe filter into amber HPLC vials and injected into a Shimadzu LC 20 Prominence 20 (Agilent Technologies, Santa Clara, CA, USA) system consisting of an autosampler, a column oven set at 30 °C, and a diode array detector. Calibration curves were fitted for standard solutions

of rutin, isoquercetin, quercetin, and epigallocatechin gallate. Determination of individual compounds concentrations was carried out in triplicates and reported based on UTR stock solutions.

5.2.2.5. Color analysis

The yellowness index (YI) and greenness values of control rutin hydrate and freeze-dried UTR, in ethanolic stock solutions (1 mg/mL) were compared with a Hunter Lab colorimeter (CR-400/CR-410, Konica Minolta, Ramsey, NJ, USA) using D65 illuminant, opening of 14 mm, and 10° standard observer, according to the ASTM D2244 method (ASTM, 2011). The colorimeter was calibrated with a white reference plate (L* = 93.49, a* = −0.25, b* = −0.09). Lightness, chroma and hue were measured for the samples and the total color difference (ΔE), and yellowness (YI) were calculated according to Boun and Huxsoll (1991) described in Chapter 3 (Section 3.2.2.6.6). Greenness values as (-a) were reported.

5.2.2.6. Morphology and elemental analysis

A Tagarno FHD prestige digital microscope, 660X magnification (Horsens, Denmark) was used to capture the physical appearance of the freeze-dried UTR samples. Surface analysis including the morphology and elemental compositional analysis of the freeze-dried UTR samples were also assessed using a Zeiss Sigma 300 VP Field Emission Scanning Electron Microscope coupled with Energy Dispersive X-ray (SEM/EDX) Spectroscopy (Carl Zeiss AG, Oberkochen, Germany).

5.2.2.7. Thermal behavior

The thermal behaviour of the freeze-dried UTR samples was studied with a Differential Scanning Calorimeter (DSC), Universal V4.7A TA Instrument, DSC Q100

V9.8 Build 296 (New Castle, DE, USA). The system was calibrated using indium as the reference standard. Rutin/UTR powder sample (1.5-6 mg) was placed in an aluminium pan and purged under a nitrogen flow rate of 50 mL/min, then heated from 25 to 210 ℃ at a heating rate of 10 ℃/min.

5.2.2.8. Application of UTR samples in barley starch pyrodextrinization

5.2.2.8.1. Barley starch pyrodextrinization

Waxy barley white flour (>99% amylopectin) was wet processed for starch isolation according to the method described in Chapter 3, Section 3.2.2.1. Pyroconversion of barley starch isolate with total starch content of 95.84±1.56% dm mixed with rutin was carried out according to Orozco-Martínez and Betancur-Ancona (2004) with slight modifications. In a 30 mL bootex crucible, 0.5 mL of 1 mg/mL ethanolic solution (control rutin hydrate, or freeze-dried UTR in absolute ethanol) was added to barley starch isolate (3 g). Then, 3 mL of 2.2 M HCl was added, the mixture was stirred for 1 min using a spatula, and quantitatively rinsed off with 2 mL ethanol. The mixture was covered with a crucible lid and left to react for 24 h at room temperature (23 ℃). The hydrolyzed starch in the crucible was transferred to a convection oven at 90 ℃ for 1 h. The final product was a light-yellow to brown coloured syrup, which was left to cool in a desiccator. The barley starch-rutin, and barley starch dextrinized syrups were stored at -18 ℃ until further analysis. Pyrodextrinization of barley starch was carried out in triplicates.

5.2.2.8.2. Soluble starch determination and reducing end group assay

The hydrolysis of barley starch by the pyrodextrinization process was verified by determination of total starch content in the final syrups according to the Megazyme total starch assay procedure for soluble starch. The total starch content in total syrup volume was

presented in grams (g). Reducing end group was determined according to the method described by Imoto and Yagishita (1971). Briefly, 0.45 mL of the sample was mixed with 0.6 mL of 0.5 g/L potassium ferricyanide solution containing 0.5 M sodium carbonate. The mixture was transferred to boiling water bath and heated for 15 min, after cooling, the absorbance was read at 420 nm. Reducing end yield was presented as mg glucose equivalent/ mL dextrin syrup.

5.2.2.8.3. Antioxidant activity by ABTS inhibition assay

The ethanolic supernatant from the soluble starch determination was analysed for antioxidant activity using the ABTS inhibition assay according to Dudonné et al. (2009) with slight modifications. Firstly, 10 mL of 7 mM ABTS stock solution was mixed with 10 mL of 2.45 mM potassium persulfate and placed in an amber bottle. The mixture was left in the dark to stabilize for 14 h and form the ABTS cation (ABTS$^{\bullet+}$) solution. Thereafter, the ABTS$^{\bullet+}$ solution was diluted with deionized water to an absorbance of 0.70 ±0.02 read at 734 nm. In the assay, 3.0 mL of diluted ABTS$^{\bullet+}$ solution was added to 0.1 mL of the ethanolic extract from dextrins. The mixture was mixed for 5 s and incubated at 30 °C for 10 min. The blank used was 90% ethanol. Positive controls used were serial dilutions of BHA in 90% ethanol (0.02–0.2 mg/mL). Absorbance based on decolorization of the ABTS cation was measured at 734 nm using a Jenway Genova spectrophotometer (Stone, Staffordshire, UK). Analysis was carried out in triplicates. The inhibition percentage was calculated using Equation 5.5:

Inhibition (%) = 1- (A$_S$/A$_B$) x 100 (5.5)

where, As is absorbance of the UTR sample, and A$_B$ is the absorbance of the blank solution.

5.2.2.8.4. HPLC determination of malto-oligosaccharides

Pyrodextrinized syrup was diluted (1 mL to 50 mL) using deionized water. The pH of the hazy acidic solution (pH 2), was then modified to pH 6, using 1 M Na_2CO_3. Samples were filtered through a 0.2 µm nylon syringe filter into glass vials and injected into a HPLC system.

The determination of malto-oligosaccharides was carried out using a Shimadzu-10A HPLC system equipped with a Shimadzu RID-10A refractive index detector set at 40 °C, an autosampler Shimadzu SIL-10A set at 25 °C and a column heater EchoTherm™ CO20 (Torres Pines Scientific, La Jolla, CA, USA). The separation was carried out with an Aminex ® HPX-42A column, 300 mm x 7.8 mm coupled with a Micro-Guard De-Ashing guard column (Bio-rad Laboratories, Hercules, CA, USA). The mobile phase was deionized water (Fisher Scientific, Ottawa, ON, Canada) set at 85 °C. The elution was in isocratic mode at a flow rate of 0.3 mL/min. The injection volume was 10 µL and the total run time was 50 min.

Peak identification was performed using the following standards: glucose, maltose, maltotriose, maltotetraose, maltopentaose, maltohexaose, and maltoheptaose from Sigma Aldrich (Oakville, ON, Canada). Glucose and malto-oligosaccharides were quantified by comparing peak areas to a standard curve of each compound. Standard curves were generated by plotting the area against the concentration (serial dilutions) of standards.

5.2.3. Statistical analysis

All experiments were carried out in at least duplicates. The data obtained were analyzed by One-way Analysis of Variance (ANOVA) using Minitab 18 statistical software

(Minitab Inc., State College, PA, USA), and values were reported as mean ± standard deviation, comparing the means for significant differences at $p < 0.05$ by Tukey's test.

5.3. Results and Discussion

5.3.1. Physical appearance of UTR before freeze-drying

The ultrasound treatment in water formed colloidal solutions of rutin (Figure 5.1.) which might indicate the presence of charged ions from the ultrasonication in water (Bermudez-Aguirre, 2017), and the formation of charged rutin nanoparticles. Recrystallized rutin in the citric acid and NaCl media (at 47 ºC), and in water (at 86 ºC) sedimented. Rutin in citric acid and NaCl treated with heat (at 86 ºC) showed needle-like shapes by visual observation. Khalifa et al. (1983) also reported the appearance of rutin as pale-yellow needles. The shape and height of the recrystallized sediments might indicate structural change of rutin. Mass of freeze-dried UTR varied from 13 to 28 mg.
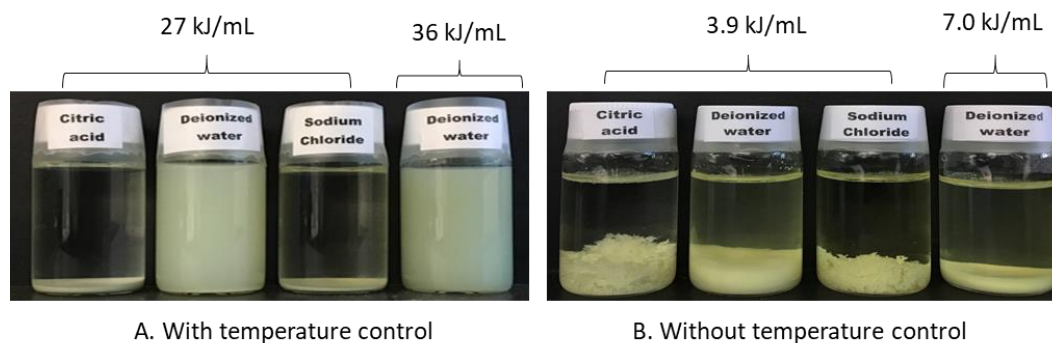
Figure 5.1. Recrystallized rutin in aqueous citric acid (0.01g/mL), deionized water, and aqueous sodium chloride (0.01 g/mL), after ultrasonication, with temperature control (A), and without temperature control (B).

5.3.2. Zeta size and potential

The colloidal suspensions (Figure 5.1A) of UTR in water, at 15 min (27 kJ/mL), had a zeta size of 820.15±9.26 nm (Polydispersity index, 0.378), and zeta potential of -43.7±1.27 mV. The UTR in water, at 15 min (36 kJ/mL), which had a zeta size

287.40±17.25 nm (Polydispersity index, 0.354), and zeta potential of -29.4±1.56 mV. The lower the negative zeta potential (surface charge velocity), the more stable the colloidal suspension. These results indicate that the longer ultrasonication duration (20 min), created more cavitation impact on particle size reduction, but fewer negative charge on the particles. The hydroxide ions (OH$^-$) produced during ultrasonication may have participated in the formation of oxygen gas (Bermudez-Aguirre, 2017).

5.3.3. Transmission Electron Microscopy (TEM)

Rutin particles from the colloidal suspensions in water (Figure 5.1A) were further studied by TEM (Figure 5.2). In Figure 5.2A, the particles are separate from one another showing different shapes and sizes. The particles in Figure 5.2B are stringed together and appears to be part of the particle breaking off from the parent particle. In Figure 5.2C, the interior of the 'rutin' particle is made up of a network of fine threads wound together like a web. The thin longitudinal particles to the top left corner (Figure 5.2C) may be the smaller sized particles breaking off from the web of threads.

Control (rutin hydrate)   Ultrasound treated rutin in water   Ultrasound treated rutin in water
(27 kJ/mL)   (36 kJ/mL)
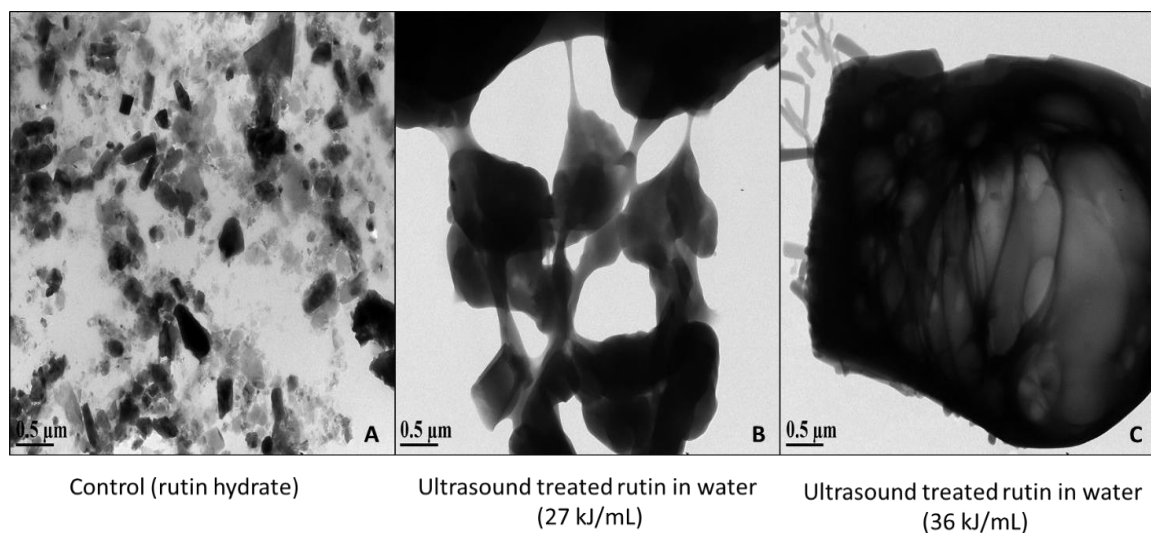
Figure 5.2. Transmission Electron Microscope images of rutin hydrate (A), and ultrasound treated rutin in water for 15 min, 27 kJ/mL (B), and for 20 min, 36 kJ/mL.

5.3.4. Composition of insoluble fraction (freeze-dried UTR) by HPLC

The flavonoid compounds identified in the untreated rutin hydrate, and the insoluble fractions (with and without temperature control), were rutin (1.0-1.4 mg/mL), isoquercetin (0.005-0.010 mg/mL), quercetin (0.01-0.02 mg/mL), and epigallocatechin gallate (0.01-0.02 mg/mL). However, epigallocatechin gallate was not observed in the insoluble fraction of UTR water at 27 kJ/mL. Epigallocatechin gallate produced at this treatment condition may have been carried in free form with the water-phase supernatant. This is because the solubility of epigallocatechin gallate in water is 20 mg/mL (Nguyen et al., 2017), therefore epigallocatechin gallate identified in the insoluble fractions may have been bound to other flavonoids. Quercetin was identified in the insoluble fractions of UTR water, 36 kJ/mL and 7.0 kJ/mL, and NaCl, 27 kJ/mL, 3.9 kJ/mL, which were not observed in the methanolic solutions in the previous study (Chapter 4, Table 4.2, and Table 4.3). It is possible that the methanolic solutions were over-diluted, and therefore the quantifiable quercetin was below the detection limit.

5.3.5. Color of ethanolic solution and physical appearance of freeze-dried UTR

All ethanolic solutions of UTR at 36 kJ/mL (water media) and 27 kJ/mL showed greenish color with (a) values of -1.9±0.4 (control); -3.1±0.2 (water, 36 kJ/mL); -3.2±0.1 (NaCl); -2.7±0.3 (water), and -1.8±0.0 (citric acid). The greenish colors of UTR samples including the control were not significantly different. However, the control and UTR-citric acid were significantly different from other UTR samples in both ΔE, and YI (Figure 5.3A). In the freeze-dried solid form (Figure 5.4A), the control was yellow, and the UTRs were deep green.

Total colour differences (ΔE) were 3.83±0.07 (control), 4.28±0.71 (UTR-citric acid), and 7.44±0.19 (UTR-NaCl). Yellowness indices (YI) were 7.63±0.13 (control), 8.20±0.96 (UTR-citric acid), and 12.89±0.32 (UTR-NaCl). The ΔEs and YIs were highly correlated with Pearson's correlation coefficient (r=0.999, and P value=0.00). The greenness, ΔE, and YI could be a result of structure change in rutin during the ultrasound treatment.
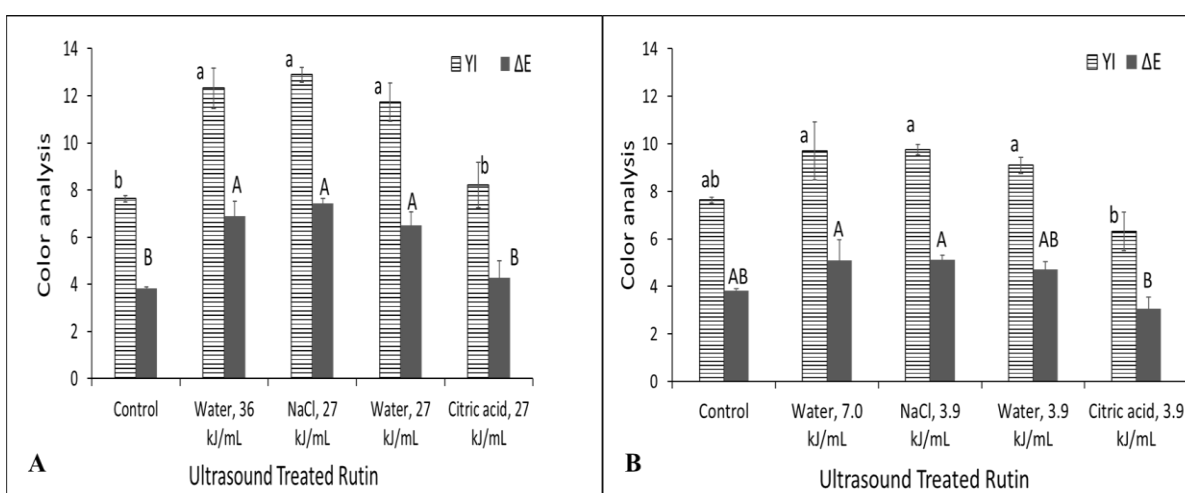
Figure 5.3. Yellowness index (YI), and total color difference (ΔE) of insoluble fractions obtained after ultrasonication treatment of rutin, with temperature control (A) and without temperature control (B).

(Values within each graph that share same lowercase letters (a-b) are not significantly different at p>0.05. Values within each graph that share same uppercase letters (A-B) are not significantly different at p>0.05).

Generally, flavonoids with different structures are associated with different colors, which are developed during natural biosynthesis or altered by engineering the biosynthetic pathway of transgenic plants (Winkel-Shirley, 2001). Structure-related color changes in flavonoids may be from the addition of sugars, methyl, or ferulate groups (Winkel-Shirley, 2001), pH and metal-complexation (Panhwar and Memon, 2014). It was reported that dilute solutions of rutin showed dark green color when added to ferric chloride (The Merck Index, 2006; Sando and Lloyd, 1924). This green color reaction might be related to the chelating

or electron donation of rutin to ferrous ion, which can be inferred from Figure 5.4 A, or water and citric acid UTR are 'oxidized' derivatives of rutin. Free radicals produced during ultrasonication may have been scavenged by rutin. The greenish-yellow UTR (Figure 5.4A) might also indicate the extent of anti-oxidation reactions of rutin during the ultrasonication process. However, the UTR-citric acid had same yellowness index as the control rutin, which may indicate the presence of stable rutin structure. In this study, since the ultrasound probe was used directly, there might have been metal contamination in the UTR.
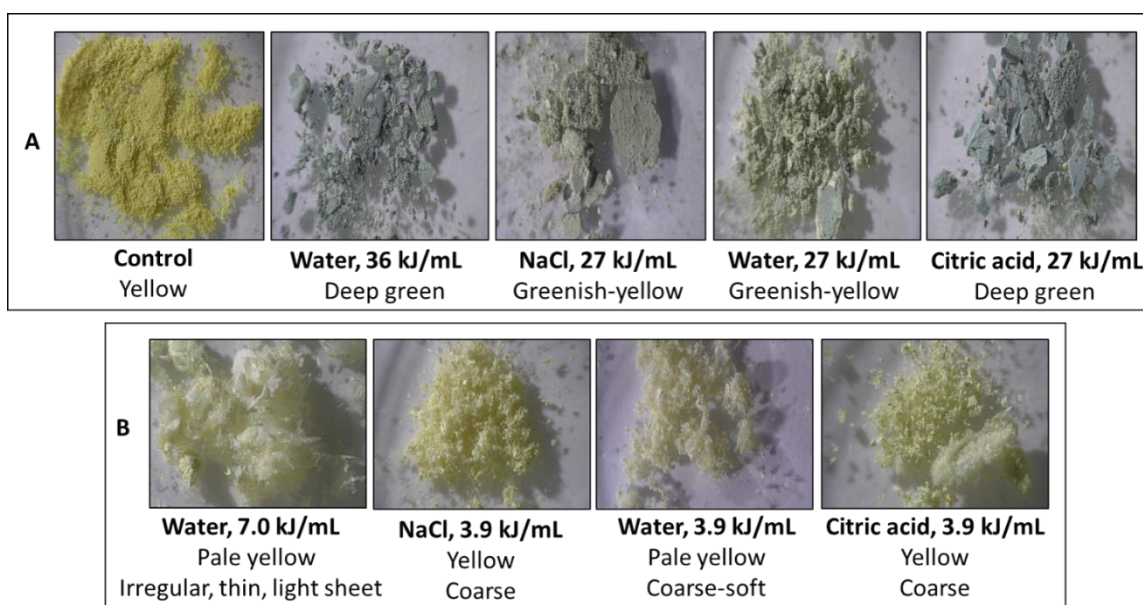
Figure 5.4. Physical appearance of rutin hydrate powder (control) and the insoluble fractions from ultrasound treatments of rutin in different solvents, with temperature control (A) and without temperature control (B).

The ultrasound treatment with ΔED at 0.1-7.0 kJ/mL did not have significant effects on the yellowness index, total color difference (Figure 5.3B) and greenness of the UTR samples. Greenness values were -2.24±0.09 (water, 7.0 kJ/mL); -2.24±0.03 (NaCl); -1.81±0.40 (water), and -1.39±0.20 (citric acid). The rise in temperature from 47 °C (with temperature control) to 86 °C (without temperature control) may have minimized the cavitation effect during the process (Paniwnyk et al., 2001). Therefore, the structural

modification of rutin may have been greatly influenced by heat and less by cavitation. This may explain the stable yellow color of the freeze-dried UTR after 86 °C (Figure 5.4B), and UTR-citric acid after 47 °C (Figure 5.3A).

5.3.6. Surface morphology and elemental analysis

The scanning electron micrographs (Figure 5.5) show particle morphology of the control (rutin hydrate) (A-B). The surface of the particle (B) is masked with a coating layer. The UTR particles shown in (A) are stacks of broken fragments or smaller particles of rutin held together possibly by van der Waals forces.
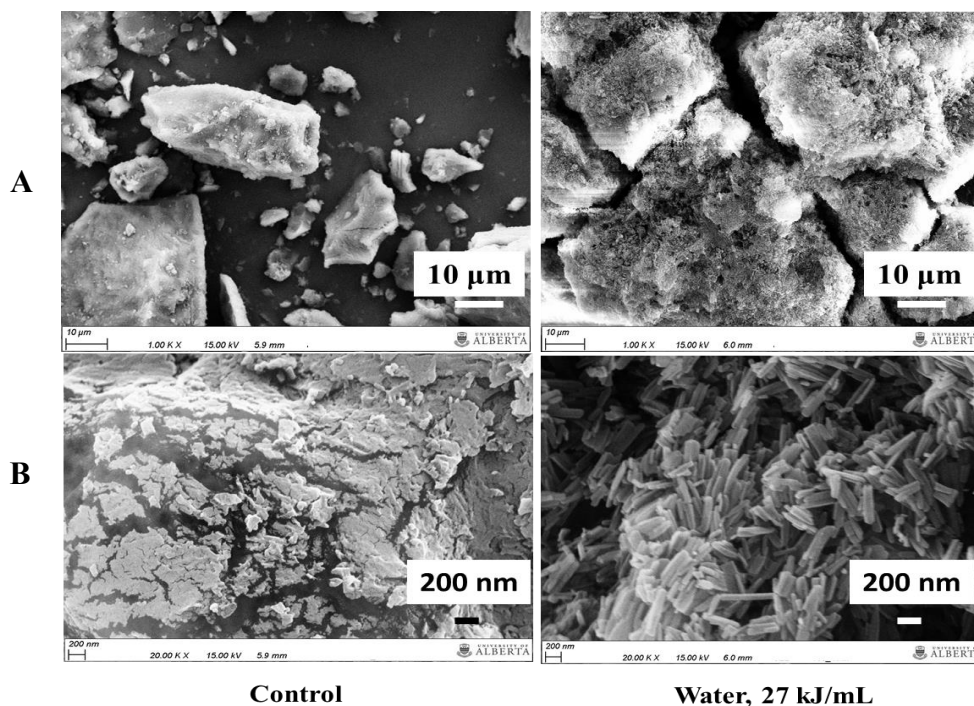
Figure 5.5. Scanning Electron Microscopy images of rutin and ultrasound treated rutin powder with temperature control: Powder particles (A, 1KX magnification), Lone/agglomerated particle(s) and Lone/agglomerated particle(s) (B, 20KX magnification).

These stacks of particles (A-B) show that the individual fragments are slender, longitudinal, stick like shapes with widths <200 nm. Scanning electron micrographs of fragmentary, and stick shape crystals were reported for rutin in ethanol (Peng et al., 2009).

Raw rutin was first treated in boiling water twice for recrystallization and vacuum-dried at 135.05 °C for 12 h, followed by dissolution in ethanol (Peng et al., 2009). It is possible that the mechanical disintegration of rutin by ultrasound energy at 27, and 36 kJ/mL reduced rutin into smaller sized rutin and derivatives particles. Fragmented UTR was also observed for water at 36 kJ/mL, and citric acid, and NaCl at 27 kJ/mL treatment conditions (not shown) but are similar in description to images in Figure 5.5. The Energy-Dispersive X-ray spectroscopy (Table 5.1) indicates presence of sodium, chlorine, aluminium and titanium in the samples. The presence of aluminium and titanium may be from the ultrasound probe and could have interfered with rutin reactions by forming rutin-metal complexes (Malešev and Kuntić, 2007). Sodium and chlorine elements may be impurities from the starting rutin sample.

Table 5.1. Energy-Dispersive X-ray spectroscopy on ultrasound treated rutin powders

Treatment	Elements (wt %)					
	Carbon	Oxygen	Sodium	Chlorine	Aluminium	Titanium
Control	54.2	45.7	nd	nd	nd	nd
Water, 36 kJ/mL	53.6	42.5	nd	nd	0.3	3.5
NaCl, 27 kJ/mL	51.6	39.5	1.9	2.8	0.3	3.9
Water, 27 kJ/mL	58.1	38.5	1.5	1.8	nd	nd
Citric acid, 27 J/mL	49.2	44.8	nd	nd	0.3	5.6
Water, 7.0 kJ/mL	54.8	45.2	nd	nd	nd	nd
NaCl, 3.9 kJ/mL	53.9	45.6	0.2	0.3	nd	nd
Water, 3.9 kJ/mL	55.6	44.4	nd	nd	nd	nd
Citric acid, 3.9 J/mL	49.3	48.7	0.6	0.5	nd	0.9

*nd, not detectable.

Figure 5.6A showed that the UTR without temperature control (86 °C) lost the granule-like particle shape of the control (Figure 5.5). The loss of shape was more extreme with UTR-water at 7.0 kJ/mL with numerous undefined boundaries. This extreme thermal effect at this condition may refer to the absence of interference of solutes compared to other media. In Figure 5.6B, the UTRs were made up of multiple agglomerates of thin-long fibre

strands, some of which appeared as thick sheets (NaCl, water, 3.9 kJ/mL), and clumps (citric acid).
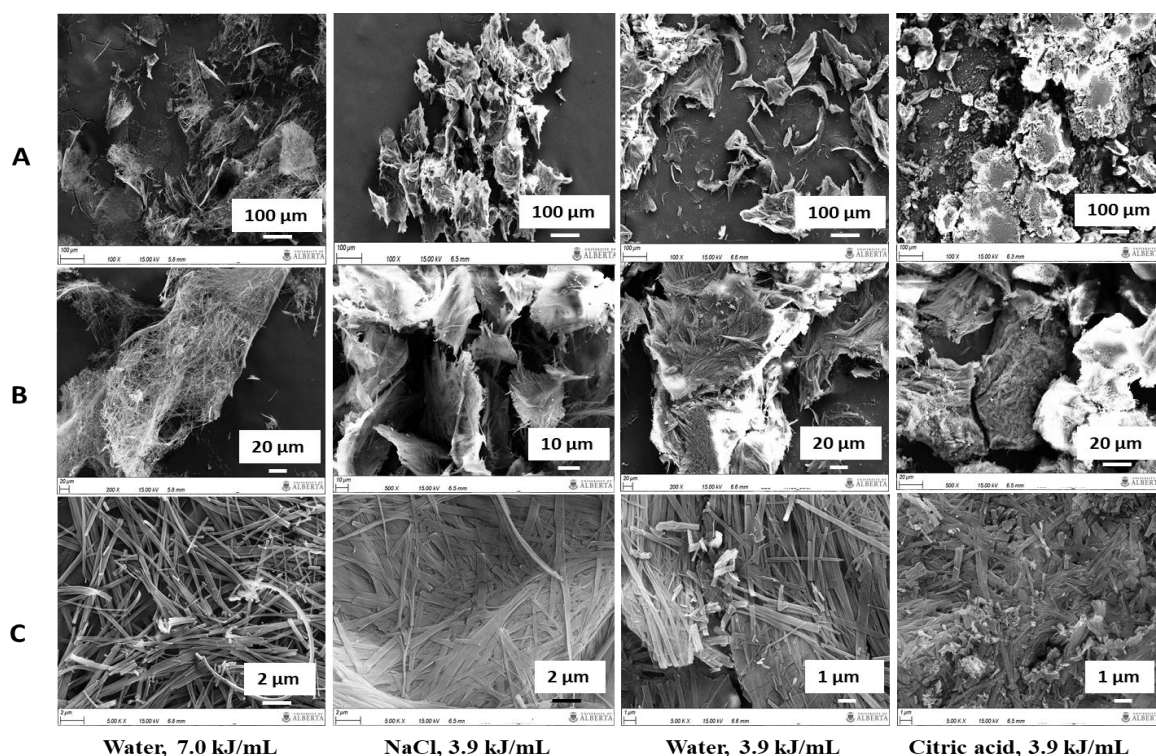
Figure 5.6. Scanning Electron Microscopy images of ultrasound treated rutin powders without temperature control: Particles (A, 100X magnification), Lone/agglomerated particle(s) (B, 200/500X magnification) Lone/agglomerated particle(s) (C, 5KX magnification).

In Figure 5.6C, the fibre strands of UTR at water, 7.0 kJ/mL were loose, while the others (NaCl, water, citric acid at 3.9 kJ/mL) were firmly held together in a common layer. From the scales, each fibre strand width is at least 500 nm.

5.3.7. Thermal behavior

The phase transitions of UTR powder with response to heat flow are shown in Figure 5.7. The peak melting point for the crystalline control was 174.16 ± 1.17 ℃, which agrees with literature data of commercial rutin (Montes et al., 2016). However, enthalpies

for rutin differ as 157.10±6.79 J/g was obtained in this study compared to 33.42 J/g from literature data (Montes et al., 2016). Enthalpies are obtained by integrating the heat capacity curves (area of the melting), and represent an estimate of crystallinity (Gabbott, 2008).
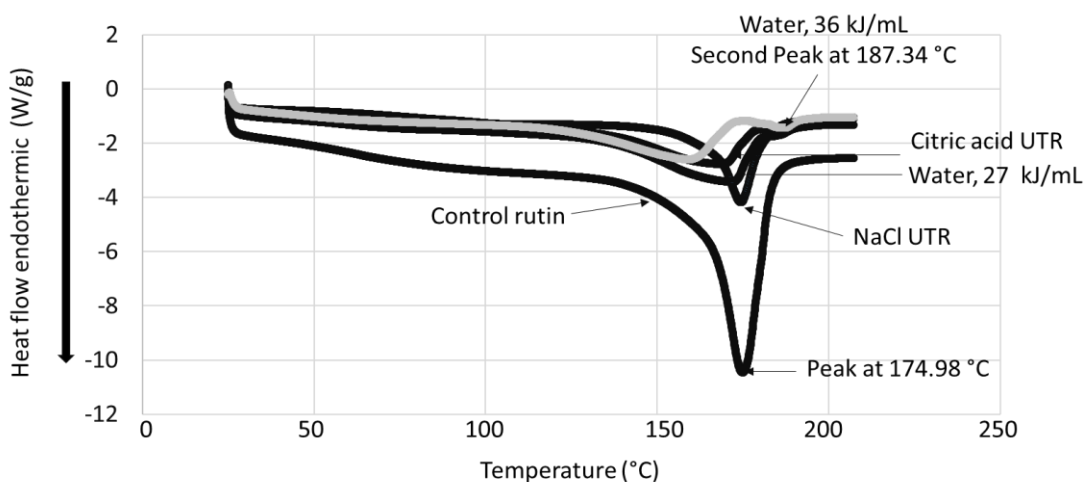
Figure 5.7. DSC thermograms of rutin and modified rutin after ultrasonication treatments using water, citric acid, and NaCl with temperature control.

The UTR particles at 27 kJ/mL (NaCl, water, and citric acid) showed one melting peak not significantly different from the control. However, endotherm for UTR powder in water at 36 kJ/mL was significantly different from the control, and the other treatments showing two melting peaks at 159.86±0.71 °C, and 187.38±0.06 °C. This is an indication of the presence of two rutin polymorphs formed at this condition and could be a result of molecular rearrangement or mass loss (Saunders, 2008; da Costa et al., 2002). Khalifa et al. (1983) reported that raw rutin crystals ($C_{27}H_{30}O_{16}.3H_2O$) lose water at 125 °C, and melt at 188.7 °C. Another raw rutin material was reported to have two melting peaks around 140 °C and 185 °C (Wei et al., 2017). It is also possible that the peak at 159.86±0.71 °C represents a 'glycosylated' rutin while the peak at 187.38±0.06 °C represents an aglycone, both existing together, as glycosylated flavonoids (Chebil et al., 2007). From the

125

compositional HPLC analysis of the control rutin, and the UTRs tested for DSC, rutin was the major component as 96-98%, with <2% contents of isoquercetin, quercetin, and epigallocatechin gallate. Therefore, the thermograms were interpreted based on the major component, rutin. The enthalpies of all UTR with temperature control except water at 36 kJ/mL (Table 5.2) were not significantly different. Therefore, all UTR are crystals of rutin.

In Figure 5.8, all the UTR showed two melting peaks at 154.78 °C and 182.43 °C, which indicates that two rutin polymorphs were formed at 86 °C, different from the control of a single polymorph (Figure 5.7). The enthalpies for UTR rutin (including water at 36 kJ/mL) were not significantly different for peak 1 as 71.84 J/g to 95.18 J/g, and peak 2 as 5.31 J/g to 10.44 J/g (Table 5.2).
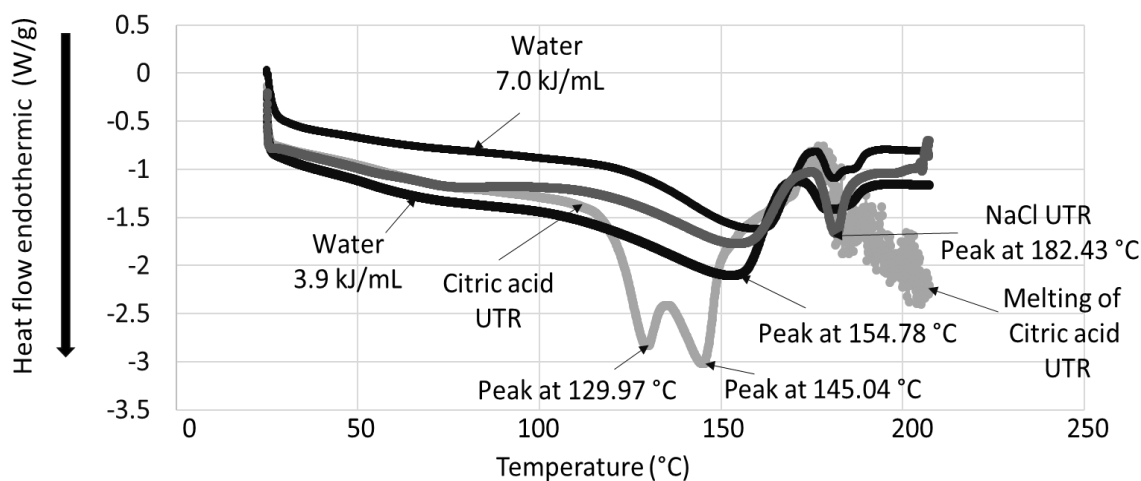
Figure 5.8. DSC thermograms of modified rutin after ultrasonication treatments using water, citric acid, and NaCl without temperature control.

The UTR of citric acid at 3.9 kJ/mL showed two overlapped melting peaks at 129.97 °C and 145.04 °C, and a decomposition peak at 179.47 °C. The peak at 129.97 °C may represent anhydrous rutin crystals (Khalifa et al., 1983). The other peak at 145.04 °C,

and the melting peak at 179.47 °C, both indicate a different rutin polymorph formed in citric acid treatment compared to the treatment by ultrasound in water and NaCl media.

Table 5.2. Enthalpy of endotherms of ultrasound treated rutin

Condition	Treatment	Enthalpy of first peak (J/g)	Enthalpy of second peak (J/g)
	Control	157.10±6.79[A]	nd
With temperature control	Water, 27 kJ/mL	142.65±3.32[A]	nd
	NaCl, 27 kJ/mL	106.50±9.05[B]	nd
	Citric acid, 27 kJ/mL	131.00±9.33[AB]	nd
	Water, 36 kJ/mL	81.55±0.49[a]	5.31±0.19[b]
Without temperature control	Water, 3.9 kJ/mL	95.18±2.79[a]	9.71±0.59[ab]
	NaCl, 3.9 kJ/mL	71.84±6.40[a]	10.44±0.33[a]
	Water, 7.0 kJ/mL	82.73±24.71[a]	7.88±2.38[ab]
	*Citric acid, 3.9 kJ/mL	145.90±17.68 J/g	

*One enthalpy for overlapped peaks. nd – not detectable. [A-B]Values with same uppercase letters are not significantly different at p>0.05. [a-b]Values with same lowercase letters are not significantly different at p>0.05.

5.3.8. Total starch determination and reducing end yield

The modified starch product (syrup) from the pyrodextrinization process weighed an average of 5.9 g, and a final volume of 5.2 mL of light-yellow to brown syrup. Total starch in the syrups was calculated as 0.03 g in the total volume of syrup and was not significantly different in all dextrin produced. The low starch content represents the presence of α-amylase digestible starch (Megazyme method), therefore it was assumed that by difference, at least 99% of the initial starch content (wet basis) was modified to other linkages of pyrodextrins during the process. Reducing end yield ranged from 266.36±7.41 to 423.72±5.82 mg glucose equivalent group/mL dextrin syrup and was not significantly different among the treatments with the different ultrasound treated rutin).

5.3.9. Antioxidant activity by ABTS

The ethanolic extract from the precipitation of saccharides showed ABTS$^{•+}$ inhibition capacity for all rutin/UTR dextrin samples as 2-3% and were not significantly different from one another. The positive control of BHA (0.02 mg/mL) showed 24% ABTS$^{•+}$ inhibition capacity. ABTS$^{•+}$ inhibition capacity was not detected in the saccharides pellet. It is possible that rutin, isoquercetin, quercetin, and epigallocatechin gallate were degraded during the pyroconversion of starch and may have contributed to antioxidant activity.

5.3.10. Identification and quantification of malto-oligosaccharides

The combined acid and heat treatment of the starch, with and without rutin produced light yellow-brown syrups. According to Figure 5.9, all dextrin syrups contained glucose and malto-oligosaccharides with degree of polymerization (DP) 2, 3, 4, 5, 6, and 7, namely maltose, maltotriose, maltotetraose, maltopentaose, maltohexaose, and maltoheptaose, respectively. Since the same starch was used in all treatments, then the same amylopectin architecture (distribution of chain length and placement of branches, Wang and Copeland, 2015) was available for the acid hydrolysis. This may explain the similar order of amounts of malto-oligosaccharides produced from all treatments in the order from DP 4, 1, 3, 5, 2, 7, and 6.
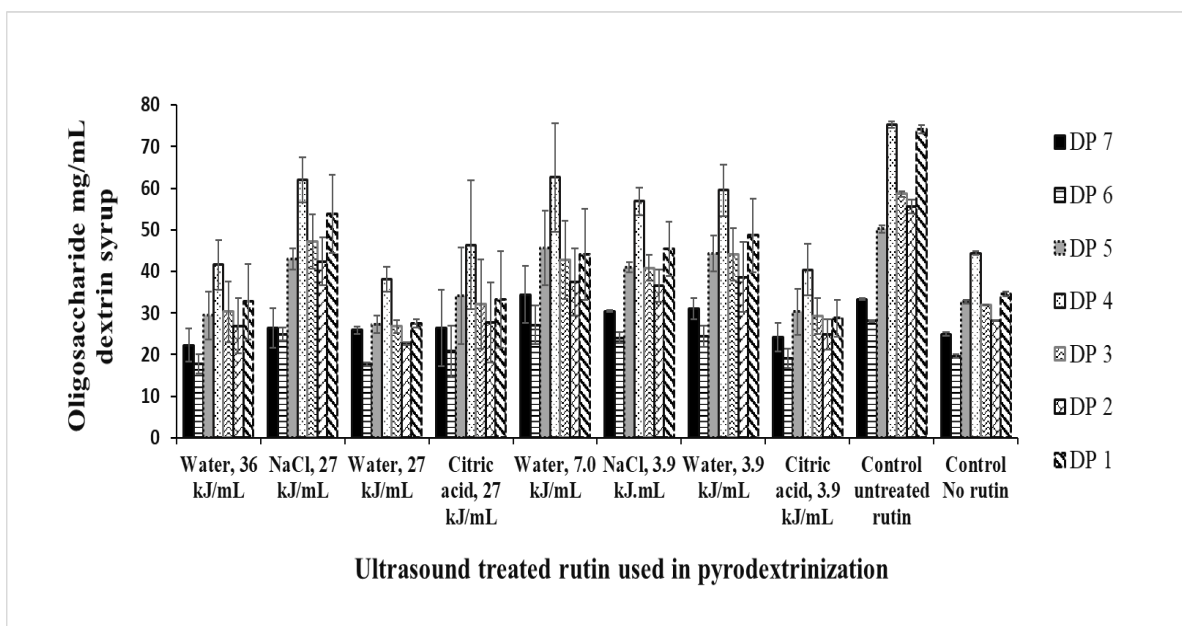
Figure 5.9. Influence of ultrasound treated rutin on production of malto-oligosaccharides in barley starch pyrodextrinized syrups.

The malto-oligosaccharides produced with or without rutin were DP 4 (38.05±3.02-75.19±0.79 mg/mL dextrin syrup), DP 1 (27.49±0.32-74.21±0.95 mg/mL dextrin syrup), DP 3 (26.75±1.52-58.58±0.73 mg/mL dextrin syrup), DP 5 (27.19±2.13-50.20±0.85 mg/mL dextrin syrup), DP 2 (22.53±0.32-55.54±1.60 mg/mL dextrin syrup), DP 7 (22.25±3.91-34.43±6.93 mg/mL dextrin syrup), and DP 6 (17.67±0.49-28.05±0.25 mg/mL dextrin syrup).

From Figure 5.9, the increase in the amounts of malto-oligosaccharides from treatment with control (no rutin) to control (untreated rutin) might be as a result of the release of glucose molecules from the combined acid and thermal hydrolysis of rutin to free rhamnose, and free quercetin (Yang et al., 2019).

Figure 5.10. is a proposed mechanism for modification of rutin during ultrasonication.
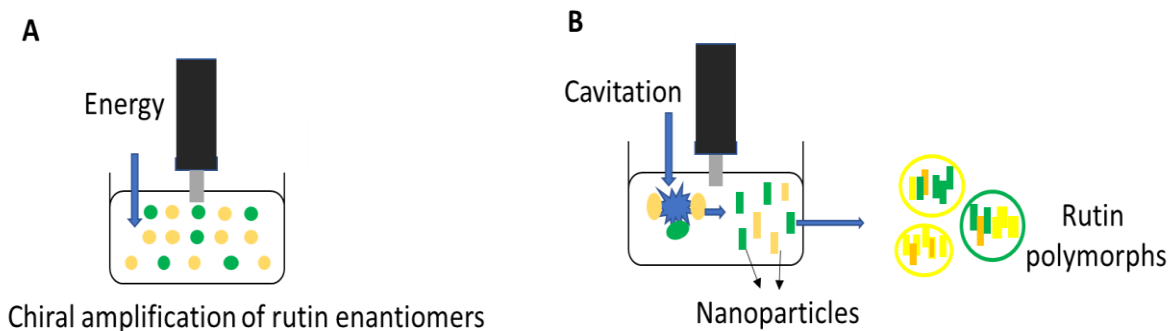
Figure 5.10. Possible mechanism for increase in rutin content by ultrasonication in Chapter 4 (A), and characteristics of polymorphs influenced by clustering of nanoparticles (B).

5.3.   Conclusions

Ultrasonication reduces micro-size rutin to nano-size rutin in acidic media (pH 2, 5, & 6). The extent of structural disintegration was determined by temperature change at 47-86 °C. Ultrasound treatment of rutin in water with temperature control at 47 °C produced greenish, short and thin pieces of flavonoid, while ultrasound treatment of rutin without temperature control at 86 °C produced yellow, long, slender, and loosely held flavonoid strands. The ultrasound treated rutin were of at least one-dimension of diameter in the nanoscale (100-820 nm). Changes in color, morphology, and melting peaks indicate structural modification of rutin by cavitation to produce different rutin polymorphs. Dextrins produced with rutin have enhanced antioxidant activity by ABTS.

Chapter 6. Structural characterization of starch isolates from the electrolysis treatment of barley flour[4]

6.1.   Introduction

Electrolysis involves the passage of electricity via metal electrodes inserted in an electrolyte to create ionic species and form new products through non-spontaneous chemical reactions (Petrucci et al., 2007). In the case of flour treatment, the electrolyte could be the flour slurry in water due to the release of ions from the wheat flour components such as starch, and gluten (Clements 1977a). Clements (1977b) further reported increases in electrical conductivity of flour suspensions and aqueous extracts in relation to ash contents. However, this inherent electrical conductivity of flour was not reported for electrolysis treatment of flour.

The major component of cereal flour is starch, a polymer consisting of α-1,4 and α-1,6 linked glucopyranose molecules, amylose and amylopectin. Earlier, starch obtained from tuber, sweet potato, was modified with electrolysis treatment using a platinum anode, and cathode (cathode material not mentioned) spaced 10 mm apart and inserted in 0.8 g/100 mL sodium chloride (an electrolyte) at a voltage of 90 V for 30 min (Xijun et al., 2012). Afterwards, the electrolysed starch was heat treated at 120 ºC for 30 min prior to cooling for the development of sweet potato retrograded (resistant) starch with a yield of 30.3% compared to 7.7% yield from the control starch at 0 V (Xijun et al., 2012). Recently, Trinh and Dang (2019) reported the structural properties of cassava starch including retrogradation, swelling factor, and gel clarity after the utilization of sodium chloride

---

[4] A version of this chapter will be submitted as Ekaette, I., and Saldaña, M.D.A. Structural characterization of starch isolates from electrolysis treatment of barley flour, and the influence of rutin. Food Engineering.

concentrations (0.5 to 5.0 % w/v) on cassava starch during electrolysis at 10 V/ 3A, using titanium electrodes 10 cm apart for 1 h at 30 °C. Retrogradation increased with an increase in sodium chloride concentration (Trinh and Dang, 2019). These methods added an external electrolyte (sodium chloride) in the electrolysis treatment of the tuber starches. Retrogradation of starch, which usually relates to the cooling of gelatinized starch, is the reassociation of starch molecule chains through hydrogen bonding in a more ordered (Wang et al., 2015) and compact structure. Chen et al. (2017) reported the increase in hardness of rice starch gels in cold storage from 100 to 1050 g in a 22-day period. To the best of my knowledge, the effect of electrical voltage with a flour slurry as an electrolyte has not been reported for structural modification of barley flour components. It was hypothesized that the ionic species produced during water electrolysis might interact with the starch molecules.

Barley *Hordeum vulgare* was selected as an important cereal grain in Canada, having high starch content (52-68%), and other components including protein (8.7-16%), and dietary fibre (4.7-23.8%) (Gao et al., 2009; You and Izydorczyk, 2002; Andersson and Andersson, 2001). Rutin, a flavonoid glycoside was chosen as a functional ingredient, and structural modifier of starch as described in Tables 2.3-2.4 to enhance understanding of the effect of electrolysis on the structure of barley starch gel. Interactions of starch and phenolic compounds were discussed in detail by Zhu (2015a). Barley starch-rutin interactions in subcritical water was also reported in Chapter 3, Section 3.3.2. The objectives of this study were to: 1) understand the effect of electrical voltage and electrode length on the structural properties of barley starch isolates and 2) understand electrolysed barley starch behavior in the presence of rutin.

6.2.   Materials and Methods

6.2.1. Materials

Barley flour (CDC Fibar, 0% amylose content) was provided by the Grain Processing and Technology Laboratory, Department of Agricultural, Food and Nutritional Science, University of Alberta (Edmonton, AB, Canada). Sodium carbonate, rutin hydrate, isoquercetin, quercetin, and glycerol were purchased from Sigma Aldrich (Oakville, ON, Canada). Light mineral oil was purchased from Fisher Scientific (Ottawa, ON, Canada) and APTS (8-aminopyrene-1,3,6 – trisulfonic acid, trisodium salt) was purchased from AAT Bioquest, Inc. (Sunnyvale, CA, USA). All other chemicals were of analytical grade and solvents were of high-performance liquid chromatography (HPLC) grade.

6.2.2. Methods

6.2.2.1. Compositional analysis

Barley flour was characterized for starch content according to the Megazyme total starch assay procedure (Megazyme International Ireland Limited, Wicklow, Ireland). Protein content of barley flour was carried out using Flash 2000, Organic Elemental (CHN-O) analyzer (Thermo Fisher Scientific, Mississauga, ON, Canada). Total ash was determined according to standard method (AACC, 1995). Briefly, 3 g of barley flour was incinerated in a muffle furnace at 550 $^{\circ}$C until a light grey ash was obtained. The crucible containing the residue was left to cool in a desiccator and ash content was calculated using Equation 6.1.

Ash (%) = (weight of residue/sample weight) x 100   (6.1)

6.2.2.2. Electrolysis

Barley CDC Fibar flour (100 g) was placed in a 1 L pyrex glass beaker and 600 g deionized water was added to the flour. The suspension was mixed using a magnetic stirrer for 1 h to equilibrate the release of ions (Clements, 1977b). Using a pH and conductivity meter (Denver Instrument, Model 220 Arvada, CO, USA), measurements of conductivity, pH and total dissolved solids in the barley flour slurry were taken before and after 1 h of mixing. Platinum rods (99.99% pure, 0.15 cm diameter x 15 cm length) obtained from Surepure Chemetals (Florham Park, NJ, USA) were fitted through rubber hoses and held 2.5 cm apart on plastic lid. The electrolysis chamber consisted of the plastic lid placed on the 1 L beaker while inserting the platinum rods into the slurry at rod lengths of 4, 6, and 8 cm. The upper ends of the rods were connected to a DC supply and the voltage supply varied at 2, 5, 10, 15, 20, 25 and 30 V. The rods were considered as the electrodes. The experiment was carried out in an open electrolysis chamber at constant stirring for 30 min (Figure 6.1). Temperatures after the electrolysis experiment ranged from 22-29 ºC. Experiments were carried out in at least duplicates.
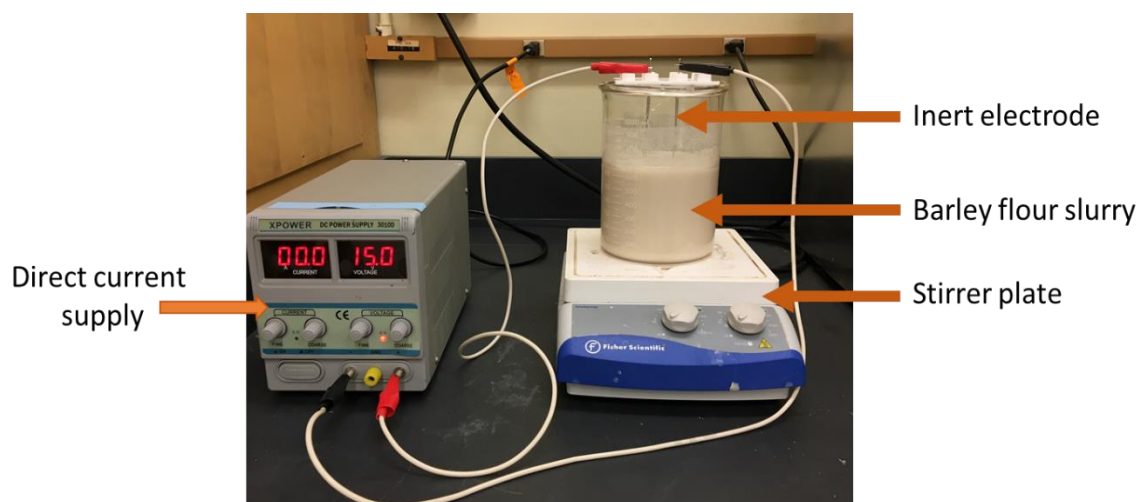
Figure 6.1. Electrolysis treatment of barley flour slurry.

6.2.2.3. Starch isolation

The electrolysed flour was centrifuged at 1593 g for 10 min. The supernatant was discarded, and the residue was carefully removed by scraping the brownish top layers until the whitish layer (starch concentrate) was visible. The remaining (whitish) layer was re-washed with deionized water followed by centrifugation at 1593 g for 10 min, and the top layers were re-scraped until the whitish layer was clean of brownish residue. Total washing times was four from the electrolysed barley flour to the wet starch recovery. The starch portion was dispersed with 95% ethanol and dried at 40 °C overnight.

Alkali-extraction method of barley starch was carried out by stirring 150 g barley flour in 1.3 L deionized water with 200 mg of sodium carbonate (pH 6.0 for the final mixture). This procedure was determined from pre-trials to obtain a simplified starch isolation procedure particular to the CDC Fibar cultivar (0% amylose). The mixture was centrifuged at 1593 g for 10 min (Megazyme method). The supernatant was discarded, and the residue was re-suspended in 1.3 L water and sodium carbonate was used to adjust the pH to 10.4 (Wood et al., 1989). The alkali-barley flour slurry was left to stand for 3 h, after which centrifugation (1593 g, and 10 min) and washing steps were repeated four times. The wet starch was recovered by similarly scraping off the protein brown layers from the wet residues until the whitish layer was visibly free of brown deposits. The recovered starch was re-dispersed with 95% ethanol in aluminium pans and dried in a convection oven at 40 °C overnight.

All dried starch fractions from electrolysis and alkali-method were milled through a 0.5 mm sieve using a Retsch ZM 200 laboratory mill (Retsch Inc. Newtown, PA, USA), and stored in air-tight containers at ambient temperature (23 °C). The dried starches were

characterized for moisture, starch, and protein contents according to AACC standard methods (AACC, 1995) described in Chapter 3 (Section 3.2.2.2).

6.2.2.4. Elemental analysis

Elemental composition of the ash powder was carried out with a Zeiss Sigma 300 VP Field Emission Scanning Electron Microscope coupled with Energy Dispersive X-ray (SEM/EDX) Spectroscopy (Carl Zeiss AG, Oberkochen, Germany). Ash powder was dispersed on carbon conductive adhesive tapes without coating and scanned in back scattered electrons (BSE) mode for the surface compositional analysis.

6.2.2.5. Preparation of rutin solution and HPLC determination

Rutin hydrate (83.9 mg) was mixed with 600 mL of deionized water and filtered through a Whatman filter paper (No. 1). This procedure was conducted in triplicates and the supernatants were analyzed for flavonoid content using HPLC method described in Section 4.2.2.4). The supernatant is named as rutin solution in the starch gel preparation.

6.2.2.6. Preparation of starch gels

Barley starch (as is) and deionized water or rutin solution were mixed in the proportion 10% (w/w) in 20 mL plastic vial. The plastic vial was transferred to an open water bath with a maximum temperature of 75 °C. After shaking at 250 rpm for 10 min, the starch gel was left in the water bath for another 5 min. Starch gel internal temperature was measured as 67 °C. The starch gel was left to cool at ambient temperature of 23 °C for 40 days to examine the long shelf life storage. Starch gels with rutin solution were covered with aluminium foil during storage for light protection of rutin. Preparations of starch gels for each experimental condition were carried out in duplicates.

6.2.2.7. Fourier Transform Infrared (FT-IR) spectroscopy

An ALPHA II FTIR spectrometer (Bruker, Billerica, MA, USA) fitted with Platinum ATR cell and an OPUS software was used to obtain FT-IR spectra of freeze-dried starch gels. Each sample was subjected to 16 scans at 4 cm^{-1} resolution in the wavenumber range of 4000–400 cm^{-1}.

6.2.2.8. Absorption capacity

Barley starch gels after 40 days storage, were transferred to liquid nitrogen for 2 min fast-freezing process. The frozen starch gels were then freeze-dried, and the dried starch gels were used for determination of absorption capacity. Irregularly shaped pieces of the dried gel starches with two of the dimensions in the range of 0.5 cm to 2.3 cm and weight between 0.05 g and 0.34 g were submerged into 25 mL of solvent either deionized water, 50% v/v aqueous ethanol, 50% v/v aqueous glycerol, or light paraffin oil, for 9 h to achieve maximum absorption at ambient temperature. After 9 h, each soaked starch gel was removed from the respective solvent and placed in paper towel within 5 s. The paper towel was used to remove excess solvent from the surfaces of the gel. The weight of the dabbed starch gel was taken immediately, and the absorption capacity was calculated according to Equation 6.2. This procedure was also carried out on a random selection of the whole dried pre-gel cylinders (2 cm diameter, 4 cm height, and 1.4 g). Absorption capacity was determined in at least duplicates.

Absorption capacity (AC) = (W$_s$ – W$_d$)/ W$_d$ x 100   (6.2)

where W$_s$ is weight of soaked starch gel, and W$_d$ is the weight of dried gel.

6.2.2.9. Light microscopy

Starch gel was submerged in deionized water, 50% v/v aqueous ethanol, 50% v/v aqueous glycerol, or light mineral oil, for 9 h. A cross section of the wet gel was mounted between glass slides. The microstructure images were taken at 20X magnification with Differential Interference Contrast (DIC), using an Axiocam 506 mono lens, and an Axio Imager M2 (Carl Zeiss Microscopy GMBH, Göttingen, Germany).

6.2.2.10. Texture Analysis

Texture analysis was carried out on starch gels after 18 h (0.75 days), and 40 days storage at ambient temperature, using a TA.XT plus texture analyzer (Texture Technologies Corp., Scarsdale, NY, USA). Starch gel was compressed with a spherical probe (12.7 mm diameter) at a test speed of 1 mm/s to 10 mm. The strain was 10%, and trigger force 1 g. Plots of force (g) against time (s) were used to obtain values for firmness of the starch gels.

6.2.3. Statistical analysis

All experiments were carried out in at least duplicates and data were reported as mean ± standard deviation and were analyzed by One-way Analysis of Variance (ANOVA) using Minitab 18 statistical software (Minitab Inc., State College, PA, USA). The means were compared for significant differences at $p<0.05$ by Tukey's test.

6.3. Results and Discussion

6.3.1. Chemical composition, conductivity, pH, and total dissolved solids of barley flour

The starting barley flour was composed of starch 69.560±1.313% dm, protein 13.080±0.060% dm, and ash 1.060±0.003% dm. The measured conductivity of barley starch flour slurry increased from 1.16 Ms/cm after 1 h of mixing to 1.45 Ms/cm after

electrolysis. This increase in electrical conductivity might be related to further release of ions from flour ash (Clements 1977a,b). In general, the pH of slurry decreased from 5.39 after 1 h of mixing to 4.55 after electrolysis, which indicated an increase in hydrogen ions (H^+), and slightly acidic content. From a study on amylopectin (in 90% dimethyl sulfoxide) complexation with metal salts of iron (Fe^{2+}), copper (Cu^{2+}), chromium (Cr^{2+}), nickel (Ni^{2+}), and lead (Pb^{2+}), Peres et al. (2016) associated the decrease in conductivity and reduction in solution pH to the release of hydrogen ions (of the hydroxyl groups of the amylopectin molecule), the participation of hydroxyl groups from water molecules in the metal coordination spheres, or the presence of counterions. However, the increase in conductivity in this study is contrary to the reported decrease in conductivity for amylopectin-metal complexation (Peres et al., 2016) where the decrease in pH was suggested in relation to the formation of starch(amylopectin)-metal chelates. Furthermore, the total dissolved solids increased from 581 mg/L measured after 1 h of mixing to 702 mg/L measured after electrolysis, which indicated increased content of minerals, metals, organic materials, phenolic compounds, and salts. Possible reasons are that the electrolysis process may have served as an extraction treatment (Gachovska et al., 2006) of water-soluble solutes from flour components; and, there could have been enhanced solubility of inorganic, and organic compounds during the electrolysis process.

6.3.2. Total starch, protein, and ash contents of electrolysed starch isolates

The average mass of starch isolates was 31 g (as is). The individual starch contents varied from 91.24±3.06% (dm) of alkali-treated starch to 99.26±0.52% (dm) of electrolysed starches and were not significantly different as shown in (Appendix D, Table D.1). The individual protein contents were also not significantly different between 0.25±0.02% (dm)

of alkali-treated starch to 0.95±0.01% (dm) of electrolysed starches (Table D.1). Ash content of alkali-treated starch was 0.32±0.02% (dm), and was not significantly different from ash content of 0.14±0.00 to 0.28±0.04% (dm) of the electrolysed starches (Table D.1), however, the color of all ash from electrolysed starches was black, which was different from the color of the ash from the alkali treated starch (whitish), and the color of the ash from starting barley flour (grey). Color differences might suggest metal compositional differences and reactions, involving transition metals (Figure 6.2).

Figure 6.2. Physical appearance of ash powders from barley flour (A), alkali-treated starch (B), and electrolysed starch at 15 V, 120 min (C).

6.3.3. Elemental composition of ash powders

The high sodium content of the alkali-treated starch in Table 6.1 was from the addition of sodium carbonate used for pH adjustment during the starch isolation process and that contributed to the whitish ash color.

The alkaline pH (10.4) may also have enhanced magnesium (Mg^{2+}) complexation with the protein fraction aggregation (Zhu and Damodaran, 1994), thereby causing lesser magnesium content in the alkali-treated starch compared to the magnesium content in the electrolysed starch.

Table 6.1. Elemental composition of ash from barley flour and isolated starches

Ash source	Element mass (%)								
	Na	Mg	Al	Si	P	S	K	Ca	Fe
Barley flour	0.28 ± 0.04^b	4.09 ± 0.58^a	0.12 ± 0.02^b	0.04 ± 0.01^b	18.32 ± 2.23^a	nd	nd	nd	nd
Alkali-treated starch	35.08 ± 0.93^a	0.75 ± 0.04^c	0.74 ± 0.08^a	trace	3.53 ± 0.17^c	0.37 ± 0.04	2.87 ± 0.01^b	2.71 ± 0.02^a	nd
Electrolysed starch at 15V, 8 cm	0.13 ± 0.01^b	2.90 ± 0.19^b	0.19 ± 0.01^b	0.20 ± 0.01^a	12.93 ± 0.79^b	nd	2.06 ± 0.12^b	2.32 ± 0.17^{ab}	0.21 ± 0.05
Electrolysed starch at 25V, 8 cm	0.09 ± 0.01^b	3.17 ± 0.36^{ab}	0.05 ± 0.01^b	0.23 ± 0.05^a	9.91 ± 0.97^b	nd	3.96 ± 0.47^a	2.07 ± 0.17^b	nd

[a-c]Values with same lowercase letters per column are not significantly different, nd – not detectable.

The aluminium, and silicon contents of barley flour (starting material), which are lower than the same elements' contents in the isolated starches maybe related to the interaction of aluminum and silicon elements as an alloy composite in the flour ash (Liang et al., 2001; Hammond et al., 1995). The absence of sulfur, potassium, calcium and iron in the initial barley flour ash also suggests these elements existed as metal oxides, thereby limiting their detection at the surface. The elemental composition of the electrolysed starches was advantageous over the alkali-treated starch by higher phosphorus content. The loss of phosphorus from 18.32±2.23% in barley flour to 3.53±0.17% in the alkali-treated starch might be related to phosphorus (phytic acid) interactions with the top layer aggregated proteins (Mittal et al., 2016). The increased potassium content (3.96±0.47% at 25 V, 8 cm), and the presence of iron content (0.21±0.05% at 15 V, 8 cm) including the absence of sulfur in the electrolysed starches maybe related to the effect of electric field on protein secondary structure (Singh et al., 2016). Proteins can respond to electric fields by exposure of the sulfhydryl groups, intermolecular disulphide interactions, and self-aggregation via the sulphide bonds, for example, self-aggregation of ovalbumin was observed when pulsed electric field intensity exceeded 25 kV/cm (Zhao and Yang, 2012), but no self-aggregation of bovine serum albumin protein occurred between 20 and 35 kV/cm (Zhao and Yang, 2012). The involvement of sulfhydryl groups in self-aggregation of proteins limits its complexation with metals. Therefore, at the conditions investigated (15 V, and 25 V at 8 cm), it is possible that the sulfhydryl groups of barley proteins were involved in metal complexation. Heavy metal (Hg^{2+}, Cd^{2+}, and Pb^{2+}) complexation was reported for thiol-containing (sulfhydryl) peptides of soy glycinin hydrolysates (Ding et al., 2015).

6.3.4. Starch structure by FT-IR

The FT-IR spectra (Figure 6.3) showed that the electrolysed starches increased in hydrogen bonding interactions. This was deduced from the band at 994 cm $^{-1}$ which was not present for the alkali-treated starch (control). The band at 994 cm $^{-1}$ represents intramolecular hydrogen bonding of the hydroxyl group at C6 and is water sensitive (van Soest et al., 1995). This also enhanced hydration capacity for the electrolysed starches. Also observed was the band at 1016 cm $^{-1}$ which had a higher intensity for the alkali-treated compared to the starch treated at 25 V with rutin, and 5 V with rutin. The 1016 cm $^{-1}$ represents amorphous region of the retrograded starch (van Soest et al., 1995), and is not pronounced in the starches without rutin (5 V, 15 V, and 25 V), with rutin (15 V, and alkali-treated). This might imply that the presence of rutin disrupted the crystalline packing in the electrolysed starches.
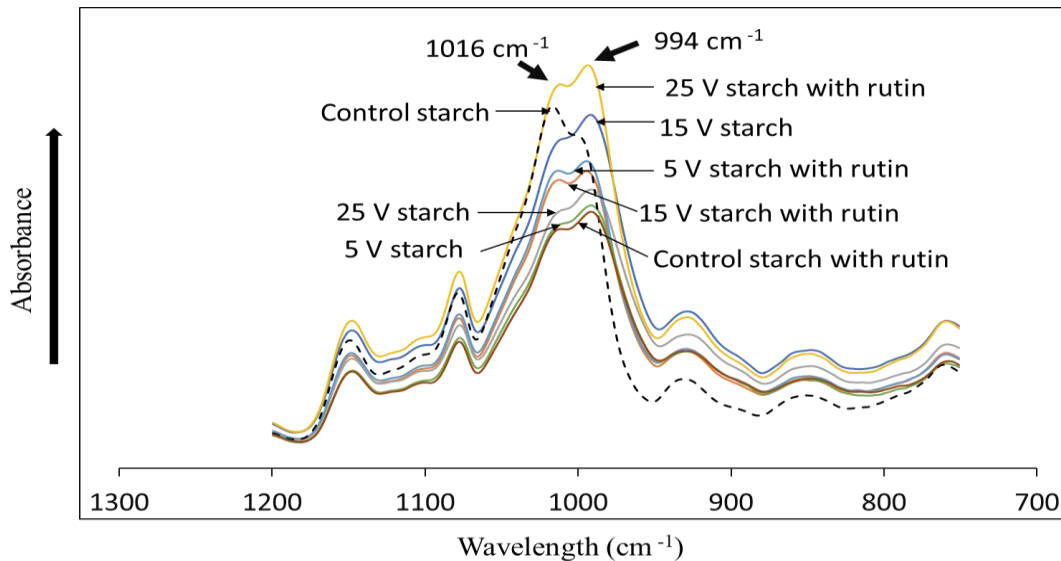
Figure 6.3. FT-IR spectra of freeze-dried gels of barley starch isolated by alkali-treatment, and electrolysis.

This type of disruption was reported for the influence of tea polyphenols on rice starch (Xiao et al., 2011; 2013). Furthermore, the ratio of band 1077 cm $^{-1}$ to 1016 cm $^{-1}$ is

representative of the short-range order in retrograded starch. Lower ratio of absorbances 1077 cm $^{-1}$ /1016 cm $^{-1}$ is correlated with loss of crystalline order (disruption of double helices) (van Soest et al., 1995). Ratio of 1077 cm $^{-1}$ /1016 cm $^{-1}$ of control (alkali-treated) starch is 0.481, control starch with rutin (0.537), 25 V starch (0.568), 25 V starch with rutin (0.520), 15 V starch (0.559), 15 V starch with rutin (0.523), 5 V starch (0.545), and 5 V starch with rutin (0.519). Electrolysed starches (25, 15, & 5V) showed higher crystallinity than control starch. Rutin increased crystallinity in control starch but reduced crystallinity in the electrolysed starch (25, 15 and 5 V). Rutin possibly disrupted the double helices, and chelated metals in the starch granule/gel during gelatinization.

In general, the presence of rutin influenced the bands between 1200-1000 cm $^{-1}$ in the fingerprint region of starch, which represent the CH-OH and CH_2-OH groups stretching.

6.3.5. Absorption capacity

The effect of electrolysis was also determined on absorption capacity for rehydrated starch gels in various hydrophilic and hydrophobic solvents (Figure 6.4). Significant difference among voltage treatments was only observed for absorption capacity of rehydrated starch gels in water at 8 cm. This may be related to the increased rate of reactions after electrode length of 6 cm, because of the increased surface area using longer the electrode (8 cm).

The absorption capacity (Figure 6.4) for all electrolysed starch gels were higher than that of the alkali-treated starch gel (no voltage treatment), which suggests that electrolysis treatment increased the affinity of the treated starches for hydrophilic and hydrophobic groups compared to the control. Kuang et al. (2011) reported that capillary

absorption of water by starch sulfate-based hydrogels was based on surface hydrophilicity and pore structure.
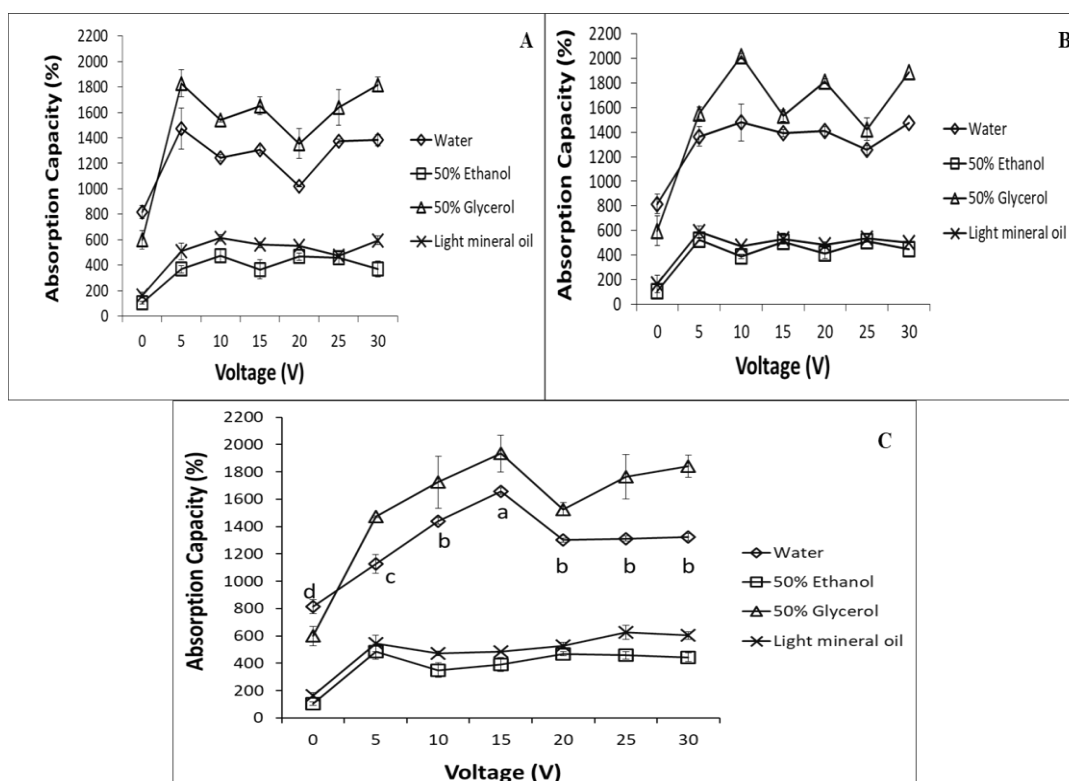
Figure 6.4. Absorption capacity of freeze-dried gel barley starches in hydrophilic and hydrophobic solvents. Barley starches were isolated using electrolysis (5-30 V) with electrode lengths of 4 cm (A), 6 cm (B), and 8 cm (C).

The chemical reactions in the barley flour slurry were assumed to follow the cell reactions of water electrolysis, because of the positions of hydrogen and oxygen in the electrochemical series considering that multiple metal ions of barley flour were also present in the slurry during electrolysis. Water is reduced at the cathode to produce hydrogen gas and hydroxide ions according to Equation 6.3a, and the hydroxide ions or water molecules are oxidized at the anode (Equation 6.3b-c). The overall (cell) reaction is provided in Equation 6.3d (Silberberg, 2009). Therefore, starch may have had increased interactions with OH^- and H^+ ions during the electrolysis process.

Reduction half-reaction:

$$2H_2O(l) + 2e^- \rightarrow H_2(g) + 2OH^-(aq) \hspace{4cm} (6.3a)$$

Oxidation half-reactions:

$$2OH^-(aq) - 2e^- \rightarrow O_2(g) + 2H^+(aq) \hspace{4cm} (6.3b)$$

$$2H_2O(l) \rightarrow O_2(g) + 4H^+(aq) + 4e^- \hspace{4cm} (6.3c)$$

Overall (cell) reaction:

$$2H_2O(l) \rightarrow 2H_2(g) + O_2(g) \hspace{4cm} (6.3d)$$

The densities of solvents (Table 6.2) may also have contributed to the absorption capacity, as all starches showed higher absorption capacity in 50% glycerol (highest density), and water compared to 50% ethanol, and light mineral oil (lower densities).

Table 6.2. Properties of solvents

Solvent	Chemical formula	Density (g/cm^3)
Water	H_2O	0.99705[a]
50% v/v Aqueous Glycerol	$C_3H_5(OH)_3$	1.12375[b]
50% v/v Aqueous Ethanol	C_2H_5OH	0.93062[c]
Light mineral oil	$C_{16}H_{10}N_2Na_2O_7S_2$	0.83000[d]

[a] www.engineeringtoolbox.com, at 25ºC, [b] Physical properties of glycerin and its solutions, at 25ºC, [c] Steffen's chemistry at 20ºC, [d] Fisher Safety Data Sheet.

From Figure 6.4C, the absorption capacity in water increased with increase in voltage from 1126.15±69.34% at 5 V to 1659.05±24.69% at 15 V, then reduces to 1300.13±14.84% at 20 V. It is possible that after 15 V, other reactions such as metal complexation may have competed for the availability of the hydroxide or hydrogen ions. The absorption capacity range observed in this study is comparable to absorption capacity (1519%) reported for chemically modified corn starch-based hydrogels by reactive mixing, utilizing 10 g starch, an initiator (ceric ammonium nitrate, 3.75%), a crosslinker (N,N' – methylene-bisacrylamide, 1.0%), a saponification agent (NaOH; 30%), and urea (200%)

(Xiao et al., 2017). Figure 6.5 shows increase in dimensions of the whole cylinder of barley starch isolate from the treatment with 15 V/ 8 cm for 2 h.
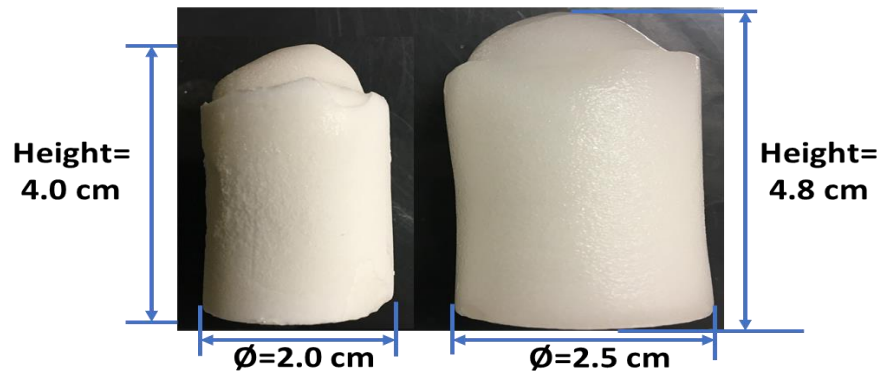
Figure 6.5. Electrolysed starch: freeze-dried gel (left) and swollen starch gel (right)

6.3.6. Effect of rutin solution on absorption capacity

The HPLC identification of the rutin solution showed a composition of rutin (10.08±0.85 µg/mL), isoquercetin (0.36±0.06 µg/mL), quercetin (1.97±0.04 µg/mL), and epigallocatechin gallate (2.59±0.02 µg/mL). Therefore, the 12.5 mL rutin solution used per gel formation had an approximate solute mass of 187 µg. Based on Figure 6.4C, selected samples at 5 V, 15 V, and 25 V were tested for the effect of rutin on absorption capacity.

Figure 6.6A shows that rutin could have interacted with the gel hydroxide ions via hydrogen bonding, thereby reducing the number of hydroxide ions available for water interaction and absorption. Also, with the presence of rutin, the water absorption 565.88±69.98% at 15 V was lower than 825.73±28.39%, and 886.44±0.79% of 5 V, and 25 V, respectively.
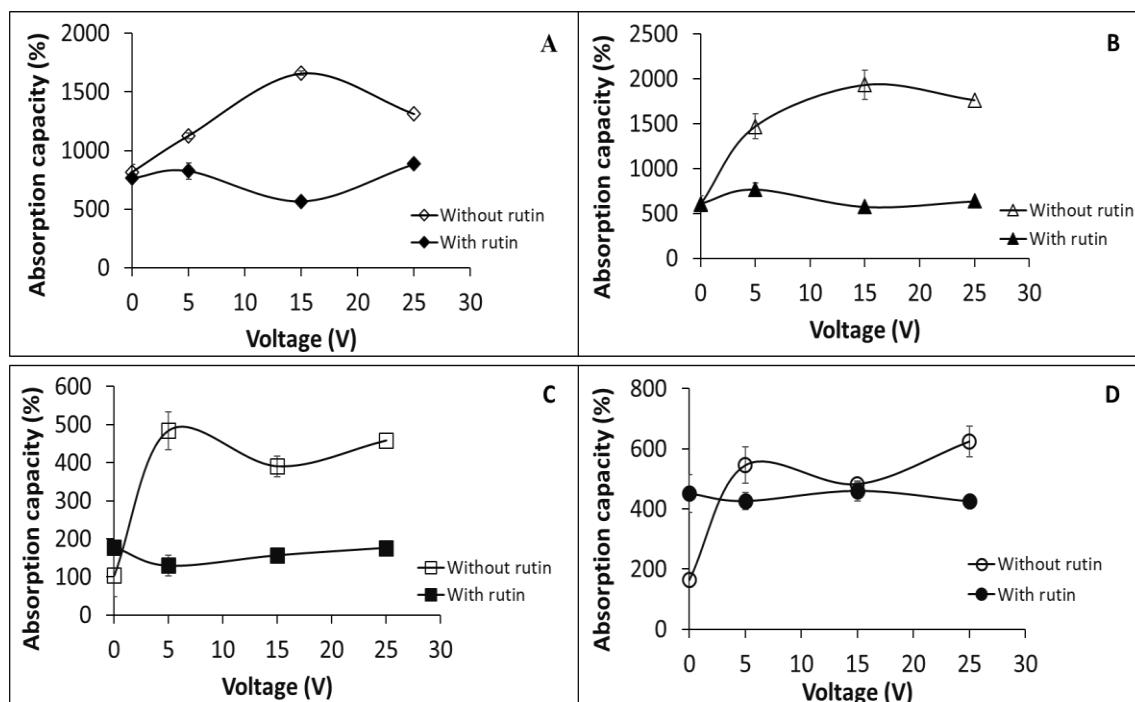
Figure 6.6. Absorption capacity of freeze-dried gel starches from starch isolates treated with electrode length 8 cm. Gels were prepared in deionized water and with rutin solution. Solvents used for absorption were water (A), 50% v/v glycerol (B), 50% v/v ethanol (C), and light mineral oil (D).

This opposite behavior from the 'without rutin' gels suggests the influence of other rutin-starch interactions on water absorption in the gel, which may include rutin complexation with metals (Table 6.1). Figure 6.6 A-C compared to Figure 6.6D shows that hydrophilic groups contribute to the flexibility of the starch chains necessary to enhance water uptake. In both water and 50% v/v glycerol solvents, the presence of rutin did not change the absorption capacity of the control alkali-treated starch but decreased the absorption capacity of electrolysed starches. However, in Figure 6.6C-D, the presence of rutin, and other hydrophobic (flavonoid) compounds enhanced the absorption capacity for 50% v/v ethanol and light mineral oil for the alkali-treated starch by an increase from

103.71±10.75% to 177.66±2.46%, and from 163.62±21.99% to 451.55±6.03%, respectively.

Figure 6.7 illustrates the shrinking behavior of the rutin-loaded electrolysed starch (25 V, 8 cm) gel in water, after 9 h. The decrease in dimensions (height and diameter) confirms the anti-swelling effect of rutin on absorption capacity of starch.
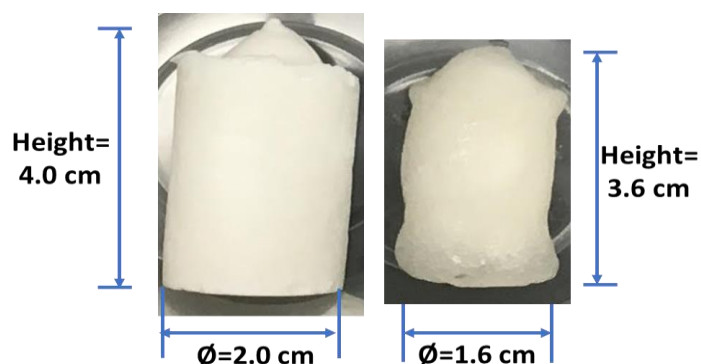
Figure 6.7. Electrolysed starch at 25 V, 8 cm: freeze-dried gel loaded with rutin (left) and shrunken gel (right) after steeping in water for 9 h.

6.3.7. Microstructure of starch gels

The light microscope images (Figure 6.8, A1-2, B1-2), shows fragmented starch granules dispersed in the starch gels of the alkali-treated (0 V), and the electrolysed (15 V) starches. However, the paste of the electrolyzed starch gel without rutin, (Figure 6.8.A2) appeared denser compared to the electrolysed starch gel with rutin (Figure 6.8.B2). The presence of fragmented starch granules in starch pastes was also observed in the light microscopy images of starch gels after absorption in 50% v/v glycerol, and 50 v/v ethanol.
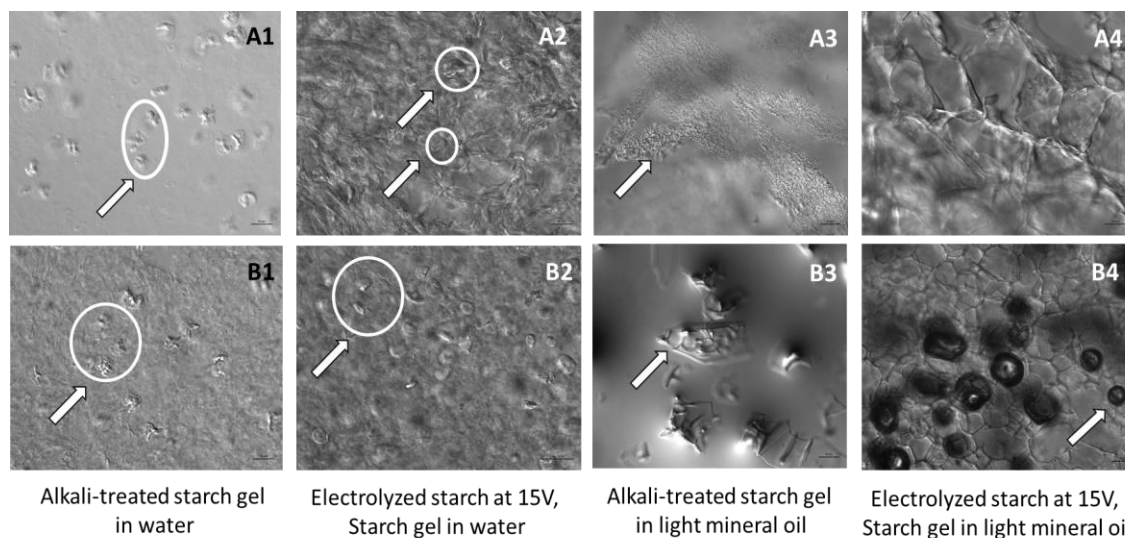
Figure 6.8. Light microscope images showing microstructure of freeze-dried starch gels after absorption in water and light mineral oil: Without rutin (A1-4), With rutin (B1-4).

The alkali-treated starch gel (without rutin), after immersion in light mineral oil was firm, and maintained its original size. This suggests that starch chains were not flexible in the hydrophobic solvent. Light microscope image of its cross section (Figure 6.8.A3) showed a continuous network, but the appearance of individual dispersed starch granules was not observed (Figure 6.8.A3). The alkali-treated starch gel (with rutin), after immersion in light mineral oil was less firm; a cross section was like melt, showing protrusions that were glassy, and irregular in shape (Figure 6.8.B3). The microstructure of alkali-treated starch gel in light mineral oil (B), may have been influenced by rutin-mineral oil interactions (Figure 6.6D).

The effect of voltage on microstructure of starch gels in light mineral oil, was observed in (Figure 6.8. A4, and B4). Similar to Figure 6.8.A2, gel in Figure 6.8.A4 was thick. Figure 6.8. B4, showed a network with defined borders, with dark areas which might represent air bubbles around starch granules. For applications in oil-based products, these images might contribute to understanding of texture of rutin-starch gels.

150

6.3.8. Gel firmness

The effect of retrogradation on alkali-treated starch gel was determined at 40 days of storage. Its firmness decreased from 15.3±0.2 g to 2.1±0.0 g, but the presence of rutin enhanced the firmness with an increase from 2.1±0.0 g to 5.8±0.8 g (~176 %) (Table 6.3). The loss of firmness of the starch gels, might be related to the degradation of external branches and inter-cluster regions of amylopectin molecule, thereby limiting the formation of double helices (Palacios et al., 2004). But the presence of rutin and other flavonoids, might have minimized this degradation by interactions with the double helices of the glucan chains. Keetels et al. (1996) reported that during recrystallization (retrogradation) of amylopectin gels, stiffening of the gels was either caused by the formation of crystalline clusters along the α-1,4 glucan chains or the development of crosslinks between adjacent clusters. It is possible that rutin also developed crosslinks that enhanced the firmness of the gels. Increased firmness also means increased gel elastic modulus (Palacios et al., 2004). Figure 6.9A shows the influence of rutin on firmness and flow behavior.

Table 6.3. Texture profile of alkali-treated barley starch and electrolysed barley starches

Presence of rutin	Duration of storage (days)	Firmness (g)			
		Alkali-treated starch	Electrolysed starch at 8cm		
			5 V	15 V	25 V
No rutin	0.75	15.3±0.2[e]	22.6±0.5[abc]	19.0±0.0[bcde]	20.2±1.3[abcde]
Rutin	0.75	16.9±0.5[de]	24.3±0.6[ab]	21.9±2.5[abcd]	22.5±0.6[abc]
No rutin	40.00	2.1±0.0[f B]	24.7±0.8[a]	18.4±0.0[cde]	23.4±0.4[abc]
Rutin	40.00	5.8±0.8[f A]	25.0±0.1[a]	22.1±0.0[abcd]	20.0±4.1[abcde]

[a-e]Values with same lowercase letters are not significantly different across all values at $p>0.05$. [A-B]Values with different uppercase letters are significantly different for alkali-treated starch after 40 days at $p<0.05$.

The firmness of the electrolysed starches without and with rutin (18.4 to 25.0 g) did not change at 40 days of storage. Also, possibly, there was no significant retrogradation within the duration of storage studied. This agreed with Zhu and Wang (2012), who observed no retrogradation (%) for waxy rice starch (1.6% amylose content), and normal rice starch with rutin (22% amylose content) after storage at 4 $^{\circ}$C, and 7 days. But they observed retrogradation (%) for high amylose rice starch (32% amylose content) with and without rutin after 4 $^{\circ}$C, and 7 days.
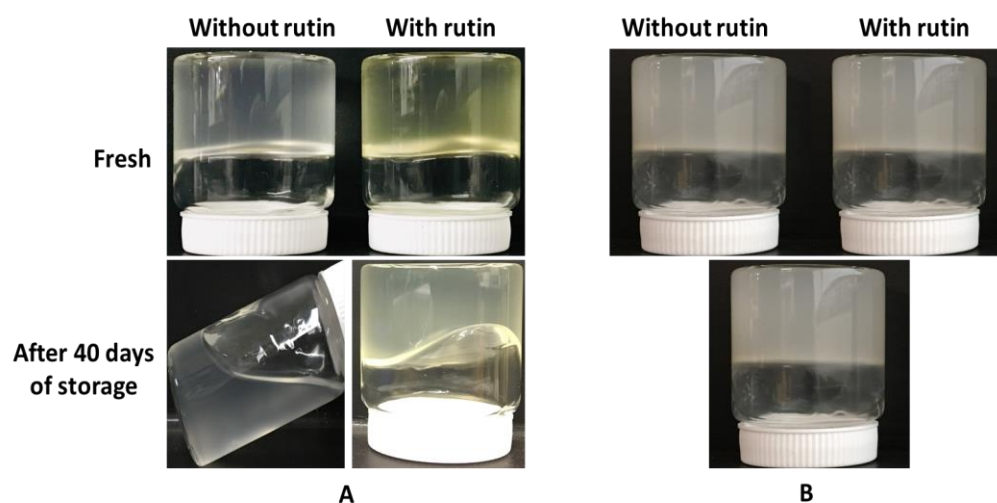
Figure 6.9. Barley starch gels (10% w/w) from alkali-treated starch (A), and electrolysed starch (B), stored at room temperature.

These results suggest that amorphous regions in starch enhances retrogradation, and not the presence of rutin. However, the opacity of the electrolysed starch gels (Figure 6.9B), compared to the alkali-treated starch, might suggest a new alignment of the amylopectin straight chains due to polarization in the electric field. Opaque starch gels are common with normal to high amylose starches (Amani et al., 2005). Therefore, it is assumed that in the electrolysed starches, a new structure of amorphous regions was formed. However, according to Figure 6.2, band at 994 cm^{-1} which represents amorphous

regions, was lower in intensity for the electrolysed starches compared to the alkali-treated starch. Therefore, the opacity or no retrogradation may have also been caused from the increased intramolecular bonding for the electrolysed starches (band at 994 cm^{-1}) within the amylopectin molecule.

The loss of rutin yellow color (Figure 6.9A) during storage, indicates degradation of rutin. The negative correlation of rutin content and storage time of dried inflorescence of black elder plant for 1 year (at 22 °C) was reported by Dadáková et al. (2011). Because of the opacity of the electrolysed starch gels, the degradation of rutin color was not observed.

Figure 6.10. is a proposed mechanism for electrolysed starch modification. Electrolysed starch is enriched with metal ions. The release of metal ions during gelatinization occupies spaces in starch gel which contribute to gel opacity.
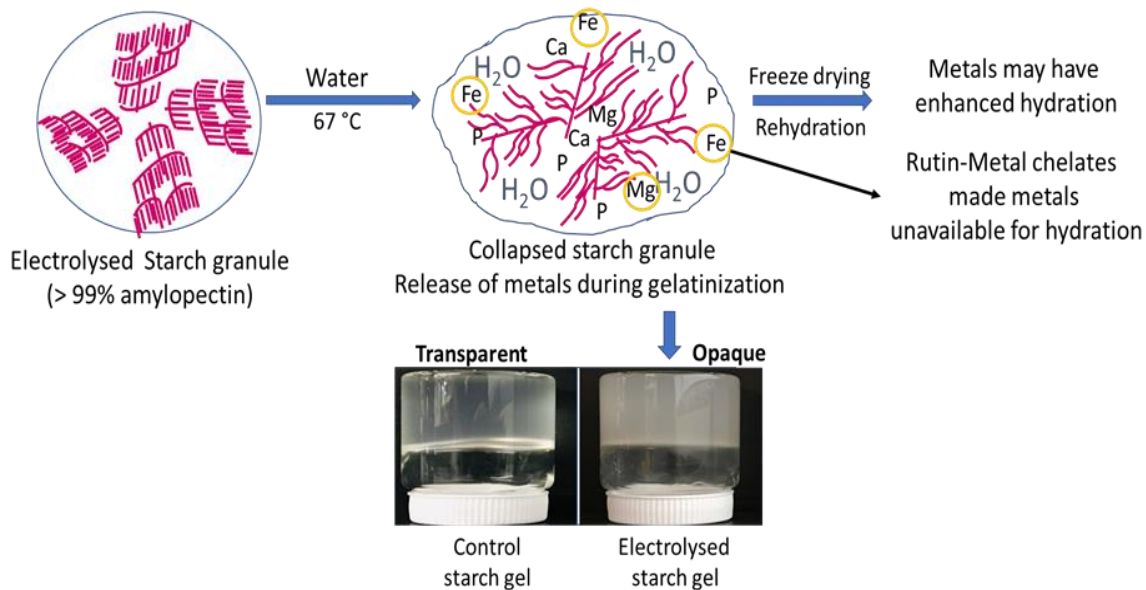
Figure 6.10. Possible mechanism for electrolysed starch and rutin interaction.

6.4.   Conclusions

The choice of starch isolation treatment from a flour matrix can confer modifying properties on the starch. The conventional alkali-treatment, and the electrolysis treatment of barley flour produced modified starches with varying elemental composition. The retrograded starch conformations (FT-IR), absorption capacity, and firmness, all indicate different structural characteristics of the starches. Electrolysis (voltage treatment) and rutin, separately increase the crystallinity of retrograded starch. Barley starch treated at 15 V, 8 cm highest absorption capacity between 5 V, and 25 V at 8 cm, and the lowest when rutin was added between 5 V and 25 V at 8 cm. The firmness of the electrolysed starches without and with rutin were not significantly different from one another at 40 days of storage at room temperature.

Chapter 7. Conclusions and recommendations

7.1. Conclusions

This PhD thesis research has explored the potential of three emerging technologies for starch and rutin processing as food ingredient. In the first study (Chapter 3), barley starch combined with rutin was treated under pressurized water at 80 °C and subcritical water temperatures of 100-160 °C. Based on the results, subcritical water technology offers the option of tunable temperatures for desirable barley starch-rutin interactions, including the amount of rutin that can be incorporated in the modified starch. Some of the proposed mechanisms for barley starch-rutin interactions include hydrogen bonding, amylose inclusion, and the disruption of the starch crystallite. After 120 °C, high amylose content of 37%, is required to increase rutin content in modified starch. In this thesis, the effect of the subcritical water treatment was only investigated on the starch behavior. The rutin hydrolysates (isoquercetin, quercetin, epigallocatechin gallate, catechin), from the thermal hydrolysis of rutin were not quantified. These rutin hydrolysates may have contributed to the molecular structure of the SCW modified starch.

In the second study (Chapter 4), the flavonoid rutin was treated with ultrasonication for rutin hydrolysis to isoquercetin and quercetin. Ultrasonication of rutin suspensions in water (pH 5.0), aqueous citric acid (pH 2.2) and aqueous sodium chloride (pH 6.3) was selective in the production of quercetin at different energy densities, utilizing non-thermal and thermal conditions. Quercetin production was highest in citric acid media at 600 W, 20 min, and without temperature control (86 °C). The quantification was carried out using a HPLC with a diode array detector (DAD). It was observed that rutin yield increased by 42% in all pH media studied, with no significant difference. Modified rutin structure may

have influenced its antioxidant capacities studied by DPPH, FRAP, ABTS, iron (II) -chelating and copper (II) -chelating activities. Also, ultrasonication of rutin without temperature control at 86 $^{\circ}$C in water (pH 5) and NaCl (pH 6.3) media increased the production of levorotatory enantiomer of rutin. This study offers the option of producing quercetin at low temperatures compared to high temperatures (>120 $^{\circ}$C) with degradation products as reported in literature.

In study 3 (Chapter 5), the ultrasound treatments of rutin in Chapter 4 were repeated at extreme conditions of energy density (27 and 36 kJ/mL) to produce rutin nanocrystals. The rutin nanocrystals (100-820 nm) from ultrasound processing had a green coloration at 47 $^{\circ}$C but maintained the yellow color similar to the control at 86 $^{\circ}$C. The ultrasonication effect in water at 36 kJ/mL (47 $^{\circ}$C), produced two rutin polymorphs identified by melting peak temperatures of 155 $^{\circ}$C and 182 $^{\circ}$C. These same melting peak temperatures were also identified for rutin polymorphs produced from the ultrasound treatment in water, and sodium chloride at 86 $^{\circ}$C. All parameters studied in Chapters 4 and 5 for the ultasonication of rutin (media pH, energy density and temperature) seem to have an interactive effect on the modified rutin properties.

The final study (Chapter 6) involved the first step of isolating barley starch after electrolysis treatment of barley flour, and then adding rutin solution as the dispersed phase for the electrolysed starch gelatinization process. The isolated electrolysed starch showed increased metal content in starch. Based on FT-IR results, electrolysed starch had increased crystallinity. However, rutin decreased the crystallinity of electrolysed starch as opposed to rutin increasing the crystallinity of alkai-treated starch. It was assumed that the crystallinity of the electrolysed starch was enhanced by starch-metal complexation. Also, the

electrolysed starch gels had superior absorption capacities and firmness compared to the alkali-treated isolated starch. The electrolysed starches were opaque and may provide light protection for rutin. The presence of rutin enhanced understanding of the structure of electrolysed barley starch.

The limitations of these research studies are: 1) The purity level of starting material (rutin hydrate ≥ 94%) indicate the presence of other flavonoid compounds and unknown impurities. Flavonoid compounds identified by HPLC such isoquercetin, quercetin, and epigallocatechin gallate may have influenced the results. 2). Pure barley starch is not commercially available. Therefore, barley starch isolation from barley flour for studies 1 and 3 was performed. 3). Method of starch isolation requires barley flour with high starch content to enhance high starch recovery after scraping off protein layer. 4). The antioxidant activity of the new SCW rutin-barley starches/hydrogels was not determined. To uncomplex the rutin molecules, a modified protocol used for defatting starch may be applied. This protocol to uncomplex lipid from V-amylose- lipid complexes requires a boiling process of starch in 75% v/v propan-2-ol. Further heat treatment of rutin-starches produced in this thesis might further hydrolyse the rutin compound, and influence antioxidant activity.

The novelty and scientific contributions of these research studies are: 1). Rutin might undergo an increase in its content if exposed to thermal and/or ultrasound treatment. 2). The feasibility of high temperature treatment of high amylose starch in excess water at of 140 °C and 160 °C was possible in the presence of rutin; As observed in study 1 (Chapter 3) under the same treatment conditions, high amylose starch treatments without rutin were

not possible. 3). Superabsorbent starch hydrogels can be produced with electrolysis. 4). The protocols in this thesis are applicable to other cereal starches, like maize, or wheat.

In summary, rutin was incorporated into barley starch producing modified starch products such as expanded starches, dextrins, and hydrogels. The expanded starch can be used as functional ingredient in creams, sauces, soups, and baked products; the dextrin can be used as coating material for nuts, and gums; and the hydrogel can be used in personal care products, including pads, and cosmetics.

7.2. Recommendations

Based on the information collected in this thesis, subcritical water technology offers a one-step, and time-efficient protocol for barley starch-rutin interactions, compared to the two-step, and time-consuming protocols of the ultrasonication-pyrodextrinization, and the electrolysis-gelatinization appraoches. However, future work is required.

Pressurized water in the subcritical region acts as an acid and a base because of the increase in hydronium and hydroxide ions. It would be important to investigate the pH properties of barley starch gel under subcritical water conditions. Therefore, further experiments can be performed with pH measurement of the process, the untreated starch suspensions and subcritical water treated starch gels. Knowledge of the pH will provide better understanding of the effect of pH on starch-rutin complexation, and final starch color.

Starch chemical composition includes metals like calcium, and iron, which might react with rutin under high temperatures. Therefore, the analysis by X-ray crystallinity of the subcritical water modified starches will show influence of inorganic metals (starch-metal complexation) on the starch X-ray diffractogram. This information can enhance

understanding into the mode of complexation between starch and rutin under subcritical water conditions.

In Chapter 4, the identification and quantification of rutin derivatives can be performed using liquid chromatography-mass spectroscopy (LC-MS/MS), and chiral chromatography. These will enhance understanding on the molecular weight and structure of the rutin derivatives.

The ultrasound processing of rutin can be set up to prevent the direct contact of the probe with the rutin suspension. Alternatively, an inert (platinum) probe can be used to eliminate metal contamination and other side reactions that may have occurred between rutin, its derivatives and the probe metal (Chapters 4, and 5).

Nuclear Magnetic Resonance (NMR) studies of the freeze-dried rutin can improve understanding on functional groups, and linkages formed in the obtained rutin polymorphs. Also, an X-ray diffraction analysis on the freeze-dried rutin, will enhance knowledge on the crystallite structure of the nanocrystals.

The isolation of the oligosaccharide's fractions, identified by HPLC in Chapter 5, can be done, followed by molecular studies such as mass spectrometry and NMR. These studies together with the identification of cyclic oligosaccharides using HPLC will provide more insight to the molecular structure of the proposed rutin-dextrin conjugates.

Due to possible electrical discharges during ultrasonication and electrolysis, the ultrasound treated rutin and electrolysis treated starches should be tested for residual electrons.

The subcritical water treated starches, pyrodextrins, and electrolysed starch gels loaded with rutin can be tested for rutin release, and its stability for antioxidant and anti-microbial applications.

Kinetic studies can be carried out on the subcritical water treatment of starch, with and without rutin. Also, a kinetic study will provide more insight to the cavitation threshold on rutin hydrolysis.

Resistant starch is a dietary fibre that may be produced by starch-phenolic interactions. Resistant starch analysis can be determined for subcritical water treated starches, pyrodextrins, and electrolysed starches, with or without rutin.

Subcritical water treatment can be carried out on starch types of B and/or C X-ray crystallinity from tubers and legumes, in the presence of rutin.

Effect of ultrasonication can be carried out on water-soluble rutin.

References

AACC (1995) Approved Methods of the American Association of Cereal Chemists AACC (1995). 9th ed., vol 2. American Association of Cereal Chemists, Inc. St Paul, MN, USA.

AAFC (2019) Agriculture and Agri-Food Canada http://www.agr.gc.ca/eng/news/scientific-achievements-in-agriculture/barley-is-in-when-it-comes-to-heart- health/?id=1378999685709, accessed on November 21, 2019.

Ababio, O. Y. (1990). New School Chemistry. In Akpanisi, L.E.S., Igwe, H. (Ed.) African First Publishers PLC, Onitsha, Nigeria. pp 200-229.

Adkins, G.K., & Greenwood, C.T. (1966). The isolation of cereal starches in the laboratory. *Die Stärke*, 18, 213-218.

Afanas'ev, I.B., Dorozhko, A.I., Brodskii, A.V., Kostyuk, V.A., Potapovitch, A.I. (1989) Chelating and free radical scavenging mechanisms of inhibitory action of rutin and quercetin in lipid peroxidation, *Biochemical Pharmacology*, 38, 11, 1763-1769.

Agbor, V.B., Cicek, N., Sparling, R., Berlin, A., & Levin, D.B. (2011). Biomass pretreatment: Fundamentals toward application. *Biotechnology Advances,* 29,75-685.

Ahmed, A., Khalid, N., Ahmad, A., Abbasi, N.A., Latif, M.S.Z., & Randhawa, M.A. (2013). Phytochemicals and biofunctional properties of buckwheat: a review. *Journal of Agricultural Science*, 1-21.

Ainsworth, E.A., & Gillespie, K. M. (2007). Estimation of total phenolic content and other oxidation substrates in plant tissues using Folin–Ciocalteu reagent. *Nature Protocols*, 2, 4, 875-877.

Akulichev, V. A. (1966). Hydration of ions and the cavitation resistance of water, *Soviet Physics Acoustics,* 12, 144.

Al-Roujeaie, A.S., Abuohashish, H.M., Ahmed, M.M., & Alkhamees, O.A. (2017). Effect of rutin on diabetic-induced erectile dysfunction: Possible involvement of testicular biomarkers in male rats. *Andrologia.* 49, e12737.

Alvarez, V.H., Cahyadi, J., D. Xu, & Saldaña, M.D.A. (2014). Optimization of phytochemicals production from potato peel using subcritical water: Experimental and Dynamic modeling, *Journal of Supercritical Fluids,* 90, 8-17.

Amani, N.G., Kamenan, A., Rolland-Sabaté, A., & Colonna, P. (2005). Stability of yam starch gels during processing. *African Journal of Biotechnology,* 4,1, 94-101.

Andersson, A. A. M., Andersson, R., & Åman, P. (2001) Starch and by-products from a laboratory-scale barley starch isolation procedure. *Cereal Chemi*stry, 78, 5, 507–513.

Andrea, B., Baviello, G., Zannettino, C., Corsini, G., Sándor, G., & Végvári, G. (2009). The use of *fagopyrum tataricum gaetn*. whole flour to confer preventive contents of rutin to some traditional Tuscany biscuits. The Annals of the University Dunarea de Jos of Galati, Fascicle VI, *Food Technology*, 34, 1, 38-41.

Antunes, A. B. d. F., Geest, B.G.D., Vervaet, C., & Remon, J. P. (2013). Solvent-free drug crystal engineering for drug nano- and micro suspensions. *European Journal of Pharmaceutical Sciences* 48, 121–129.

Ao, Z., & Jane, J-L. (2007). Characterization and modeling of the A- and B-granule starches of wheat, triticale, and barley. *Carbohydrate Polymers*, 67, 46–55.

ASTM, 2011 Standard Practice for Calculation of Color Tolerance and Color Difference from Instrumentally Measured Color Coordinates, ASTM, International, West Conshohocken, PA, 2011 (ASTM D2244-11).

Atchley, A.A., Crum, L.A., Reidy, J.R. & Roy, R.A. (1984). The influence of the dissolved ion concentration on the acoustic cavitation threshold of water. *The Journal of the Acoustical Society of America* 75, S35.

Bai, Y., & Shi, Y-C. (2016). Chemical structures in pyrodextrin determined by nuclear magnetic resonance spectroscopy. *Carbohydrate Polymers* 151, 426–433.

Ball, S. G.; van de Wal, M.H.B., & Visser, R.G.F. (1998). Progress in understanding the biosynthesis of amylose. *Trends in Plant Science*, 3,12, 462-467.

Baks, T., Ngene, I.S., van Soest, J.J.G., Janssen, A.E.M., & Boom, R.M. (2007). Comparison of methods to determine the degree of gelatinisation for both high and low starch concentrations. *Carbohydrate Polymers,* 67, 481-490.

Balasundram, N., Sundram, K., & Samman, S. (2006). Phenolic compounds in plants and agri-industrial by-products: antioxidant activity, occurrence, and potential uses. *Food Chemistry,* 99, 191-203.

Bamdad, F., Wu, J., & Chen, L. (2011) Effects of enzymatic hydrolysis on molecular structure and antioxidant activity of barley hordein. *Journal of Cereal Science* 54, 20-28.

Barros, F., Awika, J.M. & Rooney, L.W. (2012). Interaction of tannins and other sorghum phenolic compounds with starch and effects on *in vitro* starch digestibility. *Journal of Agricultural and Food Chemistry*, 60, 11609-11617.

Bathgate, G.N., & Palmer, G.H. (1972). A reassessment of the chemical structure of barley and wheat starch granules. *Die Stärke*, 10, 336-341.

Bello-Pérez, L.A., Agama-Acevedo, E., Zamudio-Flores, P.B., Mendez-Montealvo, G., & Rodriguez-Ambriz, S.L. (2010). Effect of low and high acetylation degree in the morphological, physicochemical and structural characteristics of barley starch. *LWT - Food Science and Technology,* 43, 1434-1440.

Benzie, I, F.F., & Strain, J.J. (1996). The ferric reducing ability of plasma (frap) as a measure of ''antioxidant power'': the FRAP assay. *Analytical Biochemistry*, 239, 70–76.

Bergthaller W., & Hollmann, J. (2007). Starch. *Comprehensive Glycoscience, 2,* 579-612.

Berlim, L.S., Bezerra Jr., A.G., Pazina, W.M., Ramin, T.S., Schreiner, W.H., & Ito, A.S. (2018). Photophysical properties of flavonoids extracted from *Syngonanthus nitens*, the golden grass. *Journal of Luminescence,* 194, 394-400.

Bermudez-Aguirre, D. (2017) Sonochemistry of foods. *Ultrasound: Advances in Food Processing and Preservation*, Ed. Daniela Bermudez-Aguirre, Academic press, Elsevier, pp 131-143.

Bertoft, E., Qin, Z., & Turku, R.M. (1993). Studies on the structure of pea starches part 3: amylopectin of smooth pea starch. *Starch-Stärke* 45 (11), 377-382.

Bhatty, R. S. (1999). The potential of hull-less barley. *Cereal Chem*istry 76, 589-599.

Bhatty, R.S., & Rossnagel, B.G. (1998). Comparison of pearled and unpearled canadian and japanese barleys. *Cereal Chem*istry, 75, 1, 15-21.

Boun, H., & Huxsoll, C. (1991). Control of minimally processed carrot (*Daucus carota*) surface discoloration caused by abrasion peeling. *Journal of Food Science*, 56, 416-418.

Brunner, G. (2014). Hydrothermal and Supercritical Water Processes, Elsevier, Kidlington, Oxford, UK. pp 666.

Byars, J.A., Fanta, G.F., & Kenar. J.A. (2013). Effect of amylopectin on the rheological properties of aqueous dispersions of starch–sodium palmitate complexes. *Carbohydrate Polymers*, 95, 171-176.

Canadian Grain Commission. (2019). https://grainscanada.gc.ca/en/grain-research/export-quality/cereals/food-barley/, accessed on December 13, 2019.

Campechano-Carrera, E., Corona-Cruz, A., Chel-Guerrero, L., & Betancur-Ancona, D. (2007). Effect of pyrodextrinization on available starch content of Lima bean (*Phaseolus lunatus*) and Cowpea (*Vigna unguiculata*) starches. *Food Hydrocolloids* 21, 472–479.

Cao, X., Zhang, M., Qian, H., Mujumdar, A.S., & Wang, Z. (2017). Physicochemical and nutraceutical properties of barley grass powder microencapsulated by spray drying. *Drying Technology*, 35, 11, 1358-1367.

Cárcel, J.A., García-Pérez, J.V., Benedito, J., & Mulet, A. (2012). Food process innovation through new technologies: use of ultrasound. *Journal of Food Engineering,* 110, 200–207.

Carlson, T. L.-G., Lund, K.L., Goteborg, N.D.-N., & Brabrand, N.K. (1979). A study of the amylose-monoglyceride complex by raman spectroscopy. *Starch-Stärke* 31(7), 222-224.

Chai, Y., Wang, M., & Zhang, G. (2013). Interaction between amylose and tea polyphenols modulates the postprandial glycemic response to high-amylose maize starch. *Journal of Agricultural and Food Chemistry*, 61, 8608-8615.

Chaiwanichsiri, S., Ohnishi, S., Suzuki, T., Takai, R. & Miyawaki, O. (2001). Measurement of electrical conductivity, differential scanning calorimetry and viscosity of starch and flour suspensions during gelatinisation process. *Journal of the Science of Food and Agriculture,* 81,1586-1591.

Chatel, G. & Colmenares, J. C. (2017). Sonochemistry: from basic principles to innovative applications. *Topics in Current Chemistry* (Z) 375:8. Springer International Publishing Switzerland 2016.

Chebil, L., Humeau, C., Anthoni, J., Dehez, F., Engasser, J-M., & Ghoul, M. (2007). Solubility of flavonoids in organic solvents, *Journal of Chemical and Engineering Data*, 52, 1552-1556.

Chemat, F., Rombaut, N., Meullemiestre, A., Turk, M., Perino, S., Fabiano-Tixier, A-S., & Abert-Vian, M. (2017). Review of green food processing techniques. preservation, transformation, and extraction. *Innovative Food Science and Emerging Technologies*, 41, 357-377.

Chemat, F., Zill-e-Huma, & Khan, M. K. (2011). Applications of ultrasound in food technology: processing, preservation and extraction. *Ultrasonics Sonochemistry*, 18, 813-835.

Chen, C., Hu, W., Zhang, R., Jiang, A., & Zou, Y. (2016). Levels of phenolic compounds, antioxidant capacity, and microbial counts of fresh-cut onions after treatment with a combination of nisin and citric acid. *Horticulture, Environment, and Biotechnology*, 57, 3, 266-273.

Chen, W., Li, P., & Wang, X. (2010). Chemical stability of yellow pigment extracted from the flower bud of *Sophora japonica* L. (Huaimi). *International Journal of Food Science and Technology*, 45, 1666–1672.

Chen, H., Nie, Q., Xie, M., Yao, H., Zhang, K., Yin, J., & Nie, S. (2019). Protective effects of β-glucan isolated from highland barley on ethanol-induced gastric damage in rats and its benefits to mice gut conditions. *Food Research International,* 122, 157–166.

Chen, L., Tian, Y., Tong, Q., Zhang, Z., & Jin, Z. (2017). Effect of pullulan on the water distribution, microstructure and textural properties of rice starch gels during cold storage. *Food Chemistry* 214, 702–709.

Chen, X-W., Wang, J-M., Yang, X-Q., Qi, J-R., & Hou, J-J. (2016). Subcritical water induced complexation of soy protein and rutin: improved interfacial properties and emulsion stability. *Journal of Food Science*, 81(9), 2149-2157.

Cheng, L., Ye, X.P., He, R., & Liu, S. (2009). Investigation of rapid conversion of switchgrass in subcritical water. *Fuel Processing Technology*, 90, 301-311.

Cheng, J., Zhu, M., & Liu, X. (2020). Insight into the conformational and functional properties of myofibrillar protein modified by mulberry polyphenols. *Food Chemistry,* 308, 125592.

Chen, Z-Y, Zhu, Q.Y., Tsang, D., & Huang Y. (2001). Degradation of green tea catechins in tea drinks. *Journal of Agricultural and Food Chemistry*, 49, 477-482.

Cheow, C.S., & Yu, Y.S. (1997). Effect of fish protein content, salt, sugar and monosodium glutamate on the gelatinization of starch in fish-starch mixtures. *Journal of Food Processing and Preservation*, *21*, 161-177.

Chinnaswamy, R. (1993). Basis of cereal starch expansion. *Carbohydrate Polymers*, 21, 157-167.

Chirug, L., Okun, Z., Ramon, O., & Shpigelman, A. (2018). Iron ions as mediators in pectin-flavonols interactions. *Food Hydrocolloids*, 84, 441-449.

Chua, L.S. (2013). A review on plant-based rutin extraction methods and its pharmacological activities. *Journal of Ethnopharmacology* 150*,* 805–817.

Chua, L.S., Ruzlan, N.N., & Sarmidi, M.R. (2017) Recovery of Rutin from *Labisia pumila* Extract Using Solid Phase Extraction. *Acta Chimica Slovenica, 64,* 888–894.

Clements, R.L. (1977a). Electrical conductivity of flour suspensions and extracts in relation to flour ash. *Cereal Chemi*stry 54, 4, 847-854.

Clements, R.L. (1977b). Distribution of ash among flour extracts and fractions and its relation to electrical conductivity. *Cereal Chemi*stry, 54, 4, 840-847.

Cohen, R., Orlova, Y., Kovalev, M., Ungar, Y., & Shimoni, E. (2008). Structural and functional properties of amylose complexes with genistein. *Journal of Agricultural and Food Chemistry*, 56, 4212-4218.

Comin, L.M., Temelli, F., & Saldaña. (2012). Barley b-glucan aerogels as a carrier for flax oil via supercritical CO_2. *Journal of Food Engineering*, 111, 625–631.

Conde-Petit, B., Escher, F., & Nuessli, J. (2006). Structural features of starch-flavor complexation in food model systems. *Trends in Food Science and Techology,* 17, 227-235.

Covington, A.K., & Dickinson, T. (1973). Introduction and solvent properties. In: Covington AK, Dickinson T, editors. *Physical Chemistry of Organic Solvents Systems*. London: Plenum Press, pp 1–23.

Da Costa, E.M., Filho, J.M.B., do Nascimento, T.G., & Macêdo, R.O. (2002). Thermal characterization of the quercetin and rutin flavonoids, *Thermochimica Acta* 392-393, 79-84.

Dadáková, E., Vrchotová, N., Chmelová, Š., & Šerá, B. (2011). The stability of rutin and chlorogenic acid during the processing of black elder (*Sambucus nigra*) inflorescence. *Acta Alimentaria*, 40, 3, 327-334.

Dai, F., Miao, Q., Zhou, B., Yang, L., & Liu, Z-L. (2006). Protective effects of flavonols and their glycosides against free radical-induced oxidative hemolysis of red blood cells. *Life Sciences,* 78, 2488–2493.

De Araujo M.E., Franco Y.E.M, Alberto T.G, Sobreiro M.A, Conrado M.A, Priolli, D.G., & Sawaya A.C.F., Ruiz A.L., de Carvalho J.E., & de Oliveira, C.P. (2013). Enzymatic de-glycosylation of rutin improves its antioxidant and antiproliferative activities. *Food Chemistry* 141: 266-273.

Dev, B. & Jain, B.D. (1962). Spectrophotometric determination of thorium with rutin (quercetin-3-rutinoside), *Journal of the Less-Common Metals*, 4, 286-290.

Ding, X., Hua, Y., Chen, Y., Zhang, C. & Kong, X. (2015). Heavy metal complexation of thiol-containing peptides from soy glycinin hydrolysates. *International Journal of Molecular Sciences, 16*, 8040-8058.

Doctor, N. & Yang, Y. (2018). Separation and analysis of aspirin and metformin HCl using green subcritical water chromatography. *Molecules*, 23, 2258; doi:10.3390/molecules23092258.

Doublier, J.L. & Nantes. (1981). Rheological studies on starch - flow behaviour of wheat starch pastes. *Starch-Stärke* 33(12), 415-420.

Dudonné, S., Vitrac, X., Coutiére, P., Woillez, M., & Mérillon, J-M. (2009). Comparative study of antioxidant properties and total phenolic content of 30 plant extracts of industrial interest using DPPH, ABTS, FRAP, SOD, and ORAC assays. *Journal of Agricultural and Food Chemi*stry, 57, 1768–1774.

Dupuis, J.H., Tsao, R., Yada, R.Y., & Liu, Q. (2017). Physicochemical properties and in vitro digestibility of potato starch after inclusion with vanillic acid. *LWT - Food Science and Technology*, 85, 218-224.

El Halal, S.L.M., Colussi, R., Pinto, V.Z., Bartz, J., Radunz, M., Carreño, N.L.V., Dias, A. R.G., & Zavareze, E.d.R. (2015). Structure, morphology and functionality of acetylated and oxidised barley starches. *Food Chemistry*, 168, 247-256.

Elia, P., Azoulay, A., & Zeiri, Y. (2012). On the efficiency of water soluble antioxidants, *Ultrasonics Sonochemistry,* 19, 314-324.

Escandar, G.M., & Sala, L.F. (1991). Complexing behavior of rutin and quercetin, *Canadian Journal of Chemistry*, 69, 1994–2000.

Filipčev, B., Šimurina, O., Sakač, M., Sedej, I., Jovanov, P., & Bodroža-Solarov, M. (2011). Feasibility of use of buckwheat flor as an ingredient in ginger nut biscuit formulation, *Food Chemistry*, 125, 164-170.

Fisher, J.R., & Barnes, H.L. (1972). The ion-product constant of water to 350◦. *The Journal of Physical Chemistry*, 76, 1, 90–99.

Flora, G., Mittal, M., & Flora, S.J.S. (2015). Medical Countermeasures-Chelation Therapy, in: S.J.S., Flora (Ed.), Handbook of Arsenic Toxicology, Academic Press, Elsevier Science,London, pp. 589-626.

Foti, M.C., Daquino, C., & Geraci, C. (2004). Electron-Transfer Reaction of Cinnamic Acids and Their Methyl Esters with the DPPH Radical in Alcoholic Solutions, *Journal of Organic Chemistry,* 69, 2309-2314.

Friedman, M., & Jürgens, H.S. (2000). Effect of pH on the Stability of Plant Phenolic Compounds. *Journal of Agricultural and. Food Chemistry, 48,* 2101-2110.

Gabbott, P (2008). A practical introduction to differential scanning calorimetry, Principles and Applications of Thermal Analysis, (ed.) Gabbott, P., Blackwell Publishing Ltd. pp 1-50.

Gachovska, T.K., Ngadi, M.O., & Raghavan, G.S.V. (2006). Pulsed electric field assisted juice extraction from alfalfa. *Canadian Biosystems Engineering* 48:3.33-3.37.

Gao, J., Vasanthan, T., & Hoover, R. (2009). Isolation and characterization of high-purity starch isolates from regular, waxy, and high-amylose hulless barley grains. *Cereal Chem*istry, 86, 2, 157–163.

Gullón, B., Lú-Chau, T.A., Moreira, M.T., Lema, J.M., & Eibes, G. (2017). Rutin: a review on extraction, identification and purification methods, biological activities and approaches to enhance its bioavailability. *Trends in Food Science and Technology*, 67, 220-235.

Gulsun, T., Gursoy, R.N., & Oner, L. (2011). Design and characterization of nanocrystal formulations containing ezetimibe. *Chemical and Pharmaceutical Bulletin,* 59,1,41-45.

Guzar, I., Ragaee, S., & Seetharaman, K. (2012). Mechanism of hydrolysis of native and cooked starches from different botanical sources in the presence of tea extracts. *Journal of Food Science,* 77, 11, C1192-1196.

Güzel, D., & Sayar, S. (2010). Digestion profiles and some physicochemical properties of native and modified borlotti bean, chickpea and white kidney bean starches. *Food Research International*, 43, 2132–2137.

Hammond, K. E., Evans, D.E., & Hodson, M.J. (1995). Aluminium/silicon interactions in barley (*Hordeum vulgare* L.) seedlings, *Plant and Soil,* 173, 85-95.

Han, X., Kang, J., Bai, Y., Xue, M., & Shi, Y-C. (2018) Structure of pyrodextrin in relation to its retrogradation properties, *Food Chemistry,* 242, 169–173.

Hasler, C.M. (2002). Functional foods: benefits, concerns and challenges – a position paper from the American Council on Science and Health. *The Journal of Nutrition,* 132, 3772-3781.

He, C., Zhang, Z., Liu, H., Gao, J., Li, Y., & Wang, M. (2018). Effect of rutin and quercetin on the physicochemical properties of Tartary buckwheat starch. *Starch/Stärke*, 70, 1700038.

Hendriks, A.T.W.M, & Zeeman, G. (2009). Pretreatments to enhance the digestibility of lignocellulosic biomass, *Bioresource Technology*, 100, 10-18.

Hęś, M., Szwengiel, A., Dziedzic, K., Thanh-Blicharz, J.L., Kmiecik, D., & Górecka, D. (2017). The effect of buckwheat hull extract on lipid oxidation in frozen-stored meat products. *Journal of Food Science,* 82, 4, 882-889.

Hinkle, M. E. & Zobel, H. F. (1968). X-ray diffraction of oriented amylose fibers. iii. the structure of amylose-n-butanol complexes. *Biopolymers* 6, 1119-1128.

Hossain, M.A., Salehuddin, S.M., Kabir, M.J., Rahman, S.M.M., & Rupasinghe, H.P.V. (2009). Sinensetin, rutin, 30-hydroxy-5, 6, 7, 40-tetramethoxyflavone and rosmarinic acid contents and antioxidative effect of the skin of apple fruit. *Food Chemistry,* 113, 185-190.

Hoover, R., & Ratnayake, W.S. (2002). Starch characteristics of black bean, chickpea, lentil, navy bean and pinto bean cultivars grown in Canada. *Food Chemistry,* 78, 489-498.

Hossain, M.A., Salehuddin, S.M., Kabir, M. J., Rahman, S.M.M., & Rupasinghe, H.P.V. (2009). Sinensetin, rutin, 3´-hydroxy-5, 6, 7, 4´-tetramethoxyflavone and rosmarinic acid contents and antioxidative effect of the skin of apple fruit. *Food Chemistry,* 113, 185–190.

Hou, L., Zhou, B., Yang, L., & Liu, Z-L. (2004). Inhibition of human low density lipoprotein oxidation by flavonols and their glycosides. *Chemistry and Physics of Lipids,* 129, 209–219.

Hu, X., Guo, B., Liu, C., Yan, X., Chen, J., Luo, S., Liu, Y., Wang, H., Yang, R., Zhong, Y., & Wu, J. (2018). Modification of potato starch by using superheated steam. *Carbohydrate Polymers,* 198, 375–384.

Huang, D., Ou, B., & Prior, R.L. (2005). The chemistry behind antioxidant capacity assays. *Journal of Agricultural and Food Chemistry*, 53, 1841-1856.

Huang, W., Xue, A., Niu, H., Jia, Z., & Wang, J. (2009). Optimised ultrasonic-assisted extraction of flavonoids from *folium eucommiae* and evaluation of antioxidant activity in multi-test systems *in vitro*. *Food Chemistry,* 114, 1147–1154.

Huerta, R.R., & Saldaña, M.D.A. (2018). Pressurized fluid treatment of barley and canola straws to obtain carbohydrates and phenolics. *The Journal of Supercritical Fluids* 141, 12–20.

Immel, S. & Darmstadt, F.W.L. (2000). The hydrophobic topographies of amylose and its blue iodine complex. *Starch-Stärke* 52(1), 1-8.

Imoto, T., & Yagishita, K. (1971). A simple activity measurement of lysozyme, *Agricultural and Biological Chemistry*, 35, 1154–1156.

Jane, J-J (2009). Structural features of starch granules II. In J. BeMiller, & R. Whistler (Eds.), *Starch: Chemistry and Technology*, 3rd ed. New York: Elsevier. pp. 193-236.

Jeon, Y-J., Vasanthan, T., Temelli, F., & Song, B-K. (2003). The suitability of barley and corn starches in their native and chemically modified forms for volatile meat flavor encapsulation. *Food Research International,* 36, 349–355.

Jeszka-Skowron, M., Krawczyk, M., & Zgoła-Grześkowiak, A. (2015). Determination of antioxidant activity, rutin, quercetin, phenolic acids and trace elements in tea infusions: Influence of citric acid addition on extraction of metals. *Journal of Food Composition and Analysis,* 40, 70–77.

Jin, F, Z. Zhou, A. Kishita, & Enomoto, H. (2006). Hydrothermal conversion of biomass into acetic acid, *Journal of Material Science,* 41, 1495-1500.

Jouquand, C., Ducruet, V., & Le Bail, P. (2006). Formation of amylose complexes with C6-aroma compounds in starch dispersions and its impact on retention. *Food Chemistry,* 96, 461-470.

Jovanovic, S.V., Steenken, S., Tosic, M., Marjanovic, B., & Simic, M.G. (1994). Flavonoids as antioxidants. *Journal of the American Chemical Society,* 116, 4846-4851.

Jurasekova, Z., Domingo, C., Garcia-Ramos, J.V., & Sanchez-Cortes, S. (2014). Effect of pH on the chemical modification of quercetin and structurally related flavonoids characterized by optical (UV-visible and Raman) spectroscopy. *Physical Chemistry Chemical Physics,* 16, 12802.

Kalinova, J., & Dadakova, E. (2009). Rutin and total quercetin content in amaranth (*amaranthus* spp.). *Plant Foods for Human Nutrition,* 64, 68–74.

Källman, A., Bertoft, E., Koch, K., Åman, P., & Andersson, R. (2013). On the interconnection of clusters and building blocks in barley amylopectin. *International Journal of Biological Macromolecules,* 55, 75-82.

Källman, A., Vamadevan, V., Bertoft, E., Koch, K., Seetharaman, K., Åman, P., & Andersson, R. (2015). Thermal properties of barley starch and its relation to starch characteristics. *International Journal of Biological Macromolecules,* 81, 692–700.

Karunaratne, R., & Zhu, F. (2016). Physicochemical interactions of maize starch with ferulic acid. *Food Chemistry*, 199, 372-379.

Kasemwong, K., & Itthisoponkul, T. (2013). Encapsulation of flavour compounds as helical inclusion complexes of starch. In Park & Appell, *Advances in Applied Nanotechnology for Agriculture ACS Symposium Series* 9 (pp 235-245), Washington, DC, American Chemical Society.

Keetels, C.J.A.M., Oostergetel, G.T., & van Vliet, T. (1996). Recrystallization of amylopectin in concentrated starch gels. *Carbohydrate Polymers*, 30, 61-64.

Kenar, J.A., Compton, D.L., Little, J.A., & Peterson, S.C. (2016). Formation of inclusion complexes between high amylose starch and octadecyl ferulate via steam jet cooking. *Carbohydrate Polymers*, 140, 246-252.

Khalifa, T. I., Muhtadi, F. J., & Hassan, M. M. A. (1983). Rutin, *Analytical Profiles Drug Substances,* In Florey, K., (ed.) Academic Press: New York. vol. 12, pp 623-681.

Kim, D-S., & Lim, S-B. (2017). Optimization of subcritical water hydrolysis of rutin into isoquercetin and quercetin. *Preventive Nutrition and Food Science,* 22,2, 131-137.

Kim, D., Yeom, S., Park, C-S., & Kim, Y-S. (2016). Effect of high hydrostatic pressure treatment on isoquercetin production from rutin by commercial α-L-rhamnosidase. *Biotechnology Letters,* 38, 1775-1780.

Klein, E., Rimarčík, J., Senajová, E., Vagánek, A., & Lengyel, J. (2016). Deprotonation of flavonoids severely alters the thermodynamics of the hydrogen atom transfer. *Computational and Theoretical Chemistry,* 1085, 7-17.

Komulainen, S., Pursiainen, J., Perämäki, P., & Lajunen, M. (2013). Complexation of Fe(III) with water-soluble oxidized starch. *Starch-Stärke*, 65, 338-345.

Kong, X., Kasapis, S., Zhu, P., Sui, Z., Bao, J., & Corke, H. (2016). Physicochemical and structural characteristics of starches from Chinese hull-less barley cultivars. *International Journal of Food Science and Technology,* 51, 509–518.

Kong, B., & Xiong, Y.L. (2006). Antioxidant Activity of Zein Hydrolysates in a Liposome System and the Possible Mode of Action. *Journal of Agricultural and Food Chemi*stry, 54, 6059−6068.

Kowblansky, M. (1985). Calorimetric investigation of inclusion complexes of amylose with long-chain aliphatic compounds containing different functional groups. *Macromolecules, 18*, 1776–1779.

Kraujalis, P., Venskutonis, P.R., Kraujalienė, V., & Pukalskas, A. (2013). Antioxidant properties and preliminary evaluation of phytochemical composition of different anatomical parts of amaranth. *Plant Foods for Human Nutrition*, 68, 322–328.

Kreft, I., Fabjan, N., & Yasumoto, K. (2006). Rutin content in buckwheat (*Fagopyrum esculentum* Moench) food materials and products. *Food Chemistry,* 98, 508–512.

Krewson, C.F., & Naghski, J. (1952). Some physical properties of rutin. *Journal of American Pharmacists Association,* XLI (11), 582-587.

Kuang, J., Yuk, K.Y., & Huh, K.M. (2011). Polysaccharide-based superporous hydrogels with fast swelling and superabsorbent properties. *Carbohydrate Polymers* 83: 284–290.

Kumar, S., & Pandey, A.K. (2013) Chemistry and biological activities of flavonoids: an overview. *The Scientific World Journal*, vol. 2013, Article ID 162750, 16 pages.

Lee, E.J., Nomura, N., Patil, B.S., & Yoo, K.S. (2014). Measurement of total phenolic content in wine using an automatic Folin–Ciocalteu assay method. *International Journal of Food Science and Technology*, 49, 2364–2372.

Lemańska, K., Szymusiak, H., Tyrakowska, B., Zieliński, R., Soffers, A.E.M.F., & Rietjens, I.M.C.M. (2001). The influence of pH on antioxidant properties and the mechanism of antioxidant action of hydroxyflavones. *Free Radical Biology and Medicine,* 31,7, 869-881.

Li, M., Pernell, C., & Ferruzzi. M.G. (2018). Complexation with phenolic acids affect rheological properties and digestibility of potato starch and maize amylopectin. *Food Hydrocolloids,* 77, 843-852.

Li, J.H., Vasanthan, T., Hoover, R., & Rossnagel, B.G. (2004). Starch from hull-less barley: IV. Morphological and structural changes in waxy, normal and high-amylose starch granules during heating. *Food Research International*, 37, 417-428.

Li, W., Xiao, X., Zhang, W., Zheng, J., Luo, Q., Ouyang, S., & Zhang, G. (2014). Compositional, morphological, structural and physicochemical properties of starches from seven naked barley cultivars grown in China. *Food Research International,* 58, 7–14.

Liao, J., Qu, B., Liu, D., & Zheng, N. (2015). New method to enhance the extraction yield of rutin from *Sophora japonica* using a novel ultrasonic extraction system by determining optimum ultrasonic frequency. *Ultrasonics Sonochemistry*, 27, 110–116.

Liang, X., & Fan, Q. (2013). Application of sub-critical water extraction in pharmaceutical industry, *Journal of Materials Science and Chemical Engineering*, 1, 1-6.

Liang, Y. Yang, C., & Shi, H. (2001). Effects of silicon on growth and mineral composition of barley grown under toxic levels of aluminium, *Journal of Plant Nutrition*, 24: 2, 229-243.

Lin, C-L., Lin, J-H., Zeng, H-M., Wu, Y-H., & Chang, Y-H. (2018). Indigestible pyrodextrins prepared from corn starch in the presence of glacial acetic acid. *Carbohydrate Polymers*, 188, 68–75.

Lin, L-Y., Liu, H-M., Yu, Y-W., Lin, S-D., & Mau, J-L. (2009). Quality and antioxidant property of buckwheat enhanced wheat bread. *Food Chemistry,* 112, 987-991.

Lin, L-M., Wu, H-Y., Li, W-S., Chen, W-L., Lee, Y-J., Wu, D.C., Li, P., & Yeh, A. (2010). Kinetic studies of the oxidation of quercetin, rutin and taxifolin in the basic medium by (ethylenediaminetetraacetato) cobalt (III) complex. *Inorganic Chemistry Communications,* 13, 633–635.

Liu, K., & Barrows, F.T. (2017). Wet processing of barley grains into concentrates of proteins, β-glucan, and starch. *Cereal Chemistry* 94, 2, 161–169.

Liu, Y., Gou, L., Fu, X., Li, S., Lan, N., & Yin, X. (2013). Protective effect of rutin against acute gastric mucosal lesions induced by ischemia-reperfusion. *Pharmaceutical Biology*, 51, 7, 914–919.

Liu, D., Xu, H., Tian, B., Yuan, K., Pan, H., Ma, S., Yang, X., & Pan, W. (2012). Fabrication of carvedilol nanosuspensions through the anti-solvent precipitation– ultrasonication method for the improvement of dissolution rate and oral bioavailability. *AAPS Pharm Sci Tech*, 13, 1, 295-304.

Lorentz, C., Pencreac'h, G., Soultani-Vigneron, S., Rondeau-Mouro, C., de Carvalho, M., Pontoire, B., Ergan, F., & Le Bail, P. (2012). Coupling lipophilization and amylose complexation to encapsulate chlorogenic acid. *Carbohydrate Polymers*, 90, 152-158.

Lu, Y., Dong, Y., Li, X., & He, Q. (2016). The nitrite-scavenging properties of catechol, resorcinol, and hydroquinone: a comparative study on their nitration and nitrosation reactions. *Journal of Food Science,* 8, 11, *2692-2696.*

Magalhães, L.M., Segundo, M.A., Reis, S., & Lima, J.L.F.C. (2008). Methodological aspects about in vitro evaluation of antioxidant properties. *Analytica Chimica Acta* 613, 1-19.

Maheshwari, G., Sowrirajan, S., & Joseph B. (2017). Extraction and isolation of β-Glucan from grain sources-A review. *Journal of Food Science*, 82, 7, 1535-1545.

Malešev, D. & Kuntić. (2007). Investigation of metal-flavonoid chelates and the determination of flavonoids via meta-flavonoid complexing reactions. *Journal of the Serbian Chemical Society*, 72, 10, 921-939.

MarketsandMarkets (2019). https://www.marketsandmarkets.com/Market-Reports/speciality-food-ingredients-market-252775011.html. Accessed December 12, 2019.

Martínez, M., Motilva, M-J., de las Hazas, M-C. L., Romero, M-P., Vaculova, K., & Ludwig, I.A. (2018). Phytochemical composition and β-glucan content of barley genotypes from two different geographic origins for human health food production. *Food Chemistry,* 245, 61–70.

Mauludin, R., Müller, R.H., & Keck, C.M. (2009). Kinetic solubility and dissolution velocity of rutin nanocrystals. *European Journal of Pharmaceutical Sciences*, 36, 502–510.

Mcallister, T. & Meale, S. (2015). Barley grain. Feed Industry Guide (1st ed.). Agriculture and Agric-Food Canada. www.albertabarley.com, accessed on December 22, 2018.

McClements, D.J. (1995). Advances in the application of ultrasound in food analysis and processing. *Trends in Food Science and Technology,* 6, 293-299.

McDonald, A.M.L., & Stark, J.R. (1988). A critical examination of procedures for the isolation of barley starch. *Journal of Institute of Brewing*, 94, 125-132.

McMillan, T., Izydorczyk, & Li, Y. (2019). Barley Production and Quality of Western Canadian Malting Barley 2019. Canadian Grain Commission, https://grainscanada.gc.ca/en/grain-research/export-quality/cereals/malting-barley/pdf/cgc-barley-annual-report.pdf, accessed on December 13, 2019.

Medina, D.D., Gedanken, A., & Mastai, Y. (2011). Chiral amplification in crystallization under ultrasound radiation. *Chemistry - A European Journal*, 17, 11139-11142.

Medvidović-Kosanović, M., Šeruga, M., Jakobek, Lidija, & Novak, I. (2010). Electrochemical and antioxidant properties of (+)-catechin, quercetin and rutin. *Croatica Chemica Acta,* 83, 2, 197-207.

Menezes, José C. J. M. D. S., Orlikova, B., Morceau, F., & Diederich, M. (2016) Natural and synthetic flavonoids: structure–activity relationship and chemotherapeutic potential for the treatment of leukemia. *Critical Reviews in Food Science and Nutrition*, 56: S4–S28.

Merendino, N., Molinari, R. Costantini, L., Mazzucato, A., Pucci, A., Bonafaccia, F., Esti, M., Ceccantoni, B., Papeschi, C., & Bonafaccia, G. (2014). A new "functional" pasta containing tartary buckwheat sprouts as an ingredient improves the oxidative status and normalizes some blood pressure parameters in spontaneously hypertensive rats. *Food and Function*, 5, 1017-1026.

Middleton, E.J. (1998). Effect of plant flavonoids on immune and inflammatory cell function. *Advances in Experimental Medicine and Biology*, vol. 439, Flavonoids in the living system (Eds.) John A. Manthey, Bela S. Buslig, Springer Science+Business Media New York, USA. pp. 175–182.

Miles, M.J., Morris, V.J., Orford, P. D*.,* & Ring, S.G. (1985). The roles of amylose and amylopectin in the gelation and retrogradation of starch. *Carbohydrate Research*, 135, 271-281.

Mittal, V.A., Ellis, A., Ye, A., Edwards, P.J.B., Das, S., & Singh, H. (2016). Iron binding to caseins in the presence of orthophosphate, *Food Chemistry*, 190, 128-134.

Miyake, K., Arima, H., Hirayama, F., Yamamoto, M., Horikawa, T., Sumiyoshi, H., Noda, S., & Uekama, K. (2000). Improvement of solubility and oral bioavailability of rutin by complexation with 2-hydroxypropyl-β-cyclodextrin. *Pharmaceutical Development and Technology*, 5,3, 399-407.

Modig, G., Nilsson, P-O., & Wahlund, K-G. (2006). Influence of jet-cooking temperature and ionic strength on size and structure of cationic potato amylopectin starch as

measured by asymmetrical flow field-flow fractionation multi-angle light scattering. *Starch-Stärke,* 58, 55-65.

Montanari, A., Chen, J., & Widmer, W. (1998). Discovery of new flavonoids from dancy tangerine cold pressed peel oil solids and leaves, citrus flavonoids: a review of past biological activity against disease. *Advances in Experimental Medicine and Biology*, vol. 439, *Flavonoids In The Living System* (Eds.) John A. Manthey, Bela S. Buslig, Springer Science+Business Media New York, USA. pp. 103–116.

Montes, A., Wehner, L., Pereyra, C., & de la Ossa, E.J.M. (2016). Precipitation of submicron particles of rutin using supercritical antisolvent process. *Journal of Supercritical Fluids*, 118, 1-10.

Morales-Sanchez, E., Vazquez-Landaverde, P. A., Gaytan-Martinez, M., and Huerta-Ruelas, J.A. (2009) Electrical conductivity of heated cornstarch–water mixtures. *Journal of Food Process Engineering,* 32, 817–827.

Moreschi, S.R.M., Petenate, A.J., & Meireles, M.A. (2004). Hydrolysis of ginger bagasse starch in subcritical water and carbon dioxide. *Journal of Agricultural and Food Chemistry, 52,* 1753-1758.

Morikawa, K., & Nishinari, K. (2000). Effects of concentration dependence of retrogradation behaviour of dispersions for native and chemically modified potato starch. *Food Hydrocolloids, 14*, 395-401.

Morita, N., Maeda, T., Miyazaki, M., Yamamori, M., Miura, H., & Ohtsuka, I. (2002). Dough and baking properties of high-amylose and waxy wheat flours. *Cereal Chemistry, 79*, 491-495.

Nagamori, M., & Funazukuri, T. (2004). Glucose production by hydrolysis of starch under hydrothermal conditions. *Journal of Chemical Technology and Biotechnology, 79,* 229–233.

Naguleswaran, S., Vasanthan, T., Hoover, R., & Bressler, D. (2013). The susceptibility of large and small granules of waxy, normal and high-amylose genotypes of barley and corn starches toward amylolysis at sub-gelatinization temperatures. *Food Research International,* 51, 771–782.

Naguleswaran, S., Vasanthan, T., Hoover, R., & Bressler, D. (2014a). Amylolysis of amylopectin and amylose isolated from wheat, triticale, corn and barley starches. *Food Hydrocolloids,* 35, 686-693.

Naguleswaran, S., Vasanthan, T., Hoover, R., Chen, L., & Bressler, D. (2014b). Molecular characterisation of waxy corn and barley starches in different solvent systems as revealed by MALLS. *Food Chemistry,* 152, 297–299.

Nguyen, T.T.H., Kim, N.M., Yeom, S-C., Han, S., kwak, S-H., Kim, S-B., Park, J-S., Mok, I.K., & Kim, D. (2017). Biological characterization of epigallocatechin gallate complex with different steviol glucosides, *Biotechnology and Bioprocess Engineering*, 22, 512-517.

Noosuk, P., Hill, S.E., Farhat, I.A., Mitchell, J.R., & Pradipasena, P. (2005). Relationship between viscoelastic properties and starch structure in rice from Thailand. *Starch-Stärke,* 57, 587-598.

Novak, I., Janeiro, P., Seruga, M., & Oliveira-Brett, A.M. (2008). Ultrasound extracted flavonoids from four varieties of Portuguese red grape skins determined by reverse-phase high-performance liquid chromatography with electrochemical detection. *Analytica Chimica Acta,* 630, 107–115.

Nyombaire, G., Siddiq, M., & Dolan, K.D. (2011). Physico-chemical and sensory quality of extruded light red kidney bean (*Phaseolus vulgaris L.*) porridge, *LWT - Food Science and Technology* 44, 1597-1602.

Obiro, W. C., Ray, S. S., & Emmambux, M. N. (2012). V-amylose structural characteristics, methods of preparation, significance, and potential applications. *Food Reviews International*, 28, 412-438.

Okechukwu, P.E., & Rao, M.A. (1996). Role of granules size and size distribution in the viscosity of cowpea starch dispersions heated in excess water. *Journal of Texture Studies*, *27*, 159-173.

Olvera-Hernández, Betancur-Ancona, D., Chel-Guerrero, L.A., Ble-Castillo, J.L., & Castellanos-Ruelas, A.F. (2018). Morphological and physicochemical changes in great dwarf banana (*Musa cavendish* aaa) starch modified by pyrodextrinization and enzymatic hydrolysis. *Starch/Stärke*, *70*, 1700122.

Orozco-Martínez, T., and Betancur-Ancona, D. (2004). Indigestible starch of *P. lunatus* obtained by pyroconversion: changes in physicochemical properties. *Starch/Stärke,* 56, 241–247.

Ożarowski, M., Mikołajczak, P. Ł., Kujawski, R., Wielgus, K., Klejewski, A., Wolski, H., & Seremak-Mrozikiewicz, A. (2018). Pharmacological effect of quercetin in hypertension and its potential application in pregnancy-induced hypertension: review of *in vitro*, *in vivo*, and clinical studies, *Evidence-Based Complementary and Alternative Medicine*, Article ID 7421489.

Paczkowska, M., Mizera, M., Piotrowska, H., Szymanowska-Powałowska, D., Lewandowska, K., Goscianska, J., Pietrzak, R., Bednarski, W., Majka, Z., & Cielecka-Piontek, J. (2015). Complex of rutin with β-cyclodextrin as potential delivery system. *PLoS ONE* 10(3): e0120858.

Palacios, H.R., Schwarz, P.B., D'Appolonia, B.L. (2004). Effects of α-amylases from different sources on the firming of concentrated wheat starch gels: relationship to bread staling. *Journal of Agricultural and Food Chemistry*, 52, 5987-5994.

Panhwar, Q.K. & Memon, S. (2014). Synthesis, characterization and antioxidant activity of rutin complexes, *Pakistan Journal of Analytical and Environmental Chemistry*, 15, 2, 60-70.

Paniwnyk, L., Beaufoy, E., Lorimer, J.P., & Mason, T.J. (2001). The extraction of rutin from flower buds of *Sophora japonica*. *Ultrasonics Sonochemistry* 8, 299-301.

175

Paula, R.D., Rabalski, I., Messia, M.C., Abdel-aal, E.M., & Marconi, E. (2017). Effect of processing on phenolic acids composition and radical scavenging capacity of barley pasta. *Food Research International*, 102, 136–143.

Pei-Ling, L., Xiao-Song, H., & Qun, S. (2010). Effect of high hydrostatic pressure on starches: a review. *Starch/Stärke* 62, 615–628.

Pękal, A. & Pyrzynska, K. (2014). Evaluation of aluminium complexation reaction for flavonoid content assay. *Food Analytical Methods*, 7, 1776–1782.

Peng, B., Li, R., & Yan, W. (2009). Solubility of rutin in ethanol + water at (273.15 to 323.15) K, *Journal of Chemical and Engineering Data*, 54, 1378-1381.

Peres, G.L., Leite, D.C., & da Silveir, N.P. (2016). Study of complexes formation between transition metal ions and amylopectin in DMSO/H_2O solution. *Starch/Stärke*, 68, 1129–1138.

Petrucci, R.H., Harwood, W.S., Herring, F.G., & Madura, J. D. (2007). *General Chemistry: Principles and Modern Applications*. 9th ed. Prentice Hall, New Jersey, USA, pp 822-857.

Phaechamud, T. & Tuntarawongsa, S. (2016). Transformation of eutectic emulsion to nanosuspension fabricating with solvent evaporation and ultrasonication technique, *International Journal of Nanomedicine*, 11 2855–2865.

Pińkowska, P. Wolak, & Oliveros, E. (2013). Application of Doehlert matrix for determination of the optimal conditions of hydrothermolysis of rapeseed meal in subcritical water, *Fuel,* 10,258-264.

Plaza, M., & Turner, C. (2015). Pressurized hot water extraction of bioactives. *Trends in Analytical Chemistry*, 71, 39–54.

Prado, J.M, Forster-Carneiro, T., Rostagno, M.A., Follegatti-Romero, L.A., Filho, F.M., & Meireles, M.A.A. (2014). Obtaining sugars from coconut husk, defatted grape seed, and pressed palm fiber by hydrolysis with subcritical water, *Journal of Supercritical Fluids,* 89,89-98.

Přikryl, J., Hájel, T., Švecová, B., Salex, R.N., Černíková, M., Červenka, L., & Buňka, F. (2018). Antioxidant properties and textural characteristics of processed cheese spreads enriched with rutin or quercetin: The effect of processing conditions. *LWT - Food Science and Technology,* 87, 266-271.

Proctor, A. (2018). *Alternatives to Conventional Food Processing*, 2nd edition, (ed) Andrew Proctor, The Royal Society of Chemistry, pp 499.

Qu, J., Zhou, Q., Du, Y., Zhang, W., Bai, M., Zhang, Z., Xi, Y., Li, Z., & Miao, J. (2014). Rutin protects against cognitive deficits and brain damage in rats with chronic cerebral hypoperfusion. *British Journal of Pharmacology,* 171, 3702–3715.

Ravber, M., Knez, Z., & Škerget, M. (2015). Optimization of hydrolysis of rutin in subcritical water using response surface methodology. *Journal of Supercritical Fluids*, 104, 145–152.

Ravber, M., Pečar, D., Goršek, A., Iskra, J., Knez, Ž., & Škerget, M. (2016). Hydrothermal degradation of rutin: identification of degradation products and kinetics study. *Journal of Agricultural and Food Chemistry*, 64, 9196-9202.

Saldaña, M.D.A, Alvarez, V.H., & Haldar, A. (2012). Solubility and Physical properties of sugars in pressurized water. 2012. *Journal of Chemical Thermodynamics,* 55, 115-123.

Saldaña, M.D.A., & Valdivieso-Ramírez, C.S. (2015). Pressurized fluid systems: phytochemical production from biomass. *The Journal of Supercritical Fluids*, 96, 228-244.

Samarakoon, E.R.J., Waduge, R., Liu, Q., F. Shahidi, F. & Banoub, J.H. (2020). Impact of annealing on the hierarchical structure and physicochemical properties of waxy starches of different botanical origins. *Food Chemistry,* 303, 125344.

Sando, C. E., & Lloyd, J.U. (1924) The isolation and identification of rutin from the flowers of elder (*Sambucus canadensis* l.) *Journal of Biological Chemistry,* 58, 737-745.

Sarkar, S., Alvarez, V.H. & Saldaña, M.D.A. (2014). Relevance of ions in pressurized fluid extraction of carbohydrates and phenolics from barley hull, *Journal of Supercritical Fluids,* 93, 27-37.

Saunders, M. (2008). Thermal analysis of pharmaceuticals, Principles and Applications of Thermal Analysis, (ed.) Gabbott, P., Blackwell Publishing Ltd. pp 286-239. doi:10.1002/9780470697702.

Savic, I.M., Savic-Gajic, I.M., Nikolic, V.D., Nikolic, L.B., Radovanovic, B.C., & Milenkovic-Andjelkovic, A. (2016). Enhancement of solubility and photostability of rutin by complexation with β-cyclodextrin and (2-hydroxypropyl)-β-cyclodextrin. *Journal of Inclusion Phenomena and Macrocyclic Chemistry,* 86, 33-43.

Scherer, R.I. & Godoy, H.T. (2014). Effects of extraction methods of phenolic compounds from *Xanthium strumarium* L. and their antioxidant activity. *The Brazilian Journal of Medicinal Plants* 16: 41-46.

Schirmer, M., Höchstötter, A., Jekle, M., Arendt, E., & Becker, T. (2013). Physicochemical and morphological characterization of different starches with variable amylose/amylopectin ratio. *Food Hydrocolloids,* 32, 52-63.

Sedej, I., Sakač, M., Mandić, A., Mišan, A., Pestorić, M., Šimurina, O., & Čanadanović-Brunet, J. (2011). Quality assessment of gluten-free crackers based on buckwheat flour, *LWT-Food Science and Technology,* 44, 694-699.

Shaarawy, H.H., El-Rafie, S.M., El-Ghaffar, A.M.A, & El-Rafie, M.H. (2009). Electrocatalytic oxidation of rice starch using mixed oxidant generated via

titanium/rhodium thermally activated modified electrode: Part (I). *Carbohydrate Polymers*, 75, 208–213.

Sharma, K., Ko, E.Y., Assefa, A.D., Ha, S., Nile, S.H., Lee, E.T., & Park, S.W. (2015). Temperature-dependent studies on the total phenolics, flavonoids, antioxidant activities, and sugar content in six onion varieties. *Journal of Food and Drug Analysis,* 23, 243-252.

Shultz, M.J. (2007). Chemistry for Engineers, An applied approach. Houghton Mifflin Company, Boston, USA, pp 326.

Silberberg, M.S. (2009). *Chemistry: the molecular nature of matter and change* 5th ed. McGraw-Hill, Boston, USA. pp 923-966.

Simin, N., Orcic, D., Cetojevic-Simin, D., Mimica-Dukic, N., Anackov, G., Beara, I., Mitic-Culafic, D., & Bozin, B. (2013). Phenolic profile, antioxidant, anti-inflammatory and cytotoxic activities of small onion (*Allium flavum* L. subsp. *flavum*, Alliaceae). *LWT – Food Science and Technology*, 54, 139-146.

Singh, J., Kaur, L., & Singh, N. (2004). Effect of acetylation on some properties of corn and potato starches. *Starch-Stärke*, *56*, 586-601.

Singh, A., Lahlali, R., Vanga, S.K., Karunakaran, C., Orsat, V., & Raghavan, V. (2016). Effect of high electric field on secondary structure of wheat gluten*, International Journal of Food Properties* 19, 1217-1226.

Singh, P.P., & Saldaña, M.D.A. (2011). Subcritical water extraction of phenolic compounds from potato peel, *Food Research International,* 44, 2452-2458.

Soria, A.C., & Villamiel, M. (2010). Effect of ultrasound on the technological properties and bioactivity of food: a review. *Trends in Food Science & Technology,* 21, 323-331.

Součková, M., Klomfar, J., & Pátek, J. (2008). Measurement and correlation of the surface tension-temperature relation for methanol. *Journal of Chemical & Engineering Data*, 53, 2233-2236.

Sridhar, K., Rahman, H., Sosnik, A., Mukherjee, U., Natarajan, T., Siram, K. & Krishnamoorthy, B. (2016). Production of irbesartan nanocrystals by high shear homogenisation and ultra-probe sonication for improved dissolution rate. *Current Drug Delivery, 13,* 688-697.

Statista, https://www.statista.com/statistics/271973/world-barley-production-since-2008/ accessed on January 28, 2019.

Statistics Canada, https://www.grainscanada.gc.ca/barley-orge/harvest-recolte/2017/qbsm17-qosm17-2-en.html, accessed on November 13, 2018.

Stohs, S.J., & Gagchi, D. (1995). Oxidative mechanisms in the toxicity of metal ions. *Free Radical Biology and Medicine,* 18, 2, 321-336.

Su, J., Chotineeranat, S., Laoka, B., Chatakanonda, P., Vanichsriratana, W., Sriroth, K., & Piyachomkwan, K. (2018). Effect of dry heat treatment with xanthan gum on physicochemical properties of different amylose rice starches. *Starch-Stärke*, 70, 1700142.

Subpuch, N., Huang, T-C., & Suwannaporn, P. (2016). Enzymatic digestible starch from pyrodextrinization to control the release of tocopheryl acetate microencapsulation in simulated gut model. *Food Hydrocolloids* 53, 277-283.

Sutkar, V.S., & Gogate, P.R. (2010). Mapping of cavitational activity in high frequency sonochemical reactor. *Chemical Engineering Journal*, 158, 296–304.

Szawara-Nowak, D., Koutsidis, G., Wiczkowski, W., & Zieliński, H. (2014). Evaluation of the *in vitro* inhibitory effects of buckwheat enhanced wheat bread extracts on the formation of advanced glycation end-products (AGEs). *LWT- Food Science and Technology,* 58, 327-334.

Szeto, Y.T., Tomlinson, B., & Benzie, I.F.F. (2002). Total antioxidant and ascorbic acid content of fresh fruits and vegetables: implications for dietary planning and food preservation. *British Journal of Nutrition* 87, 55–59.

Takahama, U., & Hirota, S. (2010). Fatty acids, epicatechin-dimethylgallate, and rutin interact with buckwheat starch inhibiting its digestion by amylase: implications for the decrease in glycemic index by buckwheat flour. *Journal of Agricultural and Food Chemistry*, 58, 12431-12439.

Takahama, U., Yamauchi, R., & Hirota, S. (2013). Interactions of starch with a cyanidin-catechin pigment (vignacyanidin) isolated from *Vigna angularis* bean. *Food Chemistry*, 141, 2600-2605.

Takeo, K., Tokumura, A., & Kuge, T. (1973). Complexes of starch and its related materials with organic compounds. Part. X. X-ray diffraction of amylose-fatty acid complexes. *Die Stärke Jahrg,* 11, 357-362.

Tang, H., Watanabe, K., & Mitsunaga, T. (2002). Structure and functionality of large, medium and small granule starches in normal and waxy barley endosperms. *Carbohydrate Polymers,* 49, 217 -224.

The Merck Index. (2006). An encyclopedia of chemicals, drugs, and biologicals. 14th edition. Eds, O'Neil, M.J., Heckelman, P.E., Koch, C.B., Roman, K.J., Kenny, C.M., D'Arecca, M.R., Merck & Co. Inc., Whitehouse Station, NJ, USA. pp 8303.

Tongdang, T., Meenun, M., & Chainui, J. (2008). Effect of sago starch addition and steaming time on making cassava cracker (keropok). *Starch-Stärke,* 60, 568-576.

Trinh, K.S., & Dang, T.B. (2019). Structural, physicochemical, and functional properties of electrolyzed cassava starch. *International Journal of Food Science*, 9290627.

Uddin, M.H., Nanzai, B., & Okitsu, K. (2016). Effects of Na_2SO_4 or NaCl on sonochemical degradation of phenolic compounds in an aqueous solution under Ar: positive and

negative effects induced by the presence of salts. *Ultrasonics Sonochemistry* 28, 144–149.

Valentová, K., Vrba, J., Bancířová, M., Ulrichová, J., & Křen, V. (2014). Isoquercetrin: pharmacology, toxicology, and metabolism, *Food and Chemical Toxicology,* 68, 267-282.

Vamadevan, V., Bertoft,E., Soldatov, D.V., & Seetharaman, K.(2013). Impact on molecular organization of amylopectin in starch granules upon annealing. *Carbohydrate Polymers,* 98, 1045– 1055.

Van Soest, J.J.G., Tournois, H., De Wit, D., & Vliegenthart, J.F.G. (1995). Short-range structure in (partially) crystalline potato starch determined with attenuated total reflectance Fourier-transform IR spectroscopy. *Carbohydrate Research,* 279, 201-214.

Vasanthan, T., & Temelli, F. (2008). Grain fractionation technologies for cereal beta-glucan concentration, *Food Research International*, 41, 876-881.

Vetrova, E.V., Maksimenko, E.V., Khizrieva, S.S., Bugaeva, A.F., Borisenko, N.I., & Minkin, V. I. (2017). A simple way for the preparation of natural antioxidant quercetin from rutin by subcritical water. *Journal of Natural Science, Biology and Medicine*, 8,213-215.

Wang, S., & Copeland, L. (2015). Effect of acid hydrolysis on starch structure and functionality: a review. *Critical Reviews in Food Science and Nutrition*, 55, 1081-1097.

Wang, S., Li, C., Copeland, L., Niu, Q., & Wang, S. (2015). Starch retrogradation: a comprehensive review. *Comprehensive Reviews in Food Science and Food Safety,* 14, 568-585.

Wang, C., & Zuo, Y. (2011). Ultrasound-assisted hydrolysis and gas chromatography–mass spectrometric determination of phenolic compounds in cranberry products. *Food Chemistry,* 128, 562–568.

Wang, C., Tian, Z., Chen, L., Temelli, F., Liu, H., & Wang, Y. (2010). Functionality of barley proteins extracted and fractionated by alkaline and alcohol methods. *Cereal Chem*istry 87, 6, 597-606.

Watanabe. M., Ohshita, Y., & Tsushida, T. (1997). Antioxidant compounds from buckwheat (*Fagopyrum esculentum möench*) hulls. *Journal of Agricultural and Food Chemistry,* 45, 1039-1044.

Wei, Q., Keck, C.M., & Müller, R.H. (2017). Preparation and tableting of long-term stable amorphous rutin using porous silica. *European Journal of Pharmaceutics and Biopharmaceutics*, 113, 97-107.

Whittam, M.A., Orford, P.D., Ring, S.G., Clark, S.A., Parker, M.L., Cairns, P., & Miles, M.J. (1989). Aqueous dissolution of crystalline and amorphous amylose-alcohol complexes. *International Journal of Biological Macromolecules*, 11, 339-344.

Winkel-Shirley, B. (2001). Flavonoid biosynthesis. A colorful model for genetics, biochemistry, cell biology, and biotechnology, *Plant physiology*, 126, 485-493.

Wood, P.J., Weisz, J., Fedec, P., & Burrows, V.D. (1989). Large-scale preparation and properties of oat fractions enriched in (1-3)(1-4)-beta-D-glucan. *Cereal Chemistry*, 66,2, 97-103.

Wu, Y., Chen, Z., Li, X., & Li, M. (2009). Effect of tea polyphenols on the retrogradation of rice starch. *Food Research International*, 42, 221–225.

Wu, Y., Lin, Q., Chen, Z. & Xiao, H. (2011). The interaction between tea polyphenols and rice starch during gelatinization. *Food Science and Technology International*, 17, 6, 569–577.

Xia, Y., Bamdad, F., Gänzle, M., & Chen, L. (2012). Fractionation and characterization of antioxidant peptides derived from barley glutelin by enzymatic hydrolysis. *Food Chemistry*, 134, 1509–1518.

Xiao, H., Lin, Q., Liu, G-Q., Wu, Y., Tian, W., Wu, W., & Fu, X. (2011). Effect of green tea polyphenols on the gelatinization and retrogradation of rice starches with different amylose contents. *Journal of Medicinal Plants Research* 5,17, 4298-4303.

Xiao, H., Lin, Q., Liu, G-Q., Wu, Y., Wu, W., & Fu, X. (2013). Inhibitory effects of green tea polyphenols on the retrogradation of starches from different botanical sources. *Food and Bioprocess Technology*, 6:2177–2181.

Xiao, X., Yu, L., Xie, F., Bao, X., Liu, H., Ji, Z., & Chen, L. (2017). One-step method to prepare starch-based superabsorbent polymer for slow release of fertilizer. *Chemical Engineering Journal*, 309, 607–616.

Xijun, L., Kunsheng, Z., Qingfeng, L., Xu, Z., & Shuyi, Z. (2012). The effects of electrolysis at room temperature on retrogradation of sweet potato Starch. *International Journal of Biological Macromolecules,* 50, 38–42.

Yang, J., Lee, H., Sung, J., Kim, Y., Jeong, H.S., & Lee, J. (2019). Conversion of rutin to quercetin by acid treatment in relation to biological activities. *Preventive Nutrition and Food Science,* 24, 3, 313-320.

Yangcheng, H., Gong, L., Zhang, Y., & Jane, J-L. (2016). Physicochemical properties of Tibetan hull-less barley starch. *Carbohydrate Polymers,* 137, 525–531.

Ye, J., Hu, X., Luo, S., Liu, W., Chen, J., Zeng, Z., & Liu, C. (2018). Properties of starch after extrusion: a review. *Starch-Stärke,* 70, 11, 1700110.

Yoo, J., Kim, Y., Yoo, S-H., Inglett, G.E., & Lee, S. (2012). Reduction of rutin loss in buckwheat noodles and their physicochemical characterisation. *Food Chemistry,* 132, 2107-2111.

You, S., & Izydorcyk, M.S. (2002). Molecular characteristics of barley starches with variable amylose content, *Carbohydrate Polymers,* 49, 33-42.

Zhang, M., Chen, H., Li, J., Pei, Y., & Liang, Y. (2010) Antioxidant properties of tartary buckwheat extracts as affected by different thermal processing methods. *LWT - Food Science and Technology,* 43, 181–185.

Zhang, Y., Wang, D., Yang, L., Zhou, D., & Zhang, J. (2014). Purification and characterization of flavonoids from the leaves of zanthoxylum bungeanum and correlation between their structure and antioxidant activity. *PLoS One,* 9, e105725.

Zhang, W.L., Chen, J-P., Lam, K. Y-C., Zhan, J. Y-X., Yao, P., Dong, T. T-X., & Tsim, K. W-K.(2014) Hydrolysis of glycosidic flavonoids during the preparation of danggui buxue tang: an outcome of moderate boiling of chinese herbal mixture. *Evidence-Based Complementary and Alternative Medicine*, Article ID 608721, 11 pages.

Zhang, Z-L., Zhou, M-L., Tang, Y., Li, F-L., Tang, Y-X., Shao, J-R., Xue, W-T., & Wu, Y-M. (2012). Bioactive compounds in functional buckwheat food. *Food Research International,* 49, 389–395.

Zhao, Y., & Saldaña, M.D.A (2019a). Hydrolysis of cassava starch, chitosan and their mixtures in pressurized hot water media. *The Journal of Supercritical Fluids,* 147, 293–301.

Zhao, Y., & Saldaña, M.D.A. (2019b). Use of potato by-products and gallic acid for development of bioactive film packaging by subcritical water technology. The *Journal of Supercrit Fluids, 143*, 97-106.

Zhu, F. (2015a). Interactions between starch and phenolic compound. *Trends in Food Science and Technology*, 43, 129-143.

Zhu, F. (2015b). Impact of ultrasound on structure, physicochemical properties, modifications, and applications of starch. *Trends in Food Science and Technology*, 43: 1-17.

Zhu, F. (2018). Modifications of starch by electric field based techniques. *Trends in Food Science & Technology*, 75, 158–169.

Zhu, F., Cai, Y. Z., Sun, M., & Corke, H. (2008). Effect of phenolic compounds on the pasting and textural properties of wheat starch. *Starch-Stärke*, 60, 609-616.

Zhu, F., & Wang, Y. (2012). Rheological and thermal properties of rice starch and rutin mixtures. *Food Research International, 49*, 752–762.

Zhu, H. & Damodaran, S. (1994). Effects of calcium and magnesium ions on aggregation of whey protein isolate and its effect on foaming properties. *Journal of Agricultural and Food Chemistry,* 42, 856-862.

Zhao, W., & Yang, R. (2012). Pulsed electric field induced aggregation of food proteins: ovalbumin and bovine serum albumin. *Food Bioprocess Technol* 5:1706–1714.

Zieliński, H., Michalska, A., Amigo-Benavent, M., del Castillo, M.D., & Piskula, M.K. (2009). Changes in protein quality and antioxidant properties of buckwheat seeds and groats induced by roasting. *Journal of Agricultural and Food Chemistry*, 57, 4771-4776.

Appendix

Appendix A: Barley starch behavior in the presence of rutin under subcritical water conditions

(A)

$y = 2E+07x - 94119$
$R^2 = 0.9996$

(B)

$y = 4E+07x - 294834$
$R^2 = 0.9999$
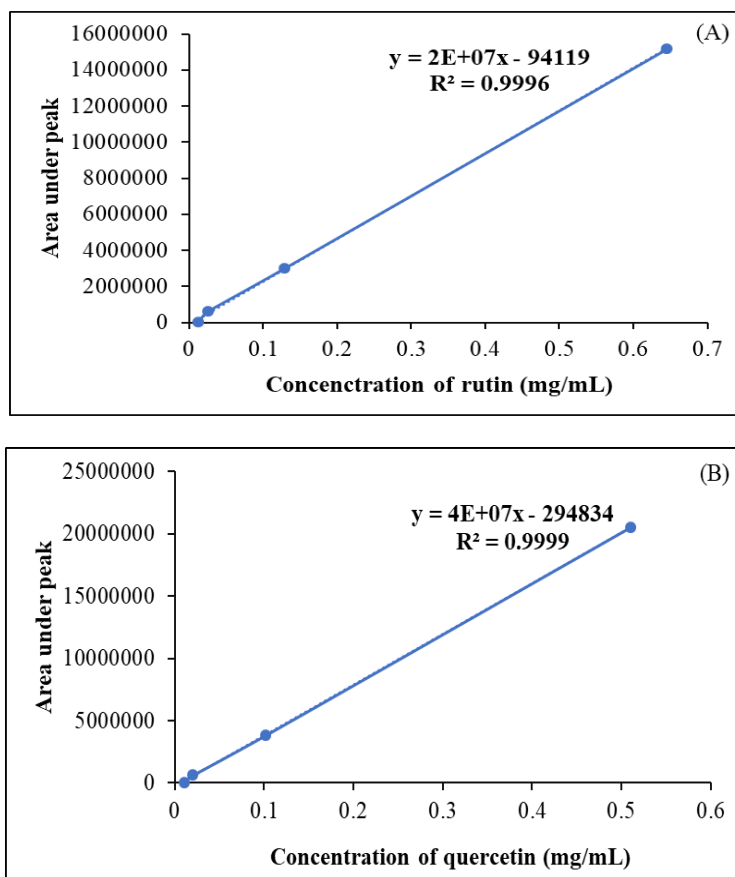
Figure A.1. Standard curves for rutin (A) and quercetin (B) determination in aqueous rutin solution using HPLC at 268 nm.
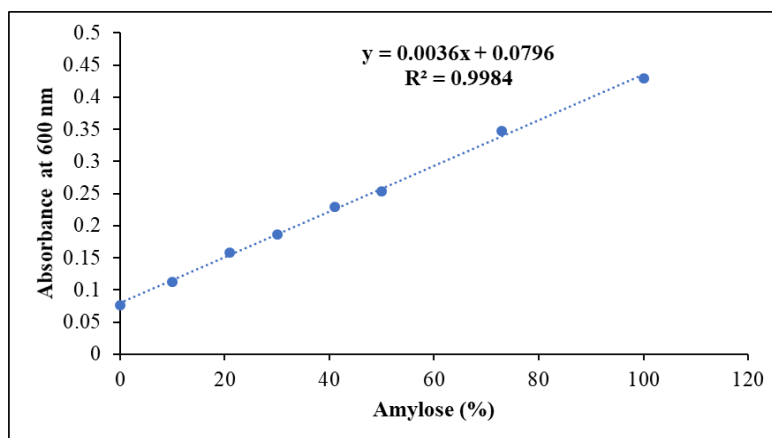
Figure A.2. Standard curve for amylose content determination using UV spectrophotometer at wavelength 600 nm.

Table A.1. Amylose content of different barley varieties

Barley variety	Abs	Amylose	Moisture content (%)	Amylose (dm)	Mean	Std dev
CDC Hilose	0.193	0.318	10.13	0.354	0.372	0.026
	0.207	0.357	8.60	0.391		
Peregrine	0.155	0.211	10.19	0.235	0.223	0.017
	0.149	0.194	7.73	0.210		
CDC Rattan	0.076	-0.011	-	-	-	-
	0.070	-0.028	-	-	-	-

Abs – absorbance, - Not available, dm – dry matter, Std dev – standard deviation
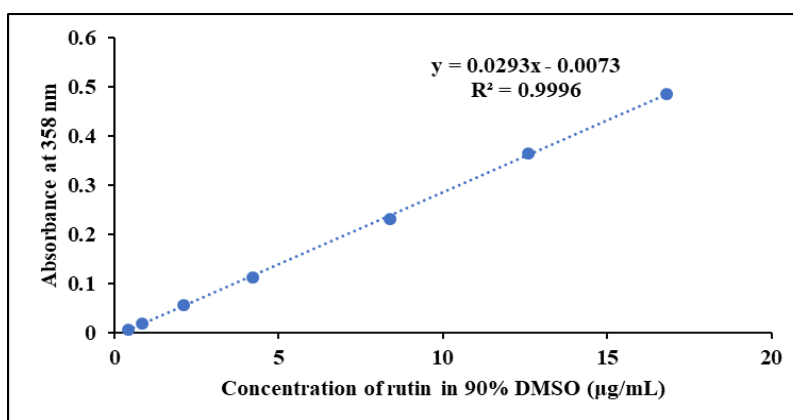
Figure A.3. Standard curve for rutin content determination using UV spectrophotometer at wavelength of 358 nm.

185

Table A.2. Purity of starch powders

Temperature (ºC)	Starch	Total starch (% dm)	Starch	Total starch (% dm)	Starch	Total starch (% dm)
80	37% amylose with rutin	87.17±2.43[c]	22% amylose with rutin	90.50±1.11[abc]	0% amylose with rutin	93.51±1.21[abc]
100		89.32±0.89[bc]		91.98±2.04[abc]		95.47±3.29[abc]
120		89.95±0.69[bc]		95.70±1.59[abc]		93.83±3.14[abc]
140		88.73±2.59[bc]		93.36±2.25[abc]		96.16±0.92[ab]
160		89.59±0.63[bc]		95.22±3.64[abc]		94.01±3.07[abc]
80	37% amylose	88.95±2.05[bc]	22% amylose	89.81±1.93[bc]	0% amylose	90.94±0.31[abc]
100		90.01±0.32[bc]		91.84±2.77[abc]		89.56±3.99[bc]
120		88.79±1.89[bc]		90.56±3.21[bc]		94.92±3.54[abc]
140		-		93.81±1.55[abc]		93.37±2.27[abc]
160		-		92.39±2.05[abc]		97.82±2.34[a]

Data shown as mean±standard deviation (*n*=3).

[a-c]Data with same lowercase letters within rows and columns are not significantly different. – not available.

Table A.3. Rutin content in starch

CDC Rattan (0% amylose starch)												
T (°C)	Starch			Rutin			Rutin	Rutin/ Starch		Rutin/ Starch		
	Mass (mg)	Mass (g)	Abs (Y)	Conc (ug/mL)	Conc (mg/mL)	Vol (mL)	mg	mg/g (as is)	MC (%)	mg/g (dm)	Mean	Std dev
80	20.0	0.02	0.131	4.720	0.005	3.0	0.014	0.708	3.180	0.731	0.696	0.003
	20.1	0.0201	0.119	4.311	0.004	3.0	0.013	0.643	3.180	0.665		
80	20.0	0.02	0.127	4.584	0.005	3.0	0.014	0.688	3.862	0.715		
	20.3	0.0203	0.121	4.379	0.004	3.0	0.013	0.647	3.862	0.673		
100	20.8	0.0208	0.219	7.336	0.007	3.0	0.022	1.058	4.450	1.107	0.871	0.060
	20.1	0.0201	0.146	4.910	0.005	3.0	0.015	0.733	4.450	0.767		
	20.1	0.0201	0.116	3.914	0.004	3.0	0.012	0.584	4.450	0.611		
100	20.8	0.0208	0.14	4.711	0.005	3.0	0.014	0.679	4.740	0.713		
	20.7	0.0207	0.152	5.110	0.005	3.0	0.015	0.741	4.740	0.777		
	20.4	0.0204	0.242	8.100	0.008	3.0	0.024	1.191	4.740	1.250		
120	20.0	0.02	0.129	4.346	0.004	3.0	0.013	0.652	6.230	0.695	0.644	0.016
	20.5	0.0205	0.128	4.312	0.004	3.0	0.013	0.631	6.230	0.673		
	20.8	0.0208	0.115	3.880	0.004	3.0	0.012	0.560	6.230	0.597		
120	20.8	0.0208	0.121	4.080	0.004	3.0	0.012	0.588	4.970	0.619		
	20.5	0.0205	0.128	4.312	0.004	3.0	0.013	0.631	4.970	0.664		
	20.3	0.0203	0.117	3.947	0.004	3.0	0.012	0.583	4.970	0.614		
140	20.6	0.0206	0.071	2.419	0.002	3.0	0.007	0.352	4.990	0.371	0.379	0.026
	20.3	0.0203	0.069	2.352	0.002	3.0	0.007	0.348	4.990	0.366		
	20.0	0.02	0.064	2.186	0.002	3.0	0.007	0.328	4.990	0.345		
140	20.4	0.0204	0.076	2.585	0.003	3.0	0.008	0.380	5.820	0.404		
	20.8	0.0208	0.075	2.551	0.003	3.0	0.008	0.368	5.820	0.391		

T- temperature, Abs – absorbance, Conc – concentration, dm – dry matter, Std dev- standard deviation, MC – moisture content.

Table A.3. Continued.

								Rutin	Rutin/ Starch		Rutin/ Starch		
T (°C)	Starch			Rutin				Rutin					
	Mass (mg)	Mass (g)	Abs (Y)	Conc (ug/mL)	Conc (mg/mL)	Vol (mL)	mg	mg/g (as is)	MC (%)	mg/g (dm)	Mean	Std dev
CDC Rattan (0% amylose starch)												
160	20.5	0.0205	0.048	1.654	0.002	3.0	0.005	0.242	5.570	0.256	0.250	0.004
	20.6	0.0206	0.047	1.621	0.002	3.0	0.005	0.236	5.570	0.250		
	20.0	0.0200	0.043	1.488	0.001	3.0	0.004	0.223	5.570	0.236		
160	20.1	0.0201	0.050	1.721	0.002	3.0	0.005	0.257	6.050	0.273		
	20.3	0.0203	0.046	1.588	0.002	3.0	0.005	0.235	6.050	0.250		
	20.1	0.0201	0.043	1.488	0.001	3.0	0.004	0.222	6.050	0.236		
Peregrine (22% amylose starch)												
80	20.5	0.0205	0.117	4.180	0.004	3.0	0.013	0.612	4.152	0.638	0.616	0.105
	20.1	0.0201	0.086	3.129	0.003	3.0	0.009	0.467	4.152	0.487		
80	20.1	0.0201	0.108	3.875	0.004	3.0	0.012	0.578	3.335	0.598		
	20.5	0.0205	0.138	4.892	0.005	3.0	0.015	0.716	3.335	0.741		
100	20.2	0.0202	0.091	3.083	0.003	3.0	0.009	0.458	4.740	0.481	0.534	0.018
	20.3	0.0203	0.108	3.648	0.004	3.0	0.011	0.539	4.740	0.566		
	20.2	0.0202	0.098	3.316	0.003	3.0	0.010	0.492	4.740	0.517		
100	20.8	0.0208	0.107	3.615	0.004	3.0	0.011	0.521	4.390	0.545		
	20.3	0.0203	0.113	3.814	0.004	3.0	0.011	0.564	4.390	0.590		
	20.6	0.0206	0.098	3.316	0.003	3.0	0.010	0.483	4.390	0.505		
120	20.7	0.0207	0.082	2.784	0.003	3.0	0.008	0.403	4.800	0.424	0.469	0.024
	20.6	0.0206	0.11	3.714	0.004	3.0	0.011	0.541	4.800	0.568		
	20.7	0.0207	0.09	3.050	0.003	3.0	0.009	0.442	4.800	0.464		
120	20.5	0.0205	0.088	2.983	0.003	3.0	0.009	0.437	4.630	0.458		
	20.8	0.0208	0.087	2.950	0.003	3.0	0.009	0.426	4.630	0.446		

T-temperature, Abs – absorbance, Conc – concentration, Vol – volume, dm – dry matter, Std dev- Standard deviation, MC – moisture content

Table A.3. Continued.

T (°C)	Starch Mass (mg)	Mass (g)	Abs (Y)	Rutin Conc (µg/mL)	Conc (mg/mL)	Vol (3mL)	Rutin mg	Rutin/Starch mg/g (as is)	MC (%)	Rutin/Starch mg/g (dm)	Mean	Std dev
120	20.3	0.0203	0.086	2.917	0.003	3.000	0.009	0.431	4.630	0.452		
140	20.7	0.0207	0.056	1.920	0.002	3.000	0.006	0.278	5.280	0.294	0.279	0.017
	20.3	0.0203	0.044	1.522	0.002	3.000	0.005	0.225	5.280	0.237		
	20.6	0.0206	0.051	1.754	0.002	3.000	0.005	0.255	5.280	0.270		
140	20.4	0.0204	0.057	1.953	0.002	3.000	0.006	0.287	5.230	0.303		
	20.3	0.0203	0.054	1.854	0.002	3.000	0.006	0.274	5.230	0.289		
	20.8	0.0208	0.054	1.854	0.002	3.000	0.006	0.267	5.230	0.282		
160	20.6	0.0206	0.036	1.256	0.001	3.000	0.004	0.183	4.370	0.191	0.191	0.000
	20.7	0.0207	0.037	1.289	0.001	3.000	0.004	0.187	4.920	0.196		
	20	0.02	0.03	1.056	0.001	3.000	0.003	0.158	4.920	0.167		
	20.6	0.0206	0.039	1.355	0.001	3.000	0.004	0.197	4.920	0.208		
CDC Hilose (37% amylose starch)												
80	20.5	0.0205	0.12	4.281	0.004	3.000	0.013	0.627	4.083	0.653	0.634	0.024
	20.5	0.0205	0.106	3.807	0.004	3.000	0.011	0.557	4.083	0.581		
80	20.4	0.0204	0.128	4.553	0.005	3.000	0.014	0.669	3.565	0.694		
	20.5	0.0205	0.112	4.010	0.004	3.000	0.012	0.587	3.565	0.609		
100	20.2	0.0202	0.151	5.332	0.005	3.000	0.016	0.792	4.354	0.828	0.647	0.042
	20.5	0.0205	0.095	3.434	0.003	3.000	0.010	0.503	4.354	0.525		
100	20.6	0.0206	0.096	3.468	0.003	3.000	0.010	0.505	4.311	0.528		
	20.5	0.0205	0.13	4.620	0.005	3.000	0.014	0.676	4.311	0.707		
120	20.4	0.0204	0.098	3.536	0.004	3.000	0.011	0.520	4.673	0.545	0.580	0.047
	19.9	0.0199	0.096	3.468	0.003	3.000	0.010	0.523	4.673	0.548		

T-temperature, Abs – absorbance, Conc – concentration, Vol – volume, dm – dry matter, Std dev- Standard deviation, MC – moisture content

Table A.3. Continued.

T (°C)	Starch Mass (mg)	Mass (g)	Abs (Y)	Rutin Conc (µg/mL)	Conc (mg/mL)	Vol (mL)	Rutin mg	Rutin/ Starch mg/g (as is)	MC (%)	Rutin/ Starch mg/g (dm)	Mean	Std dev
120	20.5	0.0205	0.11	3.942	0.004	3.00	0.012	0.577	4.271	0.603		
	20.0	0.02	0.111	3.976	0.004	3.00	0.012	0.596	4.271	0.623		
140	20.3	0.0203	0.099	3.628	0.004	3.00	0.011	0.536	4.372	0.561	0.550	0.023
	20.3	0.0203	0.101	3.696	0.004	3.00	0.011	0.546	4.372	0.571		
140	20.0	0.0200	0.092	3.389	0.003	3.00	0.010	0.508	4.676	0.533		
160	19.9	0.0199	0.052	2.024	0.002	3.00	0.006	0.305	5.063	0.321	0.344	0.032
	20.4	0.0204	0.062	2.365	0.002	3.00	0.007	0.348	5.063	0.366		

T-temperature, Abs – absorbance, Conc – concentration, dm – dry matter, Std dev- Standard deviation, MC – moisture content

Table A.4. Amylose content in starch

Peregrine (22% amylose starch)							
	Temperature (°C)	Abs	MC (%)	% amylose (as is)	% amylose (dm)	Mean	Standard deviation
With rutin	80	0.131	4.15	0.14	0.15	0.15	0.00
	80	0.131	3.33	0.14	0.15		
	100	0.144	4.74	0.18	0.19	0.20	0.01
	100	0.15	4.39	0.20	0.21		
	120	0.121	4.80	0.12	0.12	0.13	0.01
	120	0.128	4.63	0.14	0.14		
	140	0.155	5.28	0.21	0.22	0.23	0.00
	140	0.157	5.23	0.22	0.23		
	160	0.156	4.37	0.21	0.22	0.22	0.00
	160	0.154	4.92	0.21	0.22		
Without rutin	80	0.139	5.08	0.17	0.17	0.17	0.01
	80	0.133	5.08	0.15	0.16		
	100	0.145	3.80	0.18	0.19	0.19	0.01
	100	0.148	3.97	0.19	0.20		
	120	0.147	4.26	0.19	0.20	0.20	0.00
	120	0.148	4.05	0.19	0.20		
	140	0.153	2.77	0.21	0.21	0.21	0.00
	140	0.151	3.75	0.20	0.21		
	160	0.156	4.02	0.21	0.22	0.22	0.00
	160	0.157	4.02	0.22	0.23		

Abs- absorbance, MC – moisture content, dm – dry matter

Table A.4. Continued.

	Temperature (°C)	Abs	MC (%)	% amylose (as is)	% amylose (dm)	Mean	Standard deviation
CDC Hilose (37% amylose starch)							
With rutin	80	0.165	4.08	0.24	0.25	0.24	0.01
	80	0.162	3.57	0.23	0.24		
	100	0.173	4.35	0.26	0.27	0.27	0.00
	100	0.174	4.31	0.26	0.28		
	120	0.18	4.67	0.28	0.30	0.29	0.01
	120	0.176	4.27	0.27	0.28		
	140	0.187	4.37	0.30	0.31	0.31	0.01
	140	0.183	4.68	0.29	0.30		
	160	0.21	5.06	0.37	0.39	0.37	0.03
	160	0.197	5.06	0.33	0.35		
Without rutin	80	0.168	4.35	0.25	0.26	0.26	0.00
	80	0.166	4.35	0.24	0.25		
	100	0.19	6.23	0.31	0.33	0.35	0.02
	100	0.201	6.23	0.34	0.36		
	120	0.184	6.02	0.29	0.31	0.31	0.01
	120	0.181	6.02	0.28	0.30		

Abs- absorbance, MC – moisture content, dm – dry matter

Table A.5. Specific volume (Expansion) of starch

	Temperature (°C)	Weight (g)	Volume (mL)	Bulk density (g/mL)	1/BD (mL/g)	Mean	Std dev
CDC Rattan (0% amylose starch)							
	Native starch	0.37	0.50	0.74	1.35	1.32	0.04
	Native starch	0.39	0.50	0.78	1.29		
With rutin	80	0.25	0.50	0.51	1.98	1.97	0.01
	80	0.25	0.50	0.51	1.97		
	100	0.29	0.50	0.58	1.71	1.75	0.05
	100	0.28	0.50	0.56	1.78		
	120	0.26	0.50	0.52	1.92	1.88	0.06
	120	0.27	0.50	0.54	1.84		
	140	0.32	0.50	0.63	1.58	1.65	0.11
	140	0.29	0.50	0.58	1.73		
	160	0.24	0.50	0.48	2.07	2.06	0.01
	160	0.24	0.50	0.49	2.06		
Without rutin	80	0.28	0.50	0.56	1.77	1.91	0.20
	80	0.24	0.50	0.49	2.05		
	100	0.25	0.50	0.50	1.99	1.85	0.21
	100	0.29	0.50	0.59	1.70		
	120	0.32	0.50	0.65	1.55	1.58	0.04
	120	0.31	0.50	0.62	1.60		
	140	0.33	0.50	0.66	1.52	1.54	0.02
	140	0.32	0.50	0.64	1.55		
	160	0.27	0.50	0.53	1.88	1.94	0.08
	160	0.25	0.50	0.50	1.99		
Peregrine (22% amylose starch)							
	Native starch	0.43	0.50	0.85	1.18	1.19	0.03
	Native starch	0.41	0.50	0.82	1.21		
With rutin	80	0.20	0.50	0.40	2.51	2.51	0.00
	80	0.20	0.50	0.40	2.51		
	100	0.25	0.50	0.50	2.00	1.97	0.04
	100	0.26	0.50	0.51	1.94		
	120	0.25	0.50	0.50	1.98	2.07	0.12
	120	0.23	0.50	0.46	2.16		
	140	0.19	0.50	0.39	2.57	2.68	0.16
	140	0.18	0.50	0.36	2.80		
	160	0.18	0.50	0.36	2.79	2.80	0.02
	160	0.18	0.50	0.36	2.81		

BD- bulk density

Table A.5. Specific volume (Expansion) of starch (Continued).

	Temperature (°C)	Weight (g)	Volume (mL)	Bulk density (g/mL)	1/BD (mL/g)	Mean	Std dev
Peregrine (22% amylose starch)							
Without rutin	80	0.15	0.50	0.30	3.34	3.37	0.04
	80	0.15	0.50	0.29	3.40		
	100	0.24	0.50	0.48	2.08	2.06	0.03
	100	0.24	0.50	0.49	2.04		
	120	0.24	0.50	0.48	2.07	2.12	0.06
	120	0.23	0.50	0.46	2.17		
	140	0.26	0.50	0.53	1.90	1.97	0.10
	140	0.25	0.50	0.49	2.04		
	160	0.18	0.50	0.36	2.74	2.76	0.03
	160	0.18	0.50	0.36	2.78		
CDC Hilose (37% amylose starch)							
	Native starch	0.41	0.50	0.81	1.23	1.24	0.01
	Native starch	0.40	0.50	0.80	1.25		
With rutin	80	0.23	0.50	0.45	2.21	2.27	0.09
	80	0.21	0.50	0.43	2.34		
	100	0.15	0.50	0.30	3.33	3.15	0.26
	100	0.17	0.50	0.34	2.96		
	120	0.16	0.50	0.31	3.21	3.03	0.25
	120	0.18	0.50	0.35	2.85		
	140	0.12	0.50	0.24	4.20	4.62	0.60
	140	0.10	0.50	0.20	5.04		
	160	0.08	0.50	0.17	5.97	6.10	0.17
	160	0.08	0.50	0.16	6.22		
Without rutin	80	0.23	0.50	0.46	2.18	2.10	0.11
	80	0.25	0.50	0.49	2.03		
	100	0.26	0.50	0.52	1.92	1.91	0.01
	100	0.26	0.50	0.53	1.90		
	120	0.22	0.50	0.43	2.31	2.24	0.10
	120	0.23	0.50	0.46	2.17		

BD- bulk density, Std dev – Standard deviation

Table A.6. Viscoelastic properties of starch with rutin.

Frequency (Hz)	CDC Rattan (0% amylose starch)											
	80 °C				100 °C				120 °C			
	Storage modulus (Pa)				Storage modulus (Pa)				Storage modulus (Pa)			
	a	b	Mean	Std dev	a	b	Mean	Std dev	a	b	Mean	Std dev
0.10	320.15	88.78	204.46	163.60	138.09	146.56	142.32	5.99	211.64	73.06	142.35	97.99
0.16	332.40	93.57	212.98	168.88	143.20	151.63	147.41	5.96	219.60	76.58	148.09	101.13
0.25	345.62	99.07	222.34	174.34	148.66	157.14	152.90	5.99	230.27	80.72	155.50	105.74
0.40	362.35	105.58	233.97	181.56	155.58	164.27	159.92	6.14	240.81	86.35	163.58	109.22
0.63	383.30	115.44	249.37	189.41	164.06	172.84	168.45	6.20	256.44	94.33	175.39	114.63
1.00	409.66	129.30	269.48	198.25	178.58	186.83	182.71	5.84	276.42	107.28	191.85	119.60
1.58	449.04	154.38	301.71	208.36	203.31	211.39	207.35	5.71	307.96	129.81	218.89	125.98
2.51	514.16	203.08	358.62	219.97	251.67	259.57	255.62	5.59	363.67	175.29	269.48	133.20
3.98	638.04	306.94	472.49	234.12	355.89	363.28	359.59	5.23	475.36	275.11	375.24	141.60
6.31	900.72	546.00	723.36	250.83	596.67	602.82	599.74	4.34	721.49	508.58	615.03	150.54
10.00	1502.87	1119.52	1311.20	271.07	1175.58	1177.98	1176.78	1.70	1299.16	1073.39	1186.28	159.64
15.85	2947.13	2524.82	2735.98	298.62	2598.01	2589.40	2593.71	6.09	2700.89	2464.49	2582.69	167.16
25.00	6416.05	5938.63	6177.34	337.59	6056.45	6020.98	6038.72	25.08	6096.61	5849.89	5973.25	174.46
	140 °C				160 °C							
0.10	27.27	35.86	31.56	6.07	15.73	11.32	13.53	3.11				
0.16	30.21	38.88	34.55	6.13	19.24	14.60	16.92	3.28				
0.25	33.27	42.05	37.66	6.21	24.53	19.46	22.00	3.58				
0.40	37.62	47.04	42.33	6.66	32.10	25.62	28.86	4.58				
0.63	44.48	54.07	49.28	6.78	42.34	35.33	38.84	4.95				
1.00	55.69	65.44	60.56	6.89	58.42	50.78	54.60	5.40				
1.58	76.66	87.16	81.91	7.42	86.37	77.85	82.11	6.02				
2.51	120.49	131.75	126.12	7.96	139.32	130.73	135.03	6.08				
3.98	219.72	231.85	225.79	8.57	249.51	242.07	245.79	5.26				
6.31	455.00	468.09	461.55	9.26	498.19	488.44	493.32	6.89				
10.00	1028.09	1042.89	1035.49	10.47	1083.26	1066.55	1074.91	11.82				
15.85	2447.89	2463.91	2455.90	11.33	2528.86	2553.99	2541.43	17.77				
25.00	5872.87	5928.39	5900.63	39.26	6020.66	5947.75	5984.21	51.56				

a– experiment, b- duplicate of experiment, Std dev- standard deviation

Table A.7. Viscoelastic properties of starch with rutin.

Frequency (Hz)	Peregrine (22% amylose starch)											
	80 °C				100 °C				120 °C			
	Loss modulus (Pa)				Loss modulus (Pa)				Loss modulus (Pa)			
	a	b	Mean	Std dev	a	b	Mean	Std dev	a	b	Mean	Std dev
0.10	328.00	341.44	334.72	9.50	191.09	158.90	174.99	22.76	136.71	161.59	149.15	17.60
0.16	271.81	352.63	312.22	57.15	172.54	196.83	184.68	17.17	136.41	196.86	166.63	42.74
0.25	271.27	275.06	273.17	2.68	214.39	209.26	211.82	3.63	160.28	177.16	168.72	11.93
0.40	350.31	355.33	352.82	3.55	219.97	208.48	214.23	8.13	174.46	222.51	198.48	33.97
0.63	378.92	385.38	382.15	4.56	252.74	228.99	240.87	16.79	198.01	250.76	224.39	37.30
1.00	389.31	419.47	404.39	21.33	288.18	259.81	273.99	20.06	223.06	272.88	247.97	35.22
1.58	463.23	460.54	461.89	1.90	327.55	302.03	314.79	18.04	258.27	326.40	292.34	48.18
2.51	508.81	531.17	519.99	15.81	373.53	353.04	363.28	14.49	294.30	375.18	334.74	57.19
3.98	572.95	590.66	581.80	12.52	436.18	406.62	421.40	20.90	344.53	434.30	389.41	63.48
6.31	658.06	676.45	667.26	13.00	510.90	474.33	492.61	25.86	403.23	507.26	455.24	73.55
10.00	750.01	769.54	759.77	13.81	601.43	555.99	578.71	32.13	476.47	597.79	537.13	85.79
15.85	864.88	885.66	875.27	14.69	709.85	657.32	683.59	37.14	564.58	707.79	636.19	101.27
25.00	1010.29	1036.53	1023.41	18.55	845.32	784.44	814.88	43.05	681.06	853.04	767.05	121.61
	140 °C				160 °C							
0.10	229.96	200.01	214.99	21.18	450.61	464.65	457.63	9.93				
0.16	230.92	243.45	237.19	8.86	441.30	526.68	483.99	60.37				
0.25	231.85	223.80	227.82	5.69	510.12	558.99	534.56	34.56				
0.40	276.75	246.17	261.46	21.62	507.15	503.95	505.55	2.26				
0.63	291.99	266.54	279.27	18.00	562.32	522.40	542.36	28.22				
1.00	326.18	308.09	317.13	12.80	634.58	588.35	611.46	32.69				
1.58	367.73	347.61	357.67	14.23	653.49	608.42	630.95	31.87				
2.51	421.76	392.13	406.95	20.95	726.45	690.72	708.59	25.26				
3.98	480.63	446.43	463.53	24.19	794.61	767.50	781.05	19.17				
6.31	556.56	513.57	535.06	30.40	895.62	857.03	876.33	27.29				
10.00	647.04	598.81	622.93	34.10	1015.84	973.42	994.63	30.00				
15.85	761.36	702.48	731.92	41.64	1163.86	1118.18	1141.02	32.30				
25.00	906.73	841.71	874.22	45.97	1351.44	1300.13	1325.79	36.28				

a– experiment, b- duplicate of experiment, Std dev- standard deviation

Table A.8. Color of rutin powders

Starch	Temp (°C)	L	a	b	(L*-L)^2	(a*-a)^2	(b*-b)^2	ΔE	Mean ΔE	Std dev
Calibration with white tile L*=92.32, a*=0.86, b*=0.83										
CDC Hilose (37% amylose)	80	98.63	-0.64	2.12	39.82	2.25	1.66	6.61	6.61	0.01
	80	98.62	-0.64	2.12	39.69	2.25	1.66	6.60		
	100	99.33	-0.46	2.29	49.14	1.74	2.13	7.28	7.33	0.07
	100	99.53	-0.40	1.81	51.98	1.59	0.96	7.38		
	120	98.57	-0.37	1.10	39.06	1.51	0.07	6.38	6.69	0.45
	120	99.19	-0.37	1.46	47.20	1.51	0.40	7.01		
	140	99.46	-0.26	0.91	50.98	1.25	0.01	7.23	7.23	0.00
	140	99.46	-0.25	0.91	50.98	1.23	0.01	7.23		
	160	97.29	-0.24	1.13	24.70	1.21	0.09	5.10	5.09	0.02
	160	97.27	-0.23	1.13	24.50	1.19	0.09	5.08		
Peregrine (22% amylose)	80	97.99	-1.78	4.55	32.15	6.97	13.84	7.28	8.03	1.06
	80	99.82	-1.52	4.72	56.25	5.66	15.13	8.78		
	100	97.18	-0.73	2.62	23.62	2.53	3.20	5.42	5.35	0.10
	100	97.07	-0.72	2.49	22.56	2.50	2.76	5.27		
	120	96.76	-0.35	1.76	19.71	1.46	0.86	4.69	4.97	0.39
	120	97.41	-0.31	1.26	25.91	1.37	0.18	5.24		
	140	96.74	-0.18	2.07	19.54	1.08	1.54	4.71	4.70	0.01
	140	96.73	-0.17	2.06	19.45	1.06	1.51	4.69		
	160	98.96	-0.13	1.67	44.09	0.98	0.71	6.77	6.77	0.00
	160	98.96	-0.12	1.67	44.09	0.96	0.71	6.76		
CDC Rattan (0% amylose)	80	97.71	-0.75	3.86	29.05	2.59	9.18	6.39	6.49	0.14
	80	98.10	-0.89	3.47	33.41	3.06	6.97	6.59		
	100	96.12	-0.66	4.67	14.44	2.31	14.75	5.61	5.62	0.01
	100	96.14	-0.67	4.67	14.59	2.34	14.75	5.63		
	120	96.21	-0.30	2.78	15.13	1.35	3.80	4.50	4.29	0.30
	120	95.60	-0.33	2.95	10.76	1.42	4.49	4.08		
	140	93.42	-0.19	2.63	1.21	1.10	3.24	2.36	2.35	0.01
	140	93.42	-0.16	2.62	1.21	1.04	3.20	2.34		
	160	93.28	-0.02	2.49	0.92	0.77	2.76	2.11	2.11	0.00
	160	93.27	-0.02	2.49	0.90	0.77	2.76	2.11		

L scale – Light versus dark, a scale – red versus green, b scale – yellow versus blue, ΔE – total color difference. Std dev- standard deviation

Table A.8. Continued.

	Temp (°C)	L	a	b	YI	Mean YI	Std dev
Calibration with white tile L*=92.32, a*=0.86, b*=0.83							
CDC Hilose (37% amylose)	80	98.63	-0.64	2.12	3.07	3.07	0.00
	80	98.62	-0.64	2.12	3.07		
	100	99.33	-0.46	2.29	3.29	2.95	0.49
	100	99.53	-0.40	1.81	2.60		
	120	98.57	-0.37	1.10	1.59	1.85	0.36
	120	99.19	-0.37	1.46	2.10		
	140	99.46	-0.26	0.91	1.31	1.31	0.00
	140	99.46	-0.25	0.91	1.31		
	160	97.29	-0.24	1.13	1.66	1.66	0.00
	160	97.27	-0.23	1.13	1.66		
Peregrine (22% amylose)	80	97.99	-1.78	4.55	6.63	6.69	0.09
	80	99.82	-1.52	4.72	6.76		
	100	97.18	-0.73	2.62	3.85	3.76	0.13
	100	97.07	-0.72	2.49	3.66		
	120	96.76	-0.35	1.76	2.60	2.22	0.53
	120	97.41	-0.31	1.26	1.85		
	140	96.74	-0.18	2.07	3.06	3.05	0.01
	140	96.73	-0.17	2.06	3.04		
	160	98.96	-0.13	1.67	2.41	2.41	0.00
	160	98.96	-0.12	1.67	2.41		
CDC Rattan (0% amylose)	80	97.71	-0.75	3.86	5.64	5.35	0.42
	80	98.10	-0.89	3.47	5.05		
	100	96.12	-0.66	4.67	6.94	6.94	0.00
	100	96.14	-0.67	4.67	6.94		
	120	96.21	-0.30	2.78	4.13	4.27	0.20
	120	95.60	-0.33	2.95	4.41		
	140	93.42	-0.19	2.63	4.02	4.01	0.01
	140	93.42	-0.16	2.62	4.01		
	160	93.28	-0.02	2.49	3.81	3.81	0.00
	160	93.27	-0.02	2.49	3.81		

Temp: temperature, L scale – Light versus dark, a scale – red versus green, b scale – yellow versus blue, YI – yellowness index, Std dev- standard deviation.

Table A.8. Continued.

Amy-lose	Temp (°C)	L	a	b	(100-L)^2	(100-L)^2 + a^2 + b^2	^0.5	WI	Mean WI	Std dev
Calibration with white tile L*=92.32, a*=0.86, b*=0.83									
CDC Hilose 37%	80	98.63	-0.64	2.12	1.88	6.78	2.60	97.40	97.39	0.00
	80	98.62	-0.64	2.12	1.90	6.81	2.61	97.39		
	100	99.33	-0.46	2.29	0.45	5.90	2.43	97.57	97.83	0.37
	100	99.53	-0.40	1.81	0.22	3.66	1.91	98.09		
	120	98.57	-0.37	1.10	2.04	3.39	1.84	98.16	98.22	0.09
	120	99.19	-0.37	1.46	0.66	2.92	1.71	98.29		
	140	99.46	-0.26	0.91	0.29	1.19	1.09	98.91	98.91	0.00
	140	99.46	-0.25	0.91	0.29	1.18	1.09	98.91		
	160	97.29	-0.24	1.13	7.34	8.68	2.95	97.05	97.05	0.01
	160	97.27	-0.23	1.13	7.45	8.78	2.96	97.04		
22%	80	97.99	-1.78	4.55	4.04	27.91	5.28	94.72	94.88	0.23
	80	99.82	-1.52	4.72	0.03	24.62	4.96	95.04		
	100	97.18	-0.73	2.62	7.95	15.35	3.92	96.08	96.09	0.00
	100	97.07	-0.72	2.49	8.58	15.30	3.91	96.09		
	120	96.76	-0.35	1.76	10.50	13.72	3.70	96.30	96.70	0.57
	120	97.41	-0.31	1.26	6.71	8.39	2.90	97.10		
	140	96.74	-0.18	2.07	10.63	14.94	3.87	96.13	96.13	0.00
	140	96.73	-0.17	2.06	10.69	14.97	3.87	96.13		
	160	98.96	-0.13	1.67	1.08	3.89	1.97	98.03	98.03	0.00
	160	98.96	-0.12	1.67	1.08	3.88	1.97	98.03		
CDC Rattan 0%	80	97.71	-0.75	3.86	5.24	20.71	4.55	95.45	95.70	0.35
	80	98.10	-0.89	3.47	3.61	16.44	4.05	95.95		
	100	96.12	-0.66	4.67	15.05	37.30	6.11	93.89	93.90	0.01
	100	96.14	-0.67	4.67	14.90	37.16	6.10	93.90		
	120	96.21	-0.30	2.78	14.36	22.18	4.71	95.29	94.99	0.42
	120	95.60	-0.33	2.95	19.36	28.17	5.31	94.69		
	140	93.42	-0.19	2.63	43.30	50.25	7.09	92.91	92.91	0.00
	140	93.42	-0.16	2.62	43.30	50.19	7.08	92.92		
	160	93.28	-0.02	2.49	45.16	51.36	7.17	92.83	92.83	0.01
	160	93.27	-0.02	2.49	45.29	51.49	7.18	92.82		

Temp – temperature, L scale – Light versus dark, a scale – red versus green, b scale – yellow versus blue, WI- whiteness index, Std   dev- standard deviation

Appendix B: Effect of ultrasonication on rutin and its derivatives
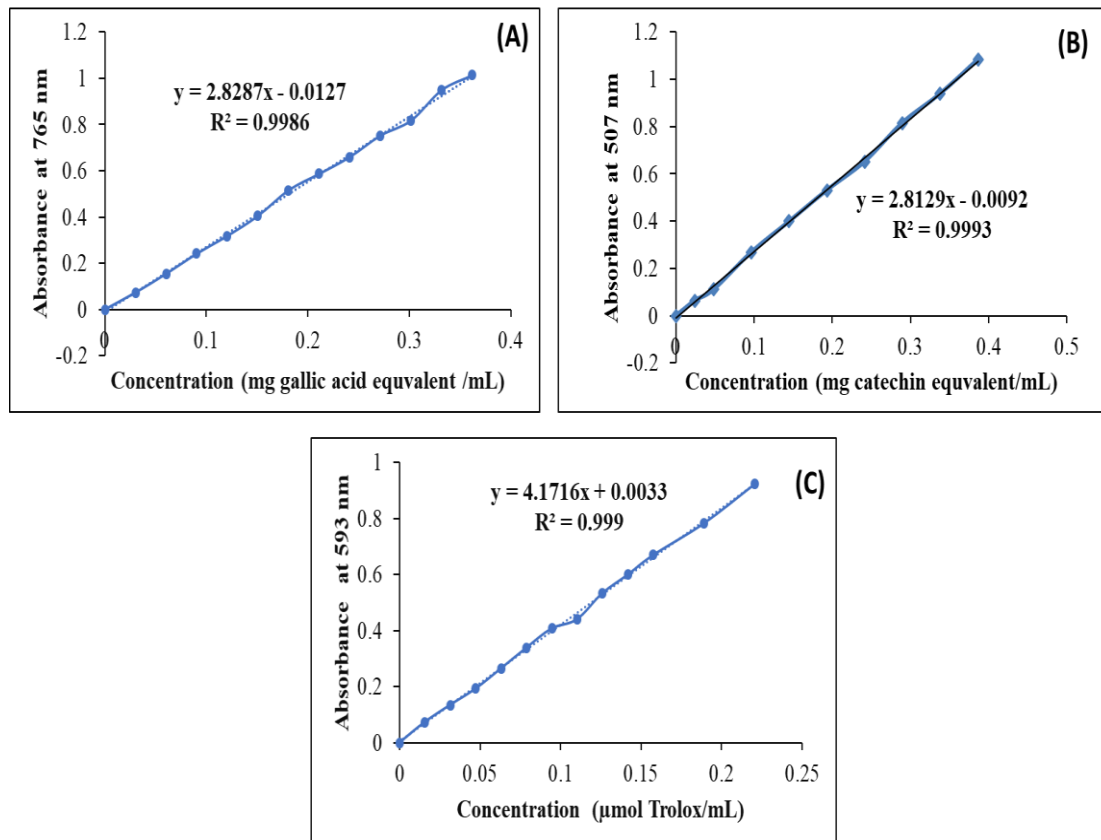
Figure B.1. Standard curves for determination of total phenolic content (A), total flavonoid content (B), and Ferric reducing antioxidant power (C).

Table B.1. Total phenolic content (with temperature control)

Media	Time (min)	ED (kJ/mL)	Mass (mg)	Abs 1	Abs 2	Abs 3	Avg abs (Y)	Conc x (mg/mL)	x*50mL (mg)	mg gallic acid	Mean	Std dev
Water	0	Untreated	20.0	0.290	0.288		0.289	0.11	5.33	0.27	0.28	0.02
			20.9	0.333	0.325		0.329	0.12	6.04	0.29		
	2	3.6	20.0	0.449	0.445		0.447	0.16	8.13	0.41	0.38	0.03
			20.5	0.410	0.406		0.408	0.15	7.44	0.36		
	5	9	20.4	0.448	0.448		0.448	0.16	8.14	0.40	0.42	0.02
			19.9	0.476	0.473		0.475	0.17	8.61	0.43		
	10	18	20.1	0.488	0.492		0.490	0.18	8.89	0.44	0.45	0.02
			20.6	0.531	0.531		0.531	0.19	9.61	0.47		
	15	27	20.8	0.563	0.583		0.573	0.21	10.35	0.50	0.49	0.02
			20.1	0.523	0.532		0.528	0.19	9.55	0.48		
	20	36	20.7	0.498	0.500		0.499	0.18	9.04	0.44	0.43	0.00
			20.9	0.498	0.495		0.497	0.18	9.00	0.43		
NaCl	0	Untreated	20.4	0.306	0.311		0.31	0.11	5.68	0.28	0.27	0.02
			20.0	0.286	0.266		0.28	0.10	5.10	0.26		
	2	3.6	20.5	0.447	0.456	0.448	0.45	0.16	8.18	0.40	0.41	0.01
			20.8	0.483	0.481	0.478	0.48	0.17	8.72	0.42		
	5	9	20.9	0.486	0.475	0.484	0.48	0.17	8.74	0.42	0.42	0.01
			20.9	0.498	0.495	0.499	0.50	0.18	9.02	0.43		
	10	18	20.3	0.506	0.508	0.514	0.51	0.18	9.23	0.45	0.45	0.00
			20.5	0.512	0.509	0.503	0.51	0.18	9.20	0.45		
	15	27	20.4	0.488	0.495	0.491	0.49	0.18	8.91	0.44	0.43	0.00
			20.2	0.480	0.481	0.482	0.48	0.17	8.73	0.43		
	20	36	20.6	0.509	0.509	0.513	0.51	0.18	9.25	0.45	0.45	0.00
			20.6	0.506	0.508	0.523	0.51	0.19	9.28	0.45		

ED- energy density, Abs- absorbance, Avg- average, Conc – concentration, Std dev- standard deviation

Table B.1. Continued.

Media	Time (min)	ED (kJ/mL)	Mass (mg)	Abs 1	Abs 2	Abs 3	Avg abs (Y)	Conc x (mg/mL)	x*50mL (mg)	mg gallic acid	Mean	Std dev
Citric acid	0	Untreated	20.2	0.313	0.319		0.32	0.12	5.81	0.29	0.29	0.00
			20.1	0.321	0.317		0.32	0.12	5.86	0.29		
	2	3.6	20.2	0.467	0.487	0.465	0.47	0.17	8.59	0.43	0.42	0.01
			20.8	0.472	0.480	0.472	0.47	0.17	8.61	0.41		
	5	9	20.6	0.468	0.466	0.467	0.47	0.17	8.48	0.41	0.42	0.02
			20.4	0.492	0.484	0.489	0.49	0.18	8.86	0.43		
	10	18	20.5	0.506	0.514	0.523	0.51	0.19	9.32	0.45	0.46	0.00
			20.3	0.502	0.517	0.518	0.51	0.19	9.28	0.46		
	15	27	20.0	0.494	0.498	0.522	0.50	0.18	9.14	0.46	0.46	0.00
			20.7	0.513	0.529	0.521	0.52	0.19	9.43	0.46		
	20	36	20.4	0.521	0.512	0.503	0.51	0.19	9.27	0.45	0.45	0.00
			20.4	0.508	0.513	0.503	0.51	0.18	9.20	0.45		

ED- energy density, Abs- absorbance, Avg- average, Conc – concentration, Std dev- standard deviation

Table B.2. Total phenolic content (without temperature control)

Media	Time (min)	ΔED (kJ/mL)	Mass (mg)	Abs 1	Abs 2	Avg Abs (Y)	Conc x (mg/mL)	x*50mL (mg)	mg gallic acid/mg rutin hydrate	Mean	Std dev
Water	2	0.1	20.3	0.457	0.453	0.455	0.17	8.27	0.41	0.40	0.01
			20.6	0.452	0.455	0.454	0.16	8.24	0.40		
	5	0.5	20.1	0.486	0.457	0.472	0.17	8.56	0.43	0.42	0.00
			20.4	0.469	0.484	0.477	0.17	8.65	0.42		
	10	1.5	20.4	0.483	0.486	0.485	0.18	8.79	0.43	0.44	0.01
			20.5	0.513	0.507	0.510	0.18	9.24	0.45		
	15	3.9	20.5	0.519	0.511	0.515	0.19	9.33	0.46	0.45	0.00
			20.4	0.516	0.504	0.510	0.18	9.24	0.45		
	20	7.0	20.0	0.504	0.510	0.507	0.18	9.19	0.46	0.45	0.01
			20.7	0.504	0.500	0.502	0.18	9.10	0.44		
NaCl	2	0.1	20.1	0.454	0.456	0.455	0.17	8.27	0.41	0.41	0.00
			20.3	0.460	0.460	0.460	0.17	8.36	0.41		
	5	0.5	20.2	0.414	0.422	0.418	0.15	7.61	0.38	0.39	0.02
			20.7	0.471	0.469	0.470	0.17	8.53	0.41		
	10	1.5	20.5	0.499	0.495	0.497	0.18	9.01	0.44	0.45	0.01
			20.4	0.513	0.508	0.511	0.18	9.25	0.45		
	15	3.9	20.6	0.508	0.504	0.506	0.18	9.17	0.45	0.44	0.00
			20.4	0.491	0.498	0.495	0.18	8.97	0.44		
	20	7.0	20.5	0.490	0.487	0.489	0.18	8.86	0.43	0.44	0.01
			20.3	0.508	0.480	0.494	0.18	8.96	0.44		

ΔED- change in energy density, Abs- absorbance, Avg- average, Conc – concentration, Std dev- standard deviation

Table B.2. Continued.

Media	Time (min)	ΔED (kJ/mL)	Mass (mg)	Abs 1	Abs 2	Abs 3	Avg abs (Y)	Conc x (mg/mL)	x*50mL (mg)	mg gallic acid/mg rutin hydrate	Mean	Std dev
Citric acid	2	0.1	20.7	0.470	0.474	0.466	0.470	0.17	8.53	0.41	0.41	0.01
			20.5	0.449	0.450	0.449	0.449	0.16	8.17	0.40		
	5	0.5	20.7	0.505	0.515	0.513	0.511	0.19	9.26	0.45	0.44	0.01
			20.4	0.483	0.479	0.478	0.480	0.17	8.71	0.43		
	10	1.5	20.7	0.500	0.505	0.511	0.505	0.18	9.16	0.44	0.45	0.01
			20.4	0.508	0.518	0.518	0.515	0.19	9.32	0.46		
	15	3.9	19.9	0.501	0.507	0.504	0.504	0.18	9.13	0.46	0.45	0.01
			20.3	0.499	0.505	0.495	0.500	0.18	9.06	0.45		
	20	7.0	20.2	0.566	0.520	0.000	0.543	0.20	9.82	0.49	0.47	0.02
			20.3	0.527	0.507	0.000	0.517	0.19	9.36	0.46		

ΔED- change in energy density, Abs- absorbance, Avg- average, Conc – concentration, Std dev- standard deviation

Table B.3. Total flavonoid content (with temperature control)

Media	Time (min)	ED (kJ/mL)	Mass (mg)	Abs 1	Abs 2	Avg Abs (Y)	Conc x (mg/mL)	x*50mL (mg)	mg catechin/mg rutin hydrate	Mean	Std dev
Water	0	Untreated	20.0	0.276	0.270	0.273	0.10	5.02	0.25	0.26	0.01
			20.9	0.322	0.277	0.300	0.11	5.49	0.26		
	2	3.6	20.5	0.445	0.444	0.445	0.16	8.06	0.39	0.36	0.04
			20.4	0.373	0.366	0.370	0.13	6.73	0.33		
	5	9	20.4	0.435	0.432	0.434	0.16	7.87	0.39	0.39	0.01
			19.9	0.447	0.435	0.441	0.16	8.00	0.40		
	10	18	20.1	0.479	0.479	0.479	0.17	8.68	0.43	0.44	0.01
			20.6	0.507	0.524	0.516	0.19	9.33	0.45		
	15	27	20.8	0.526	0.538	0.532	0.19	9.62	0.46	0.45	0.02
			20.1	0.470	0.484	0.477	0.17	8.64	0.43		
	20	36	20.7	0.458	0.455	0.457	0.17	8.28	0.40	0.40	0.01
			20.9	0.456	0.444	0.450	0.16	8.16	0.39		
NaCl	0	Untreated	20.4	0.366	0.366	0.366	0.13	6.67	0.33	0.32	0.01
			20.0	0.338	0.332	0.335	0.12	6.12	0.31		
	2	3.6	20.5	0.479	0.391	0.435	0.16	7.90	0.39	0.38	0.01
			20.8	0.457	0.398	0.428	0.16	7.76	0.37		
	5	9	20.9	0.439	0.413	0.426	0.15	7.74	0.37	0.37	0.00
			20.9	0.447	0.417	0.432	0.16	7.84	0.38		
	10	18	20.3	0.465	0.437	0.451	0.16	8.18	0.40	0.40	0.01
			20.5	0.455	0.430	0.443	0.16	8.03	0.39		
	15	27	20.4	0.457	0.406	0.432	0.16	7.83	0.38	0.38	0.00
			20.2	0.462	0.394	0.428	0.16	7.77	0.38		
	20	36	20.6	0.460	0.457	0.459	0.17	8.31	0.40	0.40	0.01
			20.6	0.447	0.449	0.448	0.16	8.13	0.39		

ED- energy density, Abs- absorbance, Avg- average, Conc – concentration, Std dev- standard deviation

Table B.3. Continued.

Media	Time (min)	ED (kJ/mL)	Mass (mg)	Abs 1	Abs 2	Avg Abs (Y)	Conc x (mg/mL)	x*50mL (mg)	mg catechin/mg rutin hydrate	Mean	Std dev
Citric acid	0	Untreated	20.2	0.380	0.372	0.376	0.14	6.85	0.34	0.35	0.01
			20.1	0.407	0.376	0.392	0.14	7.12	0.35		
	2	3.6	20.2	0.399	0.374	0.387	0.14	7.03	0.35	0.35	0.00
			20.8	0.393	0.402	0.398	0.14	7.23	0.35		
	5	9	20.6	0.384	0.372	0.378	0.14	6.88	0.33	0.35	0.02
			20.4	0.414	0.400	0.407	0.15	7.40	0.36		
	10	18	20.5	0.431	0.423	0.427	0.16	7.75	0.38	0.38	0.00
			20.3	0.420	0.419	0.420	0.15	7.62	0.38		
	15	27	20.0	0.392	0.398	0.395	0.14	7.18	0.36	0.36	0.01
			20.7	0.414	0.426	0.420	0.15	7.63	0.37		
	20	36	20.4	0.430	0.412	0.421	0.15	7.65	0.37	0.38	0.00
			20.4	0.416	0.431	0.424	0.15	7.69	0.38		

ED- energy density, Abs- absorbance, Avg- average, Conc- concentration, dm – dry matter, Std dev- standard deviation

206

Table B.4. Total flavonoid content (without temperature control)

Media	Time (min)	ΔED (kJ/mL)	Mass (mg)	Abs 1	Abs 2	Avg Abs (Y)	Conc x (mg/mL)	x*50mL (mg)	mg catechin/mg rutin hydrate	Mean	Std dev
Water	2	0.09	20.3	0.437	0.417	0.427	0.16	7.75	0.38	0.36	0.03
			20.6	0.394	0.370	0.382	0.14	6.95	0.34		
	5	0.47	20.1	0.362	0.329	0.346	0.13	6.30	0.31	0.34	0.04
			20.4	0.421	0.397	0.409	0.15	7.43	0.36		
	10	1.46	20.4	0.399	0.419	0.409	0.15	7.43	0.36	0.38	0.03
			20.5	0.469	0.442	0.456	0.17	8.26	0.40		
	15	3.86	20.5	0.434	0.439	0.437	0.16	7.92	0.39	0.39	0.00
			20.4	0.433	0.445	0.439	0.16	7.97	0.39		
	20	6.99	20.0	0.413	0.413	0.413	0.15	7.50	0.38	0.38	0.00
			20.7	0.415	0.448	0.432	0.16	7.83	0.38		
NaCl	2	0.09	20.1	0.412	0.381	0.397	0.14	7.21	0.36	0.36	0.00
			20.3	0.402	0.414	0.408	0.15	7.42	0.37		
	5	0.47	20.2	0.377	0.348	0.363	0.13	6.61	0.33	0.34	0.02
			20.7	0.390	0.403	0.397	0.14	7.21	0.35		
	10	1.46	20.5	0.430	0.436	0.433	0.16	7.86	0.38	0.39	0.00
			20.4	0.453	0.418	0.436	0.16	7.90	0.39		
	15	3.86	20.6	0.440	0.445	0.443	0.16	8.03	0.39	0.38	0.02
			20.4	0.413	0.414	0.414	0.15	7.51	0.37		
	20	6.99	20.5	0.418	0.421	0.420	0.15	7.62	0.37	0.38	0.01
			20.3	0.425	0.434	0.430	0.16	7.80	0.38		

ΔED- change in energy density, Abs- absorbance, Avg- average, Conc- concentration, Std dev- standard deviation

Table B.4. Continued.

Media	Time (min)	ΔED (kJ/mL)	Mass (mg)	Abs 1	Abs 2	Avg Abs (Y)	Conc x (mg/mL)	x*50mL (mg)	mg catechin/mg rutin hydrate	Mean	Std dev
Citric acid	2	0.09	20.7	0.387	0.395	0.391	0.14	7.11	0.34	0.35	0.01
			20.5	0.400	0.406	0.403	0.15	7.33	0.36		
	5	0.47	20.7	0.433	0.459	0.446	0.16	8.09	0.39	0.38	0.02
			20.4	0.427	0.400	0.414	0.15	7.51	0.37		
	10	1.46	20.7	0.440	0.434	0.437	0.16	7.93	0.38	0.38	0.00
			20.4	0.415	0.435	0.425	0.15	7.72	0.38		
	15	3.86	19.9	0.412	0.401	0.407	0.15	7.39	0.37	0.37	0.00
			20.3	0.413	0.427	0.420	0.15	7.63	0.38		
	20	6.99	20.2	0.480	0.471	0.476	0.17	8.62	0.43	0.40	0.04
			20.3	0.419	0.409	0.414	0.15	7.52	0.37		

ΔED- change in energy density, Abs- absorbance, Avg- average, Conc - concentration, Std dev- standard deviation

Table B.5. Ferric reducing antioxidant power (with temperature control)

Media	Time (min)	ED (kJ/mL)	Mass (mg)	Abs 1	Abs 2	Avg Abs	Conc x (mg/mL)	Conc x (μmol/mL)	x*50ml (μmol trolox)	μmol trolox/mg rutin	Mean	Std dev
Water	0	Untreated	20.0	0.311	0.306	0.309	0.07	0.29	14.62	0.73	0.77	0.06
			20.9	0.355	0.364	0.360	0.09	0.34	17.06	0.82		
	2	3.6	20.0	0.480	0.480	0.480	0.11	0.46	22.83	1.14	1.12	0.04
			20.5	0.475	0.465	0.470	0.11	0.45	22.35	1.09		
	5	9	20.4	0.471	0.478	0.475	0.11	0.45	22.56	1.11	1.16	0.08
			19.9	0.508	0.510	0.509	0.12	0.48	24.22	1.22		
	10	18	20.1	0.546	0.530	0.538	0.13	0.51	25.61	1.27	1.30	0.04
			20.6	0.575	0.578	0.577	0.14	0.55	27.45	1.33		
	15	27	20.8	0.637	0.606	0.622	0.15	0.59	29.60	1.42	1.39	0.05
			20.1	0.584	0.557	0.571	0.14	0.54	27.16	1.35		
	20	36	20.7	0.538	0.524	0.531	0.13	0.51	25.27	1.22	1.22	0.01
			20.9	0.532	0.533	0.533	0.13	0.51	25.34	1.21		
NaCl	0	Untreated	20.4	0.355	0.370	0.363	0.09	0.34	17.20	0.84	0.80	0.06
			20.0	0.321	0.321	0.321	0.08	0.30	15.21	0.76		
	2	3.6	20.5	0.499	0.514	0.507	0.12	0.48	24.10	1.18	1.17	0.01
			20.8	0.512	0.505	0.509	0.12	0.48	24.19	1.16		
	5	9	20.9	0.519	0.524	0.522	0.12	0.50	24.82	1.19	1.18	0.02
			20.9	0.516	0.507	0.512	0.12	0.49	24.34	1.16		
	10	18	20.3	0.529	0.505	0.517	0.12	0.49	24.60	1.21	1.23	0.03
			20.5	0.537	0.545	0.541	0.13	0.51	25.75	1.26		
	15	27	20.4	0.531	0.535	0.533	0.13	0.51	25.37	1.24	1.24	0.00
			20.2	0.542	0.509	0.526	0.13	0.50	25.01	1.24		
	20	36	20.6	0.535	0.542	0.539	0.13	0.51	25.63	1.24	1.24	0.00
			20.6	0.547	0.530	0.539	0.13	0.51	25.63	1.24		

ED- energy density, Abs- absorbance, Avg- average, Conc – concentration, Std dev- standard deviation

Table B.5. Continued.

Media	Time (min)	ED (kJ/mL)	Mass (mg)	Abs 1	Abs 2	Avg Abs	Conc x (mg/ml)	Conc x (µmol/ml)	x*50ml (µmol trolox)	µmol trolox/mg rutin	Mean	Std dev
Citric acid	0	Untreated	20.2	0.394	0.388	0.391	0.09	0.37	18.57	0.92	0.92	0.00
			20.1	0.379	0.394	0.387	0.09	0.37	18.35	0.91		
	2	3.6	20.2	0.539	0.555	0.547	0.13	0.52	26.04	1.29	1.28	0.01
			20.8	0.548	0.564	0.556	0.13	0.53	26.47	1.27		
	5	9	20.6	0.531	0.533	0.532	0.13	0.51	25.32	1.23	1.28	0.07
			20.4	0.572	0.568	0.570	0.14	0.54	27.14	1.33		
	10	18	20.5	0.577	0.569	0.573	0.14	0.55	27.28	1.33	1.36	0.04
			20.3	0.578	0.603	0.591	0.14	0.56	28.12	1.39		
	15	27	20.0	0.595	0.573	0.584	0.14	0.56	27.81	1.39	1.39	0.00
			20.7	0.604	0.603	0.604	0.14	0.57	28.74	1.39		
	20	36	20.4	0.590	0.602	0.596	0.14	0.57	28.38	1.39	1.44	0.07
			20.4	0.647	0.625	0.636	0.15	0.61	30.30	1.49		

ED- energy density, Abs- absorbance, Avg- average, Conc- concentration, Std dev- standard deviation

Table B.6. Ferric reducing antioxidant power (without temperature control)

Media	Time (min)	ΔED (kJ/mL)	Mass (mg)	Abs 1	Abs 2	Avg Abs	Conc x (mg/ml)	Conc x (μmol/ml)	x*50ml (μmol trolox)	μmol trolox/mg rutin	Mean	Std dev
Water	2	0.09	20.3	0.497	0.497	0.497	0.12	0.47	23.64	1.16	1.15	0.02
			20.6	0.488	0.495	0.492	0.12	0.47	23.38	1.13		
	5	0.47	20.1	0.492	0.485	0.489	0.12	0.46	23.24	1.16	1.12	0.05
			20.4	0.459	0.474	0.467	0.11	0.44	22.18	1.09		
	10	1.46	20.4	0.508	0.509	0.509	0.12	0.48	24.19	1.19	1.22	0.04
			20.5	0.532	0.541	0.537	0.13	0.51	25.53	1.25		
	15	3.86	20.5	0.546	0.554	0.550	0.13	0.52	26.18	1.28	1.28	0.00
			20.4	0.554	0.544	0.549	0.13	0.52	26.13	1.28		
	20	6.99	20.0	0.559	0.555	0.557	0.13	0.53	26.52	1.33	1.29	0.06
			20.7	0.523	0.562	0.543	0.13	0.52	25.82	1.25		
NaCl	2	0.09	20.1	0.446	0.443	0.445	0.11	0.42	21.13	1.05	1.07	0.02
			20.3	0.475	0.448	0.462	0.11	0.44	21.94	1.08		
	5	0.47	20.2	0.469	0.470	0.470	0.11	0.45	22.33	1.11	1.08	0.03
			20.7	0.461	0.462	0.462	0.11	0.44	21.94	1.06		
	10	1.46	20.5	0.497	0.485	0.491	0.12	0.47	23.36	1.14	1.16	0.03
			20.4	0.505	0.509	0.507	0.12	0.48	24.12	1.18		
	15	3.86	20.6	0.485	0.505	0.495	0.12	0.47	23.55	1.14	1.13	0.02
			20.4	0.486	0.473	0.480	0.11	0.46	22.80	1.12		
	20	6.99	20.5	0.497	0.501	0.499	0.12	0.47	23.74	1.16	1.15	0.01
			20.3	0.494	0.480	0.487	0.12	0.46	23.16	1.14		

ΔED- change in energy density, abs- absorbance, Avg- average, Conc- concentration, Std dev- standard deviation

Table B.6. Continued.

Media	Time (min)	ΔED (kJ/mL)	Mass (mg)	Abs 1	Abs 2	Avg Abs	Conc x (mg/mL)	Conc x (μmol/mL)	x*50ml (μmol trolox)	μmol trolox/mg rutin	Mean	Std dev
Citric acid	2	0.09	20.7	0.570	0.548	0.559	0.13	0.53	26.61	1.29	1.26	0.04
			20.5	0.529	0.529	0.529	0.13	0.50	25.17	1.23		
	5	0.47	20.7	0.577	0.574	0.576	0.14	0.55	27.40	1.32	1.30	0.03
			20.4	0.550	0.549	0.550	0.13	0.52	26.16	1.28		
	10	1.46	20.7	0.583	0.580	0.582	0.14	0.55	27.69	1.34	1.34	0.00
			20.4	0.579	0.571	0.575	0.14	0.55	27.38	1.34		
	15	3.86	19.9	0.576	0.571	0.574	0.14	0.55	27.31	1.37	1.36	0.02
			20.3	0.601	0.545	0.573	0.14	0.55	27.28	1.34		
	20	6.99	20.2	0.631	0.647	0.639	0.15	0.61	30.44	1.51	1.44	0.09
			20.3	0.589	0.583	0.586	0.14	0.56	27.90	1.37		

ΔED- change in energy density, abs- absorbance, Avg- average, Conc- concentration, Std dev- standard deviation

Table B.7. DPPH radical scavenging activity (with temperature control).

Media	Time (min)	ED (kJ/mL)	Abs 1	Abs 2	Avg Abs	Control	%DPPH	Mean	Std dev
Water	0	Untreated	0.114	0.164	0.139	0.717	80.61	81.83	1.73
			0.119	0.124	0.122	0.717	83.05		
	2	3.6	0.053	0.048	0.051	0.668	92.44	92.48	0.05
			0.049	0.051	0.050	0.668	92.51		
	5	9	0.060	0.055	0.058	0.668	91.39	91.95	0.79
			0.046	0.054	0.050	0.668	92.51		
	10	18	0.061	0.050	0.056	0.668	91.69	91.28	0.58
			0.068	0.054	0.061	0.668	90.87		
	15	27	0.058	0.049	0.054	0.668	91.99	92.37	0.53
			0.043	0.054	0.049	0.668	92.74		
	20	36	0.055	0.054	0.055	0.668	91.84	91.77	0.11
			0.060	0.051	0.056	0.668	91.69		
NaCl	0	Untreated	0.086	0.087	0.087	0.613	85.89	85.85	0.06
			0.089	0.085	0.087	0.613	85.81		
	2	3.6	0.043	0.075	0.059	0.651	90.94	92.93	2.82
			0.044	0.022	0.033	0.651	94.93		
	5	9	0.044	0.051	0.048	0.651	92.70	92.70	0.00
			0.030	0.065	0.048	0.651	92.70		
	10	18	0.053	0.020	0.037	0.651	94.39	93.05	1.90
			0.030	0.078	0.054	0.651	91.71		
	15	27	0.076	0.028	0.052	0.651	92.01	91.78	0.33
			0.065	0.045	0.055	0.651	91.55		
	20	36	0.036	0.036	0.036	0.651	94.47	92.51	2.77
			0.068	0.055	0.062	0.651	90.55		
Citric acid	0	Untreated	0.192	0.193	0.193	0.613	68.60	68.84	0.35
			0.193	0.186	0.190	0.613	69.09		
	2	3.6	0.063	0.084	0.074	0.680	89.19	88.79	0.57
			0.082	0.076	0.079	0.680	88.38		
	5	9	0.085	0.097	0.091	0.680	86.62	87.98	1.92
			0.073	0.072	0.073	0.680	89.34		
	10	18	0.056	0.074	0.065	0.680	90.44	90.59	0.21
			0.062	0.064	0.063	0.680	90.74		
	15	27	0.072	0.071	0.072	0.680	89.49	90.04	0.78
			0.069	0.059	0.064	0.680	90.59		
	20	36	0.068	0.054	0.061	0.680	91.03	90.70	0.47
			0.067	0.064	0.066	0.680	90.37		

ED- energy density, Abs- absorbance, Avg- average, DPPH - 1,1-Diphenyl-2-picrylhydrazine Std dev- standard deviation

Table B.7. DPPH radical scavenging activity (without temperature control).

Media	Time (min)	ΔED (kJ/mL)	Abs 1	Abs 2	Avg Abs	Control	%DPPH	Mean	Std dev
Water	2	0.09	0.050	0.058	0.054	0.717	92.47	92.75	0.39
			0.050	0.050	0.050	0.717	93.03		
	5	0.47	0.051	0.061	0.056	0.717	92.19	91.49	0.99
			0.067	0.065	0.066	0.717	90.79		
	10	1.46	0.056	0.068	0.062	0.717	91.35	91.70	0.49
			0.060	0.054	0.057	0.717	92.05		
	15	3.86	0.051	0.052	0.052	0.717	92.82	91.07	2.47
			0.090	0.063	0.077	0.717	89.33		
	20	6.99	0.123	0.136	0.130	0.717	81.94	82.88	1.33
			0.104	0.128	0.116	0.717	83.82		
NaCl	2	0.09	0.109	0.117	0.113	0.668	83.08	80.73	3.33
			0.148	0.141	0.145	0.668	78.37		
	5	0.47	0.132	0.087	0.110	0.668	83.61	81.62	2.81
			0.145	0.127	0.136	0.668	79.64		
	10	1.46	0.099	0.114	0.107	0.668	84.06	85.40	1.91
			0.092	0.085	0.089	0.668	86.75		
	15	3.86	0.135	0.114	0.125	0.668	81.36	84.06	3.81
			0.095	0.082	0.089	0.668	86.75		
	20	6.99	0.126	0.122	0.124	0.668	81.44	83.68	3.18
			0.093	0.095	0.094	0.668	85.93		
Citric acid	2	0.09	0.064	0.085	0.075	0.682	89.08	88.01	1.50
			0.079	0.099	0.089	0.682	86.95		
	5	0.47	0.082	0.084	0.083	0.682	87.83	87.32	0.73
			0.095	0.085	0.090	0.682	86.80		
	10	1.46	0.068	0.070	0.069	0.682	89.88	89.08	1.14
			0.076	0.084	0.080	0.682	88.27		
	15	3.86	0.080	0.073	0.077	0.682	88.78	88.86	0.10
			0.077	0.074	0.076	0.682	88.93		
	20	6.99	0.077	0.064	0.071	0.682	89.66	89.15	0.73
			0.068	0.087	0.078	0.682	88.64		

ΔED- change in energy density, Abs- absorbance, Avg- average, DPPH - 1,1-Diphenyl-2-picrylhydrazine Std dev- standard deviation

Table B.8. ABTS Inhibition (with temperature control).

Media	Time (min)	ED (kJ/mL)	Abs 1	Abs 2	Avg Abs	Control	%ABTS	Mean	Std dev
Water	0	Untreated	0.003	0.012	0.008	0.660	98.86	98.64	0.32
			0.001	0.020	0.011	0.660	98.41		
	2	3.6	0.002	0.002	0.002	0.642	99.69	99.65	0.06
			0.000	0.005	0.003	0.642	99.61		
	5	9	0.002	0.003	0.003	0.642	99.61	99.77	0.22
			0.000	0.001	0.001	0.642	99.92		
	10	18	0.002	0.001	0.002	0.642	99.77	99.69	0.11
			0.002	0.003	0.003	0.642	99.61		
	15	27	0.002	0.003	0.003	0.642	99.61	99.61	0.00
			0.003	0.002	0.003	0.642	99.61		
	20	36	0.004	0.003	0.004	0.642	99.45	99.45	0.00
			0.002	0.005	0.004	0.642	99.45		
NaCl	0	Untreated	0.013	0.013	0.013	0.652	98.01	97.93	0.11
				0.014	0.014	0.652	97.85		
	2	3.6	0.005	0.004	0.005	0.652	99.31	99.12	0.27
			0.002	0.012	0.007	0.652	98.93		
	5	9	0.014	0.014	0.014	0.652	97.85	98.20	0.49
			0.005	0.014	0.010	0.652	98.54		
	10	18	0.012	0.013	0.013	0.652	98.08	98.12	0.05
			0.014	0.010	0.012	0.652	98.16		
	15	27	0.005	0.013	0.009	0.652	98.62	98.39	0.33
			0.006	0.018	0.012	0.652	98.16		
	20	36	0.014	0.013	0.014	0.652	97.93	98.35	0.60
			0.002	0.014	0.008	0.652	98.77		
Citric acid	0	Untreated	0.369	0.363	0.366	0.660	44.55	45.64	1.55
			0.354	0.349	0.352	0.660	46.74		
	2	3.6	0.323	0.321	0.322	0.665	51.58	52.29	1.01
			0.312	0.313	0.313	0.665	53.01		
	5	9	0.314	0.318	0.316	0.665	52.48	52.74	0.37
			0.312	0.313	0.313	0.665	53.01		
	10	18	0.307	0.294	0.301	0.665	54.81	54.92	0.16
			0.298	0.300	0.299	0.665	55.04		
	15	27	0.314	0.309	0.312	0.665	53.16	54.32	1.65
			0.296	0.296	0.296	0.665	55.49		
	20	36	0.309	0.302	0.306	0.665	54.06	54.29	0.32
			0.305	0.300	0.303	0.665	54.51		

ED- energy density, Abs- absorbance, Avg- average, ABTS - 2,2'-Azino-bis(3-ethylbenzothiazoline-6-sulphonic acid, Std dev- standard deviation

Table B.8. ABTS Inhibition (without temperature control).

Media	Time (min)	ΔED (kJ/mL)	Abs 1	Abs 2	Avg Abs	Control	%ABTS	Mean	Std dev
Water	2	0.09	0	0	0	0.642	100.00	100.00	0.00
			0	0	0	0.642	100.00		
	5	0.47	0	0	0	0.642	100.00	100.00	0.00
			0	0	0	0.642	100.00		
	10	1.46	0	0	0	0.642	100.00	100.00	0.00
			0	0	0	0.642	100.00		
	15	3.86	0	0	0	0.642	100.00	100.00	0.00
			0	0	0	0.642	100.00		
	20	6.99	0	0	0	0.642	100.00	100.00	0.00
			0	0	0	0.642	100.00		
NaCl	2	0.09	0.011	0.005	0.008	0.659	98.79	98.79	0.00
			0.003	0.013	0.008	0.659	98.79		
	5	0.47	0.005	0.016	0.011	0.659	98.41	97.99	0.59
			0.014	0.018	0.016	0.659	97.57		
	10	1.46	0.015	0.016	0.016	0.659	97.65	97.69	0.05
			0.011	0.019	0.015	0.659	97.72		
	15	3.86	0.012	0.016	0.014	0.659	97.88	98.03	0.21
			0.008	0.016	0.012	0.659	98.18		
	20	6.99	0.015	0.012	0.014	0.659	97.95	97.95	0.00
			0.005	0.022	0.014	0.659	97.95		
Citric acid	2	0.09	0.311	0.318	0.315	0.663	52.56	53.39	1.17
			0.315	0.292	0.304	0.663	54.22		
	5	0.47	0.303	0.297	0.300	0.663	54.75	54.83	0.11
			0.295	0.303	0.299	0.663	54.90		
	10	1.46	0.301	0.289	0.295	0.663	55.51	55.47	0.05
			0.299	0.292	0.296	0.663	55.43		
	15	3.86	0.299	0.294	0.297	0.663	55.28	55.88	0.85
			0.294	0.283	0.289	0.663	56.49		
	20	6.99	0.268	0.270	0.269	0.663	59.43	57.96	2.08
			0.289	0.288	0.289	0.663	56.49		

ΔED- change in energy density, Abs- absorbance, Avg- average, ABTS - 2,2'-Azino-bis(3-ethylbenzothiazoline-6-sulphonic acid Std dev- standard deviation

Figure B.2 Chromatogram of flavonoid mix showing peaks and retention times of standards
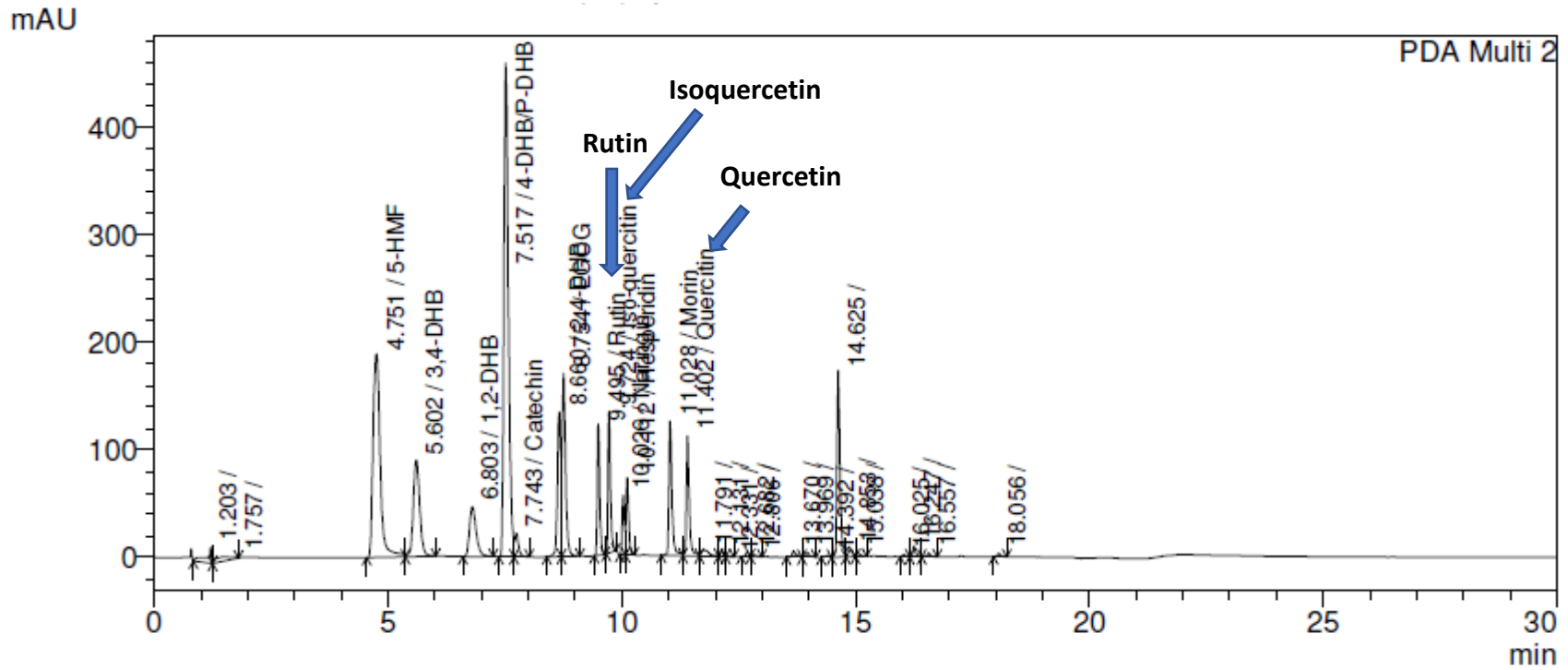
PeakTable

PDA Ch2 268nm 4nm

Peak#	Ret. Time	Area	Height	Area %	Height %	Name
1	1.203	106898	14768	0.899	0.744	
2	1.757	98830	2058	0.831	0.104	
3	4.751	2030403	189588	17.071	9.553	5-HMF
4	5.602	859272	89816	7.224	4.526	3,4-DHB
5	6.803	462572	46442	3.889	2.340	1,2-DHB
6	7.517	3069544	459512	25.807	23.154	4-DHB/P-DHB
7	7.743	120490	22013	1.013	1.109	Catechin
8	8.660	711152	134570	5.979	6.781	2,4-DHB
9	8.754	840481	170768	7.066	8.605	EGCG
10	9.495	446121	122453	3.751	6.170	Rutin
11	9.724	473040	132168	3.977	6.660	Iso-quercitin
12	10.026	194561	55447	1.636	2.794	Naringin

Figure B.3. Standard curves for rutin and isoquercetin (A1), and extrapolation of A1 for rutin (A2). Data of Table 4.2, and 4.3 were based on (A1); data were close to values obtained by A2. HPLC determination of methanolic rutin solutions was carried out at 268 nm.
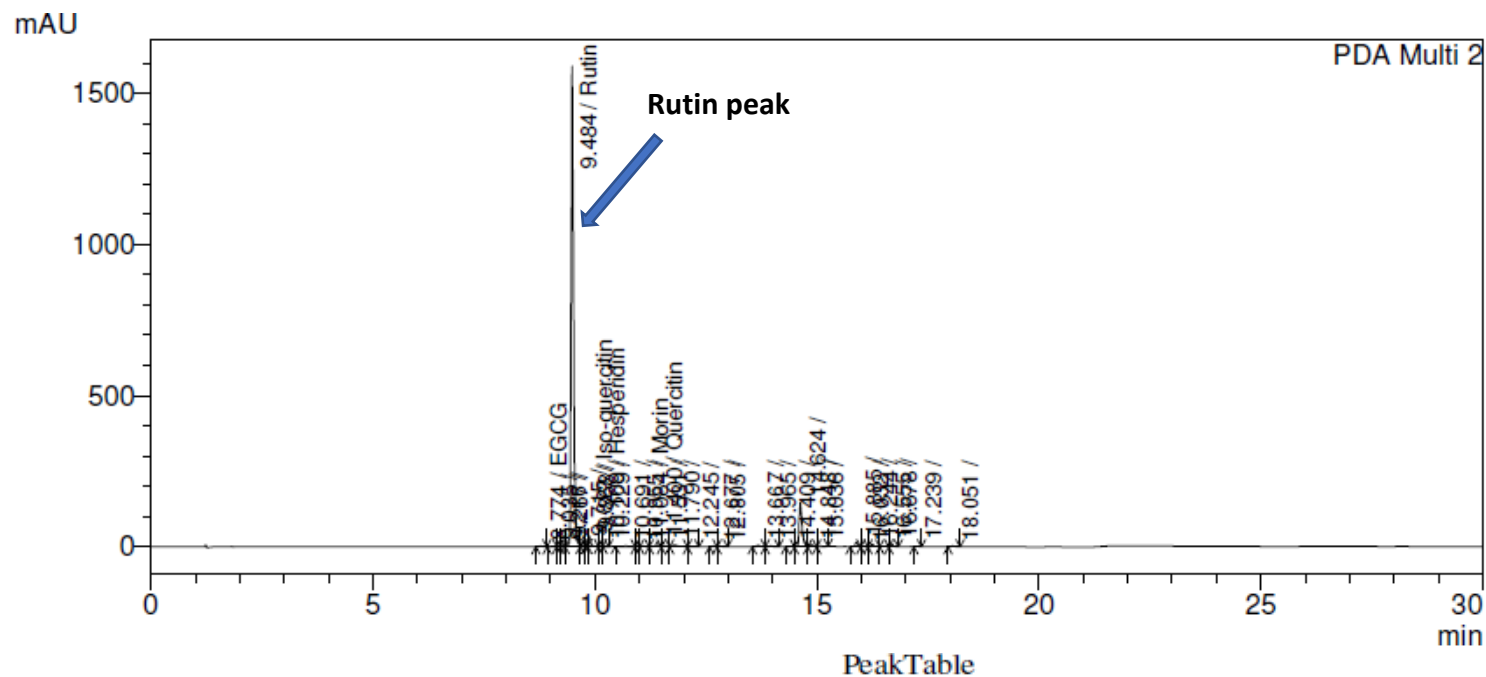
PDA Ch2 268nm 4nm

Peak#	Ret. Time	Area	Height	Area %	Height %	Name
1	8.774	10368	2403	0.138	0.125	EGCG
2	9.035	2679	517	0.036	0.027	
3	9.216	3098	785	0.041	0.041	
4	9.267	17819	3327	0.237	0.174	
5	9.484	5997362	1588914	79.865	82.869	Rutin
6	9.715	58279	13665	0.776	0.713	
7	9.823	70667	24029	0.941	1.253	Iso-quercitin
8	9.868	125621	35430	1.673	1.848	
9	10.109	365	142	0.005	0.007	Hesperidin
10	10.229	1090	355	0.015	0.019	
11	10.691	17058	1624	0.227	0.085	
12	10.955	2431	718	0.032	0.037	

Figure B.4 Chromatogram of ultrasonication rutin sample treated at 27 kJ/mL in water media.

Table B.8. Identification and quantification of flavonoids

ED (kJ/mL)	Rutin peak area	Conc (mg/ml)	mg in 50 mL	Starting mass (mg)	(mg in 50 mL/starting mass) *100	Mean	Std dev
Water media							
3.6	5368851	0.535	26.752	20.0	133.761	131.59	3.07
	5324465	0.531	26.530	20.5	129.416		
9	5257277	0.524	26.194	20.4	128.403	130.02	2.28
	5257277	0.524	26.194	19.9	131.630		
15	5804254	0.579	28.929	20.1	143.926	148.43	6.37
	6319494	0.630	31.505	20.6	152.939		
27	6530528	0.651	32.561	20.8	156.541	152.64	5.52
	5997362	0.598	29.895	20.1	148.730		
36	5587152	0.598	29.895	20.7	144.419	138.82	7.92
	5587152	0.557	27.844	20.9	133.223		
0	4640963	0.462	23.113	20.9	110.587	107.71	4.06
	4212085	0.419	20.968	20.0	104.842		
Isoquercetin peak area							
3.6	54379	0.003	0.149	20.0	0.746	0.71	0.05
	50226	0.003	0.139	20.5	0.677		
9	51913	0.003	0.143	20.4	0.701	0.71	0.01
	51913	0.003	0.143	19.9	0.719		
15	62344	0.003	0.169	20.1	0.841	0.82	0.03
	60779	0.003	0.165	20.6	0.802		
27	65651	0.004	0.177	20.8	0.853	0.90	0.07
	70667	0.004	0.190	20.1	0.945		
36	58093	0.004	0.190	20.7	0.917	0.91	0.01
	58093	0.004	0.190	20.9	0.909		
0	52661	0.003	0.145	20.9	0.693	0.65	0.06
	42851	0.002	0.120	20.0	0.602		

ED- energy density, Conc – concentration, Std dev -standard deviation

Table B.8. Continued.

NaCl media							
ΔED (kJ/mL)	Rutin peak area	Conc (mg/ml)	mg in 50 mL	Starting mass (mg)	(mg in 50 mL/starting mass)*100	Mean	Std dev
0.09	5561377	0.554	27.715	20.5	135.194	131.65	5.01
	5347730	0.533	26.647	20.8	128.109		
0.47	5556692	0.554	27.691	20.9	132.495	131.32	1.66
	5458470	0.544	27.200	20.9	130.145		
1.46	5717629	0.570	28.496	20.3	140.375	140.80	0.59
	5808260	0.579	28.949	20.5	141.216		
3.86	5732692	0.571	28.571	20.4	140.056	138.28	2.51
	5533240	0.551	27.574	20.2	136.506		
6.99	5622844	0.560	28.022	20.6	136.030	136.78	1.06
	5684588	0.567	28.331	20.6	137.528		
0	4282693	0.426	21.321	20.4	104.517	99.99	6.40
	3836882	0.382	19.092	20	95.462		
Isoquercetin peak area							
0.09	56242	0.003	0.154	20.5	0.750	0.73	0.03
	53206	0.003	0.146	20.8	0.703		
0.47	55657	0.003	0.152	20.9	0.729	0.75	0.03
	59228	0.003	0.161	20.9	0.772		
1.46	57465	0.003	0.157	20.3	0.773	0.78	0.01
	59445	0.003	0.162	20.5	0.790		
3.86	61277	0.003	0.166	20.4	0.816	0.63	0.27
	29847	0.002	0.088	20.2	0.435		
6.99	61949	0.003	0.168	20.6	0.816	0.82	0.00
	62331	0.003	0.169	20.6	0.821		
0	49735	0.003	0.138	20.4	0.674	0.63	0.07
	40900	0.002	0.115	20	0.577		

ΔED- change in energy density, Conc – concentration, Std dev -standard deviation
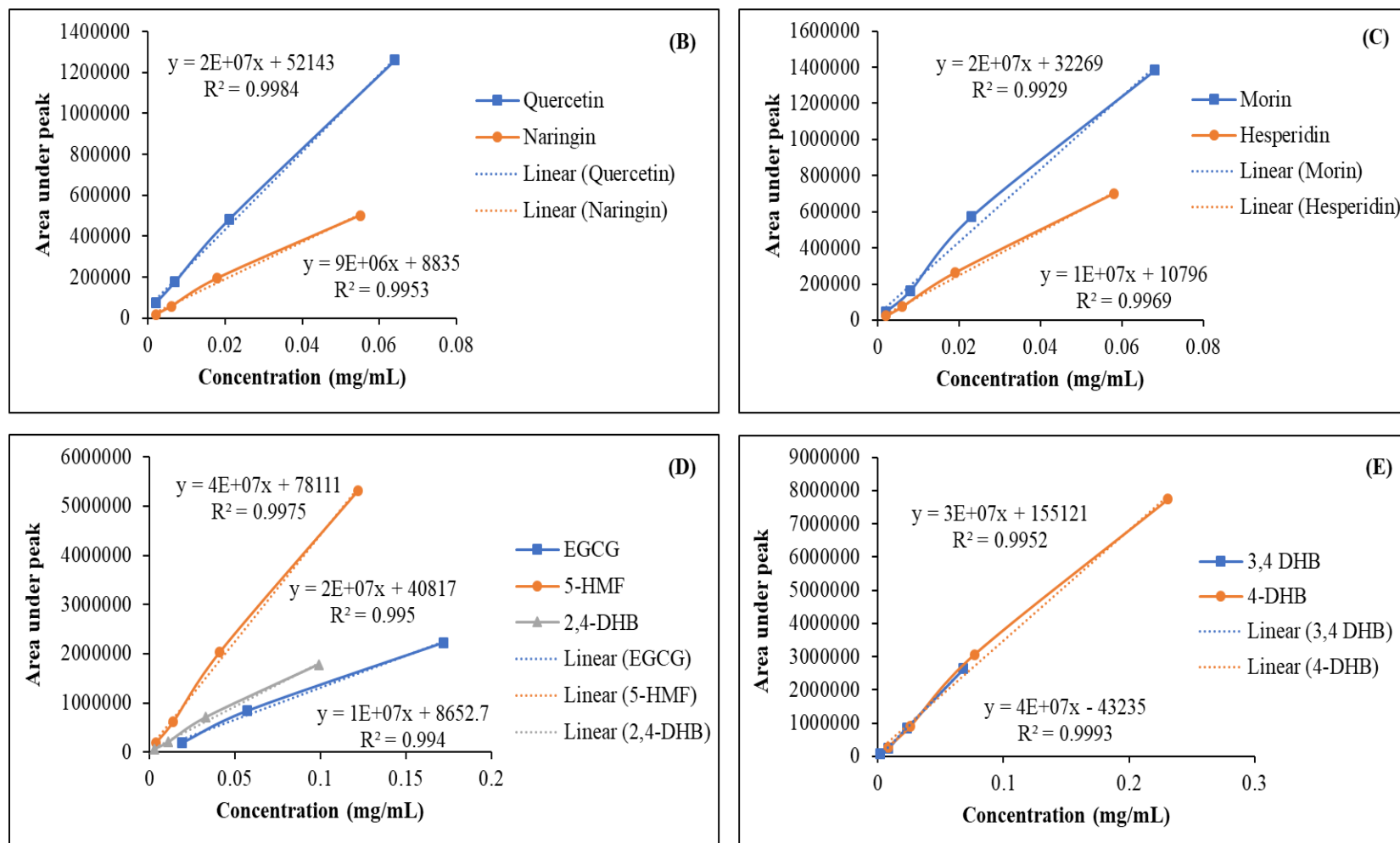
Figure B.5. Standard curves for quercetin and naringin (B), morin and hesperidin (C), EGCG – Epigallocatechin gallate, 5-HMF – 5-(Hydromethyl furfural), 2,4-DHB (D), 3,4 DHB, 4-DHB (E). HPLC determination of methanolic rutin solutions was carried out at 268 nm.*DHB – dihydrobenzoic acid.
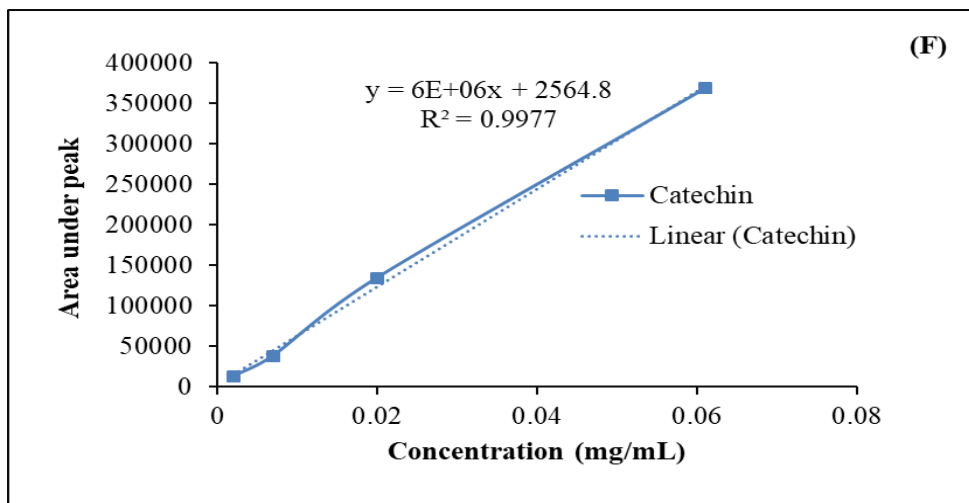
Figure B.6. Standard curve for catechin.
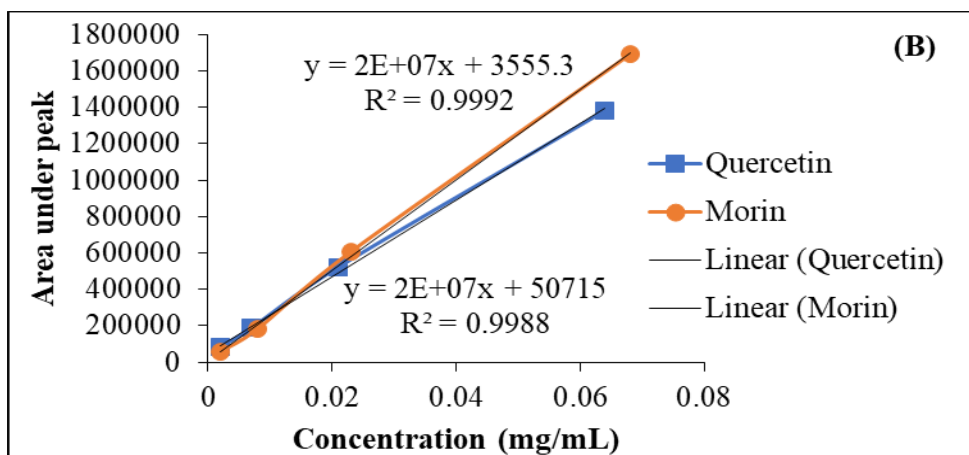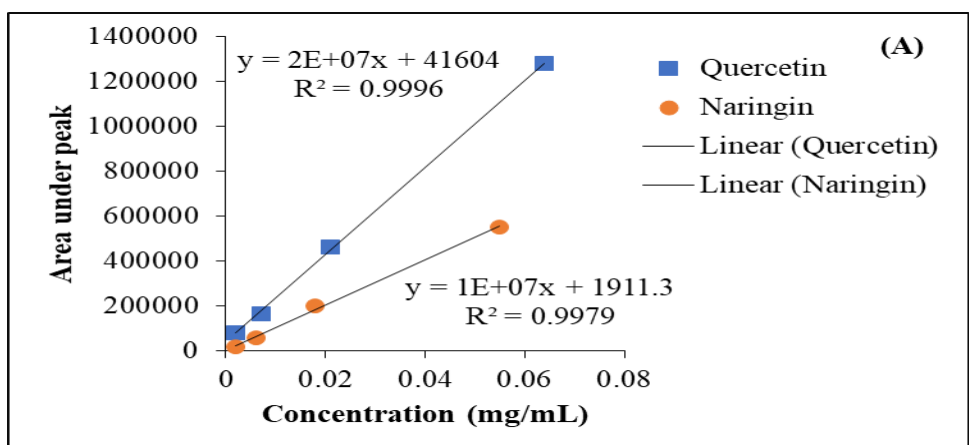
Figure B.7. Standard curve for quercetin (Used for citric acid samples).

Table B.8. Continued.

ED/ ΔED (kJ/mL)	Quercetin peak area	Conc (mg/ml)	mg in 50 mL	Starting mass (mg)	(mg in 50 mL/starting mass) *100	Mean	Std dev
Citric acid media							
3.6	111952	0.0035	0.176	20.2	0.87	0.84	0.04
	109562	0.0034	0.170	20.8	0.82		
9	104395	0.0031	0.157	20.6	0.76	0.77	0.01
	104395	0.0031	0.157	20.4	0.77		
15	102755	0.0031	0.153	20.5	0.75	0.74	0.01
	101266	0.0030	0.149	20.3	0.73		
27	99091	0.0029	0.144	20	0.72	0.73	0.02
	103391	0.0031	0.154	20.7	0.75		
36	71322	0.0015	0.074	20.4	0.36	0.36	0.00
	71383	0.0015	0.074	20.4	0.36		
0	64364	0.0011	0.057	20.2	0.28	0.34	0.09
	74249	0.0016	0.082	20.1	0.41		
0.09	108825	0.0029	0.145	20.7	0.70	0.72	0.03
	111803	0.0031	0.153	20.5	0.74		
0.47	127751	0.0039	0.193	20.7	0.93	0.89	0.05
	120402	0.0035	0.174	20.4	0.85		
1.46	162674	0.0056	0.280	20.7	1.35	1.35	0.01
	159986	0.0055	0.273	20.4	1.34		
3.86	180377	0.0065	0.324	19.9	1.63	1.69	0.08
	192101	0.0071	0.353	20.3	1.74		
6.99	233193	0.0091	0.456	20.2	2.26	2.23	0.04
	229887	0.0090	0.448	20.3	2.21		

ED – energy density, ΔED- change in energy density, Conc – concentration, Std dev- standard deviation

Appendix C: Effect of ultrasonication on rutin and its derivatives and its effect on pyrodextrinization

Table C.1. Color analysis of ethanolic rutin solutions

ED/ΔE (kJ/mL)	Media	L	a	b	L*-L	b*-b	a*-a
7	W	101.98	-2.56	7.55	-0.45	-5.70	0.12
		102.00	-2.05	6.31	-0.47	-4.46	-0.39
3.9	N	102.08	-2.28	7.08	-0.55	-5.23	-0.16
	N*	102.37	-2.25	6.88	-0.71	-1.27	0.58
3.9	W	102.43	-2.18	6.70	-0.90	-4.85	-0.26
		101.76	-2.00	6.31	-0.23	-4.46	-0.44
3.9	C	102.17	-1.06	4.11	-0.64	-2.26	-1.38
		102.54	-1.43	4.94	-1.01	-3.09	-1.01
36	W	100.77	-2.75	8.26	0.76	-6.41	0.31
		100.89	-3.13	9.13	0.64	-7.28	0.69
27	N	102.33	-3.22	9.07	-0.80	-7.22	0.78
		102.00	-3.28	9.36	-0.47	-7.51	0.84
27	W	101.81	-2.88	7.94	-0.28	-6.09	0.44
		101.58	-3.00	8.74	-0.05	-6.89	0.56
27	C	102.94	-2.00	6.40	-1.41	-4.55	-0.44
		102.49	-1.59	5.40	-0.96	-3.55	-0.85
0	60% MeoH	102.51	-1.62	5.41	-0.98	-3.56	-0.82
		102.43	-1.67	5.54	-0.90	-3.69	-0.77

ED – energy density, ΔED- change in energy density, W- water, N- NaCl, C- citric acid.
L*=101.53, a*=-2.44, b*=1.85, N* had a different calibration: L*=101.66, a*=-1.67, b*=5.61,
ΔE – total color difference, Std dev – standard deviation.

Table C.1. Continued.

ED/ΔE (kJ/mL)	Media	L*-L	b*-b	a*-a	(L*-L)^2	(b*-b)^2	(a*-a)^2	sum	sum^0.5	ΔE	Std dev
7	W	-0.45	-5.70	0.12	0.20	32.49	0.01	32.71	5.72	5.11	0.86
		-0.47	-4.46	-0.39	0.22	19.89	0.15	20.26	4.50		
3.9	N	-0.55	-5.23	-0.16	0.30	27.35	0.03	27.68	5.26	5.13	0.18
	N*	-0.71	-1.27	0.58	0.50	1.61	0.34	2.45	5.00		
3.9	W	-0.90	-4.85	-0.26	0.81	23.52	0.07	24.40	4.94	4.71	0.32
		-0.23	-4.46	-0.44	0.05	19.89	0.19	20.14	4.49		
3.9	C	-0.64	-2.26	-1.38	0.41	5.11	1.90	7.42	2.72	3.06	0.48
		-1.01	-3.09	-1.01	1.02	9.55	1.02	11.59	3.40		
36	W	0.76	-6.41	0.31	0.58	41.09	0.10	41.76	6.46	6.90	0.62
		0.64	-7.28	0.69	0.41	53.00	0.48	53.88	7.34		
27	N	-0.80	-7.22	0.78	0.64	52.13	0.61	53.38	7.31	7.44	0.19
		-0.47	-7.51	0.84	0.22	56.40	0.71	57.33	7.57		
27	W	-0.28	-6.09	0.44	0.08	37.09	0.19	37.36	6.11	6.51	0.57
		-0.05	-6.89	0.56	0.00	47.47	0.31	47.79	6.91		
27	C	-1.41	-4.55	-0.44	1.99	20.70	0.19	22.88	4.78	4.28	0.71
		-0.96	-3.55	-0.85	0.92	12.60	0.72	14.25	3.77		
0	60% MeoH	-0.98	-3.56	-0.82	0.96	12.67	0.67	14.31	3.78	3.83	0.07
		-0.90	-3.69	-0.77	0.81	13.62	0.59	15.02	3.88		

ED – energy density, ΔED- change in energy density, W- water, N- NaCl, C- citric acid.

L*=101.53, a*=-2.44, b*=1.85, N* had a different calibration: L*=101.66, a*=-1.67, b*=5.61, ΔE – total color difference, Std dev – standard deviation.

Table C.1. Continued.

ED/ΔE (kJ/mL)	Media	L	a	b	YI	Mean	Std dev	% error	Greenness	Mean	Std dev
7	Water	101.98	-2.56	7.55	10.58	9.71	1.23	12.67	-2.31	-2.24	0.10
		102	-2.05	6.31	8.84				-2.17		
3.9	NaCl	102.08	-2.28	7.08	9.91	9.75	0.22	2.23	-2.27	-2.24	0.04
	NaCl*	102.37	-2.25	6.88	9.60				-2.22		
3.9	Water	102.43	-2.18	6.7	9.34	9.10	0.34	3.78	-2.09	-1.81	0.40
		101.76	-2	6.31	8.86				-1.53		
3.9	Citric acid	102.17	-1.06	4.11	5.75	6.31	0.80	12.72	-1.25	-1.39	0.20
		102.54	-1.43	4.94	6.88				-1.53		
36	Water	100.77	-2.75	8.26	11.71	12.32	0.86	6.99	-2.94	-3.06	0.17
		100.89	-3.13	9.13	12.93				-3.18		
27	NaCl	102.33	-3.22	9.07	12.66	12.89	0.32	2.45	-3.25	-3.17	0.12
		102	-3.28	9.36	13.11				-3.08		
27	Water	101.81	-2.88	7.94	11.14	11.72	0.81	6.94	-2.94	-2.72	0.31
		101.58	-3	8.74	12.29				-2.50		
27	Citric acid	102.94	-2	6.4	8.88	8.20	0.96	11.68	-1.80	-1.81	0.02
		102.49	-1.59	5.4	7.53				-1.83		
Untreated	60% MeoH	102.51	-1.62	5.41	7.54	7.63	0.13	1.73	-1.65	-1.93	0.40
		102.43	-1.67	5.54	7.73				-2.21		

ED – energy density, ΔED- change in energy density, YI – yellowness index, Std dev- standard deviation.
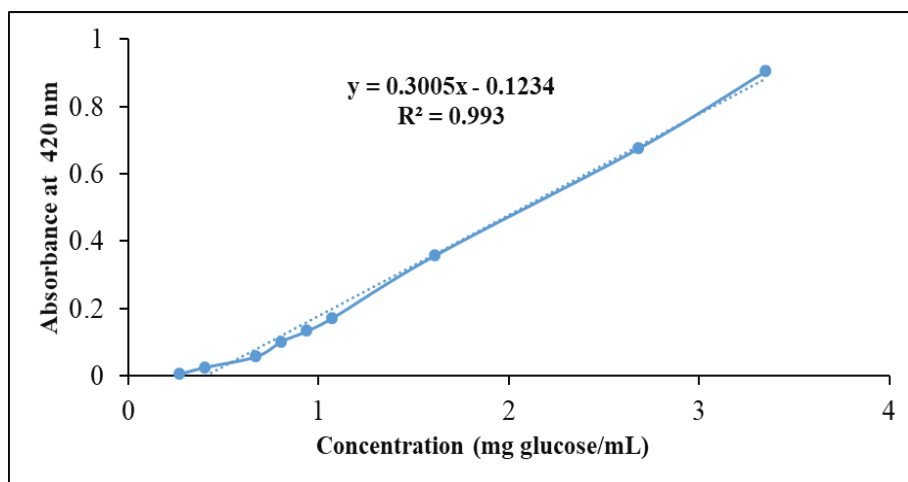
Figure C.1. Standard curve for determination of reducing end group
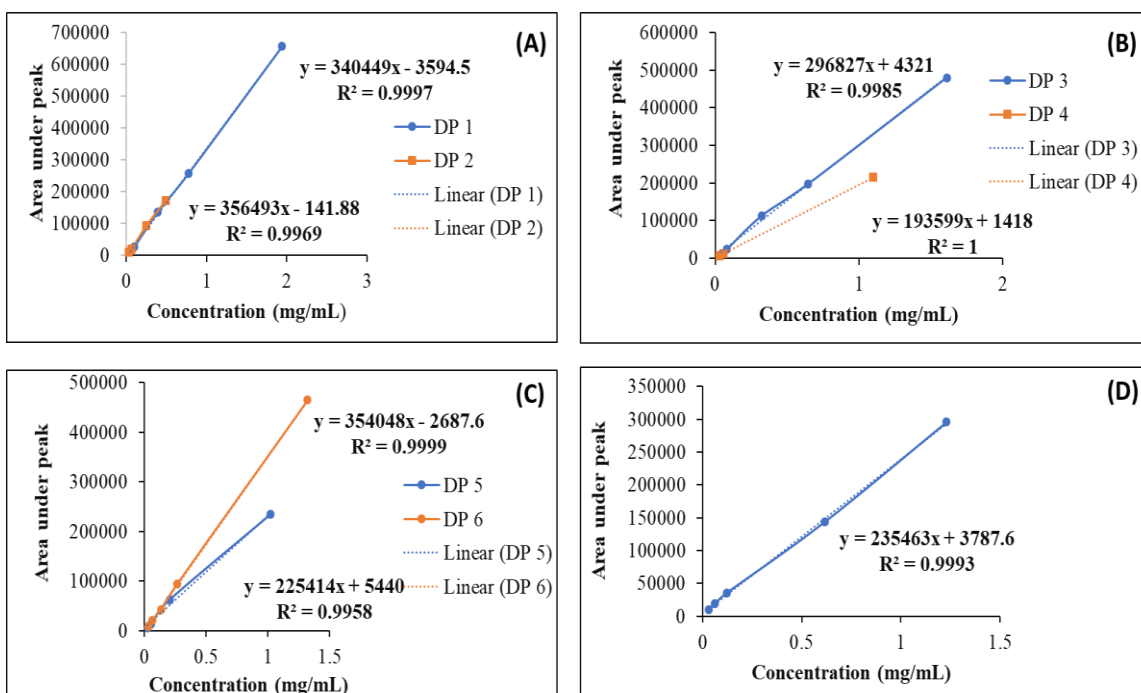
Figure C.2. Standard curves for determination of glucose and malto-oligosaccharides with DP1, 2 (A), DP 3,4 (B), DP 5,6 (C), and DP 7 (D).

Table C.2. Quantification of Malto-oligosaccharide

ED/ΔE (kJ/mL)	Media	DP 7	Conc (mg/ml)	Mean	Std dev	DP 6	Conc (mg/ml)	Mean	Std dev
7	Water	142887	29.54	34.44	6.93	166049	23.83	27.13	4.67
		189035	39.34			212788	30.43		
3.9	NaCl	146200	30.24	30.43	0.27	161262	23.15	24.04	1.26
		147987	30.62			173858	24.93		
3.9	Water	158373	32.83	30.99	2.60	183309	26.27	24.43	2.60
		141039	29.15			157305	22.59		
3.9	Citric acid	106003	21.71	24.11	3.40	121378	17.52	19.15	2.31
		128680	26.52			144475	20.78		
36	Water	95556.4	19.49	22.25	3.91	111642	16.15	17.77	2.30
		121605	25.02			134694	19.40		
27	NaCl	102790	21.02	25.90	0.90	119987	17.32	17.67	0.49
		108807	22.30			124904	18.02		
27	Water	148726	30.78	26.39	4.81	165894	23.81	24.93	1.58
		147297	30.47			181717	26.04		
27	Citric acid	97119	19.82	26.36	9.25	113776	16.45	20.81	6.16
		158728	32.90			175509	25.17		
Untreated rutin	60% MeoH	160075	33.19	33.31	0.17	194702	27.88	28.05	0.25
		161222	33.43			197179	28.23		
No rutin		122505	25.21	24.93	0.39	138762	19.98	19.61	0.51
		119900	24.66			133609	19.25		

ED – energy density, ΔED- change in energy density, Std dev- standard deviation.

Table C.2. Continued.

ED/ΔE (kJ/mL)	Media	DP 5	Conc (mg/ml)	Mean	Std dev	DP 4	Conc (mg/ml)	Mean	Std dev
7	Water	182328	39.24	45.59	8.99	208088	53.38	62.62	13.08
		239630	51.95			279709	71.87		
3.9	NaCl	185943	40.04	40.93	1.25	212366	54.48	56.80	3.28
		193940	41.81			230304	59.11		
3.9	Water	218696	47.30	44.29	4.26	248689	63.86	59.46	6.23
		191551	41.28			214591	55.06		
3.9	Citric acid	124196	26.34	30.27	5.56	140688	35.97	40.35	6.20
		159639	34.20			174631	44.74		
36	Water	119566	25.31	29.37	5.73	146109	37.37	41.56	5.92
		156114	33.42			178553	45.75		
27	NaCl	121260	25.69	27.19	2.13	140490	35.92	38.05	3.02
		134820	28.70			157035	40.19		
27	Water	191058	41.17	43.01	2.60	226312	58.08	61.92	5.42
		207630	44.85			256013	65.75		
27	Citric acid	122440	25.95	34.14	11.57	138767	35.47	46.38	15.42
		196236	42.32			223227	57.29		
Untreated rutin	60% MeoH	229051	49.60	50.20	0.85	290395	74.63	75.19	0.79
		234478	50.80			294727	75.75		
No rutin		154079	32.97	32.71	0.37	174288	44.65	44.36	0.41
		151698	32.44			172034	44.06		

ED – energy density, ΔED- change in energy density, Std dev- standard deviation.

Table C.2. Continued.

ED/ΔE (kJ/mL)	Media	DP 3	Conc (mg/ml)	Mean	Std dev	DP 2	Conc (mg/ml)	Mean	Std dev
7	Water	218208	36.03	42.69	9.42	226459	31.78	37.48	8.05
		297334	49.36			307670	43.17		
3.9	NaCl	233822	38.66	40.85	3.10	240893	33.81	36.50	3.82
		259883	43.05			279370	39.20		
3.9	Water	292602	48.56	44.13	6.27	317702	44.58	38.61	8.44
		239957	39.69			232601	32.64		
3.9	Citric acid	159396	26.12	29.20	4.36	157863	22.16	24.78	3.70
		195974	32.28			195177	27.39		
36	Water	153282	25.09	30.25	7.29	157876	22.16	26.86	6.64
		214517	35.41			224839	31.55		
27	NaCl	156732	25.67	26.75	1.52	158836	22.30	22.53	0.32
		169477	27.82			162105	22.76		
27	Water	257356	42.62	47.26	6.55	273606	38.39	42.40	5.66
		312360	51.89			330721	46.41		
27	Citric acid	149825	24.51	32.07	10.70	149159	20.94	27.69	9.54
		239637	39.64			245374	34.43		
Untreated rutin	60% MeoH	355132	59.09	58.58	0.73	387809	54.41	55.54	1.60
		348978	58.06			403899	56.67		
No rutin		193179	31.81	31.86	0.07	199594	28.01	28.15	0.19
		193745	31.91			201468	28.28		

ED – energy density, ΔED- change in energy density, std dev- standard deviation.

Table C.2. Continued.

ED/ΔE (kJ/mL)	Media	DP 1	Conc (mg/ml)	Mean	Std dev	Rhamnose	Conc (mg/ml)	Mean	Std dev
7	Water	243730	36.32	44.09	10.99	19728	4.53	4.53	0.00
		349564	51.87			19728	4.53		
3.9	NaCl	274369	40.82	45.43	6.51	15870	3.79	4.11	0.45
		337096	50.04			19192	4.42		
3.9	Water	370458	54.94	48.63	8.91	15934	3.80	3.40	0.56
		284645	42.33			11781	3.01		
3.9	Citric acid	170386	25.55	28.72	4.48	7440	2.17	2.61	0.62
		213521	31.89			12000	3.05		
36	Water	175506	26.30	32.74	9.10	7025	2.09	2.45	0.50
		263155	39.18			10718	2.80		
27	NaCl	178690	26.77	27.49	1.01	13044	3.25	3.14	0.15
		188454	28.21			11937	3.04		
27	Water	316993	47.08	53.80	9.50	13602	3.35	3.78	0.60
		408439	60.51			18064	4.21		
27	Citric acid	167134	25.07	33.30	11.63	11538	2.96	3.53	0.81
		279170	41.53			17495	4.10		
Untreated rutin	60% MeoH	497179	73.55	74.21	0.95	23788	5.30	6.24	1.32
		506279	74.88			33526	7.17		
No rutin		234569	34.98	34.56	0.59	14151	3.46	3.43	0.05
		228866	34.14			13802	3.39		

ED – energy density, ΔED- change in energy density, Std dev- standard deviation.

Appendix D: Structural characterization of starch isolates from electrolysis treatment of barley flour

Table D.1. Starch, protein and ash contents of electrolysed starches

Voltage (V)	Starch content % (dm)			Protein content % (dm)		
	Electrode Length			Electrode Length		
	4 cm	6 cm	8 cm	4 cm	6 cm	8 cm
0	91.24±3.06[a]	91.24±3.06[a]	91.24±3.06[a]	0.25±0.02[c]	0.25±0.02[c]	0.25±0.02[c]
5	92.09±1.45[a]	97.44±8.47[a]	93.92±0.74[a]	0.74±0.09[ab]	0.76±0.01[ab]	0.70±0.06[ab]
10	94.12±1.34[a]	94.50±0.72[a]	94.87±0.66[a]	0.95±0.01[a]	0.84±0.00[ab]	0.76±0.13[ab]
15	93.92±6.12[a]	97.44±1.89[a]	95.74±1.06[a]	0.70±0.12[ab]	0.76±0.09[ab]	0.86±0.10[ab]
20	97.00±0.45[a]	92.30±2.90[a]	95.98±0.30[a]	0.75±0.13[ab]	0.97±0.10[a]	0.65±0.06[ab]
25	99.26±0.52[a]	94.62±7.41[a]	92.20±1.02[a]	0.79±0.17[ab]	0.79±0.15[ab]	0.85±0.08[ab]
30	92.82±5.71[a]	96.21±2.50[a]	98.68±2.62[a]	0.50±0.00[bc]	0.58±0.07[bc]	0.52±0.00[bc]

0V means alkali-treated starch, dm – dry matter, [a-c]values with same lowercase letters per component are not significantly different.

Table D.1. Continued.

Voltage (V)	Ash content % (dm)		
	Electrode Length		
	4 cm	6 cm	8 cm
0	0.32±0.02[a]	0.32±0.02[a]	0.32±0.02[a]
5	0.14±0.01[b]	0.17±0.01[b]	0.26±0.04[ab]
10	0.23±0.03[ab]	0.26±0.00[ab]	0.22±0.04[ab]
15	0.22±0.12[ab]	0.26±0.02[ab]	0.18±0.02[b]
20	0.28±0.04[ab]	0.23±0.01[ab]	0.23±0.04[ab]
25	0.22±0.00[ab]	0.19±0.04[ab]	0.25±0.04[ab]
30	0.22±0.05[ab]	0.21±0.08[ab]	0.18±0.02[ab]

0V means alkali-treated starch, dm – dry matter,
[a-c]values with same lowercase letters per component are not significantly different.

Table D.2. Absorption capacity of freeze-dried starch gel

Electrode length (4 cm)						
Absorption in Water						
Voltage (V)	**Dry weight (g)**	**Wet weight (g)**	**Difference (g)**	**Absorption capacity (%)**	**Mean**	**Std dev**
5	0.31	5.26	4.94	1585.09	1470.92	161.47
5	0.24	3.45	3.21	1356.74		
10	0.10	1.43	1.32	1263.51	1244.50	26.89
10	0.10	1.35	1.25	1225.49		
15	0.12	1.72	1.60	1328.43	1307.92	29.00
15	0.20	2.78	2.58	1287.42		
20	0.15	1.65	1.50	1021.45	1019.15	3.26
20	0.16	1.79	1.63	1016.84		
25	0.04	0.65	0.61	1364.88	1374.88	14.15
25	0.15	2.27	2.12	1384.89		
30	0.15	2.26	2.12	1413.84	1381.94	45.11
30	0.11	1.63	1.52	1350.04		
Absorption in 50% Ethanol						
Voltage (V)	**Dry weight (g)**	**Wet weight (g)**	**Difference (g)**	**Absorption capacity (%)**	**Mean**	**Std dev**
5	0.33	1.48	1.15	349.06	367.99	26.77
5	0.22	1.09	0.87	386.91		
10	0.05	0.27	0.23	506.89	472.74	48.29
10	0.14	0.74	0.60	438.59		
15	0.05	0.27	0.22	422.18	367.23	77.72
15	0.04	0.18	0.14	312.27		
20	0.13	0.74	0.60	447.92	467.16	27.21
20	0.16	0.91	0.76	486.40		
25	0.05	0.28	0.23	423.93	458.71	49.18
25	0.06	0.36	0.30	493.49		
30	0.05	0.22	0.17	324.75	369.52	63.31
30	0.11	0.58	0.46	414.29		

Std dev- standard deviation

Table D.2. Continued.

Electrode length (4 cm)						
Absorption in 50% Glycerol						
Voltage (V)	**Dry weight (g)**	**Wet weight (g)**	**Difference (g)**	**Absorption capacity (%)**	**Mean**	**Std dev**
5	0.29	5.78	5.49	1905.06	1828.42	108.39
5	0.10	1.94	1.83	1751.77		
10	0.13	2.09	1.97	1530.27	1539.52	13.08
10	0.14	2.34	2.20	1548.77		
15	0.05	0.92	0.87	1601.11	1651.16	70.78
15	0.06	1.05	0.99	1701.20		
20	0.15	2.05	1.90	1272.40	1354.54	116.16
20	0.10	1.53	1.43	1436.67		
25	0.17	2.81	2.64	1541.71	1640.64	139.91
25	0.14	2.58	2.44	1739.57		
30	0.05	0.97	0.92	1776.49	1817.86	58.50
30	0.07	1.32	1.25	1859.23		
Absorption in Paraffin oil						
Voltage (V)	**Dry weight (g)**	**Wet weight (g)**	**Difference (g)**	**Absorption capacity (%)**	**Mean**	**Std dev**
5	0.30	1.94	1.64	554.58	508.18	65.61
5	0.09	0.51	0.42	461.79		
10	0.09	0.65	0.56	632.62	613.54	26.98
10	0.09	0.65	0.56	594.46		
15	0.04	0.27	0.23	577.41	561.06	23.13
15	0.09	0.58	0.49	544.70		
20	0.05	0.33	0.28	560.36	549.48	15.38
20	0.04	0.27	0.23	538.60		
25	0.12	0.67	0.55	474.66	475.36	0.99
25	0.13	0.75	0.62	476.06		
30	0.08	0.55	0.48	620.10	596.20	33.80
30	0.06	0.39	0.33	572.30		

Std dev- standard deviation

Table D.2. Absorption capacity of freeze-dried starch gel

Electrode length (6 cm)						
Absorption in Water						
Voltage (V)	**Dry weight (g)**	**Wet weight (g)**	**Difference (g)**	**Absorption capacity (%)**	**Mean**	**Std dev**
5	0.14	2.00	1.86	1306.89	1364.05	80.83
5	0.22	3.32	3.10	1421.21		
10	0.18	2.90	2.73	1535.14	1478.65	79.89
10	0.12	1.89	1.76	1422.16		
15	0.13	1.74	1.61	1285.59	1391.52	149.81
15	0.13	2.07	1.94	1497.45		
20	0.11	1.68	1.57	1386.27	1407.90	30.59
20	0.15	2.29	2.14	1429.53		
25	0.11	1.50	1.39	1226.88	1253.71	37.94
25	0.22	3.06	2.84	1280.53		
30	0.18	2.84	2.66	1503.67	1474.95	40.63
30	0.21	3.21	3.00	1446.22		
Absorption in 50% Ethanol						
Voltage (V)	**Dry weight (g)**	**Wet weight (g)**	**Difference (g)**	**Absorption capacity (%)**	**Mean**	**Std dev**
5	0.18	1.19	1.01	565.64	524.14	58.69
5	0.10	0.57	0.47	482.64		
10	0.11	0.54	0.43	396.48	389.23	10.26
10	0.06	0.30	0.24	381.98		
15	0.16	0.96	0.80	493.98	506.42	17.60
15	0.16	1.02	0.86	518.87		
20	0.10	0.49	0.39	400.92	410.68	13.81
20	0.09	0.47	0.38	420.45		
25	0.07	0.43	0.36	541.59	512.08	41.73
25	0.09	0.55	0.45	482.57		
30	0.10	0.57	0.46	442.41	445.48	4.34
30	0.06	0.30	0.25	448.55		

Std dev- standard deviation

Table D.2. Continued.

Electrode length (6 cm)						
Absorption in 50% Glycerol						
Voltage (V)	Dry weight (g)	Wet weight (g)	Difference (g)	Absorption capacity (%)	Mean	Std dev
5	0.14	2.24	2.09	1467.90	1553.96	121.70
5	0.14	2.47	2.32	1640.01		
10	0.09	1.90	1.81	1983.21	2019.05	50.69
10	0.07	1.59	1.51	2054.89		
15	0.11	1.73	1.62	1516.06	1532.54	23.30
15	0.15	2.42	2.28	1549.01		
20	0.06	1.11	1.05	1846.67	1812.81	47.88
20	0.04	0.71	0.68	1778.95		
25	0.11	1.60	1.49	1405.94	1421.87	22.53
25	0.12	1.79	1.67	1437.80		
30	0.06	1.33	1.26	1950.54	1885.57	91.88
30	0.07	1.33	1.26	1820.61		
Absorption in Paraffin oil						
Voltage (V)	Dry weight (g)	Wet weight (g)	Difference (g)	Absorption capacity (%)	Mean	Std dev
5	0.09	0.70	0.60	637.38	587.48	70.57
5	0.05	0.32	0.27	537.58		
10	0.09	0.57	0.48	503.27	469.80	47.32
10	0.04	0.20	0.16	436.34		
15	0.08	0.52	0.43	522.83	532.14	13.17
15	0.09	0.56	0.48	541.46		
20	0.09	0.50	0.41	452.34	484.18	45.04
20	0.09	0.58	0.49	516.03		
25	0.06	0.37	0.31	553.17	535.12	25.53
25	0.09	0.56	0.47	517.07		
30	0.06	0.38	0.32	491.90	503.05	15.77
30	0.07	0.41	0.34	514.20		

Std dev- standard deviation

Table D.2. Continued.

Electrode length (8 cm)						
Absorption in Water						
Voltage (V)	**Dry weight (g)**	**Wet weight (g)**	**Difference (g)**	**Absorption capacity (%)**	**Mean**	**Std dev**
5	0.12	1.40	1.29	1077.12	1126.15	69.34
5	0.17	2.12	1.95	1175.18		
10	0.17	2.63	2.46	1458.21	1440.88	24.51
10	0.13	1.92	1.79	1423.55		
15	0.17	2.97	2.80	1641.59	1659.05	24.69
15	0.16	2.77	2.62	1676.50		
20	0.11	1.62	1.50	1310.63	1300.13	14.84
20	0.11	1.53	1.42	1289.64		
25	0.34	4.90	4.56	1325.46	1311.40	19.88
25	0.15	2.11	1.96	1297.35		
30	0.22	3.05	2.84	1303.77	1322.34	26.26
30	0.19	2.79	2.60	1340.91		
Absorption in 50% Ethanol						
Voltage (V)	**Dry weight (g)**	**Wet weight (g)**	**Difference (g)**	**Absorption capacity (%)**	**Mean**	**Std dev**
5	0.07	0.37	0.31	445.34	484.13	54.87
5	0.10	0.62	0.52	522.93		
10	0.11	0.55	0.44	385.85	348.61	52.67
10	0.13	0.52	0.40	311.36		
15	0.13	0.59	0.46	355.51	390.48	49.46
15	0.15	0.78	0.63	425.45		
20	0.07	0.39	0.33	478.89	468.18	15.14
20	0.03	0.17	0.14	457.47		
25	0.11	0.65	0.53	477.57	458.15	27.46
25	0.10	0.56	0.46	438.73		
30	0.11	0.58	0.47	420.23	443.74	33.23
30	0.15	0.86	0.71	467.24		

Std dev- standard deviation

Table D.2. Continued.

Electrode length (6 cm)						
Absorption in 50% Glycerol						
Voltage (V)	Dry weight (g)	Wet weight (g)	Differenc e (g)	Absorption capacity (%)	Mean	Std dev
5	0.10	1.64	1.53	1467.34	1471.69	6.16
5	0.06	0.94	0.88	1476.05		
10	0.10	1.73	1.63	1588.28	1723.37	191.04
10	0.10	1.98	1.88	1858.46		
15	0.13	2.53	2.40	1838.27	1934.14	135.59
15	0.07	1.39	1.33	2030.02		
20	0.05	0.89	0.84	1560.07	1526.44	47.57
20	0.10	1.55	1.45	1492.81		
25	0.10	1.72	1.62	1649.44	1764.18	162.26
25	0.11	2.12	2.01	1878.92		
30	0.07	1.34	1.27	1782.49	1840.09	81.46
30	0.06	1.30	1.23	1897.69		
Absorption in Paraffin oil						
Voltage (V)	Dry weight (g)	Wet weight (g)	Differenc e (g)	Absorption capacity (%)	Mean	Std dev
5	0.06	0.34	0.28	502.66	545.32	60.33
5	0.05	0.34	0.29	587.98		
10	0.09	0.53	0.44	485.51	473.44	17.06
10	0.06	0.33	0.27	461.38		
15	0.08	0.49	0.40	477.74	482.40	6.59
15	0.15	0.89	0.74	487.06		
20	0.07	0.47	0.40	546.76	527.92	26.64
20	0.05	0.33	0.27	509.09		
25	0.08	0.64	0.56	660.80	624.28	51.65
25	0.09	0.61	0.52	587.75		
30	0.08	0.52	0.45	583.99	602.89	26.73
30	0.04	0.31	0.27	621.79		

Std dev- standard deviation

Table D.3. Absorption capacity of freeze-dried gel (of alkali-treated starch)

Control (Without rutin)						
Solvent	Dry weight (g)	Wet weight (g)	Difference (g)	Swelling capacity (%)	Mean (%)	Std dev
Water	0.09	0.89	0.79	853.18	815.24	51.53
	0.11	0.92	0.81	756.57		
	0.09	0.84	0.75	835.97		
50% Glycerol	0.08	0.49	0.41	547.23	597.99	71.78
	0.04	0.27	0.23	648.75		
50% Ethanol	0.13	0.25	0.12	96.11	103.71	10.75
	0.06	0.12	0.06	111.30		
Paraffin oil	0.06	0.17	0.11	179.17	163.62	21.99
	0.07	0.18	0.11	148.07		

Std dev- standard deviation

Table D.4. Absorption capacity of freeze-dried gel with rutin

Electrode length (8 cm)						
Absorption in Water						
Voltage (V)	Dry weight (g)	Wet weight (g)	Difference (g)	Absorption capacity (%)	Mean	Std dev
0	0.12	0.95	0.83	692.75	764.95	102.11
0	0.10	0.98	0.88	837.15		
5	0.13	1.20	1.07	805.66	825.73	28.38
5	0.08	0.77	0.69	845.80		
15	0.14	0.88	0.74	516.40	565.88	69.98
15	0.17	1.23	1.06	615.36		
25	0.10	0.95	0.85	885.88	886.44	0.79
25	0.10	1.01	0.91	887.00		
Absorption in 50% Ethanol						
Voltage (V)	Dry weight (g)	Wet weight (g)	Difference (g)	Absorption capacity (%)	Mean	Std dev
0	0.07	0.20	0.13	179.40	177.66	2.46
0	0.08	0.23	0.15	175.92		
5	0.07	0.17	0.10	134.31	129.99	6.11
5	0.06	0.13	0.07	125.67		
15	0.11	0.29	0.19	176.06	156.85	27.17
15	0.08	0.20	0.12	137.63		
25	0.09	0.26	0.17	189.16	176.04	18.55
25	0.07	0.18	0.11	162.92		

Std dev- standard deviation

Table D.4. Continued.

Electrode length (8 cm)						
Absorption in 50% Glycerol						
Voltage (V)	**Dry weight (g)**	**Wet weight (g)**	**Difference (g)**	**Absorption capacity (%)**	**Mean**	**Std dev**
0	0.08	0.54	0.47	601.81	610.58	12.41
0	0.09	0.67	0.57	619.35		
5	0.09	0.76	0.66	707.59	768.69	86.41
5	0.07	0.67	0.60	829.79		
15	0.12	0.78	0.65	521.71	574.26	74.31
15	0.17	1.20	1.04	626.80		
25	0.11	0.77	0.67	624.60	637.30	17.96
25	0.07	0.53	0.46	650.00		
Absorption in Paraffin oil						
Voltage (V)	**Dry weight (g)**	**Wet weight (g)**	**Difference (g)**	**Absorption capacity (%)**	**Mean**	**Std dev**
0	0.08	0.43	0.35	447.28	451.55	6.03
0	0.09	0.51	0.42	455.81		
5	0.06	0.31	0.25	382.92	426.91	62.21
5	0.05	0.29	0.24	470.89		
15	0.11	0.59	0.48	439.76	460.24	28.96
15	0.05	0.29	0.24	480.72		
25	0.08	0.44	0.36	449.12	425.75	33.05
25	0.04	0.21	0.17	402.39		

Std dev- standard deviation